

**POTENTIAL IMPACTS OF CLIMATIC WARMING ON
GLACIER-FED RIVER FLOWS IN THE HIMALAYA**

Hefin Gwyn REES

School of Environment & Life Sciences
University of Salford, Salford, UK

Submitted in Partial Fulfilment of the Requirements of the
Degree of Doctor of Philosophy, September 2014

CONTENTS

Contents	i
List of Figures and Tables	v
Figures.....	v
Tables.....	xiii
Dedication	xv
Acknowledgements	xvi
Declaration	xviii
Acronyms	xix
Abstract	xxiii

PART 1

1 Introduction	1
1.1 Background of the study	1
1.2 Objectives of the study.....	4
1.3 Approach and outline of the thesis.....	5
2 Current Understanding	6
2.1 Introduction.....	6
2.2 Characteristics of the Himalayan region.....	7
2.2.1 Physical and geomorphological characteristics	7
2.2.2 Hydrological characteristics of the region	9
2.3 Glacier fluctuation	12
2.3.1 Global glacier fluctuation	12
2.3.2 Himalayan glacier fluctuation.....	13
2.4 Hydrometeorological changes: observed and projected	16
2.4.1 Observed trends in temperature and precipitation	16
2.4.2 Observed changes to glacier-fed river flows	19
2.4.3 Climate change projections.....	20
2.5 Meso-scale hydrological modelling.....	26
2.5.1 Rainfall-runoff models.....	26

2.5.2 Modelling ice-melt.....	27
2.5.3 Modelling climate change impacts in glacier-fed catchments.....	28
2.6 Macro-scale hydrological modelling	31
2.6.1 Definition of a macro-scale hydrological model	31
2.6.2 Worldwide applications of MHMs	31
2.6.3 MHM applications in the Himalaya.....	32
2.6.4 Representation of glaciers in MHMs	34
2.7 Summary	36
3 Hydrometeorological Observations	40
3.1 Introduction.....	40
3.2 Approach to data acquisition	41
3.3 Rainfall data	43
3.3.1 General characteristics of rainfall distribution in the region	43
3.3.2 Correlation Analyses.....	51
3.3.3 Exploring trends in available rainfall data	58
3.4 Temperature Data.....	61
3.4.1 General characteristics of temperature variation across the region	61
3.4.2 Correlation analyses.....	64
3.4.3 Temperature variation with elevation	66
3.4.4 Exploring trends in the available temperature data.....	68
3.5 River flow data.....	71
3.5.1 General characteristics of glacier-fed flow regimes across the region	73
3.5.2 Variability of annual runoff in glacier-fed catchments.....	78
3.5.3 Exploring trends in glacier-fed river flows	78
PART 2	
4 Model Development.....	83
4.1 Introduction.....	83
4.2 Design of the regional macro-scale hydrological model	84
4.2.1 Defining the scope of the macro-scale hydrological model.....	85
4.2.2 Understanding the physical characteristics of the study area	87
4.2.3 Assessing the availability of data.....	89
4.2.4 Identifying a suitable candidate model	91
4.3 Features of the unmodified Macro-PDM.....	91

4.3.1	General features of Macro-PDM	91
4.3.2	Snow- and ice-melt modelling within Macro-PDM	92
4.4	Modifications required for the application of Macro-PDM in the Himalaya	96
4.4.2	Precipitation lapse rate	96
4.4.3	Seasonally adjusted temperature lapse rate.....	97
4.5	Development of a regional glacier melt model.....	98
4.5.1	Scope of the glacier melt model.....	98
4.5.2	Physical processes to be represented by the model	98
4.5.3	Data availability	102
4.5.4	Identifying a suitable candidate model	103
4.5.5	Defining the model glacier.....	103
4.5.6	Modelling the glacial melt-water contribution to cell runoff.....	110
4.5.7	Representation of glacier retreat	113
5	Application of the regional model	116
5.1	Introduction.....	116
5.2	Software modifications	116
5.3	Data Conditioning.....	118
5.3.1	Map Projection.....	118
5.3.2	Masking Grids.....	121
5.3.3	Climate driving data.....	121
5.4	Model application for the 1961-90 standard-period baseline	128
5.4.1	Temporal disaggregation of the climate driving data	128
5.4.2	Average annual- and winter-runoff estimates.....	129
5.4.3	Derivation of flow estimates.....	129
5.5	Model tuning and validation	132
5.6	Future climate representation.....	141
5.7	Comparison of predicted flows.....	147
 PART 3		
6	Results & Discussion	149
6.1	Introduction.....	149
6.2	Artificial Experiment: 50% reduction in glacier cover.....	153
6.3	Analysis of modelled future river flows in the Upper Indus (Focal Area A) ..	156
6.3.1	Gilgit at Gilgit	156
6.3.2	Indus at Besham Qila.....	160

6.3.3 All sites for the +0.06 °C/year, +0.15 °C/year and RCM-based scenarios	161
6.4 Analysis of modelled future river flows of the Ganges River (Focal Area B)	166
6.4.1 Ganges (Bhagirathi) at Uttarkashi	166
6.4.2 Ganges at Allahbad	168
6.4.3 All sites for the +0.06 °C/year, +0.15 °C/year and RCM-based scenarios	171
6.5 Analysis of modelled future river flows in the Kali Gandaki-Narayani River, Nepal (Focal Area C)	174
6.5.1 Modhi Khola at Kushma	174
6.5.2 Narayani at Bharatpur	179
6.5.3 All sites for the +0.06 °C/year, +0.15 °C/year and RCM-based scenarios	181
6.6 Analysis of modelled future river flows in the Brahmaputra (Focal Area D) .	184
6.6.1 Zangpo at Samsang	184
6.6.2 Brahmaputra at Tuting	186
6.6.3 All sites for the +0.06 °C/year, +0.15 °C/year and RCM-based scenarios	188
6.7 Discussion on model results.....	192
6.7.1 The East-West divide and the influence of the summer monsoon.....	192
6.7.2 Effects of the assumed distribution of glacial ice	193
6.7.3 Comparison with other studies	196
6.7.4 Plausibility of results.....	197
7 Conclusions and future research directions.....	199
7.1 Introduction.....	199
7.2 Meeting the aims and objectives of the study	199
7.3 Impacts of the study	201
7.4 Possible improvements to the approach and method.....	202
7.4.1 Data availability	202
7.4.2 Treatment of climate input variables	204
7.4.3 Possible improvements to the regional glacier-melt model.....	206
7.4.4 Improvements to model application.....	208
7.5 Future research directions	209
References.....	213
Appendix A: The Probability Distributed Moisture model (PDM)	
Appendix B: Publications associated with this study	

LIST OF FIGURES AND TABLES

Figures

Figure 2.1 The Himalayan region, showing the track of moisture-bearing weather systems

Figure 2.2 CMIP5-based time-series of temperature and precipitation anomalies for the Western Himalaya, Central Himalaya, Eastern Himalaya and Karakoram region from 1861 to 2099 relative to 1961-1990 for four RCP scenarios

Figure 3.1 Locations of rain gauge data that were available to the study

Figure 3.2 Average Winter (October – March) Rainfall (AWR (mm), dark grey) and Average Summer (April – September) Rainfall (ASR (mm), light grey) for 12 selected rain gauges

Figure 3.3 Average Winter (October – March) Rainfall (AWR (mm), dark grey) and Average Summer (April – September) Rainfall (ASR (mm), light grey) for 12 selected rain gauges

Figure 3.4 Contrasting rainfall regimes for six selected sites, three in the “west” (Kabul, Peshawar and Srinagar) and three in the “east” (Mandi, Pokhara and Darjeeling)

Figure 3.5 Locations of 244 Nepalese rain gauges whose data were available to the study, mapped onto a the Hydro1k DEM and showing the DCW glaciers

Figure 3.6 Box and whisker plot of average monthly rainfall for 244 Nepalese rain gauges

Figure 3.7 Year-to-year variation in the annual rainfall total (mm) at Darjeeling (India) for the 111-year period, 1868 – 1978

Figure 3.8 Year-to-year variation in the annual rainfall total (mm) at Peshawar (Pakistan) for the 138 year-period, 1863 – 2000

Figure 3.9 Year-to-year variation in the annual rainfall total (mm) at Pokhara (Nepal) for the 26-year period 1970 – 1995;

Figure 3.10 Year-to-year variation in Annual Average Rainfall (mm) for 63 Nepalese rain gauges having data from 1970-95

Figure 3.11 Location of temperature gauges whose data were obtained for the study

Figure 3.12 Number of temperature gauges having data in a given year (e.g. by 1990, temperature was being recorded at 100 gauges)

Figure 3.13 Mean monthly temperature, maximum monthly temperature and minimum monthly temperature in Nepal for the period 1961-96 (all stations, n = 119)

Figure 3.14 Time-series of derived monthly lapse rates in Nepal, from January 1961 to December 1996

Figure 3.15 Average, maximum and minimum monthly temperature lapse rates (LR) in Nepal for the period 1961-96, derived from 119 temperature gauges nationally

Figure 3.16 Annual average temperatures for all 119 stations of the Nepal national network (elevation range of between 72 m and 4100 m ASL) for the period 1961-96

Figure 3.17 Average annual temperatures for the 15 highest elevation temperature gauges in Nepal, 1967-96 (all 15 stations having elevation > 1800 m ASL)

Figure 3.18 Average annual temperatures at Peshawar, 1931-2000, at an elevation of 359 m ASL

Figure 3.19 Locations of river gauging stations whose data were available to the study

Figure 3.20 Mean monthly runoff, expressed as a percentage of the average annual runoff depth (AARD), for the selected catchments in Pakistan (light grey) and Nepal (dark grey)

Figure 3.21 Coefficient of Variation of Annual Runoff (ARCV) versus the percentage of glacier area (% ice) for the selected glacier-fed catchments in Pakistan (solid circles) and Nepal (hollow circles)

Figure 3.22 The four catchments whose data show statistically significant trends at the 5% significance level according to the Mann-Kendall trend test: (a) the Hunza at Dainyor; (b) the Asotre at Doyian(c) the Shigar at Shigar; and (d) the Bhote Kosi at Barabise

Figure 4.1 Geographical extent of the study: the Indus, Ganges and Brahmaputra river basins

Figure 4.2 Some of the natural features to be represented in the regional model

Figure 4.3 A schematic of the macro-scale hydrological model, Macro-PDM, showing the various inputs to, and outputs from, the model and its key modules

Figure 4.4 Physical features of a glacier to be represented in the glacier-melt model

Figure 4.5 Determining the area of the generic model glacier

Figure 4.6 Area distribution diagram for the generic glacier, resembling the hypsometry of a typical alpine glacier in the Swiss Alps

Figure 4.7 A side elevation view of a model glacier

Figure 4.8 Schematic of snow- and ice-stores in an ice-band of the glacier-melt model

Figure 5.1 Available rain gauges mapped onto the CRU standard-period 1961-90 0.5° x 0.5 ° Average Annual Rainfall (AAR) grid for the Ganges basin

Figure 5.2 Spatial distribution of the bias in Average Annual Rainfall data: CRU gridded data versus DHM observed rain gauge data

Figure 5.3 Modelled standard-period Average Annual Runoff Depth (AARD) at 20 km resolution for the (a) Indus, (b) Brahmaputra and (c) Ganges basins

Figure 5.4 An illustration of the drainage network derived from applying the Hydro1k flow direction grid

Figure 5.5 Location of stations used for model tuning and validation of the model in the Indus and Ganges river basins

Figure 5.6 Comparison between model estimates and observations for glacier-fed (ice) and glacier-free (no-ice) catchments in the upper Indus and Ganges basins: (a) average annual runoff; (b) average winter (October-March) runoff

Figure 5.7 Comparison of results for alternative model runs in glacier-fed catchments of both basins

Figure 5.8 Absolute change (°C) in average annual temperature (T) between HadRM2 perturbed and control climate for the period 2041- 2060 in the Ganges River basin

Figure 5.9 Relative change (%) in average annual precipitation (P) between HadRM2 perturbed and control climate for the period 2041- 2060 in the Ganges River basin

Figure 5.10 Adaptation of the “Delta Change” method that allows a gradual progression of climate input variables between the “present” (1990) and “future”(2050)

Figure 5.11 Relative changes (%) in mean flows of the Indus River by decade 10, for the +0.1 °C/year incremental temperature scenario

Figure 6.1 Location of the four focal areas: (A) Upper Indus; (B) Ganges; (C) Kali Gandaki-Narayani River System, Nepal; and (D) Brahmaputra

Figure 6.2 Changes in mean flows, relative to the 1961-90 baseline, across the drainage network of the Indus basin for a 50% reduction in glacier cover

Figure 6.3 Changes in mean flows, relative to the 1961-90 baseline, in the headwaters of the Ganges in Nepal for a 50% reduction in glacier cover

Figure 6.4 Location of the 6 focal area study sites in Upper Indus

Figure 6.5 Changes in Decadal Mean Flows, relative to baseline, of the Gilgit at Gilgit for the four incremental temperature scenarios (+0.03, +0.06, +0.1 and +0.15 °C/year) over a 100-year period

Figure 6.6 Changes in Decadal Mean Flows, relative to baseline, of the Gilgit at Gilgit for two combined incremental precipitation (P) and temperature scenarios (+0.2%P with +0.06 °C/year, -0.2%P with +0.06 °C/year, with the +0.06 °C/year temperature scenario as reference) over a 100-year period

Figure 6.7 Changes in Decadal Mean Flows, relative to baseline, of the Indus at Besham Qila for the four incremental temperature scenarios (+0.03, +0.06, +0.1 and +0.15 °C/year) over a 100-year period

Figure 6.8 Changes in Decadal Mean Flows, relative to baseline, of the Indus at Besham Qila for two combined incremental precipitation (P) and temperature scenarios (+0.2%P with +0.156 °C/year, -0.2%P with +0.15 °C/year, with the +0.15 °C/year temperature scenario as reference) over a 100-year period

Figure 6.9 Changes in Decadal Winter Mean Flows, relative to baseline, of the Indus at Besham Qila for the four incremental temperature scenarios (+0.03, +0.06, +0.1 and +0.15 °C/year) over a 100-year period

Figure 6.10 Changes in Decadal Mean Flows, relative to baseline, of the Indus and its tributaries at all six study sites for the +0.06 °C/year incremental temperature scenario over a 100-year period

Figure 6.11 Changes in Decadal Mean Flows, relative to baseline, of the Indus and its tributaries at all six study sites for the +0.15 °C/year incremental temperature scenario over a 100-year period

Figure 6.12 Changes in Decadal Mean Flows, relative to baseline, of the Indus and its tributaries at all six study sites, for the HadRM2-based scenario over a 60-year period

Figure 6.13 Location of the 4 focal area study sites in the Ganges

Figure 6.14 Changes in Decadal Mean Flows, relative to baseline, of the Ganges at Uttarkashi for the four incremental temperature scenarios (+0.03, +0.06, +0.1 and +0.15 °C/year) over a 100-year period

Figure 6.15 Changes in Decadal Mean Flows, relative to baseline, of the Ganges at Uttarkashi for two combined incremental precipitation (P) and temperature scenarios (+0.2% P with +0.06 °C/year, -0.2% P with +0.06 °C/year, with the +0.06 °C/year temperature scenario as reference) over a 100-year period

Figure 6.16 Changes in Decadal Mean Flows, relative to baseline, of the Ganges at Allahabad for the four incremental temperature scenarios (+0.03, +0.06, +0.1 and +0.15 °C/year) over a 100-year period

Figure 6.17 Changes in Decadal Mean Flows, relative to baseline, of the Ganges at Allahabad for two combined incremental precipitation (P) and temperature scenarios (+0.2% P with +0.06 °C/year, -0.2% P with +0.06 °C/year, with the +0.06 °C/year temperature scenario as reference) over a 100-year period

Figure 6.18 Changes in Decadal Mean Flows, relative to baseline, of the Ganges at all four study sites for the +0.06 °C/year incremental temperature scenario over a 100-year period

Figure 6.19 Changes in Decadal Mean Flows, relative to baseline, of the Ganges at all four study sites for the +0.15 °C/year incremental temperature scenario over a 100-year period

Figure 6.20 Changes in Decadal Mean Flows, relative to baseline, of the Ganges at all four study sites for the HadRM2-based climate change scenario over a 60-year period

Figure 6.21 Location of the 4 study sites in Kali Gandaki-Narayani river system (headwaters of the Ganges) in Nepal

Figure 6.22 Changes in Decadal Mean Flows, relative to baseline, of the Modhi Khola at Kushma for the four incremental temperature scenarios (+0.03, +0.06, +0.1 and +0.15 °C/year) over a 100-year period

Figure 6.23 Changes in Decadal Mean Flows, relative to baseline, of the Modhi Khola at Kushma for two combined incremental precipitation (P) and temperature scenarios (+0.2%P with +0.15 °C/year, -0.2%P with +0.15 °C/year, with the +0.15 °C/year temperature scenario as reference) over a 100-year period

Figure 6.24 Changes in Decadal Mean Flows, relative to baseline, of the Narayani at Bharatpur for the four incremental temperature scenarios (+0.03, +0.06, +0.1 and +0.15 °C/year) over a 100-year period

Figure 6.25 Changes in Decadal Mean Flows, relative to baseline, of the Narayani at Bharatpur for two combined incremental precipitation (P) and temperature scenarios (+0.2%P with +0.06 °C/year, -0.2%P with +0.06 °C/year, with the +0.06 °C/year temperature scenario as reference) over a 100-year period

Figure 6.26 Changes in Decadal Mean Flows, relative to baseline, of the Kali Gandaki-Narayani river system at all four study sites for the +0.06 °C/year incremental temperature scenario over a 100-year period

Figure 6.27 Changes in Decadal Mean Flows, relative to baseline, of the Kali Gandaki-Narayani river system at all four study sites for the +0.06 °C/year incremental temperature scenario over a 100-year period

Figure 6.28 Changes in Decadal Mean Flows, relative to baseline, of the Kali Gandaki-Narayani river system at all four study sites for the HadRM2-based climate change scenario over a 60-year period

Figure 6.29 Location of the 4 study sites in the Brahmaputra focal-area

Figure 6.30 Changes in Decadal Mean Flows, relative to baseline, of the Zangpo at Samsang for the four incremental temperature scenarios (+0.03, +0.06, +0.1 and +0.15 °C/year) over a 100-year period

Figure 6.31 Changes in Decadal Mean Flows, relative to baseline, of the Zangpo at Samsang for two combined incremental precipitation (P) and temperature scenarios (+0.2%P with +0.15 °C/year, -0.2%P with +0.15 °C/year, with the +0.15 °C/year temperature scenario as reference) over a 100-year period

Figure 6.32 Changes in Decadal Mean Flows, relative to baseline, of the Brahmaputra at Tuting for the four incremental temperature scenarios (+0.03, +0.06, +0.1 and +0.15 °C/year) over a 100-year period

Figure 6.33 Changes in Decadal Mean Flows, relative to baseline, of the Brahmaputra at Tuting for two combined incremental precipitation (P) and temperature scenarios (+0.2%P with +0.15 °C/year, -0.2%P with +0.15 °C/year, with the +0.15 °C/year temperature scenario as reference) over a 100-year period

Figure 6.34 Changes in Decadal Mean Flows, relative to baseline, of the Brahmaputra and tributaries at all four study sites for the +0.06 °C/year incremental temperature scenario over a 100-year period

Figure 6.35 Changes in Decadal Mean Flows, relative to baseline, of the Brahmaputra and tributaries at all four study sites for the +0.15 °C/year incremental temperature scenario over a 100-year period

Figure 6.36 Changes in Decadal Mean Flows, relative to baseline, of the Brahmaputra at all four study sites for the HadRM2-based climate change scenario over a 100-year period

Figure 6.37 The importance of model glacier vertical extents on results

Tables

Table 2.1 Summary of mean flow predictions from climate impact modelling studies in the Himalayan region where glaciers have been explicitly considered

Table 3.1 Summary of hydrometeorological time-series data available to the study

Table 3.2 Summary of the twelve representative rain gauges selected for analysis

Table 3.3 Correlation analysis of average monthly (J-D), summer (SM, A-S), winter (WN, O-M) and annual (AN) rainfall data against latitude (LT), longitude (LN), and height of station (HT), for the 12 selected rain gauges

Table 3.4 Correlation analysis of average monthly (J-D), summer (SM), winter (WN) and annual (AN) rainfall data against latitude (LT), longitude (LN), and height of station (HT), for Nepal rain gauges (n = 244)

Table 3.5 Correlation analysis of monthly (J-D), summer (SM), winter (WN) and annual (AN) average temperatures at Nepalese gauges against latitude (LT), longitude (LN), and height of station (HT) (n = 119)

Table 3.6 Summary of the selected glacier-fed catchments in Nepal and Pakistan, arranged in order of descending percentage glacier cover (% ice) in each country

Table 3.7 Derived average annual and monthly runoff statistics for the 17 selected glacier-fed catchments in Pakistan and Nepal

Table 3.8 Trend-line (regression) statistics for plots of Annual Mean Flows, expressed as a percentage of the period-of-record Mean Flow (%MF), versus time (years), for the 17 selected glacier-fed catchments

Table 4.1 Key datasets readily available from international sources

Table 4.2 Model parameters and typical values they are assigned

Table 5.1 Bias results comparing, in terms of mean bias and the standard deviation (SD) of the bias, Average Annual Rainfall (AAR) and Average Winter Rainfall (AWR) derived from CRU gridded rainfall data with that observed at “CRU” rain gauges in the Indus, Ganges and Brahmaputra basins

Table 5.2 Bias results comparing, in terms of mean bias and the standard deviation (SD) of the bias, Average Annual Rainfall (AAR) and Average Winter Rainfall (AWR) derived from CRU gridded rainfall data with that observed at Nepalese rain gauges

Table 5.3 Summary of the 40 river gauging stations used for model tuning and validation

Table 5.4 Key model parameter values applied in each study basin

Table 5.5 Mean, minimum, maximum and standard deviation of bias errors between model estimates and observed Average Annual and Winter Runoff Depth (AARD and AWRD) for glacier-fed (ice) and glacier-free (no-ice) catchments in the upper Indus and Ganges basins

Table 5.6 Sensitivity-analysis increments, showing the annual incremental increases in temperature (T) and precipitation (P) and the basis of the “scenario”

Table 6.1 Selected study sites of the four focal areas, showing site name (river and location), catchment area (km²), percentage initial ice cover (% ice), annual mean flow (AMF, m³/s) and winter mean flow (WMF, m³/s) and average annual rainfall (AAR, mm) and average winter rainfall (AWR, mm)

DEDICATION

I dedicate this thesis to my mother and late father, to whom I owe everything. It saddens me deeply that he did not survive to see me finish this work. He would have been so very proud.

Mam, I chi mae hwn: diolch am bopeth!

ACKNOWLEDGEMENTS

I have benefitted from the support and encouragement of many good people over the course of this study. Above all, I am most grateful for the love, patience and understanding of my wife, Angela, and sons, Adam, Cain and Siôn, without which the study and thesis would never have been completed.

I am also hugely indebted to Prof. David N. Collins and Dr. Neil Entwistle, of the University of Salford, for their guidance, knowledge and perseverance. I thank also past Salford students, Dr. Oliver Macdonald and Nick Pelham, and administration staff, Catriona Nardone and Ashley Hopps, for their assistance.

Since embarking on this study, I have drawn on the expertise of many colleagues (past and present) at the Centre for Ecology & Hydrology. I would like to thank the following for their help: Prof. Mike Acreman, Prof. Mark Bailey, Dr. Lucy Ball, Dr. Vicky Bell, Dr. Eleanor Blyth, Dr. David Boorman, Emma Brown, Dr. Harry Dixon, Andrew Everett, Dr. Alan Gustard, Prof. Richard Harding, Matt Holmes, Dr. Chris Huntingford, Prof. Alan Jenkins, Dr. Virginie Keller, Linda Kinsella, Filip Kral, Prof. Rob Lamb, James Miller, Dr. Jeremy Meigh, Dr. Bob Moore, Dr. Heather Musgrave, David Pitson, Dr. Christel Prudhomme, Nick Reynard, Penny Sackett, Dr. Caroline Sullivan, Dr. Anita Weatherby, and Dr. Andy Young.

I am grateful also for the advice provided by many other experts, in the UK, Europe, and beyond. They include: (from the UK) Dr. Richard Jones (Met Office Hadley Centre), Drs. David Archer and Hayley Fowler (Newcastle University), Dr. Sunil Kansakar (Environment Agency), Drs. David Hannah and John Gerrard (Birmingham University), Dr. David Viner and David Lister (University of East Anglia), Martin Walshe (DFID); (from Europe) Prof. Siegfried Demuth (UNESCO), Prof. Georg Kaser (University of Innsbruck), Dr. Kerstin Stahl (University of Freiburg), Dr. Wolfgang Grabs (WMO), Dr. Sven Kotlarski (Max Planck Institute), Dr. Thomas Maurer (Federal Institute of Hydrology, Koblenz), Dr. Patrick Wagnon (IRD, Montpellier); (from North America) Andrew Barrett (NSIDC, Boulder, Colorado),

Prof. Regine Hock (University of Alaska), Prof. Jeff Kargel (University of Arizona), and Prof. Gordon Young (Wilfrid Laurier University, Canada).

The study was motivated by my love of the Himalaya, its breathtaking landscapes and wonderful people. I am especially grateful to my many friends in the region who made the study possible, namely: Adarsha Pokhrel (ex-Director General, Department of Hydrology and Meteorology, Kathmandu, Nepal), Prof. Suresh Chalise, Dr. Mats Eriksson, Dr. Arun B. Shrestha, Dr. Mandira Shrestha, Basantha Shrestha and Pradeep K. Mool, (ICIMOD, Kathmandu), Prof. Narendra Khanal and Dr. Shiba Rijal (Tribhuvan University, Kathmandu), Profs. Arun Kumar and Arun K. Saraf (IIT-Roorkee, India), Dr. Pratap Singh (National Institute of Hydrology, Roorkee), Dr. Rajesh Kumar and Prof. Syed Hasnain (Jawaharlal Nehru University, New Delhi), and Dr. Rajiv Kumar Chaturvedi, IISc-Bangalore.

The study initially was part-funded by the DFID KAR Project No. 7980, “Snow and Glacier Aspects of Water Resources Management in the Himalayas (SAGARMATHA)” (2002-2004). The majority of funding and support, however, was provided by the NERC Centre for Ecology & Hydrology. I very much thank CEH Director, Prof. Mark Bailey, and Deputy Director, Prof. Alan Jenkins, for their backing over the course of the study and for allowing me time off work to complete the thesis over the summer of 2014.

The following organisations are also gratefully acknowledged for data provided to the study: the Climate Research Unit (CRU) at the University of East Anglia, for baseline climatology data, the Land Processes Distributed Active Archive Center (LPDAAC) at the USGS EROS Data Center, for the HYDRO1k Elevation Derivative Database and Eurasia Land Cover Characteristics Database, the Land and Water Development Division of the FAO, Rome, for the Digital Soil Map of the World, the UK Met Office Hadley Centre, for the HadRM2 RCM data, ESRI Inc., USA, for the Digital Chart of the World, and the WMO Global Runoff Data Centre, Koblenz, Germany, for river flow data from gauging stations in study area.

DECLARATION

By submitting my work here I declare that:

- this work is my own
- the work of others used in its completion has been duly acknowledged
- experimental or other investigative results have not been falsified
- I have read and understood the University Policy on the Conduct of Assessed Work (Academic Misconduct Procedure)

ACRONYMS

AAR	Average Annual Rainfall
AARD	Average Annual Runoff Depth
AMF	Annual Mean Flow
AR4	IPCC Fourth Assessment Report
AR5	IPCC Fifth Assessment Report
ArcGIS	GIS software tool (by ESRI Inc)
ARCV	Coefficient of Variation of Annual Runoff
ASCII	American Standard Code for Information Interchange
ASL	Above sea level
ASR	Average Summer Rainfall
ASTER	Advanced Spacebourne Thermal Emission and Reflection Radiometer
ASTER GDEM	ASTER Global Digital Elevation Map
AWR	Average Winter Rainfall
AWRD	Average Winter Runoff Depth
CCLM	COSMO-CLM , the unified weather forecast and regional climate model of the Potsdam Institute for Climatological Research
CEH	Centre for Ecology & Hydrology
CGCM3	Third generation of the Canadian Centre for Climate Modelling and Analysis Coupled Global Climate Model
CMIP	Coupled Model Intercomparison Project
CMIP3	Third generation of CMIP GCMs
CMIP5	Fifth generation of CMIP GCMs
CO ₂	Carbon Dioxide
CRU	Climate Research Unit (of the University of East Anglia)
CSIRO	Commonwealth Scientific and Industrial Research Organisation (Australia)
CVF	Compaq Visual Fortran
DCW	Digital Chart of the World
DDF	Degree-day factor

DEM	Digital Elevation Model
DFID	Department for International Development
DHM	Department of Hydrology and Meteorology (of the Government of Nepal)
DMF	Decadal Mean Flow
DTM	Digital Terrain Model
DWMF	Decadal Winter Mean Flow
ECHAM5	Fifth version of the ECHAM GCM of the Max Planck Institute for Meteorology (EC (from ECMWF), HAM (from Hamburg))
ECMWF	European Centre for Medium-Range Weather Forecasts
ELA	Equilibrium Line Altitude
EROS	Earth Resources Observation and Science (of the USGS)
ESRI	Environmental Systems Research Institute (supplier of ArcGIS software)
EU	European Union
FAO	Food and Agriculture Organisation (of the United Nations)
FC	Field Capacity (of a soil: the amount of water held in the soil against gravity)
FRIEND	Flow Regimes from International Experimental and Network Data (project)
GBHM	Geomorphology Based Hydrological Model (macro-scale hydrological model)
GCM	General Circulation Model
GHCN	Global Historical Climatology Network
GIS	Geographical Information System
GLIMS	Global Land Ice Measurements from Space
GWAVA	Global Water Availability Assessment model (macro-scale hydrological model)
HadCM3	Hadley Centre Coupled Model, version 3
HadRM2	Hadley Centre Regional Climate Model, version 2
HadRM3	Hadley Centre Regional Climate Model, version 3
HEC	Hydrologic Engineering Center (hydrological model)

HKH	Hindu Kush – Himalaya
HKH-FRIEND	Hindu Kush – Himalayan FRIEND (project)
IAHS	International Association of Hydrological Sciences
ICESat	Ice, Cloud, and land Elevation Satellite
ICIMOD	International Centre for Integrated Mountain Development
IHACRES	Identification of unit Hydrograph and Component flows from Rainfall, Evaporation and Streamflow data
IHP	International Hydrology Programme (of UNESCO)
IIT	Indian Institute of Technology
IPCC	Intergovernmental Panel on Climate Change
IRD	Institut de Recherche pour le Développement (of France)
JNU	Jawaharlal Nehru University (New Delhi)
KAR	Knowledge and Research (programme of DFID)
LA	Lambert Azimuth (projection)
Landsat ETM+	Landsat Enhanced Thematic Mapping Plus (satellite instrument)
Landsat TM	Landsat Thematic Mapper
LPDAAC	Land Processes Distributed Active Archive Center (of the USGS EROS Data Center)
LSM	Land-surface model
MF	Mean Flow (period-of-record mean flow)
MHM	Macro-scale Hydrological Model
MODIS	Moderate Resolution Imaging Spectroradiometer (project)
NERC	Natural Environment Research Council (of the UK)
NOAA	National Oceanic and Atmospheric Administration (of the United States of America)
NSIDC	National Snow and Ice Data Center (of the United States)
ONC	Operational Navigation Chart (of United States Defense Mapping Agency)
PC	Personal Computer
PDM	Probability Distributed Moisture (model)
PE	Potential Evaporation
PRECIS	Providing REgional Climates for Impacts Studies

RCM	Regional Climate Model
RCP	Representative Concentration Pathways
REMO	RCM of the Max Planck Institute for Meteorology (derived from the Europa Modell (EM) numerical weather prediction model of the German Weather Service)
SCA	Snow Covered Area
SD	Standard Deviation
SHE	Système Hydrologique Européen (hydrological model)
smax	Soil saturation capacity
SPOT	Satellite Pour l'Observation de la Terre
SRES	Special Report Emission Scenarios
SRM	Snow Runoff Model
SRTM	Shuttle Radar Topography Mission
SWAT	Soil and Water Assessment Tool (hydrological model)
TRMM	Tropical Rainfall Measurement Mission
TSL	Transient Snow Line
UBB	Upper Brahmaputra Basin
UBC	University of British Columbia (hydrological model)
UEA	University of East Anglia
UGB	Upper Ganges Basin
UIB	Upper Indus Basin
UN	United Nations
UNESCO	United Nations Educational, Scientific and Cultural Organisation
USDMA	United States Defense Mapping Agency
USGS	United States Geological Survey
VIC	Variable Infiltration Capacity (macro-scale hydrological model)
w.e.	Water equivalent (of snow or ice)
WBM	Water Balance Model (macro-scale hydrological model)
WMF	Winter Mean Flow
WMO	World Meteorological Organisation (of the United Nations)
WWF	World Wide Fund for Nature

POTENTIAL IMPACTS OF CLIMATIC WARMING ON GLACIER-FED RIVER FLOWS IN THE HIMALAYA

ABSTRACT

The Himalayan region is one of the most highly glacierised areas on Earth. Regarded as the “water towers” of Asia, the Himalayas are the source of several of the world’s major rivers. The region is inhabited by some 140 million people and ten times as many (~1.4 billion) live in its downstream river basins. Freshwater from the mountains is vital for the region’s economy and for sustaining the livelihoods of a fast-growing population. Climatic warming and the rapid retreat of Himalayan glaciers over recent decades have raised concerns about the future reliability of mountain melt-water resources, leading to warnings of catastrophic water shortages. Several previous studies have assessed climate change impacts on specific glacier-fed rivers, usually applying meso-scale catchment models for short simulation periods during which glacier dimensions remain unchanged. Few studies have attempted to estimate the effects on a regional scale, partly because of the paucity of good quality data across the Himalaya. The aim of this study was to develop a parsimonious grid-based macro-scale hydrological model for the Indus, Ganges and Brahmaputra basins that, in order to represent transient melt-water contributions from retreating glaciers, innovatively allowed glacier dimensions to change over time. The model initially was validated over the 1961-90 standard period and then applied in each basin with a range of climate-change scenarios (sensitivity analysis- and climate-model-based) over a 100-year period, to gain insight on potential changes in mean annual and winter flows (water availability proxies) at decadal time-steps. Plausible results were obtained, showing impacts vary considerably across the region (catchments in the east appear much less susceptible to glacier retreat effects than those in the west, due to the influence of the summer monsoon), and, in central and eastern Himalayan catchments, from upstream to downstream (effects diminish rapidly downstream due to higher runoff from non-glaciated parts).

PART 1

1 Introduction

1.1 Background of the study

Mountain glaciers generally have been retreating, almost synchronously with climatic warming, since the end of the Little Ice Age in the mid-19th century (Grove, 1988). Glacier retreat initially was rapid during the first half of the 20th century but then slowed, and even reversed in some humid areas, from about 1950 to 1980 (Haeberli, 1996), in response to cooling of the Earth's atmosphere (Oerlemans, 2005). Further global warming from the late 1970s, however, has resulted in glaciers losing mass at unprecedented rates over recent decades (Dyurgerov and Meier, 2000; Haeberli and Hoelzle, 2001). The general loss of mass from the world's glaciers since the Little Ice Age coincides with observed increases in the global mean surface temperature, of $0.07\text{ }^{\circ}\text{C} \pm 0.02\text{ }^{\circ}\text{C}$ per decade, over the last hundred years, whilst recent rapid, retreat corresponds with accelerated increases, of $0.18\text{ }^{\circ}\text{C} \pm 0.05\text{ }^{\circ}\text{C}$ per decade, between 1979 and 2005 (Trenberth *et al.*, 2007). According to the latest IPCC (CMIP5) model simulations, global mean surface temperatures for 2081–2100, relative to 1986–2005, are likely to increase by between $0.3\text{ }^{\circ}\text{C}$ to $4.8\text{ }^{\circ}\text{C}$ (IPCC, 2013a, 2013b). It has been suggested that continued warming may cause “deglaciation of large parts of mountain regions in coming decades” (Zemp and Haberli, 2007).

Recent glacier retreat has led to warnings of severe water shortages in many parts of the world (Kundzewicz *et al.*, 2007; Stern, 2007). Glaciers essentially are natural freshwater reservoirs. During periods of climatic warming and glacier retreat, melting of the ice adds a component to the flow from glacierised basins in excess of that related to contemporary precipitation: a “discharge dividend” (Collins, 2008) or “excess discharge” (Lambrecht and Mayer, 2009), from the de-stocking of glaciers, that has augmented glacier-fed river flows since the glacial maximum of the Little Ice Age (Macdonald, 2004). This additional flow component cannot be sustained indefinitely because, should climatic warming continue, glaciers one day will cease to exist. Initially, though, this valuable component of flow might be expected to increase, as melting is enhanced, but eventually it will reduce, as glacier extents decline, and ultimately diminish completely, as glaciers disappear (Barnett *et al.*,

2005; Stahl and Moore, 2006), leaving flows thereafter to be derived exclusively from present-day precipitation (Collins, 2008). However, the timing and volume of these changes (if indeed such changes have yet to occur), and how they might vary spatially, to affect water resources availability in different regions, largely remains uncertain.

The Himalayan region is considered particularly vulnerable to the impacts of deglaciation (Barnett *et al.*, 2005; Zemp and Haberli, 2007). The most glacierized area outside of the polar regions (Dyurgerov, 2005), with glaciers occupying an estimated 61,000 km² (Bajracharya and Shrestha, 2011), the Himalayas are the source of several major rivers, including the Indus, Ganges, Brahmaputra, Mekong, and Yangtze (Singh *et al.*, 2006b). As such, the mountains are often referred to as the “water towers of Asia” (e.g. UNEP, 2007; Immerzeel *et al.*, 2010). An estimated 140 million people inhabit the mountainous Himalayan region itself (Papola, 2002) and almost ten times as many (~1.4 billion \equiv 20% of the global population) live downstream within its river basins (Immerzeel *et al.*, 2010; Xu *et al.*, 2007), a significant proportion of whom are impoverished (Ravallion *et al.*, 2007) and possess little capacity to adapt to environmental change (DFID, 2006).

Himalayan glaciers generally followed global glacier fluctuations for much of the 20th century (Bolch *et al.*, 2012; Mayekwski and Jeschke, 1979; Zemp *et al.*, 2008). Many studies have reported significant retreat of the region’s glaciers since the early 1970s (e.g. Kadota *et al.*, 1997; 2000; Naithani *et al.*, 2001; Fujita *et al.*, 2001; Ageta *et al.*, 2001; Ageta *et al.*, 2003; Berthier *et al.*, 2007; Kulkarni *et al.*, 2007; Raina, 2009; Scherler *et al.*, 2011; Käab *et al.*, 2012). In 1999, the Working Group on Himalayan Glaciology of the International Commission for Snow and Ice (ICSI) claimed “glaciers in the Himalayas are receding faster than in any other part of the world and, if the present rate continues, the likelihood of them disappearing by the year 2035 is very high” (Hasnain, 1999). This claim, which was re-asserted in several publications (e.g. Pearce, 1999; Samuel, 2001; WWF, 2003, 2005), including the IPCC Fourth Assessment (Cruz *et al.*, 2007), was shown to be wrong by Cogley *et al.* (2010) and Schiermeier (2010), the former pointing-out that “Himalayan rates of recession are not exceptional” and for Himalayan glaciers to disappear by 2035 “requires a 25-fold greater loss rate from 1999 to 2035 than that estimated for 1960 to 1990”. Despite

this, serious concerns remain over the potential impacts continued climatic warming and retreating glaciers will have on the economic growth of South Asia generally (Schiermeier, 2010; Zemp and Haberli, 2007), on water availability and food security (Immerzeel *et al.*, 2010; Moors and Siderius, 2012), and on the lives and livelihoods of the growing downstream population (Singh *et al.*, 2011). Improved understanding of the potential impacts of climatic warming on glacier-fed river flows across the Himalaya is vital to enable the region's decision- and policy-makers to develop appropriate adaptation strategies (Sullivan *et al.*, 2004).

Climate varies markedly within the region from aridity in the west to extreme humid conditions in the monsoonal east, and from sub-tropical on the southern Gangetic plain to arctic in the high mountains (Alford, 1992). Consequently, the effects of glacier retreat on river flows, and water resources, are unlikely to be uniform (Bolch *et al.*, 2012). Studies to determine the impact of future climatic warming on glacier-fed river flows typically require application of physically-based models to represent the various hydro-glaciological processes controlling catchment response (Beven, 2012). Such studies, however, are hampered in the Himalaya because hydrometeorological data are sparse, unrepresentative and of inferior quality due to difficult, or inaccessible, terrain, and the heterogeneity of mountain catchments (Collins *et al.*, 2013; Shankar, 1990). Many have attempted to assess the climate change impacts on Himalayan river flows (e.g. Akhtar *et al.*, 2008; Nepal *et al.*, 2013; Singh *et al.*, 2006a; Singh and Bengtsson, 2005; Singh and Jain, 2003), usually applying meso-scale ($\sim 10^1 - 10^3 \text{ km}^2$, Uhlenbrook *et al.*, 2004) catchment models for short simulation periods during which glacier dimensions (if at all considered) remain unchanged. Climatic warming is, however, progressive and glacier dimensions continually change: a model's inability to represent transitory conditions invalidates their application over longer timescales (Nepal *et al.*, 2013). Few studies have attempted to estimate the effects on a regional, macro- ($>10^4 \text{ km}^2$), scale, partly because of the paucity of good quality data across the Himalaya (exceptions include Raje *et al.*, 2013; Yang and Musiak, 2003) and fewer still account for transient-melt-water contributions from retreating glaciers (e.g. Immerzeel *et al.*, 2010; Lutz *et al.*, 2014).

1.2 Objectives of the study

The aim of this study was to develop a novel parsimonious grid-based macro-scale hydrological model (MHM) for the Indus, Ganges and Brahmaputra basins that, in order to represent transient melt-water contributions from retreating glaciers, innovatively allowed glacier dimensions to change over time. The model was to be used to assess how future climate change, as represented by a variety of sensitivity analysis- and climate-model-based scenarios, might affect future Himalayan river flows. The study focussed primarily on possible long-term changes in the mean annual and seasonal (winter half-year) flow along the Indus, Ganges and Brahmaputra rivers and their glacier-fed tributaries: such flow statistics generally being considered good indicators, or proxies, of potential water resources availability (cf. Oki and Kanae, 2006; Vörösmarty *et al.*, 2000). The three rivers basins cover a significant proportion of the whole Himalayan region. Arguably they are the most important basins on the Indian sub-continent, inhabited by over 700 million people and having a combined total area of $2.8 \times 10^6 \text{ km}^2$ (Xu *et al.*, 2007) that encompasses the mountainous countries of Nepal and Bhutan and large parts of northern India, south west China, Bangladesh, Afghanistan and Pakistan. The study's objectives were specifically stated as:

- 1) To develop a new method of representing mountain glaciers in MHMs that is capable of accounting for the varying melt-water contributions from many retreating glaciers in a large river basin, or region;
- 2) To incorporate the method into an MHM, with the resulting, combined, hydro-glaciological model tested in the region against observed river flow data;
- 3) To apply the new model with a range of different climate-change scenarios, with view to assessing how ensuing glacier-retreat might affect spatial and temporal variations in mean annual and winter flows of the Indus, Ganges and Brahmaputra rivers, and their tributaries, several decades into the future.

Some non-goals were also established from the outset. The study deliberately did not seek to predict changes to: runoff-generating processes (e.g. evapotranspiration) in glacier-free parts of catchments; the shape and magnitude of river flow regimes; the frequency and extent of extreme hydrological events (i.e. floods or drought); nor the occurrence and risk of natural hazards (e.g. glacial lake outburst floods, landslides, avalanches).

1.3 Approach and outline of the thesis

This thesis describes the development and application of the new macro-scale hydrological model and its key component, a regional glacier melt model. The thesis is the outcome of a part-time study that began in 2002 but was delayed, and then suspended from 2008 - 2014, due to family and work commitments. Despite the bulk of the research being conducted over the initial 6-year period (2002-2008), the outcomes of the study are still highly relevant and, thus, are presented very much in respect of contemporary scientific knowledge and understanding.

The thesis is presented in seven chapters, and in three parts. Part 1, which comprises Chapters 1-3, generally sets-out the background and context of the study. Following this introductory chapter (Chapter 1), Chapter 2 provides information on characteristics of the study area and outlines current understanding of global and Himalayan glacier fluctuations, of historic and projected climatic change in the region, and of previous hydrological modelling studies pertinent to this study. Chapter 3 describes the hydrometeorological data that were obtained for the study and presents the results of some cursory analyses that were undertaken with view to informing the design of the new model. Part 2 details the development (Chapter 4) of the macro-scale hydrological model, its new regional glacier-melt component in particular, and (in Chapter 5) describes the software implementation of the model and its application, first, over a standard-period baseline and, then, with a range of climate change scenarios. Part 3 presents, interprets and discusses the model results (Chapter 6) and, in conclusion (Chapter 7), assesses the impact of the study and explores areas for further research and development.

2 Current Understanding

2.1 Introduction

Himalayan glaciers have been the focus of much scientific research for the last 40 years. The research effort arguably was most intense in the 1980s and early 1990s, when several major collaborative programmes were initiated, such as the Nepal-Japan cooperation in glacier and climate research (Higuchi, 1993), the Pakistan-Canada Snow and Ice Hydrology Project (Hewitt and Young, 1993), and the Nepal-Germany collaboration, to establish a hydrometeorological monitoring network at high elevation in 6 glacierised catchments (Grabs and Pokhrel, 1993). A large number of publications resulted from the monitoring and research conducted during this period (cf. Young and Neupane, 1996). Despite political tensions between, and within, countries in the region, efforts to promote regional collaboration and cooperation in hydrological and glaciological research persisted throughout the 1990s and into the 2000s. The UNESCO-IHP HKH-FRIEND project, established in 1996 (Chalise and Khanal, 1996), did much to advance regional collaboration over this period and supported a variety of hydrological and glaciological research projects and capacity building activities (e.g. Kansakar *et al.*, 2004; Kaser *et al.*, 2003; Konz *et al.*, 2006; Rees *et al.*, 2002).

Speculation regarding the potential catastrophic consequences of deglaciation (e.g. Pearce, 1999; Samuel, 2001; Gore, 2006) that followed erroneous claims over the state and fate of Himalayan glaciers (Hasnain, 1999 in Cogley *et al.*, 2010) focussed much of the world's scientific attention onto the Himalayan region and prompted many new multilateral- and bilateral-funded programmes, projects and initiatives post-2000, such as the EU's WATCH (Harding *et al.*, 2011) and HighNoon (Moors and Siderius, 2012) projects, the DFID "Snow and Glacier Aspects of Water Resources Management in the Himalaya" (SAGARMATHA) project (Rees *et al.*, 2004b), IRD's (Institut de Recherche pour le Développement) campaign of mass balance monitoring on the Chhota Shigri glacier in India, (Wagnon, *pers. comm.*, 2005), the "Himalayan Climate Change Adaptation Programme" (HICAP) of the Norwegian and Swedish governments, and the World Bank's "Glacier Retreat in Nepal" study (Alford and Armstrong, 2010), to name but a few.

This chapter aims to distil, from the plethora of resulting research outputs, the current knowledge and understanding pertinent to this study. Its sources include books, scientific peer-reviewed papers from journals, dissertations, contract reports and websites. Major book sources included the Red Book series of the International Association of Hydrological Sciences (IAHS) and technical reports of the Kathmandu-based International Centre for Integrated Mountain Development (ICIMOD). The major scientific journal sources included: *Annals of Glaciology*; *Cryosphere*; *Current Science*; *Hydrology and Earth System Sciences*; *Hydrological Processes*; *Journal of Glaciology*; *Journal of Hydrology*; *Mountain Research and Development*; *Nature*; and *Science*.

Based on the available literature, the chapter first describes the general physiographical, hydrological and socio-economic characteristics of the Himalayan region (§2.2), summarises current knowledge on the fluctuation of Himalayan glaciers (§2.3), and outlines climatological and hydrological changes that have been observed and projected by climate change models (§2.4). It then describes modelling approaches for estimating future water resources availability, first at the catchment- (or meso-) scale (§2.5) and then at a regional, or macro-, scale (§2.6).

2.2 Characteristics of the Himalayan region

2.2.1 Physical and geomorphological characteristics

The Himalayan region extends across the north of the Indian sub-continent in a broad 3500 km arc, from Afghanistan, in the north-west, to Myanmar, in the south-east (70 - 105 °E, 40 - 25 °N). Covering an area of some 4×10^6 km², the region includes the Hindu Kush, Karakoram and Greater Himalaya mountain ranges (Figure 2.1). It is a region characterised by extremes of elevation, slope and climate. Elevation can vary dramatically over relatively short horizontal distances, from about 50 m in the Indo-Gangetic plain to over 8000 m within a distance of only some 160 km (Chalise and Khanal, 1996; Khanal *et al.*, 1998). It has been estimated that the mean snow-covered-area of the region is approximately 18.2% of the total surface area (Gurung *et al.*, 2011) and that there are over 54,000 glaciers in the region, occupying an area over 61,000 km² and displacing a volume of about 6,000 km³ (Bajracharya and Shrestha, 2011). The Himalaya, thus, is the largest natural freshwater reservoir in the world, and

its melt-waters are a significant component of flow of several major rivers, including the Indus, Ganges, Brahmaputra, Mekong, Yangtze, and Yellow rivers (Barnett *et al.*, 2005; Collins, 1996; Singh *et al.*, 2006).

The Himalaya were formed by uplift of the Earth's crust, as the northwardly moving Indo-Australian tectonic plate collided with the Eurasian some 40 - 50 million years ago (Molnar, 1986). The mountain building process (orogeny), at the boundary of the two plates, continues to this day, making the Himalaya one of the most geologically active, and fragile, regions on Earth, prone to frequent earthquakes, landslides, avalanches and glacial lake outburst floods.

Rising from the plains of the Indian sub-continent, the Himalayan region comprises a series of successively higher mountain ranges, from the Siwalik Hills (or Outer Himalaya), at elevations of 900 - 1500 m, to the Middle Mountains (Lesser Himalaya) that rise to about 2500 m, and the High (or Greater) Himalaya (4000 - 8848 m ASL) (Khanal *et al.*, 1998; Valdiya, 2002). The region encompasses the Karakoram and Hindu Kush ranges and many other sub-ranges, all of which form part of the same extended area of uplift. Beyond the Greater Himalaya, to the north, lies the Tibetan Plateau, at an average elevation of some 4500 m.

Some 8 million years ago, the mountains attained sufficient height to disrupt atmospheric circulation and bring about conditions that, to this present day, induce the South Asian summer monsoon (Molnar, 1993). The high mountains effectively form a barrier to cold northerly air masses from Asia, increasing temperature over the Indian sub-continent. Westerly winds are split northwards and southwards (Benn and Owen, 1998), diverting high-pressure centres to the north (Trenberth and Chen, 1988) and inducing areas of low pressure over northern India in summer that draw-in moisture-laden winds from the south. The Tibetan Plateau further provides a localised high-elevation heat-source in summer, creating a pressure gradient that strengthens air flow from the Bay of Bengal and increases precipitation in eastern Himalaya (Benn and Owen, 1998).

Tectonic activity, climatic change and local effects, such as landslides and glacial advances, have largely defined the Himalayan river drainage system (Brookfield,

1998). Himalayan rivers generally display a rectilinear pattern (Ives and Messerli, 1989) formed by low-gradient latitudinal (east-west/west-east) trending rivers, developed along the forelands of mountain ranges, that are intersected by steeper longitudinal (north-south) rivers running perpendicular to the mountains (Brookfield, 1998; Seeber and Gornitz, 1983). The longitudinal rivers (e.g. Kosi, Gandaki, Karnali) originate in Tibet and drain south through the Greater Himalaya in deep gorges. They are thought to have existed before the mountain building process began (Ives and Messerli, 1989; Sharma, 1977) having maintained a southerly course as river-bed erosion (incision) maintained equilibrium with tectonic uplift (Burbank *et al.*, 1996).

2.2.2 Hydrological characteristics of the region

The extreme relief of the Himalaya results in a complex mosaic of “topo-climates”, which range from sub-tropical in the southern plains, to temperate in the Middle Mountains and arctic high up in the Greater Himalaya (Alford, 1992; Alford and Armstrong, 2010). The main controls on the region’s climate, however, are weather systems that bring moist air from the Bay of Bengal during summer (the South Asian summer monsoon) and from the west in winter (Archer and Fowler, 2004; Bookhagen and Burbank, 2010). The mountains block the northward advancement of the monsoon, causing it to divert to the west. The monsoon normally starts in June and lasts until September. Onset of the monsoon, however, is delayed, and precipitation decreases, along the Himalayan arc from south-east to north-west. The Karakoram and Hindu Kush mountain ranges are usually much less affected by the monsoon than the Himalayan ranges to the east and receive much of their annual precipitation from westerly weather systems that bring moisture from the Mediterranean and Caspian Sea regions in winter (Archer and Fowler, 2004) (see Figure 2.1). Precipitation typically decreases from south to north, with each mountain range featuring windward maxima and leeward rain-shadows that culminates in the high altitude aridity of the Tibetan Plateau (Alford, 1992; Burbank *et al.*, 2003).

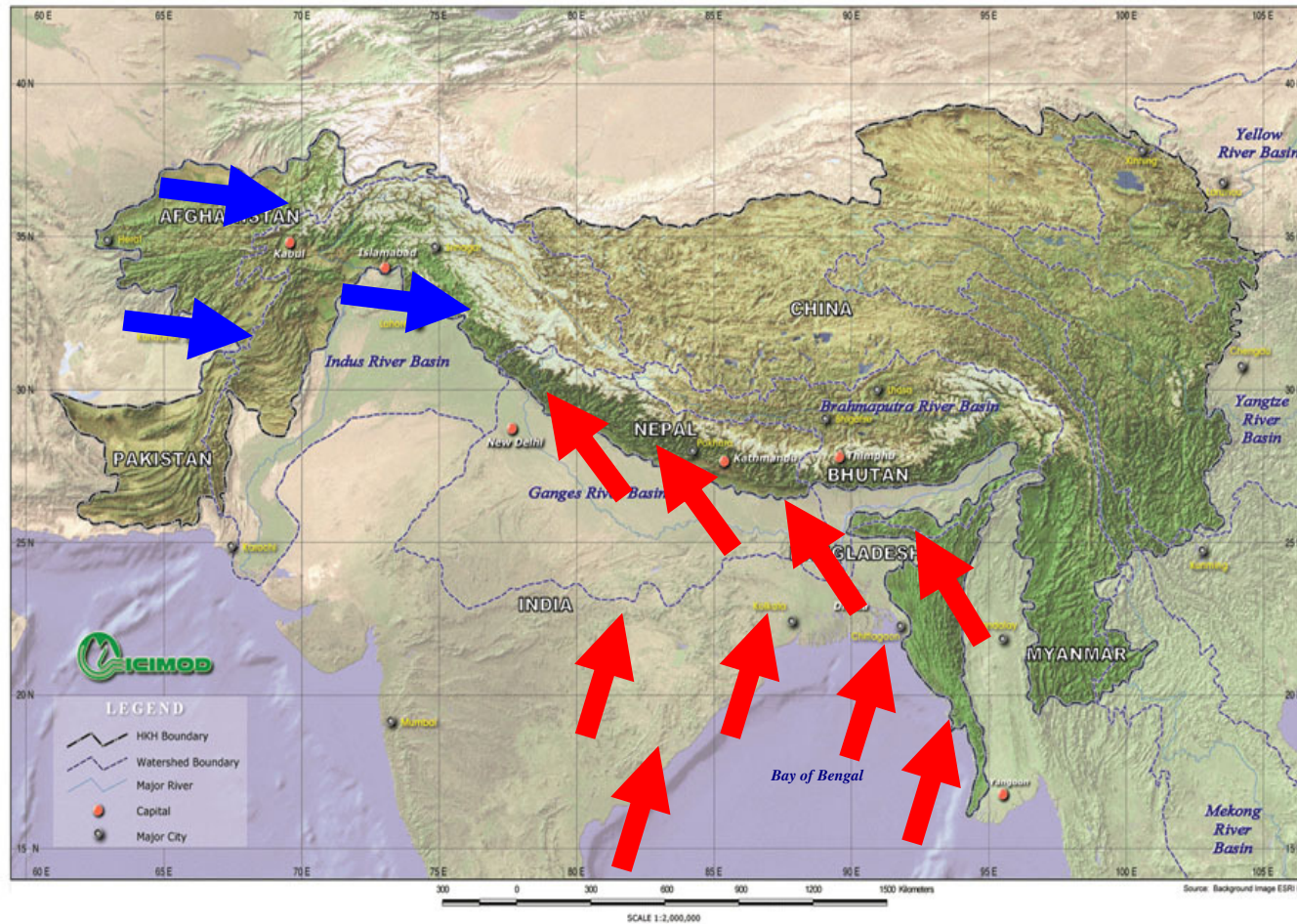


Figure 2.1 The Himalayan region, showing the track of moisture-bearing weather systems (red arrows: south-westerly summer monsoon; blue arrows: winter westerlies; adapted courtesy of ICIMOD, Nepal)

In a recent study using calibrated satellite-derived high-resolution Tropical Rainfall Measurement Mission (TRMM) data, Bookhagen and Burbank (2010) discovered a 6-fold east-west rainfall gradient in the Ganges foreland at elevations of up to 500 m ASL but no significant rainfall gradient in the same direction at higher elevations between 500 m and 5000 m. Taking transects perpendicular to the mountain ranges, they found that, in the east, the integrated annual rainfall total of mountain areas in eastern areas to be about 5 times less than that on the plains (<500 m), but, in the west, the totals were roughly equivalent. This brought them to the conclusion that “rainfall in the Himalaya responds to orographic controls, whereas rainfall in the foreland is a function of distance from the Bay of Bengal.” However, considerable variation in topography results in numerous local irregularities to the general trend of orographic precipitation and, often, extreme differences can be observed even between adjacent catchments (Alford, 1992). Annual average precipitation varies considerably across the region. The highest annual rainfall totals on Earth are experienced on the southern slopes of the eastern Himalaya. Mawsynram in Assam, north-east India, reportedly is the wettest place on Earth, with annual rainfall of 11,873 mm (Philip, 2003), whereas other areas, such as Leh in Ladakh, in north-west India, receive as little as 90 mm precipitation a year (Archer and Fowler, 2004).

Evapotranspiration increases steadily from a minimum in December to a maximum in May, the losses generally decreasing with altitude, as available thermal energy decreases (Alford, 1992). According to Bookhagen and Burbank (2010), “evapotranspiration plays only a minor role in... high-elevation mountainous catchments... generally [representing] less than 10% of the total hydrological budget”. From January minima, mean daily air temperatures rise to a maximum in late May or early June. In central and eastern parts of the region, monsoon cloud cover tends to arrest further temperature rises during remaining summer months; temperatures decline during the post-monsoon period (October to January).

The climate further ensures that all Himalayan rivers are characterised by great variations in seasonal flow, as river flow regimes are dominated by monsoonal rainfall (Hannah *et al.*, 2005). Runoff mainly is concentrated in the summer

months: the optimal period for the melting of snow and glacial ice, which, for many parts of the region, coincides with the summer monsoon. The relative contribution of melt-water to river flow generally declines from west to east. Arid conditions exist at lower elevations in the west, and, hence, melt-water from glaciers remains a major component of runoff for great distances downstream, whereas in the more humid east, monsoonal precipitation contributes much of the flow at all elevations. In the west, snow- and ice-melt contributes about 60 - 80% of the annual flow of the Indus as it emerges onto the plains (Archer and Fowler, 2004; Immerzeel *et al.*, 2010). It has been estimated that the glacier melt-water contribution is about 40% of the annual runoff of the Upper Indus (Lutz *et al.*, 2014). In the east, melt-water accounts for about 8-10% of the annual flow of the Ganges (Immerzeel *et al.*, 2010; Kattelman, 1993), with the glacier-melt contribution amounting to about 3% of the river's overall discharge (Immerzeel and Bierkens, 2012; Immerzeel *et al.*, 2010).

River flows across the region are highly seasonal, with the peak discharges that occur between June and September accounting for 65% - 75% of annual runoff (Alford, 1992). Flows recede rapidly post-monsoon, usually from October through to the following spring (Rees *et al.*, 2004a). River flows of snow-affected catchments recover earliest, as rising spring temperatures cause an initial release of snowmelt (Bookhagen and Burbank, 2010), whereas dry-season flows continue to recede in rain-fed catchments until pre-monsoon showers in April or May (Bookhagen and Burbank, 2010; Sharma, 1993). The perennial occurrence of snow- and ice-melt ahead of the summer monsoon is vital for the successful cultivation of crops, hydropower and many other water uses (Sharma, 1993).

2.3 Glacier fluctuation

2.3.1 Global glacier fluctuation

Glaciers globally have been retreating since the end of the Little Ice Age, towards the latter half of the 19th century (Barry, 2006; Grove, 1988; Oerlemans, 2005; Zemp *et al.*, 2008). Ever since the worldwide systematic collection of information on glacier changes began in 1894, observed global glacier retreats, and advances, have correlated positively with warmer, and cooler, periods of the Earth's climate

(Haerberli *et al.*, 2007). Globally, strong retreat was observed in the 1920s and 1940s, followed by stable or advancing conditions in the 1970s (Zemp *et al.*, 2008). However, since the mid-1980s, there have been “drastic” glacier retreats (Zemp *et al.*, 2008), coinciding with what is likely to have been “the warmest 30-year period of the last 1400 years” (IPCC, 2013b). Kaser *et al.* (2006) estimated the global glacier mass loss for the period 1961 - 2004 to be equivalent to a 0.5 mm (± 0.18 mm) rise in sea level per year but calculated a higher rise of 0.7 mm (± 0.22 mm) per year for the 1991 - 2004 period (in Radić and Hock, 2014). More recently, Gardner *et al.* (2013) estimated mountain glacier melt contributed to a 0.92 mm (± 0.34 mm) per year increase in sea level for the period 2003 – 2009. It is a commonly held view that climatic changes of the late twentieth century largely are a consequence of man’s emission of greenhouse gases from fossil fuels (IPCC, 2007b, 2013b). Marzeion *et al.* (2014) attribute only 25% ($\pm 35\%$) of global glacier mass loss over the period 1851 - 2010 to anthropogenic influences but assert with “high confidence” that, from 1991 to 2010, 69% ($\pm 24\%$) of the loss is due to human activity.

2.3.2 Himalayan glacier fluctuation

The Himalayan region is the most highly glacierized area outside of the polar regions (Dyurgerov, 2005; Gardner *et al.*, 2013). Estimates of the number of glaciers, and the extent of glacier cover, vary considerably, for example: Dyurgerov (2005) estimated there were some 15,000 glaciers in the region occupying a total area of between 33,000 km²; a recently prepared inventory by Bajracharya and Shrestha (2011), based on the mapping of satellite images and considering all glaciers greater than 0.01 km², reveals over 50,000 glaciers, having a total glacier area of over 61,000 km²; while the new Randolph Glacier Inventory (Arendt *et al.*, 2012), collated for the Fifth Assessment Report of the Intergovernmental Panel on Climate Change (IPCC AR5), quotes there to be about 36,800 glaciers in South Asia with a total area of 55,665 km² (Vaughan *et al.*, 2013). Numbers differ probably because of inconsistencies in the definition of glaciers and, perhaps more basically, the designation of the “Himalayan” region (i.e. whether it includes the Hindu Kush, the Karakoram and/or other mountain ranges).

As in many other parts of the World, Himalayan glaciers generally have been retreating since the end of the Little Ice Age, from about 1850 AD (Mayekwski and Jeschke, 1979; Zemp *et al.*, 2008; Bolch *et al.*, 2012; Su and Shi, 2002), except from 1920 to 1940, when stable or advancing glaciers were observed (Bolch *et al.*, 2012; Mayekwski and Jeschke, 1979), and over recent years in the Karakoram, where several glacier advances and surges have occurred (Hewitt, 2005, 2007). Many studies have reported the retreat of Himalayan glaciers over the last thirty years (e.g. Fujita *et al.*, 2001; 1997; Berthier *et al.*, 2007; Kulkarni *et al.*, 2007; Raina, 2009; Scherler *et al.*, 2011; Kääb *et al.*, 2012).

A formal systematic review of 52 glacier change studies in the region (Miller *et al.*, 2013) reaffirmed that glacier shrinkage predominates in most parts over the 20th and early part of the 21st century. The review found that, of 37 glaciers whose terminus changes had been recorded, only two Karakoram glaciers exhibited net advances: the Batura (Batura Glacier Investigation Group, 1979) and Liligo (Belò *et al.*, 2008). Most significant retreats included: 1256 m for the Imja glacier in Nepal (Bajracharya *et al.*, 2007), 1530 m over a 69 year period from 1935 for the Gangotri glacier in the northern Indian state of Uttarakhand (Kumar *et al.*, 2008), and 6569 m from 1962 to 2001 for the Parbati glacier (Kulkarni *et al.*, 2005), in the neighbouring state of Himachal Pradesh. Eleven studies, mostly in the Karakoram or western Himalaya, recorded fluctuating behaviour. Studies of glacier area changes of 39 single glaciers showed reductions of 16% over an average period of 34 years spanning 1956 (earliest) to 2008 (latest), whilst nine wider-scale regional studies recorded an average loss of 13% in glacier area over a similar period. Data from mass balance studies on seven different glaciers showed an overall trend of negative mass balance of about -0.57 m water equivalent (w.e.) per year over a 20-year period, 1986 - 2006. A lack of consistent and continuous measurements in the systematically reviewed studies prevented Miller *et al.* (2013) from quantifying whether glacier shrinkage was accelerating. Bolch *et al.* (2012) reported changes of similar magnitude in their review of Himalayan and Karakoram glacier changes, observing also that “the mass budget over large parts of the Himalaya has been negative for the past five decades”, that the rate of loss increased from about 1995, yet, region-wide, the loss rate was “close to the global mean”.

The anomalous behaviour of advancing and, in some places, surging glaciers (Hewitt, 2005) in the Karakoram appears to contradict local negative mass balance measurements (e.g. Bhutiyani, 1999). In a region-wide study, combining ICESat and SRTM data, Kääb *et al.* (2012) found that Himalayan glaciers generally thinned by -0.26 ± 0.06 m/year on average from 2003-2008, but those of the Karakoram thickened $+0.14 \pm 0.06$ m/year. Another remote-sensing-based survey, using ASTER and SPOT satellite images of the entire Himalayan region (Scherler *et al.*, 2011), showed more than 65% of monsoon-influenced glaciers to be in retreat, while 58% of studied glaciers in the Karakoram were “stable or slowly advancing”. Gardelle *et al.* (2012), likewise using satellite imagery, calculated a slight positive regional mass balance of $+0.1 \pm 0.22$ m w.e./year from Karakoram glaciers. Increases in precipitation and declining summer temperatures in northern Pakistan (Archer and Fowler, 2004) are thought to have contributed to the positive mass balances (Gardelle *et al.*, 2012; Hewitt, 2007). Hewitt (2007) points-out, however, that “huge loss of ice mass” was observed in almost all Karakoram glaciers over the 20th century until the mid-1990s and, while advances generally are “confined to the highest watersheds in the central Karakoram..., glaciers in the rest of the region continue to decline”.

These recent studies show that, although shrinkage is a dominant feature for the majority of the region’s glaciers, the behaviour clearly is not universal (Scherler *et al.*, 2011; Vaughan *et al.*, 2013). Many researchers (e.g. Bolch *et al.*, 2012; Gardelle *et al.*, 2012; Hewitt, 2007; Kääb *et al.*, 2012) cite a severe lack of representative glacier and hydrometeorological observations, and a bias towards readily accessible glaciers (Radić and Hock, 2014), as a barrier to better understanding the variability of (glacier) changes and the potential impacts to downstream water resources.

2.4 Hydrometeorological changes: observed and projected

2.4.1 Observed trends in temperature and precipitation

Glaciers are considered “sensitive climate indicators because they adjust their size in response to changes in climate (e.g. temperature and precipitation)” (Vaughan *et al.*, 2013). Long-term changes in temperature and precipitation are particularly significant because they affect the mass balance of glaciers, which, after some delay, are reflected in changes to glaciers’ dimensions (Oerlemans, 1994; Oerlemans, 1998; Paterson, 1994). Successive years of positive glacier mass balances are typically associated with thickening of glacier ice and advances of glaciers’ snouts (or termini). Years of negative mass balance, on the other hand, eventually result in thinning and retreat. Increases in precipitation falling as snow on glaciers contributes to mass gain by both increasing accumulation and suppressing ablation, as the snow insulates the ice beneath from melting. Conversely, reductions in precipitation falling as snow on glaciers promote mass loss. Air temperature, which is closely correlated to several energy balance components that determine melt (Braithwaite and Zhang, 2000; Hock, 2003), is also important. Increasing temperatures affect glacier mass by reducing the amount of precipitation that falls as snow (which reduces accumulation and provides less protection from ablation), by increasing the ablation rate (as more energy is available for melting) and by prolonging the melt season (due to a greater number of positive degree days).

The variation in regional precipitation results in Himalayan glaciers experiencing contrasting melt regimes. Glaciers in the west of the region benefit from significant winter accumulation, with ablation occurring mainly over hotter summer months. This “winter accumulation – summer melt” regime is similar to that experienced by higher latitude glaciers (e.g. European Alps, Canadian Rockies). In monsoon-affected central and eastern parts of the Himalaya, the main periods of accumulation and melt coincide, in summer. As well as being affected by general trends in climate, such “summer accumulation – summer melt” glaciers (Ageta *et al.*, 2001) are particularly susceptible to changes in the timing and intensity of the monsoon.

Studies that have attempted to assess trends in temperature and precipitation across the Himalayan region often have been hampered by a paucity of good quality long-term observations, especially at higher elevations (Bhutiya *et al.*, 2007; Chalise *et al.*, 2003; Chalise and Khanal, 1996). Of the few studies undertaken, several report general increases in temperature but no uniform trend in precipitation is apparent.

An upward trend of +0.06 °C/year was identified in annual mean maximum temperatures for 49 stations in Nepal from 1977 to 1994 (Shrestha *et al.*, 1999) and, in an extension to the earlier analysis, that trend was seen to increase to about +0.1°C/year for the period 1977-2000 (Shrestha and Aryal, 2011). However, an analysis of 78 long-term precipitation records from Nepal (Shrestha *et al.*, 2000) failed to detect any significant trend nationally, which may suggest glacier retreat in Nepal is occurring because of the increase in temperature rather than any discernible change in the precipitation regime.

Analysis of long-term monthly mean temperature data for Srinagar (Fowler and Archer, 2006), in the northern Indian state of Jammu and Kashmir (J&K), at the western margins of the Greater Himalaya, show statistically significant increases in winter (October - March) and summer (April - September) mean temperatures of +0.1 °C/decade and +0.04 °C/decade respectively from 1894-2000, but a “dramatic” increase in December to February mean temperatures of +0.51 °C/decade from 1960. Several nearby weather stations in northern Pakistan also showed significant winter warming since 1961, with winter maximum temperatures rising by between +0.27 and +0.55 °C/decade, but decreasing summer temperatures of between -0.4 and -1.11 °C/decade. Analysis of the Srinagar rainfall record, showed no significant trend over the period 1895-1999 (Archer and Fowler, 2004) but a strong upward trend in winter rainfall of about +22 mm/decade was seen from 1961. Statistically significant upward trends of winter rainfall were also found at three other locations in northern Pakistan. Again, this might explain the apparent thickening and advances of Karakoram glaciers reported by Hewitt (2005) and others.

Another study of 3 long Indian temperature records, from Shimla, Leh and Srinagar, in Himachal Pradesh and J&K, showed statistically significant positive trends in annual mean, maximum and minimum temperatures of about 1.6 °C on average over a period dating from 1901 (earliest) to 2002 (latest) (Bhutiyani *et al.*, 2007). They too observed that the rate of 20th century warming generally had increased from the late 1960s, with winters warming at a faster rate. Basistha *et al.* (2009), who analysed long-term, 80-year, records from 30 rain gauges in the neighbouring mountain state of Uttarakhand found annual and monsoonal (summer) rainfall generally to increase gradually from 1902 to 1964, only for the trend to reverse sharply from 1965-1980 over the Siwaliks and southern parts of the Lesser Himalayas.

Collins *et al.* (2013), having compiled long time-series of meteorological observations from many locations across the Himalaya, demonstrated annual monsoon precipitation to have “considerable year-to-year variability across the region... from the mid-1860s to 2000s” but apparently no regionally consistent underlying variation. Winter precipitation in western parts (e.g. Shimla and Dehradun) showed a general decrease from 1870-1970, followed by slight recovery in the 1980s. Recent (warming) trends in temperature, since the 1970s, were corroborated but, set “in the context of fluctuations since the mid-nineteenth century”, “only into the 2000s did summer temperatures... exceed earlier warmer periods”.

Ice-cores taken from the Dasuopu glacier (85.71 °E, 28.38 °N) in the central Himalayas in 1997 (Duan and Yao, 2003) provide longer-term evidence of monsoon variability over the past 300 years. The record suggests the intensity of the monsoon fluctuated in the 18th and 19th centuries, had strengthened from 1875-1920, but since then has continued to weaken. The authors showed that decreasing accumulation, and monsoon precipitation, correlates significantly with the northern hemisphere warming over the 20th century.

2.4.2 Observed changes to glacier-fed river flows

It has been claimed that the Himalayan region is the “most critical region in which vanishing glaciers will negatively affect water supply,” and that some areas are “likely to run out of water during the dry season if current warming and glacial melting trends continue” (Barnett *et al.*, 2005). The effects of glacier changes on river flows and water resources availability inevitably will vary spatially, differing according to precipitation regime (Bolch *et al.*, 2012; Radić and Hock, 2014), catchment elevation and the proportion of glacier-cover present within a catchment (Collins *et al.*, 2013; Thayyen and Gergan, 2010; Thayyen *et al.*, 2005). The glacial melt-water contribution to catchments in wetter monsoonal parts of the central and eastern Himalaya is relatively small compared to the contribution in the more generally arid western catchments (Bolch *et al.*, 2012). Declining glacier mass will, therefore, have greatest impact on river flows in drier western catchments (Miller *et al.*, 2012).

Any objective assessment of the impact of recent glacier retreat on observed river flows is difficult because very few gauging stations on glacier-fed rivers in the region have records that are sufficiently long or complete (Collins *et al.*, 2013; Shrestha and Aryal, 2011; Shrestha and Shrestha, 2005). Results from the few studies that have attempted to detect trends are summarised below.

Flow data for the Hunza River at Dainyor (a tributary of the Indus in the Karakoram region in northern Pakistan) from 1980 to 2004 show catchment average annual runoff to reduce by 3 mm/year (Khattak *et al.*, 2011). An assessment of flow data for the Beas, Chenab, Ravi and Sutlej rivers (Bhutiyan *et al.*, 2008), all glacier-fed tributaries of the Indus in north-west India, showed, for the longest available time-series (Sutlej), a statistically significant reduction in annual and summer mean flow over the period 1922 to 2004, corresponding to a reduction in monsoonal precipitation over the same period. However, reductions in winter and summer flow post-1991, a period of “average” monsoon conditions and increasing temperatures, led the authors to suggest the glacier melt-water component of discharge in the Sutlej “reached its maximum in about 1990”. From 1961-2004, the Beas was the only river (of the four) to demonstrate a statistically

significant negative trend in annual mean flow; the apparent negative trend for the Sutlej and positive trends for the Ravi and Chenab over the period were not significant.

Collins *et al.* (2013) observed a similar downward trend in annual mean flow of the Sutlej at Khab over the period 1972-2002, attributing the decline to “substantially reduced levels of monsoon precipitation” that were not off-set by increases in glacier melt. Of the relatively short flow records Collins *et al.* (2013) had obtained for gauging stations on tributaries of the Ganges in Nepal (most started in the 1960s), the record for the Kali Gandaki at Seti Beni was the only one to show a decrease in mean flow, of -12% between 1964-73 and 1983-1992. While annual flows at other stations fluctuated from year to year, their “general background level of flow was maintained from 1960s to 2000s”.

Shrestha and Aryal (2011) and Shrestha and Shrestha (2004) report two of Nepal’s largest rivers, Karnali and Sapta Koshi, having decreasing flows, while another large river, the Narayani, shows an increasing trend. Three further snow-fed rivers apparently showed a declining trend in flows, but southern (rain-fed) rivers showed none. They conclude “that trends observed in river discharge are neither consistent nor significant in magnitude, with the ambiguity due to short record lengths and high inter-annual variability in discharge data”.

2.4.3 Climate change projections

General Circulation Models (GCMs) and coupled Atmosphere-Ocean General Circulation models (AOGCMs, hereafter also referred to as GCMs) are numerical models that simulate the response of the global climate system to increasing greenhouse gas concentrations (IPCC, 2013c). Many GCMs have been developed and applied to predict future climate change under different emission scenarios. In 1995, the World Climate Programme (WCRP, 2014) established a standard protocol, the Coupled Model Intercomparison Project (CMIP), to enable scientists to analyse GCM outputs in a consistent and systematic fashion (PCMDI, 2014). Families of “reference” emission scenarios are associated with each phase of CMIP GCM models. GCM model projections in the IPCC’s Third (TAR) and Fourth

Assessment Reports (AR4) (IPCC, 2001, 2007a) were underpinned by third phase CMIP3 Special Report on Emissions Scenarios (SRES), while the latest projections in the IPCC Fifth Assessment Report (AR5)(IPCC, 2013a) were based on CMIP5 Representative Concentration Pathways (RCPs) scenarios (See Box 2.1). GCMs typically have a horizontal resolution of between 250 and 600 km (IPCC, 2013c) and are often too coarse to be representative of conditions on smaller scales. To overcome this problem, higher resolution Regional Climate Models (RCMs) have been developed (at 10 – 50 km resolution) in many parts of the world, derived either through statistical downscaling from GCMs or dynamical downscaling, where GCM output provide lateral boundary conditions to the RCM (Wilby *et al.*, 1998).

The most recent CMIP5 GCMs predict a “clear” general increase in temperature on average over South Asia of between +1.3 °C and +3.5 °C by 2100, relative to the 1986-2005 baseline period, for the RCP4.5 scenario but wide variations in precipitation (Christensen, 2013). For the Karakoram and Greater Himalaya region, Chaturvedi *et al.* (2014) report mean temperature increases of 2.4 °C, 3.5 °C, 3.8 °C and 5.5 °C by the 2080s, relative to the pre-industrial 1861–1900 period, for the four RCP scenarios (see Box 2.1), RCP2.6, RCP4.5, RCP6.0 and RCP8.5, respectively, from an ensemble of 21 CMIP5 models. The ensemble mean annual precipitation showed increases of 0.6 to 1.6 % by the 2030s for RCP2.6 and RCP8.5 respectively, and by 2.6 to 8.5 % by the 2080s, relative to the pre-industrial period, but considerable variation was reported in precipitation change projections, ranging from -20 to +40 % by 2100. The range of projected temperature and precipitation changes across the Karakoram and Himalaya can be seen in Figure 2.1 (Chaturvedi *et al.*, 2014).

In a study of two glacier-fed headwater catchments in Pakistan and Nepal, Immerzeel *et al.* (2013) stated temperature projections for the RCP4.5 scenario “reveal a region-wide warming” of about 2°C by 2021-2050, relative to 1960-1990, and a 2.2 °C temperature increase in the Upper Indus and Ganges basins. They too observed that precipitation projections showed a “modest increase of up to a few per cent on average”, albeit with “a large spread among GCMs”.

A study by Lutz *et al.* (2013), comparing potential effects of CMIP5 (RCP) and CMIP3 (SRES B1, A1B, and A2) projections on glaciers in Central Asia, observed large variations in both temperature and precipitation changes between all models and emission scenarios, yet an overall (average) increase in mean temperature of about +2°C from 1961-90 to 2021-2050. Highlighting the uncertainty in projections, Lutz *et al.*, 2013 cited the 10 and 90 percentile (%ile) projections from the CMIP3 and CMIP5 multi-model ensembles, showing temperature change projections to range from +1.3 °C (10 %ile) to +2.4 °C (90 %ile) for CMIP3, +1.7 °C to +2.9 °C for CMIP5, while precipitation changes ranged from -6 to +7% for CMIP3 and from -8 to +15% for the CMIP5 ensemble. The spread of projections of future glacier extent changes was found to be similar for both ensembles, at about 54 to 65% of the 2008 area by 2050. Chaturvedi *et al.* (2014) estimated that between 11 and 27% of glaciers in the Karakoram and Himalayan ranges could face “eventual disappearance” by 2100 under the R2.6 and R8.5 scenarios.

In another study, of possible regional climate change over South Asia, Kumar *et al.* (2013) analysed projections from ensembles of three Regional Climate Models (RCMs) - CCLM, HadRM3 and REMO - and for an ensemble of 22 CMIP3 GCMs (focussing on ECHAM5 and HadCM3 in particular), under the SRES A1B scenario over the period 1970-2099. The GCM projections for 2020-2040 showed the ensemble mean precipitation over India to increase by ~5% and temperature to rise by approximately +1.5 °C. By comparison, ECHAM5 precipitation increased by ~3% and HadCM3 by ~8%; both GCMs projected similar increases in temperature, of about +1.2 °C. Monsoonal (June-September) precipitation was projected by ECHAM and HadCM3 to increase over the Indo-Gangetic plain by 5 to 10% by 2030-2049, relative to 1970-99, and by 15 to 30% in north-west India, while annual temperature was predicted to increase by 2.5 °C to 5.5 °C in northern India and the Himalayan region by 2070-2099. Kumar *et al.* (2013) reported that, according to their RCM ensemble, precipitation was likely to increase significantly over the plains of northern India and the Himalaya for the 2070-2099 period. Similarly to the GCMs, the RCM ensembles showed “widespread warming” of 1.5 °C to 2 °C for 2030-2049, which increased to 2.5 °C to 5.5 °C by 2100. Winter (December and January) warming was found to be greatest over the Himalaya.

Box 2.1 Emission Scenarios

Emissions scenarios describe future releases into the atmosphere of greenhouse gases, aerosols, and other pollutants and, along with information on land use and land cover, provide inputs to climate models. They are based on assumptions about driving forces such as patterns of economic and population growth, technology development, and other factors. Levels of future emissions are highly uncertain, and so scenarios provide alternative images of how the future might unfold.

Special Report on Emissions Scenarios (SRES)

*SRES scenarios underpinned the climate change projections of the IPCC Third Assessment Report (TAR), published in 2001, and the IPCC Fourth Assessment Report (AR4), published in 2007. There are over 40 SRES scenarios, each based on different assumptions on future greenhouse gas pollution, land-use and other driving forces. Major “families” of SRES scenarios include: **A1** scenarios, which describe a future world of very rapid economic growth, global population that peaks in mid-century and declines thereafter, and the rapid introduction of efficient new technologies - there are three A1 sub-groups, distinguished by their technological emphasis, **A1F1** (fossil intensive), **A1T** (non-fossil energy source), and **A1B** (balance across all sources); **A2** scenarios describe a very heterogeneous world in which economic development is primarily regionally oriented and per capita economic growth and technological change are slower; **B1** scenarios represent a convergent world with the same global population that peaks in mid-century and declines thereafter, as in the A1 storyline, but with rapid changes to a service and information economy, reductions in material intensity, and the introduction of clean and resource-efficient technologies; **B2** scenarios represent a world in which emphasis is on local solutions to economic, social, and environmental sustainability, a world with continuously increasing population at a rate lower than A2, intermediate levels of economic development, and less rapid and more diverse technological change than in B1 and A1.*

Representative Concentration Pathways (RCPs)

*RCPs are a new set of climate change scenarios prepared for the Intergovernmental Panel on Climate Change (IPCC) Fifth Assessment Report (AR5). They replace the Special Report on Emissions Scenarios (SRES) used in the two previous IPCC reports. There are four pathways defined according to their total radiative forcing in 2100: **RCP 8.5** (rising radiative forcing pathway leading to 8.5 W/m² in 2100); **RCP 6.0** (stabilization without overshoot pathway to 6 W/m² at stabilization after 2100); **RCP 4.5** (stabilization without overshoot pathway to 4.5 W/m² at stabilization after 2100); and **RCP 2.6** (peak in radiative forcing at ~ 3 W/m² before 2100 and decline)*

(Adapted from: WMO, 2014)

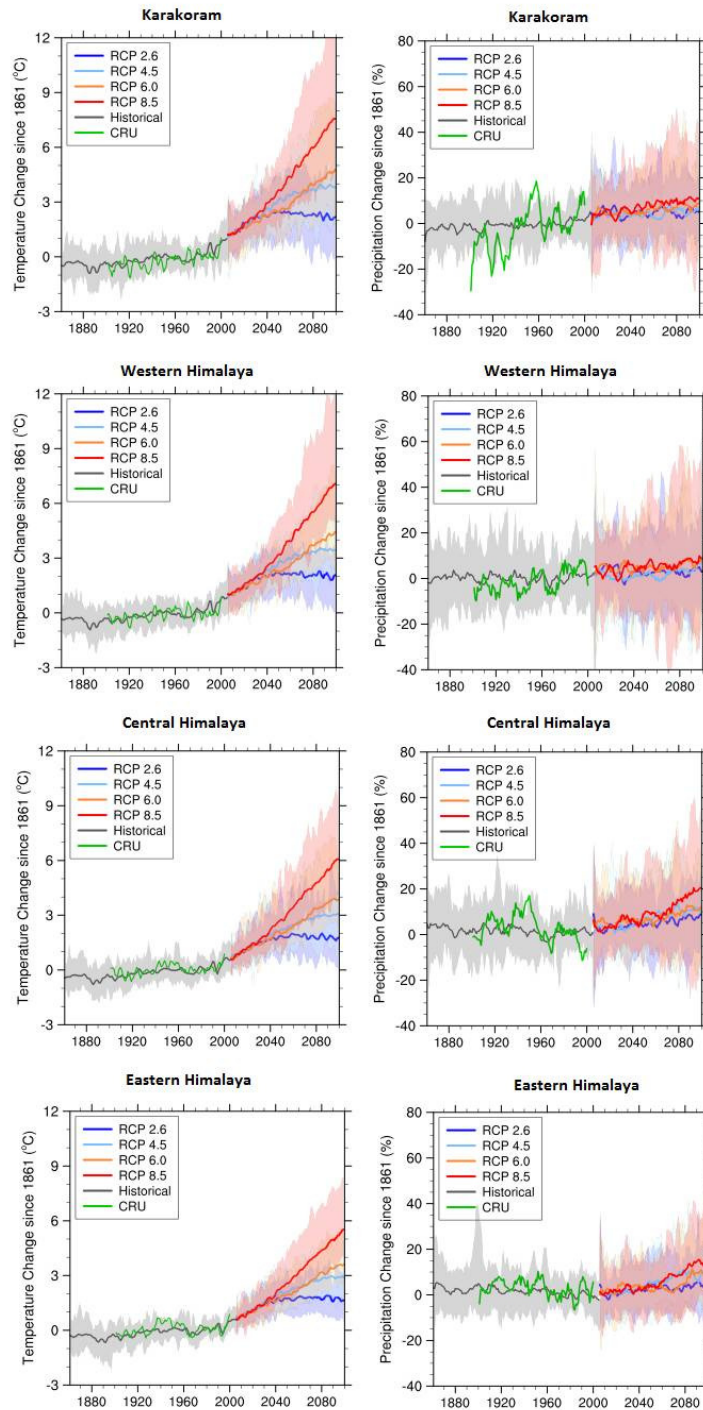


Figure 2.2 CMIP5-based time-series of temperature and precipitation anomalies for the Western Himalaya, Central Himalaya, Eastern Himalaya and Karakoram region from 1861 to 2099 relative to 1961-1990 for four RCP scenarios. The shaded area represents the range of changes projected by the 21 model ensemble; ensemble averages for each RCP are shown as thick lines; observed temperature and precipitation trends from CRU are shown by the green line and the solid black line refers to model ensemble values for historical simulations (Source: Chaturvedi, et al. 2014, with the author's permission)

Mathison *et al.* (2013) similarly assessed the potential effects of RCM projections specifically in the Ganges and Brahmaputra basins. Projections from a four-member RCM ensemble, derived from the HadRM3 and REMO RCMs under the SRES A1B scenario, were compared over two thirty-year periods, 1970-2000 (present) and 2040-2070 (future). A “near constant” increase in regional mean temperature was seen, with annual temperatures increasing by 2.5 °C to 3 °C by the 2050s. As reported by Kumar *et al.* (2013), winter temperature increases (December - February) were greater than summer. December to February and September to November temperature increases were found to be greatest in mountain regions. Considerable uncertainty and spatial variations, however, were reported in precipitation projections.

Projected changes in climate over the Indus basin, using a 17 model ensemble of the PRECIS RCM (Jones *et al.*, 2004), derived from of the HadCM3 GCM, under SRES A1B, were assessed by Rajbhandari *et al.* (2014). Comparing predictions for 3 future periods, (2011-40, 2041-70, 2071-98), relative to a 1961-90 baseline, non-uniform changes in precipitation were again observed: an increase in overall precipitation over the upper Indus, but a decrease in the lower part of the basin. Winter precipitation, however, was seen to decrease throughout. Monthly mean minimum and temperature rose consistently over each time period both in the upper and lower parts of the Indus basin. Minimum temperatures increased over the whole basin by 2 °C in the 2020s, 2.5 °C to 4 °C in the 2050s, and more than 4 °C in the 2080s, the rise in minimum temperatures being greatest on the Upper Indus. Earlier, Akhtar *et al.* (2008), also using PRECIS but under the SRES A2 emission scenario, had observed “a general increase in temperature and precipitation” for the period 2071-2100 in the Hunza, Gilgit and Asotre basins in the Upper Indus, with warming “uniformly distributed”, rising by 4.8 °C by the end of the century while mean annual precipitation increased by of 19%, 21% and 13% in the three basins respectively over the same timescale.

2.5 Meso-scale hydrological modelling

2.5.1 Rainfall-runoff models

Hydrological models are commonly used to predict conditions where data are sparse or unavailable, such as, in ungauged catchments or for some time into the future (Beven, 2012). The types of models that are most commonly used in climate impact studies are physical (process) based, deterministic, rainfall-runoff models. Such models typically use mathematical functions to describe the various individual processes that control the runoff from a catchment and link the processes through series of conceptual storage reservoirs.

A vast number of rainfall-runoff models have been developed (cf. Singh, 1995), the majority of which were developed at the catchment-, or meso- ($\sim 10^1$ to 10^3 km²), scale (Uhlenbrook *et al.*, 2004)). They range from simple, one-dimensional models (lumped models) that represent the catchment processes as a single storage reservoir whose response is described by some empirically derived function, to complex three-dimensional grid-based models (distributed models) that attempt to fully describe the behaviour of, and interactions between, catchment processes (e.g. sub-surface flows, overland flows, vegetation interception, snow- and ice-melt) on a physical basis. Rainfall-runoff models can be applied at a variety of spatial and temporal scales and at monthly, daily or sub-daily time-steps.

Calibrating the various controlling model parameters, either with reference to field observations or through numerical optimization, attains improved predictions for most catchments (Beven, 2012). Generally, the more complex the model the greater the number of parameters and the greater the difficulty of model calibration. For example, IHACRES (Jakeman *et al.*, 1990) is a simple lumped model, having two storage reservoirs in parallel (one for fast response, the other for slow), that requires only 6 parameters to be calibrated for its application in a catchment. In contrast, the distributed, grid-based SHE model, which represents catchment processes in a number of vertical layers, would require at least 18 parameters to be defined for every single grid square of the model (Beven, 2012). Depending on the level of catchment discretization (i.e. the grid-cell size), an

application of the SHE model could require the specification of literally thousands of parameters. In data sparse regions, such as the Himalayas, scope for the application of highly parameterised models is limited.

Although attempts have been made to apply the SHE model in India (e.g. Jain *et al.*, 1992; Refsgaard *et al.*, 1992), the lack of relevant data for parameter calibration has limited its application in the Himalaya. There are, however, many examples of rainfall-runoff models being applied successfully to specific catchments in the region. Early examples include the HBV-ETH model, originally developed in Scandinavia (Bergström and Forsman, 1973), and the HYCYMODEL, from Japan (Fukushima, 1988), both of which have been applied to the Langtang Khola basin in eastern Nepal by Braun *et al.* (1993) and Fukushima *et al.* (1991) respectively, the SLURP watershed model from Canada, which was used in the Satluj catchment in northern India (Jain *et al.*, 1998), the UBC watershed model (Quick and Pipes, 1977), also applied to the Satluj (Singh and Quick, 1993), the HEC model, applied to the Beas river basin in northern India (Verdhen and Prasad, 1993), and the Snowmelt-Runoff Model (SRM) (Martinec, 1975), which has been used in many Himalayan catchments including the Kabul river basin in Pakistan (Dey *et al.*, 1989) and the Beas and Parbati rivers in India (Kumar *et al.*, 1991; Kumar *et al.*, 1993). These models are more appropriately described as “semi-distributed models” because they typically contain a mixture of lumped and process-based components that are applied in a distributed manner in a catchment. As such, they generally require fewer inputs and have fewer parameters to calibrate than fully distributed models, making them more suitable in mountain areas, where data are limited.

2.5.2 Modelling ice-melt

The treatment of glaciers and ice-melt generation within catchment-scale rainfall-runoff models varies considerably, ranging from models that simply make no distinction between snow and ice (e.g. Dey *et al.*, 1989; Singh and Bengtsson, 2004) or assume all snow above a certain elevation to be considered as permanent snow or ice and adjust the melt calculation at higher elevations accordingly (Immerzeel *et al.*, 2009; Tahir *et al.*, 2011), to those that require glacier dimensions

to be mapped at high spatial resolutions and attempt to accurately represent, in a fully distributed manner, the accumulation and ablation (melt) processes across the glacier surface, the routing of melt-water through the glacier, and the glacier dynamics (e.g. Arnold *et al.*, 1998; Huss *et al.*, 2008).

A large variety of glacier melt models have been developed to calculate melt-water contributions to catchment runoff within rainfall-runoff models (Hock, 2005). These range from simple temperature-index (or degree-day) models, which describe a linear relation (the degree-day factor, DDF) between positive daily air temperature and melt rate (Hock, 2003), to more sophisticated energy-balance models that assess the energy fluxes, to and from, the glacier surface (Hock, 2005) and take into account the net radiation, global radiation, albedo, long-wave radiation, turbulent heat flux, etc. Most rainfall-runoff models (e.g. HBV, UBC, SRM) use temperature-index methods because of their intrinsic simplicity and limited data demands. Spatial variations in climate input variables are usually accounted for in such models by sub-dividing the catchment (and/or glacier) into a number of elevation bands (e.g. Singh and Bengtsson, 2005), hydrological response units (e.g. Klok *et al.*, 2001) or grid-cells (e.g. Verbunt *et al.*, 2003) and applying appropriate lapse rates (e.g. $-0.65\text{ }^{\circ}\text{C}/100\text{ m}$) from some datum. The routing (and delay) of melt-water, as it percolates through the englacial and sub-glacial drainage system to emerge at the glacier terminus (Collins, 1979), is usually represented in the models as a series of conceptual reservoirs whose storage coefficients determine the rate of melt-water release (Jansson *et al.*, 2003).

2.5.3 Modelling climate change impacts in glacier-fed catchments

Studies to assess the potential impacts of climatic change on river flows require some representation of future meteorological conditions (usually temperature and precipitation) as input to hydrological models (Akhtar *et al.*, 2008). The two approaches most commonly used are climate-model based scenarios, where GCM (or RCM) outputs are applied directly (or indirectly) as model inputs, or sensitivity analyses, in which regularly spaced adjustment (increments) are applied to key driving variables (Carter *et al.*, 2007).

There have been many studies to assess the impact of climatic warming on glacier-fed river flows in specific Himalayan catchments (e.g. Akhtar *et al.*, 2008; Braun *et al.*, 1993; Nepal *et al.*, 2013; Sharma *et al.*, 2000; Singh and Bengtsson, 2005; Singh and Kumar, 1997; Wanchang *et al.*, 2000). Due to uncertainties of climate-model predictions in the Himalaya, many of the model applications have used sensitivity analysis approaches (see Table 2.1), increasing temperature, and/or precipitation incrementally, over relatively short simulation periods, during which glaciers were treated as time-invariant, stationary elements having constant dimensions. Climatic warming is, however, progressive and glacier dimensions continually change: a model's inability to represent transient conditions arguably invalidates its application over longer timescales (Nepal *et al.*, 2013).

Over recent years, a few catchment-scale models have been developed to represent the transient behaviour of glacier retreat. One of the earliest was for an application in the 2113 km² upper Yili River basin in the Tien Shan mountains in north-west China (Ye *et al.*, 2003), where relationships, based on a glacier ice-flow model (Oerlemans, 1988; Schmeits and Oerlemans, 1997), were derived between glacier area and air temperature increases for 76 glaciers. Using a 1954-1997 baseline and a degree-day (temperature-index) approach to calculate mass balance and runoff, they found that, in all cases, glacier runoff initially would increase, attain a peak, and then decline ultimately to reach a level below baseline. The magnitude and timing of the runoff peaks depended both on glacier size and the rate of temperature increase.

Another early example was in a local (Salford) PhD study of the small 25 km² Findelenbach catchment in Switzerland (Macdonald, 2004), whereby a single alpine glacier (Findelengletcher) was conceptualised as a wedge-shaped grid box and the glacial ice was allowed to deplete in each cell according the cell's mass balance. Using HadRM2 data, Macdonald showed how glacier area changes would affect the magnitude and variability of future river flows.

In 2008, Huss *et al.* (2008) parameterised “annual glacier surface evolution” of glaciers in 3 catchments in the Zinal valley in Switzerland (Zinal, 18 km²; Moming, 10 km²; Weisshorn, 7 km²) “using an ice thickness change pattern based

on theoretical considerations of ice dynamics”. Based on a detailed 3D geometry of the glaciers and surrounding terrain, relationships were derived between annual mass balance changes (calculated using a distributed temperature-index melt model) and surface elevation change.

More recently, Immerzeel *et al.* (2012) applied an ice-flow model in a high resolution (90 m x 90 m) hydro-glaciological model of the 360 km² Langtang catchment in Nepal. Using remote sensing imagery to define glacier extent and a previous study’s data to characterise spatial variation of ice depth, the model was applied over a 100-year period, 2000-2100, with downscaled data from 5 different CMIP3 GCMs for the SRES A1B scenarios. Both temperature and precipitation were projected by the GCMs to increase on average over the period (0.06°C/year and 1.9 mm/year, respectively). Modelled glacier area correspondingly decreased continually while mean ensemble discharge “surprisingly” significantly increased annually by 0.05 m³/s (~4 mm). Immerzeel *et al.* (2013) went on to repeat the application in the Langtang and the Baltoro (1415 km², Upper Indus) catchments, using an ensemble of CMIP5 GCMs for the RCP4.5 and RCP8.5 scenarios and found “a consistent increase in total runoff for both watersheds at least until 2100” for both scenarios. Increases ranged from 31% (Langtang) to 46% (Baltoro) in 2021 -2050 for RCP4.5 (relative to the 1961-90 baseline) to 88% (Langtang) to 96% (Baltoro) in 2071 - 2100 for RCP8.5. The simulations were said to show strong glacier “retreat, downwasting and disintegration” in both cases, with retreat in the Langtang “more pronounced because the glaciers are smaller, for example for RCP8.5 the glacier area is reduced by 54% in 2100 compared with 33% in the Baltoro”.

Another, arguably, more parsimonious approach, based on glacier volume-area scaling (Bahr *et al.*, 1997; Chen and Ohmura, 1990), was developed by Stahl *et al.* (2008) and applied in an application of the HBV-EC model (Hamilton *et al.*, 2000) in the 152 km² Bridge River basin in the Canadian Rockies. The catchment was discretized into 14 elevation bands of 100 m and the model was run over a 100-year period for a range of downscaled climate change scenarios from the CGCM3 GCM. Glacier volume and area were updated each decade according to the accumulated mass balance for the period, and any reduction (or increase) in glacier

area applied to the lowest elevation bands using a “morphologic erosion operator”. For all scenarios, mass balance remained negative and glacier area and summer (August) runoff reduced continuously over the entire model period.

2.6 Macro-scale hydrological modelling

2.6.1 Definition of a macro-scale hydrological model

Macro-scale hydrological models (MHMs) typically are conceptual water-balance accounting models, resolving precipitation, evapotranspiration and discharge over regular grids, at (grid-cell) resolutions of around 10' to 3° longitude-latitude (~10 to ~300 km), spread over large geographical domains ($>10^4$ km²) (Fekete *et al.*, 2001). MHMs often provide estimates of long-term (>30 years) average runoff, at annual, seasonal and monthly timescales, from global, or regional, data that are consistently available, at an appropriate resolution, for the entire region of interest. Such models are considered particularly useful where actual observational data are sparse, and are characteristically applied without calibration at the individual catchment scale (Arnell, 1999b). MHMs normally run at a daily or monthly time-step and produce estimates of long-term average annual, seasonal, or monthly runoff. They tend to differ from land-surface models (LSMs), which consider the vertical water balance to provide lower-boundary conditions for atmospheric circulation models (GCMs and RCMs), by modelling soil moisture processes and the horizontal movement of water within, and between, cells (Döll *et al.*, 2003).

2.6.2 Worldwide applications of MHMs

Over the last 25 years, MHMs have been applied extensively in many different parts of the world to describe contemporary water availability or to assess potential impacts of future climatic change (e.g. Hidalgo *et al.*, 2009). The areal extent of applications usually ranges from large river basins (e.g. Nijssen *et al.*, 2001b; Wood *et al.*, 1997), to entire continents (e.g. Yates, 1997, for Africa) and the global land surface (e.g. Oki and Kanae, 2006). One of the earliest MHMs, the Water Balance Model (WBM), derived estimates of mean annual and monthly runoff at 0.5° resolution for South America (Vörösmarty *et al.*, 1989) and was later applied at the same spatial resolution to compute contemporary (Fekete *et al.*, 1999) and future runoff for the global land surface (Vörösmarty *et al.*, 2000b).

Macro-PDM, a macro-scale version of the Probability Distribution Moisture model (Moore, 1985), has been used to provide estimates of average annual runoff at 0.5° resolution in Europe (Arnell, 1999b), Africa (Reynard *et al.*, 1997), and the global land surface (Arnell, 1999a; 2003; Gosling and Arnell, 2011). Another MHM, the VIC model, (Liang *et al.*, 1994), also has been applied widely, at resolutions of between 0.25° and 2°, in several large river basins worldwide (e.g. Abdulla and Lettenmaier, 1997; Nijssen *et al.*, 2001a; Nijssen *et al.*, 2001b; Schaner *et al.*, 2012; Wood *et al.*, 1997), for the Indian sub-continent (Raje *et al.*, 2013), and globally (Ziegler *et al.*, 2003). VIC recently has been applied at relatively high resolutions of 0.05°, for 191 catchments in south-east Australia (Zhao *et al.*, 2012) and 5' (0.083°), in the Aksu River basin in north-west China (Zhao *et al.*, 2013). Estimates of long-term average monthly and annual runoff at 0.5° resolution have also been generated for continental Asia using the GBHM model (Yang and Musiak, 2003).

Some MHMs have evolved to combine estimates of runoff with water demand data. For example, WaterGAP2 derived 0.5 ° grids of contemporary (1961-90) and future (2025) water stress for the entire global land surface (Alcamo *et al.*, 2003), and GWAVA, a derivative of Macro-PDM, was used to develop water scarcity indicators for southern Africa (Meigh *et al.*, 1999) and to assess water availability in Central Asia (Tate and Meigh, 2001). Recently, Biemans *et al.* (2013) combined a 0.5° coupled hydrology-crop production model with a river routing scheme at the same resolution (Vörösmarty *et al.*, 2000a) to assess “water requirements and availability for current and future food requirements in five south Asian basins”, including the Indus, Ganges, Brahmaputra.

2.6.3 MHM applications in the Himalaya

Although there have been many hydro-glaciological modelling studies in the Himalaya, there have been relatively few attempts to estimate to describe water resources availability at the regional scale. Prior to this study, Nijssen *et al.* (2001b) had applied VIC at 2° resolution to the Brahmaputra basin, as part of a broader study to improve the parameterisation of the model in large river basins globally. Yang and Musiak (2003) applied the GBHM at 0.5° to calculate mean

annual water balances for 9 major Asian river basins, including the Ganges and Indus, for the period 1972-93. Gosain *et al.* (2006) used the SWAT model (Arnold and Fohrer, 2005) with HadRM2 data to assess climate change impacts on the hydrology of 12 large Indian river basins, including the Ganges, for which annual runoff was predicted to increase by over 10% by 2041-60, compared to the 1981-2000 baseline. A study of future water resources changes and sea-level rise in Bangladesh applied the GWAVA model at 0.5° resolution to the Ganges-Brahmaputra-Meghna basins (Farquharson *et al.*, 2007) for an ensemble of GCM and RCM projections, finding there were “no dramatic changes in the flow regime” between the 2050s and the 1979-99 baseline, but a strong positive trend in flows of the lower Ganges, at Hardinge Bridge, was predicted. In assessing future water availability at a 1° resolution across the whole Indian sub-continent under a range of CMIP3 GCM scenarios, Raje *et al.* (2013) predicted increases, relative to a 1965-74 baseline, to mean monthly flow and low-flows for the lower Ganges (at Farakka) for the future period 2056-2065. The aforementioned study by Biemans *et al.* (2013) applied two RCMs (HadRM3 and REMO for the SRES A1B emissions scenario) at a 0.5° resolution in the LPJmL model for two periods, 1971-2000 (representing present) and 2036 - 2065 (future), to assess future changes in water resource availability and potential crop yields for a variety of potential water use and adaptation options.

A large-scale study of the Upper Indus basin by Immerzeel *et al.* (2009), applying a modified form of the SRM model (which, strictly speaking (§2.6.1), is not a MHM) with TRRM-derived precipitation data and PRECIS regional climate model (SRES A2) output for the period 2071-2099, showed average annual runoff for the Indus and Besham Qila to increase relative to a 2001-2005 baseline, despite an assumed reduction of 50% in glacier ice by 2050 in the basin’s headwater. In a subsequent study, Immerzeel *et al.* (2010), again using a modified form of the SRM but with output from 5 GCMs for the SRES A1B scenarios over the period 2046 - 2065 and assuming glacier reduction commensurate with projected temperature and precipitation changes by 2050, modelled decreases in upstream water supply for the Upper Indus (-8.4%), Ganges (-17.6%) and Brahmaputra (-19.6%). More recently, Lutz *et al.* (2014) applied a high resolution 1 km x 1 km “cryospheric hydrological model” to “quantify the upstream hydrological regimes

of the Indus, Ganges and Brahmaputra” and assessed the potential impact of climate change using an ensemble of 4 CMIP5 GCMs (RCP4.5, RCP8.5) for the period to 2041 – 2050. Annual runoff increases were predicted in all basins, mainly due to increased precipitation and, in the Upper Indus, from accelerated melt.

2.6.4 Representation of glaciers in MHMs

Despite widespread use, the majority of MHMs traditionally have ignored glacial melt-water contributions to long-term discharge by assuming (implicitly, if not explicitly) no net change in ice volume over time. Such an assumption clearly is inappropriate in highly glacierised regions where changes in melt-water are likely to affect river flows. Prior to the commencement of this study, none of the MHMs referred to above accounted for the transient melt-water contributions from retreating glaciers. To this day, few other MHMs account for glaciers in any way.

Two recent adaptations of the VIC model by Schaner *et al.* (2012) and Zhao *et al.* (2013) are notable exceptions. Schaner *et al.* (2012) used data from GLIMS (Global Land Ice Measurements from Space) (Raup *et al.*, 2000) and the Digital Chart of the World (ESRI, 1993) to define the fractional glacier extent of every 0.25° grid cell in an application of VIC in every high-mountain area globally. Glacier melt-water contributions to cell runoff were calculated using an energy balance approach. For the entire 1998-2006 model simulation period, all glacier extents were considered invariant “uniform, flat slabs”. Zhao *et al.* (2013) similarly used an energy balance approach in their high resolution, 0.5' (0.083°), application of VIC in the 42,000 km² Aksu River in north-west China. Glacier extents were derived from the Chinese Glacier inventory and Landsat TM remote sensing data. Glacier topography (elevation, slope and aspect) were obtained from the 10" ASTER GDEM. Glacier area and glacier topography data were defined for each cell but remained constant for the whole model simulation period, 1970 – 2007.

The regional-scale studies by Immerzeel *et al.* (2009, 2010) or Lutz *et al.* (2014) did not apply MHMs (according to a strict definition of the term “MHM”) but their treatment of glaciers certainly is pertinent to this study. In the earlier, 2009, study of the Upper Indus, Immerzeel *et al.* deemed all areas above the elevation of the 5

percentile of a basin-scale snow depletion curve to be permanent snow or ice, and assumed this area to have reduced arbitrarily to 50% by the model future period, 2071 - 2099. A more sophisticated approach was adopted in the Immerzeel *et al.* (2010) study, in which initial glacier extents were calculated to have evolved by the future 2046 - 2065 period according to mass balance changes brought about by “trends in degree day and snowfall between current time and 2050”. Apart from this PhD study, Immerzeel *et al.* (2010) is the first example found of a regional climate impact study that considers progressive changes to glacier extents between present-day and future climate conditions.

The approach by Lutz *et al.* (2013, 2014) to parameterisation of glacier change in large river basins represents a further advance that could benefit future macro-scale hydrological models. Using a “delta change approach” (Kay *et al.*, 2009), similar to that adopted in this study (see §5.6), to represent transition between present-day and the perturbed future climate, Lutz *et al.* (2013) devised a scheme, based on volume-area scaling and a relationship between basin-scale hypsometry and elevation data of the fractional glacier cover in each of the model’s 1 km cells, that allowed mass balance changes to affect a change in the cell glacier cover. Recent advances in high performance computing (HPC) means that application of such high-resolution hydrological models over large domains is becoming more tractable. However, rather than being limited by the technology in future, such models are more likely to be constrained by the availability of ground-based (in-situ) measurements to define inputs and validate outputs at these high resolutions.

At a broader-scale, land-surface schemes of GCMs and RCMs conventionally characterize land-ice as a simple static ice mask, in which grid cells either are entirely covered by ice or are ice-free, the ice extent being uninfluenced by climatic change. Mountain glaciers, even in highly glacierised regions, are often ignored by such schemes because the total ice area is much smaller than that of a GCM, or RCM, grid-cell and, therefore, is considered not to significantly influence atmospheric circulation (Kotlarski, 2007). Schemes employing fractional ice masks (e.g. Dickinson *et al.*, 2006) often represent ice as a simple time-invariant geometric shape. The sub-grid parameterisation of the REMO RCM in the European Alps by Kotlarski (2007) probably was the first scheme of its kind to

explicitly model glacier mass balance and dimension change within cells, the glaciated fraction of an individual cell being adjusted “dynamically depending on accumulation and ablation conditions and following a simple volume-area [scaling] relationship”. Hirabayashi *et al.* (2010) later developed a 0.5° x 0.5° global glacier model (HYOGA) that could be coupled to both land-surface model and MHMs. It similarly allows cell-based mass balance to affect changes to the fractional glacier area according to volume-area scaling derived from observations.

2.7 Summary

This chapter’s review of recent Himalayan research reveals some interesting features of the observed and predicted hydrometeorology. Albeit for a few glaciers in the Karakoram that have been advancing, there is clear evidence of significant glacier shrinkage since the early-1970s but at rates close to the global mean. A general trend of increasing temperatures can be surmised from observations, with increases appearing to be greater in winter than in summer. No such uniform trends have been seen in either the observed precipitation or flows of glacier-fed rivers. The general warming trend in the instrumental record appears set to continue according to most climate-model-based projections for the region. Both CMIP3- and CMIP5-based GCMs consistently predict future warming, with estimates varying considerably depending on which emission scenario is considered. Future projections of precipitation appear far more uncertain, with some climate models predicting reductions in rainfall whereas others predict increases. On average, however, precipitation is expected to increase modestly over the 21st century.

Few hydrological models, whether applied at meso- or macro-scale, account of the presence of glaciers. Results from the relatively few hydrological modelling studies in the Himalaya in which glacier have been explicitly considered, are summarised in Table 2.1. Using either climate-model- or sensitivity-analysis-based scenarios, results again show no uniform trend or consistency in predictions across the region, with changes in mean flow, relative to baseline, ranging from -94% by 2100 (Gilgit at Gilgit, with PRECIS under the SRES A2 emission scenario (Akhtar *et al.*, 2008)) to +100% by 2050 (Hunza River, under a +3 °C sensitivity analysis scenario (Tahir *et al.*, 2011)).

Table 2.1 Summary of mean flow predictions from climate impact modelling studies in the Himalayan region where glaciers have been explicitly considered. The table is partitioned between studies that have used climate-model based representation of future conditions and those that have used sensitivity analysis based approaches. A model’s representation of glacier dynamics (under “Glacier representation”) is denoted “Transient” (i.e. glacier dimensions are allowed to change over time) or “Invariant” (i.e. glacier dimensions do not change over time). Changes in mean flow are as quoted in the corresponding papers albeit rounded to the nearest integer.

Reference	Study Area	Scenario	Glacier representation	Baseline period	Model period	Change in mean flow
<i>Climate-model based studies</i>						
Lutz <i>et al.</i> , 2014	Upper Indus (UIB), Ganges (UGB), Brahmaputra (UBB)	CMIP5 ensemble, RCP4.5 and RCP8.5 scenarios	Transient	1978-2007	2041-2050	-5 to +12% (UIB) up to 27% (UGB) +1 to +13% (UBB)
Immerzeel <i>et al.</i> , 2013	Langtang (360 km ² ; 46% ice) and Baltoro (1415 km ² ; 46% ice)	CMIP5 ensemble, RCP4.5 and RCP8.5	Transient	1961-1990	2021-2100	+31 to +88% (Langtang) +46 to +96% (Baltoro)
Immerzeel <i>et al.</i> , 2012	Langtang (360 km ² ; 46% ice)	CMIP3 ensemble, SRES A1B	Transient	2000-2009	2001-2099	+32% by 2050
Immerzeel <i>et al.</i> , 2010	Upper Indus, Ganges and Brahmaputra basins	CMIP3 ensemble, SRES A1B	Transient	2000-2007	2046-2065	-8% (Indus) -18% (Ganges) -20% (Brahmaputra)

Reference	Study Area	Scenario	Glacier representation	Baseline period	Model period	Change in mean flow
Immerzeel <i>et al.</i> , 2009	Upper Indus (Indus at Besham Qila)	PRECIS RCM, SRES A2, 50% glacier cover	Invariant	2001-2005	2071-2100	+7%
Akhtar <i>et al.</i> , 2008	Hunza (13,925 km ² ; 34% ice), Gilgit (12,800 km ² ; 7% ice), and Astore (3750 km ² ; 16% ice)	PRECIS RCM, SRES A2, with 100%, 50%, 0% of original glacier cover	Invariant	1961-1990	2070-2100	+88 to -65% (Hunza) +70 to -94% (Gilgit) +48 to -72% (Astore)
<i>Sensitivity analysis based studies</i>						
Nepal <i>et al.</i> , 2013	Dudh Kosi (3712 km ² ; 14% ice)	+2, +4°C	Invariant	1986-1997	n/a	+10% (+2°C) +18% (+4°C)
Tahir <i>et al.</i> , 2011	Hunza River (13,733 km ² ; 33% permanent snow or ice, > 5000m)	+10% snow covered area by 2050, +20% by 2075 +2 °C by 2025 +3 °C by 2050	Invariant	2000	2050, 2075	+7% by 2050 +14% by 2075 +64% by 2025 +100% by 2050
Singh and Bengtsson, 2005	Sutlej River (22,275 km ² ; 11% ice, relates to glacier-fed portion only)	+1 , +2, +3°C (T)	Invariant	1996-99	n/a	+16 to -50%

Reference	Study Area	Scenario	Glacier representation	Baseline period	Model period	Change in mean flow
Sharma <i>et al.</i> , 2000	Kosi River (53,000 km ²)	+4 °C	Invariant	1961-90	n/a	-2 to -8%
Wanchang <i>et al.</i> , 2000	Urumqi River (924 km ² ; 4.1% ice)	±20% (P)	Invariant	1984-1996	n/a	±48%
		+0, +1, +2, +3, +4°C (T) ±0, ±10, ±20% (P)				-37 to +28%
Singh and Kumar, 1997	Spiti River (10,000 km ² ; 2.5% ice)	+1, +2, +3°C (T) ±10% (P)	Invariant	1987-1990	n/a	-4 to +24%
		+1, +2, +3°C (T)				+3 to +18%
Braun <i>et al.</i> , 1993	Langtang (360 km ² ; 38% ice)	+2°C	Invariant	1985-90	n/a	+49 to + 91%

3 Hydrometeorological Observations

3.1 Introduction

Accessibility difficulties, due to inadequacies of infrastructure, extreme relief, ruggedness of terrain and variable weather conditions, together with the limited capacity of local measuring authorities and persistent geo-political difficulties, contrive to make hydrometeorological monitoring in the Himalayan region particularly challenging. Compared with more developed countries, the hydrometeorological networks in Himalayan countries are sparse, with the majority of monitoring stations disproportionately distributed at lower elevations (Shankar, 1990). Political tensions and mistrust between the region's countries has also engendered a reluctance by some national measuring authorities to share hydrometeorological data between each other or with the scientific community. Such difficulties clearly are a major barrier to regional hydrological studies. Consequently, our understanding and knowledge of the distribution and variability of key hydrometeorological variables in remote and high elevation areas, which strongly influence Himalayan river flow regimes, is poor, as is our understanding of the possible impacts of climate change on the region's water resources.

This chapter describes how, despite these problems, hydrometeorological data were obtained for the study (§3.2). It then presents the results of some preliminary analyses that were conducted, first, on the rainfall data that were available (§3.3), then temperature data (§3.4) and, finally, river flow data (§3.5). In each case, the general characteristics of the data are described and the possibility of any significant temporal trends explored.

3.2 Approach to data acquisition

Most of the data that were available to the study were obtained through personal contacts or collated from previous studies in the region. The greatest volume of data was obtained from contacts at the Government of Nepal Department for Hydrology and Meteorology (DHM), including all data up to 1996 from their national hydrometric (river flow) and meteorological (rainfall and temperature) networks.

A geographically extensive point-measurement rainfall dataset for other countries in the region was obtained directly from the Climate Research Unit (CRU) at the University of East Anglia, and river flow data for several major rivers in the region were obtained from the World Meteorological Organisation's (WMO) Global Runoff Data Centre (GRDC).

Additional point meteorological (rainfall mainly) and river flow data for Pakistan and India were sourced "unofficially" from various individuals. For Pakistan, these data included: rainfall, temperature and river flow data for catchments in northern Pakistan collated during earlier studies by Prof. David Collins; rainfall, evaporation and river flow data from an earlier study of the Tarbela Dam in Pakistan by CEH (Tate and Farquharson, 2000); and monthly river flow and rainfall data from Dr. David Archer (Newcastle University), who had transcribed data manually from Yearbooks whilst working in Pakistan.

For India, sourced data included: four long-term rainfall datasets for northern India, obtained circuitously from the Indian Meteorological Department (IMD); 10-day river flow data for five gauging stations along the Ganges, via Prof. Syed Hasnain (Jawaharlal Nehru University (JNU), New Delhi); and 10-day river flows for 68 gauging stations in Himachal Pradesh (India) were obtained, courtesy of Prof. Arun Kumar, at the Alternate Hydro Energy Centre (AHEC, IIT-Roorkee), from a previous CEH-led hydropower estimation project in the region (Rees *et al.* 2001). A summary of these is given in Table 3.1

Table 3.1 Summary of hydrometeorological time-series data available to the study

Data type	Country	Source of data	Number of stations	Temporal resolution	Period of Record
Rainfall	Nepal	DHM	244	Daily	1956-1996
	India	CRU	17	Monthly	1848-2000
	India	IMD	4	Daily	1973-1999
	China	CRU	29	Monthly	1935-2000
	Pakistan	CRU	20	Monthly	1861-2000
	Bangladesh	CRU	3	Monthly	1947-1998
	Afghanistan	CRU	1	Monthly	1961-1992
Temperature	Nepal	DHM	119	Monthly	1934-1996
	Pakistan	Various	3	Monthly	1882-1998
Hydrometric (river flows)	Nepal	DHM	54	Daily	1963- 2000
	India	AHEC	68	10-day	1964- 2001
		JNU	5	10-day	1991- 2001
		GRDC	5	Monthly	1949- 1974
	China	GRDC	1	Daily	1956- 1982
	Pakistan	Various	19	Daily, 10-day and monthly	1960- 1999
			6	Monthly	1973- 1982
	Bangladesh	GRDC	4	Daily	1969- 1992

3.3 Rainfall data

The locations of the point-measurement rain-gauge data that were obtained for the study are shown in Figure 3.1. As can be seen, data were available from every country in the region apart from Bhutan. In order to understand how precipitation varied across the region, data for twelve gauges only were selected for analysis. The location of the twelve can also be seen, as black triangles, in Figure 3.1. Brief details of the selected data are provided in Table 3.2. The gauges were chosen at representative locations along the Himalayan arc. All twelve gauges have reasonably long records, ranging from 18 years (Dehradun, 1981-98) to 139 years (Peshawar, 1862-2000).

3.3.1 General characteristics of rainfall distribution in the region

Analysis of the average annual rainfall (AAR, January - December), average winter rainfall (AWR, October - March) and average summer rainfall (ASR, April - September) for the twelve selected rain gauges shows a distinct variation in rainfall from west to east. In Figure 3.2, the gauges are arranged from west (left) to east (right), with the AWR and ASR totals stacked in a bar graph to give the AAR total, in mm, for each gauge. It can be clearly seen that the four most westerly gauges (Kabul, Peshawar, Gilgit and Srinagar) receive considerable less rainfall annually on average than all but one of the gauges further east. The one exception in the “east” is the Shiquahne gauge, which is located on the northern, leeward site of the Himalaya in Tibet, China, and, according to the CRU point-source data, receives only 70 mm annual rainfall on average. Shiquahne aside, the AAR totals in the east are several factors higher than those of the four westernmost gauges: AAR for the four in the west range from 113 mm (Gilgit) to 681 mm (Srinagar); by comparison, the AAR for the seven gauges in the east range from 1297 mm (Kathmandu) to 3552 mm (Pokhara). Despite the general regional differences in annual rainfall totals, considerable local variation exists probably because of gauges’ locations: Gilgit, although at high elevation, is sheltered by surrounding mountains, which would explain its apparent aridity; in the east, Kathmandu’s AAR (1297 mm) is less than half that of both Pokhara to the west (3552 mm) and Darjeeling to the east (2825 mm), probably because Kathmandu also is in a valley and in the lee of surrounding hills and mountains. The high AAR at Pokhara, the highest observed amongst all

twelve selected gauges, is likely because of its proximity to the southern, windward side of the Annapurna massif in central Nepal.

The distinction between the four westernmost gauges and the rest is seen again in Figure 3.3, where AWR (dark grey) and ASR (light grey) are normalised by the gauge's AAR. For all four "western" gauges (Kabul, Peshawar, Gilgit and Srinagar), AWR is a significantly higher proportion of AAR than with any of the easterly gauges, ranging from 68% (Kabul) to 29% (Gilgit) of AAR, compared with 16% (Mandi) to 8% (Darjeeling) in the east. A general downward trend in AWR relative to AAR can be seen from west to east. The trend is also evident when considering the four "western" gauges in isolation (Kabul – Srinagar), so too the eight "eastern" gauges (Mandi - Dibrugarh). In both Figures 3.2 and 3.3, a clear step-change is seen in the rainfall between Srinagar (74.80 °E, 34.10 °N) and Mandi (76.97 °E, 31.72 °N), indicating a change of climatological regime in that part to the Himalaya, which probably corresponds to the transition of the Greater Himalaya mountain range to the more northerly trending Karakoram. A similar discontinuity in the precipitation at this longitude was reported by Bookhagen and Burbank (2010).

These observations, regarding the regional variation in average annual and seasonal rainfall, further reaffirm statements made in the preceding chapter, concerning the region's climate and the influence of the south-westerly summer monsoon (that deposits large volumes of rainfall in the south-east of the region but then weakens progressively as it moves north and west along the Himalayan arc, often to deposit only relatively small volumes in the far north-west of the region) and westerly weather systems (that bring moisture from the Mediterranean region to the far north-west in winter).

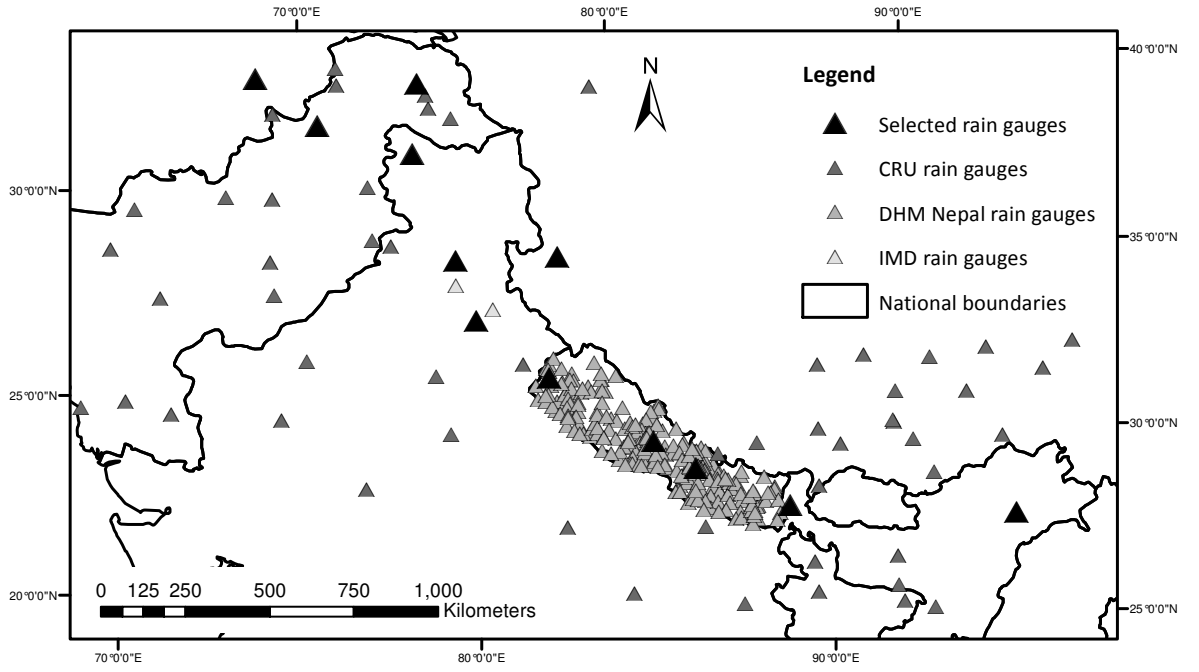


Figure 3.1 Locations of rain gauge data that were available to the study

Table 3.2 Summary of the twelve representative rain gauges selected for analysis

Gauge	Country	Location		Elevation (m ASL)	Average Annual Rainfall (mm)	Average Winter Rainfall (mm)	Period of Record
		(°E)	(°N)				
Kabul	Afghanistan	69.20	34.60	1803	303	206	1961-1992
Peshawar	Pakistan	71.60	34.00	359	363	175	1862-2000
Gilgit	Pakistan	74.33	35.92	1459	113	33	1903-1999
Srinagar	India	74.80	34.10	1587	681	329	1893-2000
Mandi	India	76.97	31.72	768	1442	234	1975-1999
Dehradun	India	78.03	30.32	648	2047	302	1981-1998
Shiquahne	China	80.08	32.50	4279	70	8	1961-1995
Dadelduhar	Nepal	80.58	29.30	1865	1300	231	1970-1994
Pokhara	Nepal	84.00	28.22	827	3552	333	1970-1995
Kathmandu	Nepal	85.37	27.70	1336	1297	143	1970-1994
Darjeeling	India	88.30	27.10	2128	2825	233	1867-1999
Dibrugarh	India	95.00	27.50	111	2711	393	1901-2000

The strong influence of these weather systems can be seen as well when inspecting the monthly rainfall regime of selected gauges (Figure 3.4). In Figure 3.4, mean monthly rainfall data for six of the selected gauges are presented. Again, the gauges are arranged west-east, reading from left-right, and the data (mean monthly rainfall values) are normalised by the AAR to enable comparison. The most westerly gauge, Kabul, is seen to have most of its rainfall over the six-month winter period, with March being the wettest month on average and June the driest of a distinct six-month dry season (June - November). The summer monsoon does not appear to penetrate beyond the Hindu Kush to Kabul. Similarly, March is the wettest month and June is the driest in Peshawar. However, in Peshawar, July and August are relatively wet (August is the second wettest month of the year on average). The increased rainfall in these two months is likely to be the result of the much weakened summer monsoon finally reaching the north-west of the region. The average August rainfall in Peshawar, at 55 mm, is still relatively small in regional terms. The winter-rain/summer-monsoon effect is also seen at Srinagar, which experiences increasing rainfall over winter months, from a November minimum to a maximum in March, then, following a dip in June rainfall, a secondary maximum in August, again presumably because of the monsoon. Only some 320 km as-the-crow-flies (Google Earth, 2013) south-east of Srinagar, in Mandi, a significantly different rainfall regime is seen, one that is dominated by the summer-monsoon. A small peak in rainfall is seen in March, but July and August are, by far, the wettest months. A recession in rainfall is then seen in September, leading to distinct dry season over the winter months, October to February. Pokahara and Darjeeling to the east of the region similarly have well-defined wet- and dry-seasons but, interestingly both have higher June rainfall, which demonstrates they experience the monsoon earlier than the more westerly gauges.

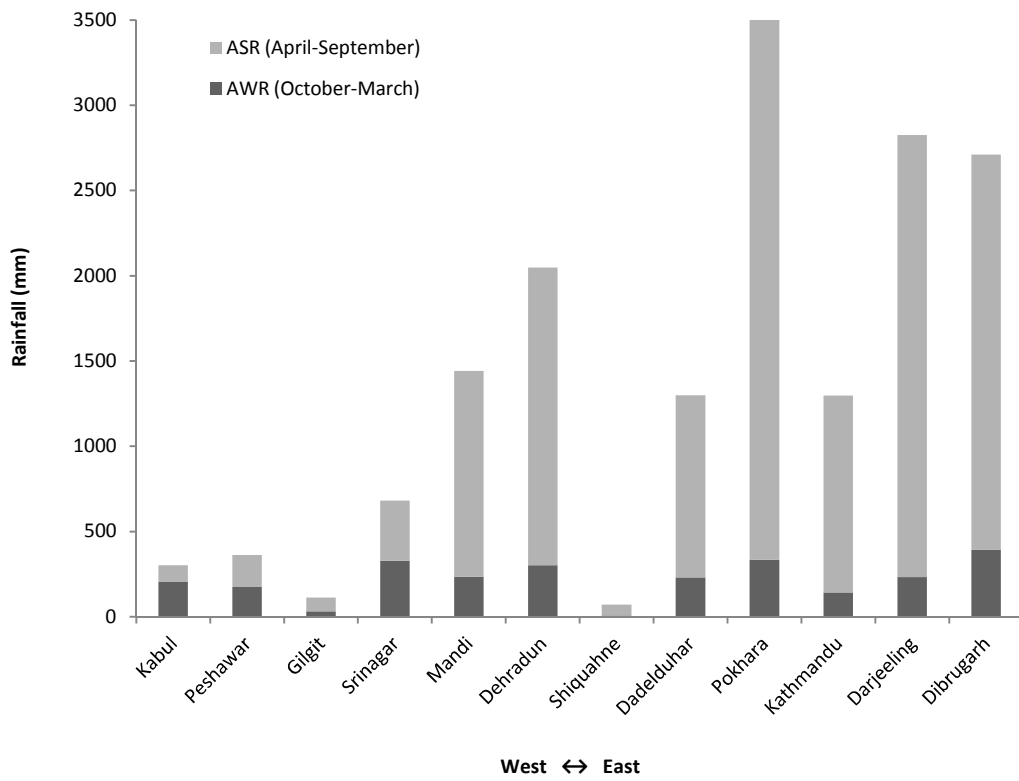


Figure 3.2 Average Winter (October – March) Rainfall (AWR (mm), dark grey) and Average Summer (April – September) Rainfall (ASR (mm), light grey) for 12 selected rain gauges, stacked to show Average Annual Rainfall (AAR) total for each gauge. Data are presented from west to east.

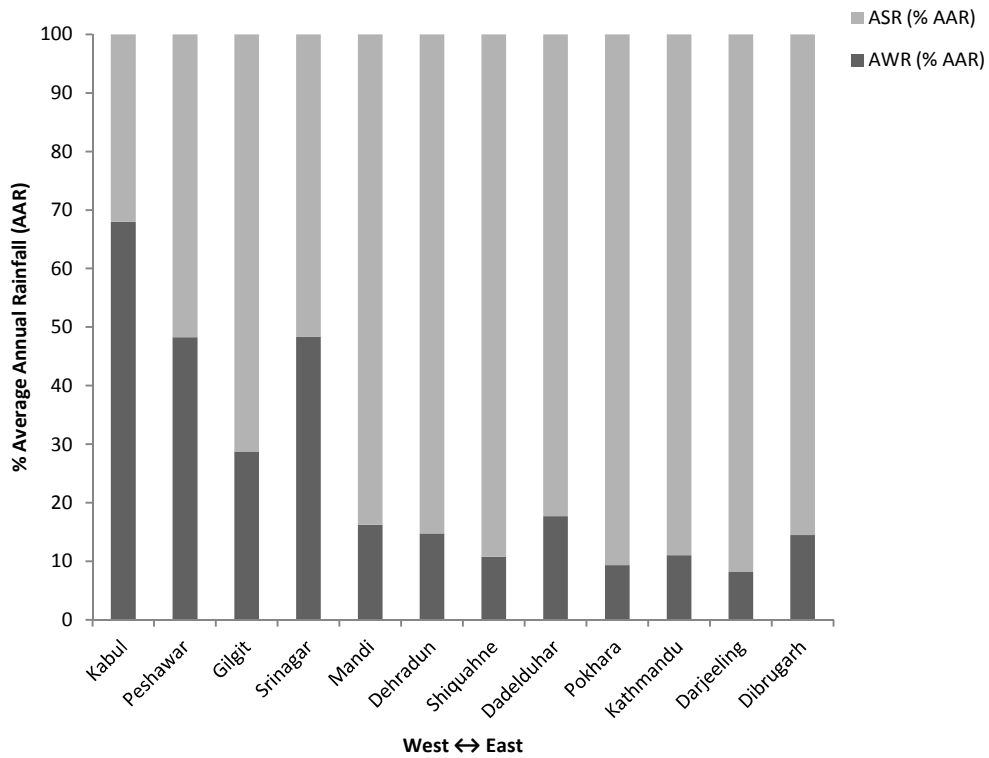


Figure 3.3 Average Winter (October – March) Rainfall (AWR (mm), dark grey) and Average Summer (April – September) Rainfall (ASR (mm), light grey) for 12 selected rain gauges, stacked and shown as a percentage (%) of the Average Annual Rainfall (AAR) total. Data are arranged from west to east.

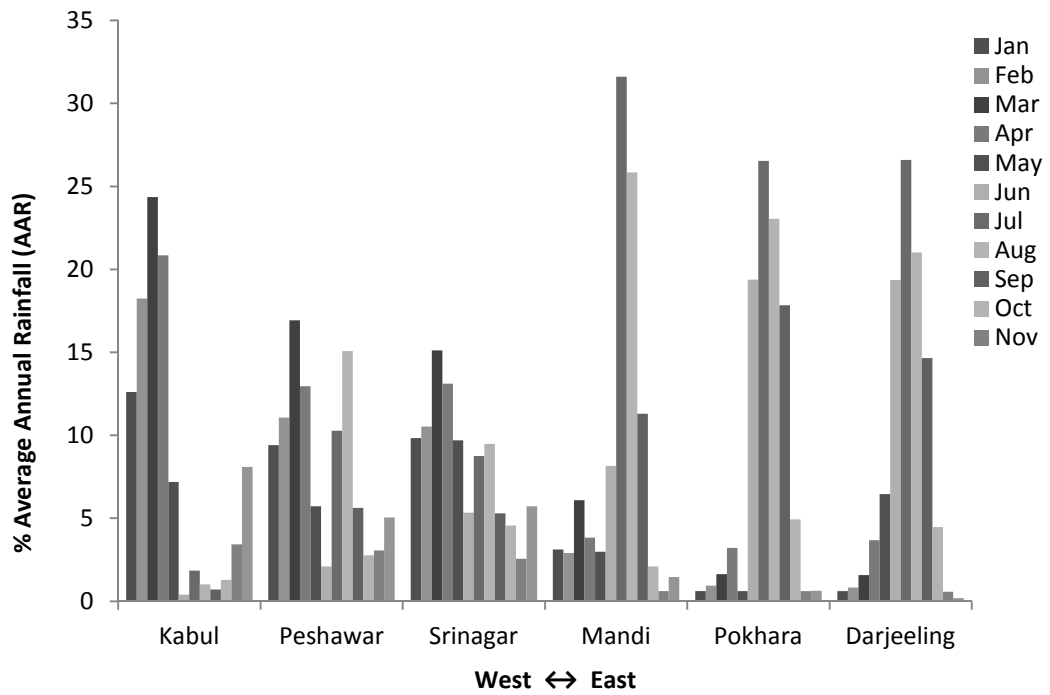


Figure 3.4 *Contrasting rainfall regimes for six selected sites, three in the “west” (Kabul, Peshawar and Srinagar) and three in the “east” (Mandi, Pokhara and Darjeeling); mean monthly rainfall totals shown as a percentage (%) of Average Annual Rainfall.*

A separate analysis of monthly rainfall data from the 244 Nepalese rain gauges, whose locations are shown in Figure 3.5, reveals the rainfall regime in Nepal, not surprisingly, to be dominated by the summer monsoon (Figure 3.6). On average, 90% of the national Average Annual Rainfall (calculated simply as the arithmetic mean of all gauges' average annual rainfall (i.e. no areal weighting applied)) occurs in the summer six-month period, April-September. As seen earlier, in Figure 3.4 with the easterly rain gauges, July and August are the wettest months, with average monthly rainfall totals of 457 mm and 394 mm respectively. Rainfall reduces sharply post-monsoon, reaching a minimum of just 1 mm on average in November, the driest month of a six-month dry-season between October and March. A small increase in rainfall is seen in April, then a further dip is seen with May rainfall before the onset of the monsoon in June. Figure 3.6 shows there is considerable variability nationwide in the average monthly rainfall totals for the wetter months (June – September), as indicated by the extent of the boxes and whiskers, but strong coherence over the drier months.

3.3.2 Correlation Analyses

Correlation analyses were conducted to explore whether relationships exist between observed average annual, seasonal and monthly rainfall totals and the location of rain gauges, as described by their longitude (°E), latitude (°N), and elevation (m ASL), that might help either the definition of the model or the later interpretation of results. The output of a correlation analysis between any two variables is a “correlation coefficient”, which is a “measure of the extent the variables vary together, that is, whether large values of one variable tend to be associated with large values of the other (positive correlation), whether small values of one variable tend to be associated with large values of the other (negative correlation), or whether values of both variables tend to be unrelated (correlation near zero). The correlation coefficient is scaled so that its value is independent of the units in which the two variables are expressed and has a value of between -1 and +1 inclusive” (Microsoft, 2014).

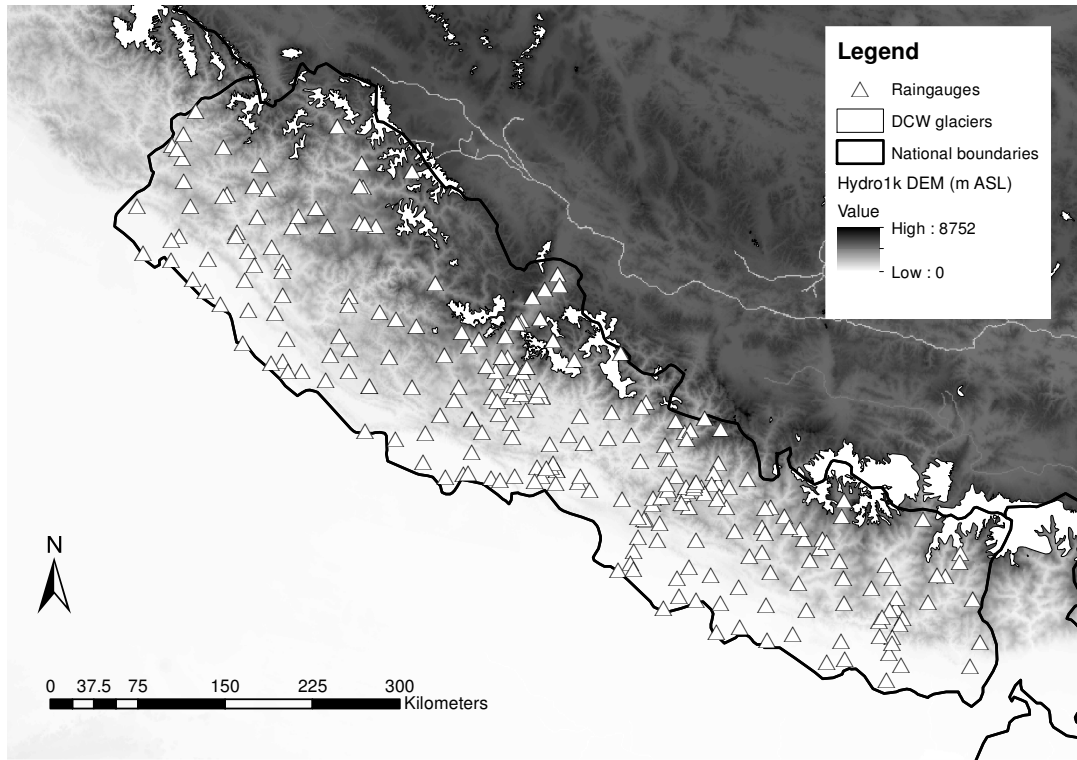


Figure 3.5 Locations of 244 Nepalese rain gauges whose data were available to the study, mapped onto a the Hydro1k DEM and showing the DCW glaciers

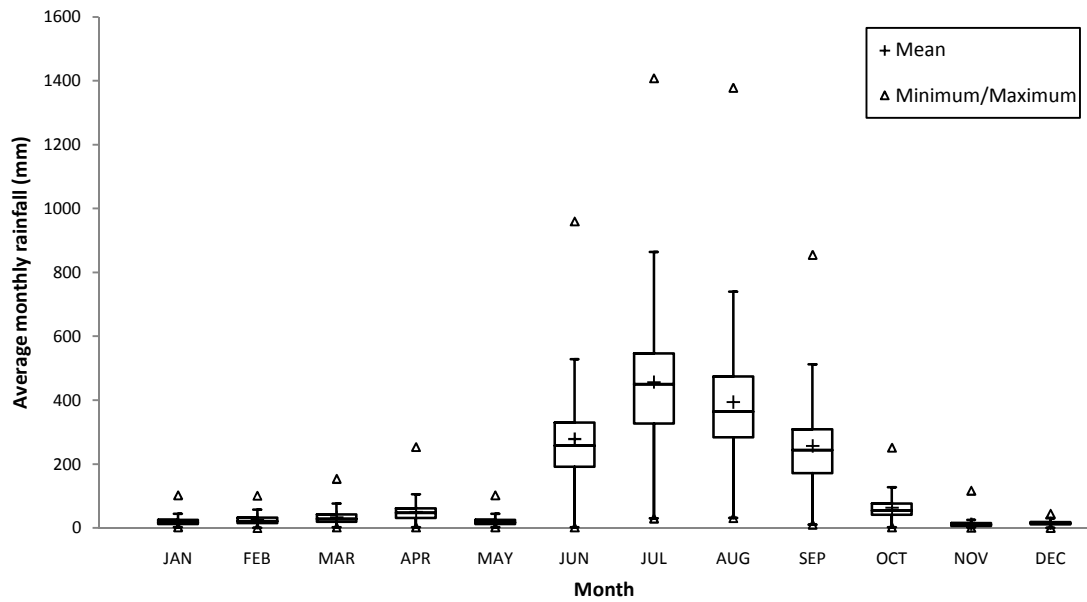


Figure 3.6 Box and whisker plot of average monthly rainfall for 244 Nepalese rain gauges, showing the mean (of average monthly values) (+), median (central line of the box), first and third quartile values (extremes of the box), ± 1.5 times the inter-quartile range (extremes of the whiskers), and minimum and maximum values (triangles) for each month.

The correlation analysis was conducted separately on two sets of data: first, on the average annual, seasonal and monthly rainfall data, and location data, of the twelve selected “representative” rain gauges listed in Table 3.2; and, second, on the equivalent data of the 244 Nepalese rain gauges shown in Figure 3.5. The results of both analyses are shown in Tables 3.3 and 3.4, respectively. The correlation coefficients in both tables are colour coded red to blue, to help legibility, with red signifying a positive correlation of +1, blue a negative correlation of -1.

Considering, first, the results in Table 3.3, for the twelve “representative” rain gauges, as might be expected, the analysis shows Average Annual Rainfall (abbreviated to AN in the table) is perfectly correlated with Average Summer Rainfall (SM), with a correlation coefficient, r , of +1.00, and is also very strongly correlated with the average monthly rainfall for June ($r = +0.96$), July (+0.98), August (+0.95), September (+0.98) and October (+0.97). There appears to be no correlation ($r \approx 0$) between AN and December (+0.01), January (-0.03) or February (+0.11) average monthly rainfall. It is interesting to note the strong negative correlation ($r = -0.83$) between AN and the latitude (LT) of gauges, and the slightly weaker positive correlation ($r = +0.73$) between AN and their longitude (LN). This indicates that the horizontal location of a gauge has strong influence on annual and summer rainfall and confirms the earlier analysis that rainfall totals appear generally to reduce from east to west and south to north. Surprisingly, AN and SM appear to be negatively correlated, albeit rather weakly, with the elevation (HT) of the rain gauge ($r = -0.41$ and -0.37 , respectively). This is surprising because rainfall is generally expected to increase with elevation up to certain thresholds (Adam *et al.*, 2006; Singh and Kumar, 1997, Lauer, 1975). The inclusion of Gilgit, Shiquahne and Kathmandu in the analysis (each at high-elevation yet having depressed rainfall due to local rain-shadow effects) possibly explains this unexpected divergence. Average Winter Rainfall (WN) in the table appears to be strongly positively correlated with rainfall November (+0.9), February (+0.81) and March (+0.87). Slightly weaker correlations are seen between WN and December and January rainfall ($r = +0.68$ and $+0.69$, respectively). Recalling Figure 3.4, this is probably because of the mix of rainfall regimes that comprise this rather limited dataset. WN is reasonably positively correlated with AN (+0.70). WN only

weakly correlates with the horizontal location of gauges ($r = +0.37$ for LN and -0.46 for LT) and slightly more strongly and negatively with elevation HT (-0.64).

Considering Table 3.4, the results of the correlation analysis between all 244 Nepalese rain gauges, we see, again, AN perfectly correlated with SM, very strongly correlated with each month's rainfall from June to September ($r = +0.95$ to $+0.97$), and not correlated ($r = +0.14$ to $+0.23$) with December to February rainfall. Surprisingly, there is a distinct lack of correlation between the average rainfall statistics and either the horizontal location (latitude and longitude) or elevation of rain gauges in Nepal (e.g. $r = +0.07$, -0.12 and -0.15 for LN, LT and HT versus AN). This could be a result of the considerable variability in the spatial distribution and magnitude of rainfall in Nepal. Temporally, however, the results confirm Nepal's rainfall universally is strongly seasonal.

Table 3.3 Correlation analysis of average monthly (J-D), summer (SM, A-S), winter (WN, O-M) and annual (AN) rainfall data against latitude (LT), longitude (LN), and height of station (HT), for the 12 selected rain gauges

	LN	LT	HT	J	F	M	A	M	J	J	A	S	O	N	D	AN	SM	WN
LN	1.00																	
LT	-0.88	1.00																
HT	-0.10	0.16	1.00															
J	-0.26	0.13	-0.44	1.00														
F	-0.09	-0.03	-0.50	0.94	1.00													
M	0.03	-0.12	-0.65	0.88	0.91	1.00												
A	0.70	-0.56	-0.51	0.25	0.47	0.54	1.00											
M	0.73	-0.51	-0.31	0.11	0.31	0.40	0.87	1.00										
J	0.78	-0.84	-0.28	-0.15	0.01	0.13	0.67	0.52	1.00									
J	0.67	-0.83	-0.35	-0.02	0.06	0.26	0.51	0.39	0.93	1.00								
A	0.60	-0.78	-0.38	0.03	0.11	0.32	0.45	0.32	0.87	0.98	1.00							
S	0.70	-0.81	-0.33	-0.09	0.04	0.19	0.60	0.41	0.98	0.97	0.93	1.00						
O	0.79	-0.81	-0.38	-0.05	0.13	0.27	0.77	0.61	0.98	0.90	0.86	0.96	1.00					
N	0.53	-0.49	-0.58	0.42	0.58	0.67	0.92	0.72	0.69	0.59	0.57	0.67	0.81	1.00				
D	-0.25	0.08	-0.41	0.90	0.89	0.75	0.27	-0.04	-0.05	0.00	0.03	0.01	0.03	0.43	1.00			
AN	0.73	-0.83	-0.41	0.04	0.18	0.35	0.68	0.53	0.96	0.98	0.95	0.98	0.97	0.74	0.07	1.00		
SM	0.75	-0.85	-0.37	-0.03	0.11	0.28	0.65	0.51	0.97	0.98	0.95	0.98	0.96	0.70	0.01	1.00	1.00	
WN	0.37	-0.46	-0.64	0.69	0.81	0.87	0.78	0.56	0.56	0.59	0.61	0.59	0.67	0.90	0.68	0.70	0.65	1.00

Table 3.4 Correlation analysis of average monthly (J-D), summer (SM), winter (WN) and annual (AN) rainfall data against latitude (LT), longitude (LN), and height of station (HT), for Nepal rain gauges (n = 244)

	LN	LT	HT	J	F	M	A	M	J	J	A	S	O	N	D	AN	SM	WN
LN	1.00																	
LT	-0.82	1.00																
HT	0.02	0.44	1.00															
J	-0.59	0.64	0.18	1.00														
F	-0.47	0.60	0.24	0.85	1.00													
M	-0.17	0.47	0.40	0.70	0.81	1.00												
A	0.43	-0.19	0.14	0.10	0.31	0.57	1.00											
M	-0.59	0.64	0.18	1.00	0.85	0.70	0.10	1.00										
J	0.17	-0.20	-0.17	0.01	0.08	0.29	0.54	0.01	1.00									
J	0.06	-0.19	-0.25	0.04	0.09	0.19	0.41	0.04	0.91	1.00								
A	-0.02	-0.03	-0.11	0.12	0.17	0.29	0.36	0.12	0.89	0.94	1.00							
S	0.13	-0.22	-0.21	0.03	0.06	0.21	0.46	0.03	0.88	0.94	0.90	1.00						
O	0.36	-0.35	-0.14	-0.03	0.04	0.27	0.64	-0.03	0.76	0.72	0.65	0.81	1.00					
N	0.20	-0.07	0.15	0.10	0.06	0.34	0.43	0.10	0.58	0.45	0.49	0.56	0.52	1.00				
D	-0.45	0.47	0.12	0.69	0.75	0.63	0.23	0.69	0.11	0.18	0.19	0.15	0.07	-0.02	1.00			
AN	0.07	-0.12	-0.15	0.14	0.20	0.35	0.52	0.14	0.95	0.97	0.96	0.96	0.78	0.56	0.23	1.00		
SM	0.08	-0.15	-0.18	0.08	0.14	0.29	0.48	0.08	0.95	0.98	0.97	0.96	0.76	0.54	0.19	1.00	1.00	
WN	-0.09	0.24	0.16	0.64	0.71	0.85	0.66	0.64	0.59	0.53	0.57	0.59	0.67	0.54	0.60	0.67	0.61	1.00

3.3.3 Exploring trends in available rainfall data

A cursory analysis was undertaken to explore whether temporal trends existed in the annual rainfall data of the twelve representative rain gauges. An interesting picture emerged from the available data, showing a distinct difference, again, between east and west, with annual rainfall totals appearing to decrease over time in the east but increasing in the west. Figure 3.7 shows a plot of annual rainfall totals at Darjeeling (in the east) for the 111-year period, 1868 – 1978, with a linear least-squares trend-line fitted that shows annual rainfall declining at a rate of about 4.5 mm per year, c. 0.16% of the Average Annual Rainfall (AAR). In contrast, the plot of annual rainfall totals in Peshawar (Figure 3.8) shows annual rainfall increasing over the 138-year period, 1863 – 2000, at a rate of about 0.7 mm per year (c. 0.18% of the AAR). Both trends were found to be statistically significant at the 5% level using Student's t-test (t -value > 2 and $p < 0.05$) and the Mann-Kendall trend test (Hirsch *et al.*, 1982). A plot of annual rainfall totals at the more centrally located Pokhara (Figure 3.9) for a shorter 26-year period, 1970-95, revealed no significant trend.

Further analysis of 63 of the longest records in Nepal, each having complete 26 years' data, shows the annual average rainfall (of all 63) appearing to decline over the period 1970 – 1995 (Figure 3.10). However, regression statistics and the Mann-Kendall trend test found this apparent trend not to be statistically significant at the 5% level, possibly because of the limited duration of the annual time-series. A more detailed analysis of trends in the region's rainfall data was considered to be beyond the scope of the study.

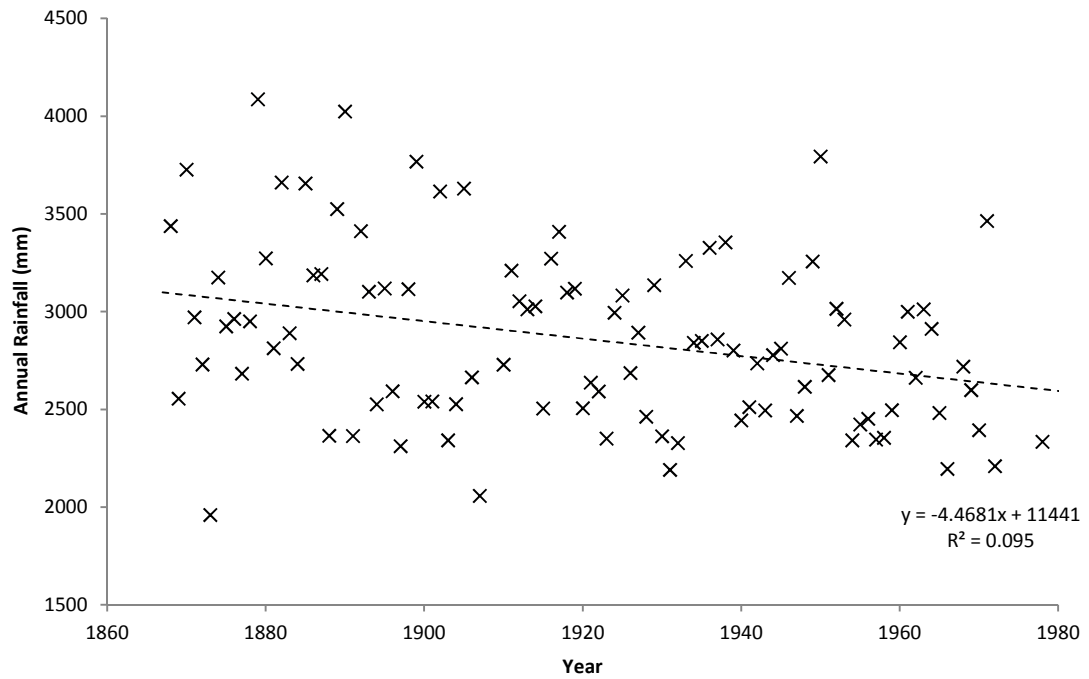


Figure 3.7 Year-to-year variation in the annual rainfall total (mm) at Darjeeling (India) for the 111-year period, 1868 – 1978; the apparent downward trend is statistically significant at the 5% level

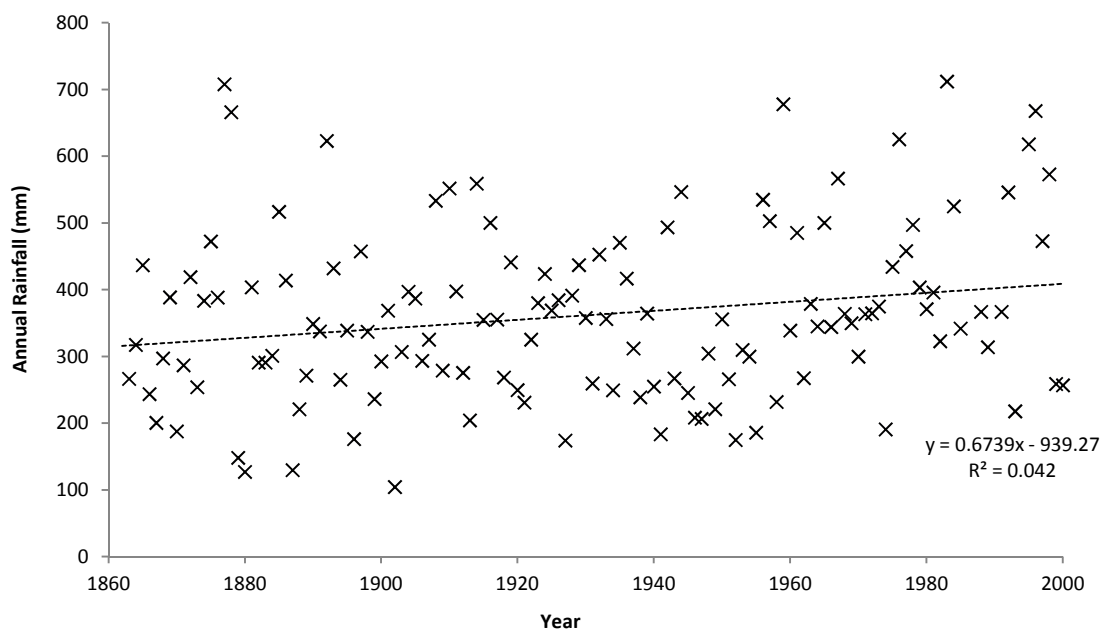


Figure 3.8 Year-to-year variation in the annual rainfall total (mm) at Peshawar (Pakistan) for the 138 year-period, 1863 – 2000; the apparent upward trend is statistically significant at the 5% level

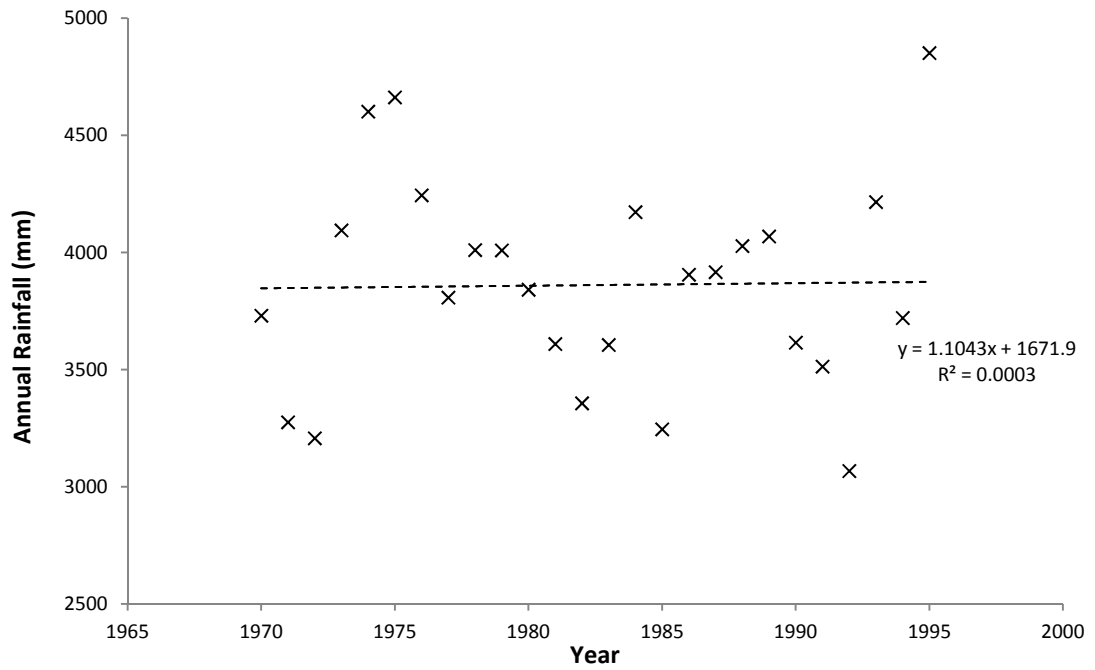


Figure 3.9 Year-to-year variation in the annual rainfall total (mm) at Pokhara (Nepal) for the 26-year period 1970 – 1995; no trend is seen

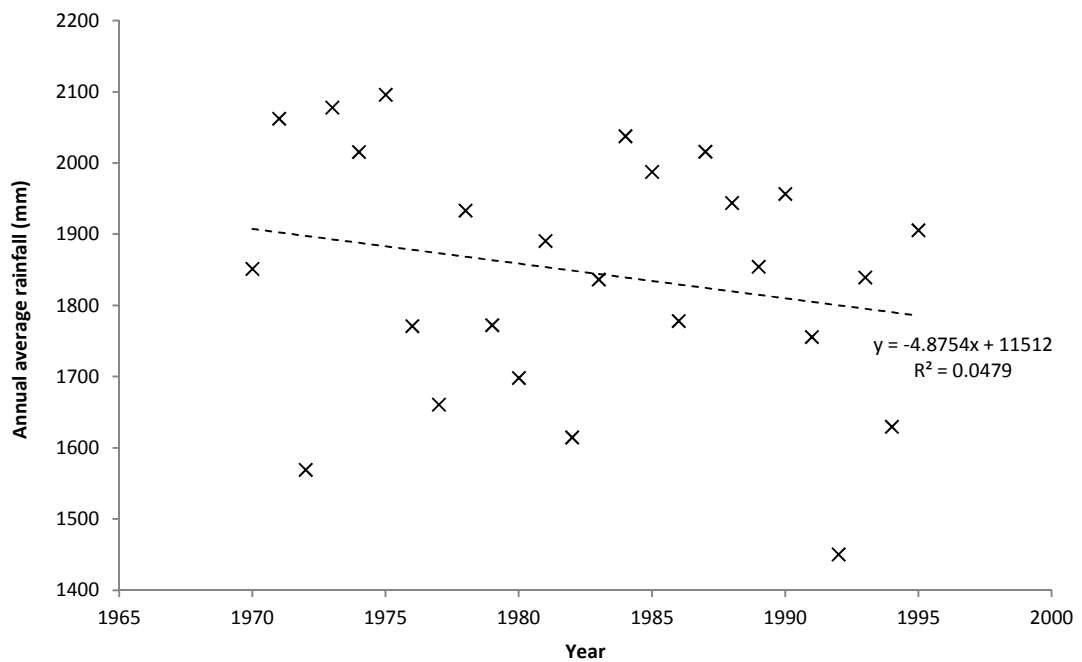


Figure 3.10 Year-to-year variation in Annual Average Rainfall (mm) for 63 Nepalese rain gauges having data from 1970-95; the apparent trend is not statistically significant

3.4 Temperature Data

Air temperature is likely to be a key factor in determining the future response of glaciers to climatic warming. It was considered important, therefore, for the design of the proposed regional hydrological model, to gain an understanding of how temperature varied across the region through the analysis of available data.

3.4.1 General characteristics of temperature variation across the region

Monthly mean temperature data were obtained for 119 gauges having at least 5 years' data from the Nepalese climatology network; their spatial distribution is shown in Figure 3.11. The earliest observation dates back to 1934 and the latest available to 1996. Figure 3.12 illustrates the temporal evolution of the network over this period: with only 6 stations having observations pre-dating 1961, the network tripled in size between 1961 and 1966 and then grew steadily for the next 10 years, until about 1976, at which point the national network comprised some 73 gauges. Network growth continued modestly over the next couple of decades, attaining maximum coverage of 100 stations in 1991. Due to this continual growth, no attempt was made in this study to define a common period as the basis for the temperature analyses. Instead, the following analyses were conducted on the basis of all available data from 1961 to 1996.

Inspection of 12 mean monthly temperatures for Nepal (calculated as the arithmetic means for each respective month from all available monthly time-series) reveals (Figure 3.13) that February is the coldest month and that temperatures rise steadily thereafter, reaching a maximum in May or June, prior to the summer monsoon. Further increases in mean monthly temperatures are probably suppressed in July and August due to the cooling effect of the monsoon. Temperatures decline, as expected, over post-monsoon, autumn, months. The coldest monthly (mean) temperature recorded over the 1961-96 period is -11.4°C at Tengboche in central Nepal, at an elevation of 3857 m ASL, in February 1978. The warmest monthly (mean) temperature over the same period is $+37.5^{\circ}\text{C}$, recorded in May 1972 at Paklihawa in the south east of the country, at an elevation of 100 m ASL.

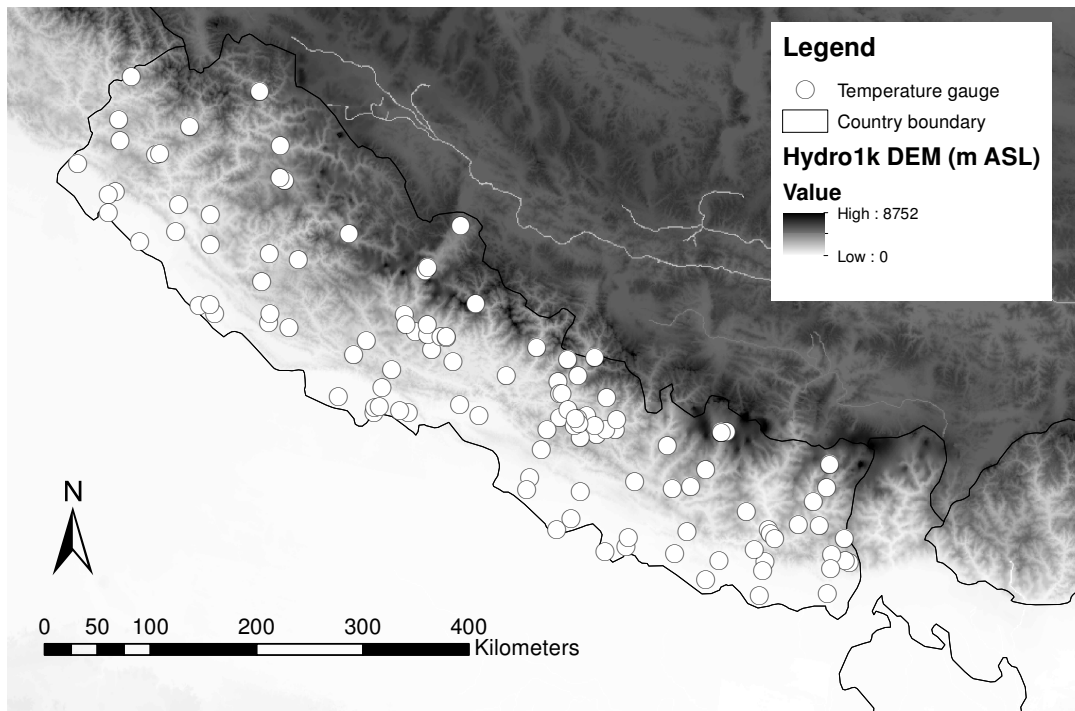


Figure 3.11 Location of temperature gauges whose data were obtained for the study

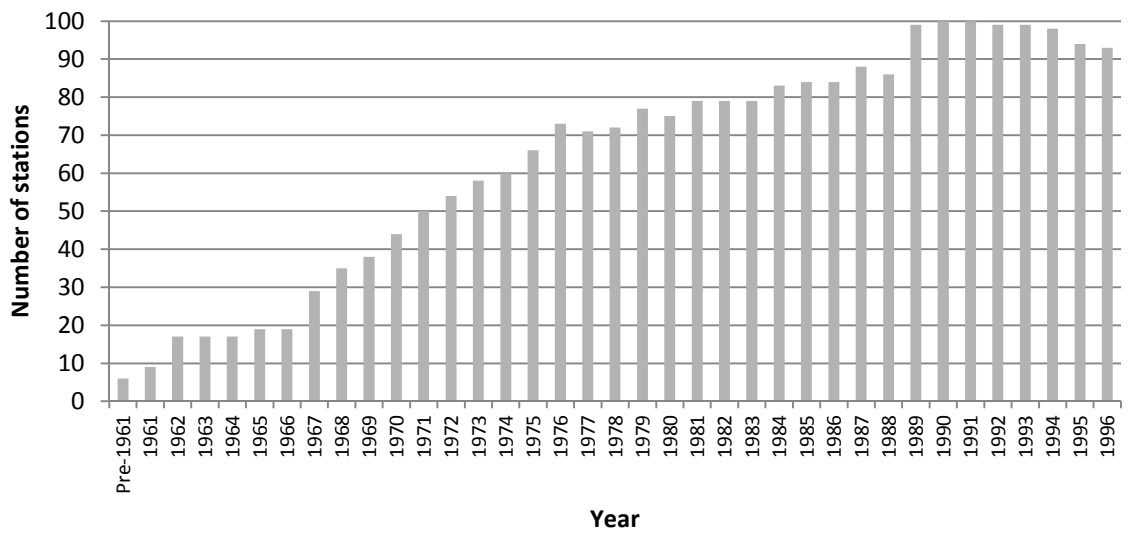


Figure 3.12 Number of temperature gauges having data in a given year (e.g. by 1990, temperature was being recorded at 100 gauges)

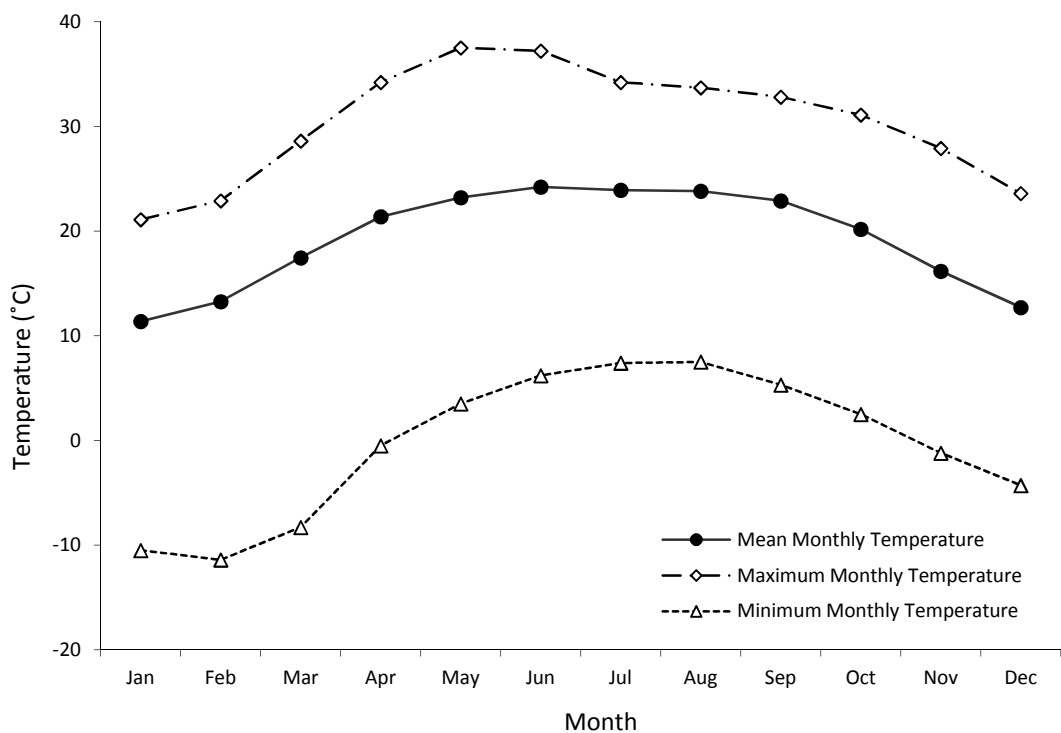


Figure 3.13 Mean monthly temperature, maximum monthly temperature and minimum monthly temperature in Nepal for the period 1961-96 (all stations, n =119)

3.4.2 Correlation analyses

Mean annual (AN), seasonal (summer (SM) and winter (WN)) and monthly (J-D) temperature values were derived for every temperature gauge from their monthly mean temperature time series. Correlation analysis was applied to explore the relationship between the mean annual, seasonal and monthly temperatures and gauge locations, as defined by their longitude (LN), latitude (LT) and elevation (HT, m ASL). The results, shown in Table 3.5, indicate that annual mean temperatures (AN) correlate perfectly ($r = +1.0$) with the summer seasonal temperatures (SM) and those of the summer months (May to September). Very strong positive correlations are seen between AN and every month's data ($r \geq +0.97$) and also from month to month, with the mean monthly temperature for any month very strongly, if not perfectly, correlated ($r = +0.99$ or $+1.0$) with the temperature of the previous and following months. Interestingly, strong positive correlations are maintained even between the most distant months (e.g. January – June), where $r = +0.95$. This is probably because any gauge having a high June temperature relative to others can be expected to have a relatively high January temperature too, with elevation likely to be the determining factor on a gauge's temperature at any time of year.

Annual, seasonal and mean monthly temperatures (J-D) are all very strongly negatively correlated with elevation (HT), with r ranging from -0.96 to -0.98 , which confirms that mean temperatures in Nepal universally reduce with elevation. However, there appears only to be a weak negative correlation between the mean monthly temperatures and gauges' horizontal locations (LN and LT), with r ranging from -0.09 to -0.31 with LN and from -0.21 to -0.37 with LT. This apparent lack of correlation with horizontal location may be explained by the weak correlation between HT and LN ($+0.19$) and LT ($+0.32$), which indicates the elevation of temperature gauges (an important factor in determining temperature) is variable in Nepal and not dependant on horizontal location.

Table 3.5 Correlation analysis of monthly (J-D), summer (SM), winter (WN) and annual (AN) average temperatures at Nepalese gauges against latitude (LT), longitude (LN), and height of station (HT) (n = 119)

	LN	LT	HT	J	F	M	A	M	J	J	A	S	O	N	D	AN	SM	WN
LN	1.00																	
LT	-0.70	1.00																
HT	0.19	0.32	1.00															
J	-0.12	-0.34	-0.96	1.00														
F	-0.12	-0.34	-0.96	1.00	1.00													
M	-0.14	-0.34	-0.97	0.99	1.00	1.00												
A	-0.20	-0.31	-0.97	0.98	0.99	0.99	1.00											
M	-0.29	-0.23	-0.97	0.96	0.97	0.98	0.99	1.00										
J	-0.31	-0.21	-0.97	0.95	0.96	0.97	0.98	0.99	1.00									
J	-0.28	-0.22	-0.97	0.96	0.96	0.97	0.97	0.99	1.00	1.00								
A	-0.26	-0.24	-0.97	0.96	0.97	0.97	0.98	0.99	0.99	1.00	1.00							
S	-0.25	-0.26	-0.97	0.97	0.97	0.98	0.98	0.99	0.99	1.00	1.00	1.00						
O	-0.17	-0.32	-0.98	0.98	0.99	0.99	0.99	0.98	0.98	0.98	0.99	0.99	1.00					
N	-0.12	-0.35	-0.97	0.99	0.99	0.99	0.99	0.97	0.96	0.97	0.97	0.98	0.99	1.00				
D	-0.09	-0.37	-0.96	1.00	0.99	0.99	0.98	0.96	0.95	0.95	0.96	0.97	0.99	1.00	1.00			
AN	-0.20	-0.30	-0.98	0.99	0.99	0.99	1.00	0.99	0.99	0.99	0.99	0.99	1.00	0.99	0.99	1.00		
SM	-0.26	-0.25	-0.98	0.97	0.97	0.98	0.99	1.00	1.00	1.00	1.00	1.00	0.99	0.98	0.97	1.00	1.00	
WN	-0.13	-0.35	-0.97	1.00	1.00	1.00	0.99	0.97	0.97	0.97	0.97	0.98	0.99	1.00	1.00	0.99	0.98	1.00

3.4.3 Temperature variation with elevation

As evidenced in the previous sub-section, temperature generally decreases with elevation in Nepal. The rate at which temperature decreases with increasing elevation is called the *lapse rate*. The average atmospheric temperature lapse rate globally is about $-6.5^{\circ}\text{C}/\text{km}$ but this value can vary depending to time and location (Barry, 2008).

Analysis of the Nepalese data reveals some interesting features about the variation of temperature and lapse rates in the Himalaya. Using all available data, a single national time series of monthly lapse rates was derived by applying a simple linear regression between monthly mean temperature and station elevation for all available temperature gauges for every month from 1961 to 1996. The slope of each month's regression line (dT/dH) provides the monthly lapse rate and the intercept corresponds to the mean monthly seal-level temperature, at 0 m ASL. The resulting time-series (Figure 3.14) reveals some consistent behaviour in lapse rates from year-to-year, with maxima (most negative lapse rates) regularly occurring immediately pre- and post-monsoon (in April/May and October), and two distinct minima (most positive lapse rates) in December/January and July/August. This "M" shaped profile is more clearly seen when taking the average of the monthly lapse rates (Figure 3.15): the average monthly lapse for Nepal varies from about $-4.7^{\circ}\text{C}/\text{km}$ in December and $-4.9^{\circ}\text{C}/\text{km}$ in July, to about $-6.4^{\circ}\text{C}/\text{km}$ in April. This variation in lapse rates is possibly to be determined by air moisture content, which, in Nepal is strongly dependent on the monsoon: the drier the air the higher (more negative) the lapse rate becomes (*pers. comm.* Richard Harding).

Such temporal variations in temperature lapse rates potentially have significant implications for hydrological modelling, affecting both the partitioning of rain and snow and the melting of snow and ice. Several studies (e.g. Blandford *et al.*, 2008; Chiu *et al.*, 2014; Rolland, 2003; Komatsu *et al.*, 2010) have shown lapse rates varying seasonally under different conditions, yet, temperature lapse rate is held constant in most hydrological models. A notable exception is a model applied by Wanchang *et al.* (2000) in the Urumqui River basin in China, where monthly temperature lapse rates were applied for each month of a 1984-1996 simulation.

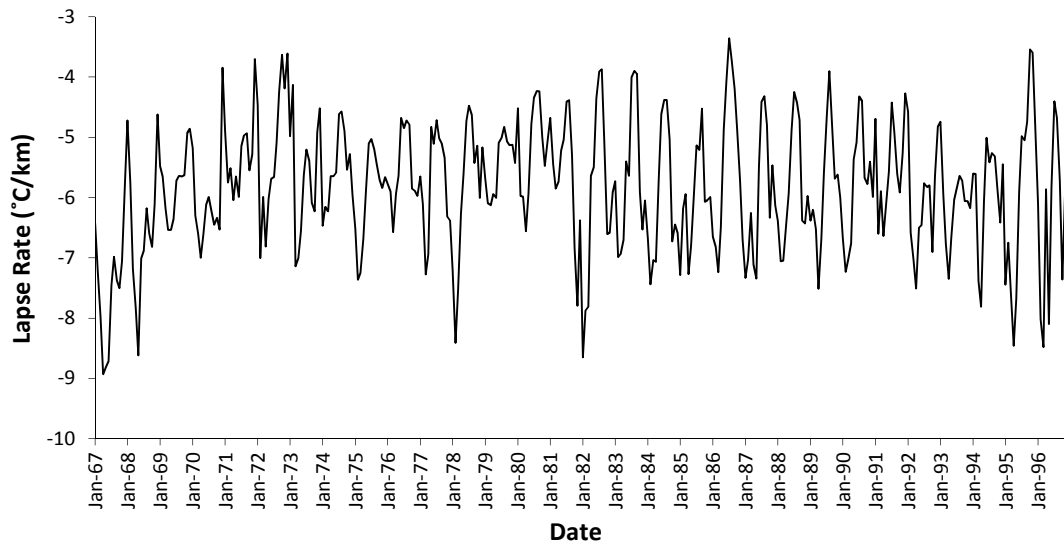


Figure 3.14 Time-series of derived monthly lapse rates in Nepal, from January 1961 to December 1996

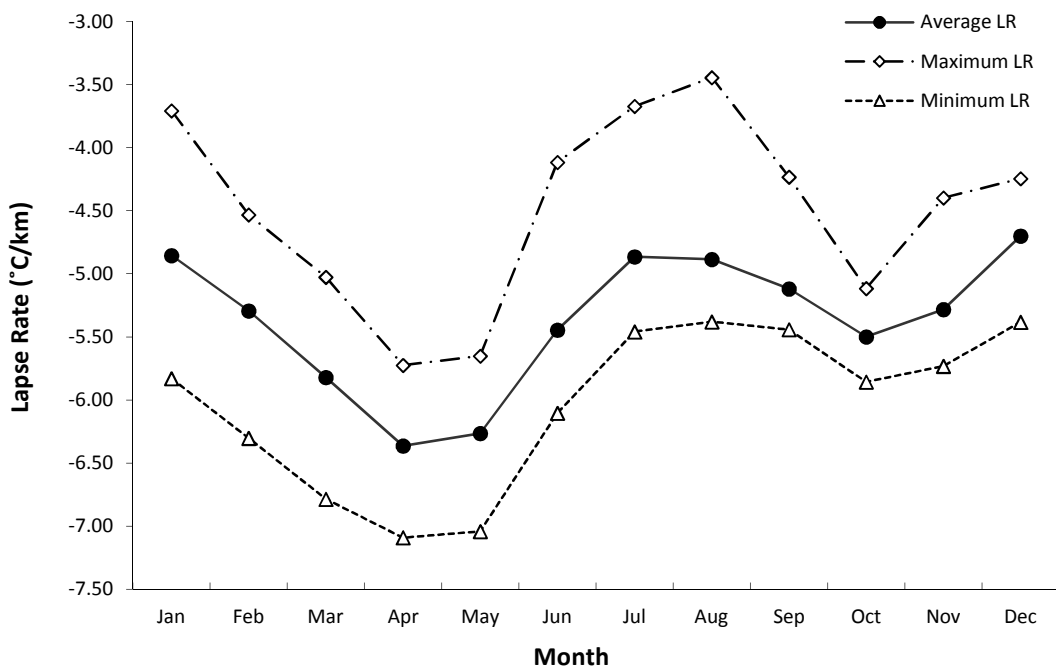


Figure 3.15 Average, maximum and minimum monthly temperature lapse rates (LR) in Nepal for the period 1961-96, derived from 119 temperature gauges nationally

3.4.4 Exploring trends in the available temperature data

Analysing the annual mean temperatures of the 119 temperature gauges in Nepal reveals a statistically significant upward trend in temperature over the period 1961 to 1996 (Figure 3.16), showing a rate of increase of almost 0.07 °C/year. The result is consistent with that of Shrestha *et al.* (1999) who reported similar increases in annual maximum temperatures in Nepal. Figure 3.16 represents the annual mean temperature for all 119 gauges whose elevations range from between 72 m and 4100 m above sea level (ASL). However, on inspecting of annual mean temperature values for the 15 highest temperature gauges in Nepal (Figure 3.17), at elevations above 1800 m (approximately 1 standard deviation above the national mean station elevation), even higher annual increases, of about 0.14 °C/year, are seen, albeit over a shorter thirty-year period, from 1967 to 1996. The apparent trend was found to be statistically significant at the 5% level, according to Student's t-test and the Mann-Kendall trend test. Such observed increases in temperature, particularly at high elevation, coupled with a possible downward trend in rainfall as described in §3.3, could help to explain the reported rapid retreat of Nepalese glaciers (Chapter 2).

Few long time-series of temperature data were available beyond Nepal. One of the longest was for a gauge in Peshawar, Pakistan, which had monthly mean temperature data from 1931 to 2000. Annual mean temperatures were derived from the monthly series for each year of the period of record and plotted, as shown in Figure 3.18. A linear least-squares trend-line fitted through the points suggests a small increase in annual temperature over the period, but this trend was found not to be statistically significant at the 5% significance level.

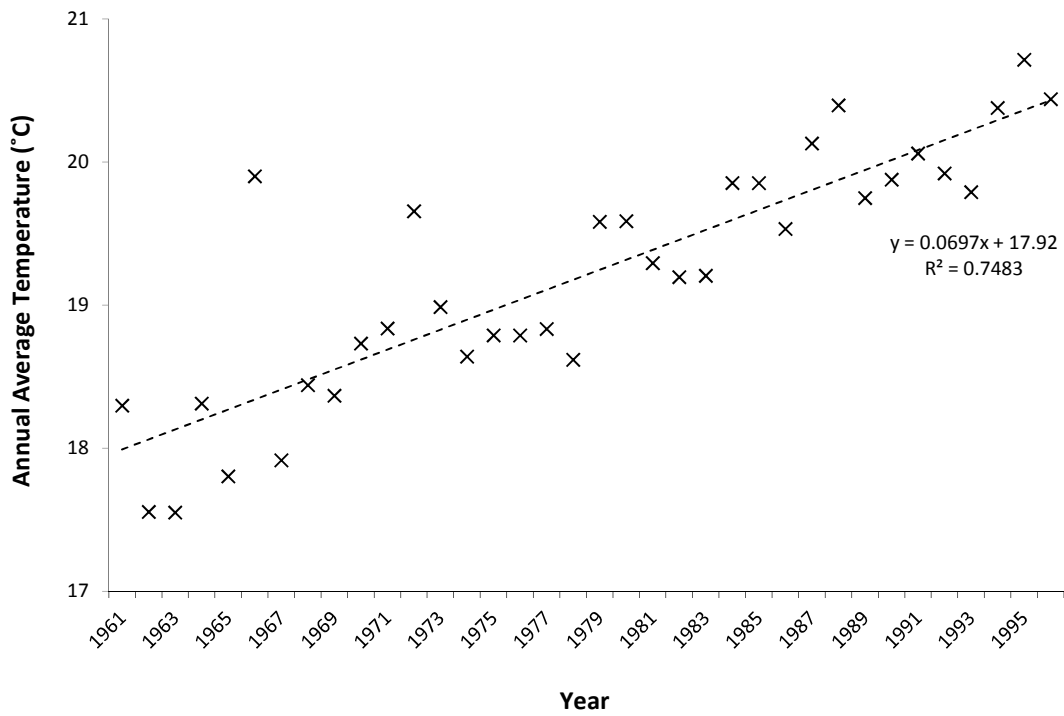


Figure 3.16 Annual average temperatures for all 119 stations of the Nepal national network (elevation range of between 72 m and 4100 m ASL) for the period 1961-96

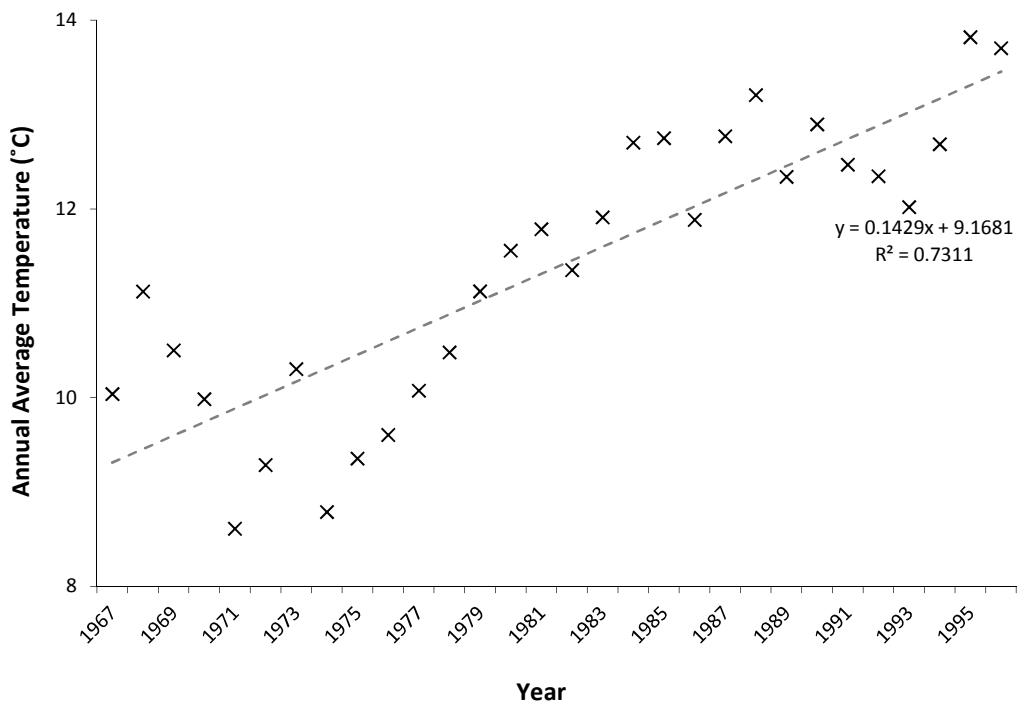


Figure 3.17 Average annual temperatures for the 15 highest elevation temperature gauges in Nepal, 1967-96 (all 15 stations having elevation > 1800 m ASL)

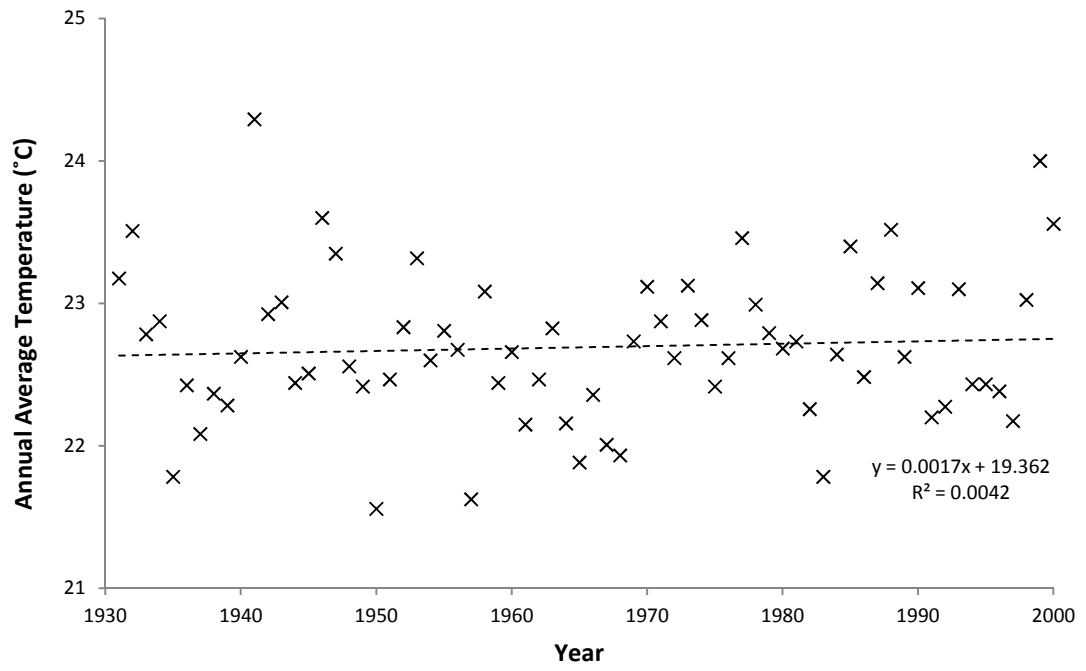


Figure 3.18 Average annual temperatures at Peshawar, 1931-2000, at an elevation of 359 m ASL

3.5 River flow data

River flow data (synonymously referred to as streamflow- or discharge-data) arguably are the most useful type of hydrological data because they represent the combined response of all physical processes in the upstream catchment (Hersch, 1995). River flow is the rate at which water travels through a given river cross-section and usually is expressed in units of m^3/s . Measurement generally involves the automatic or manual recording of water level, or stage, at a gauging station and the subsequent application of a stage-discharge relationship to derive an estimate of flow (Rees, 2008).

Most countries globally have long-established hydrometric networks comprising many gauging stations, from which data are used for a variety of purposes, ranging from water resources management and planning to flood control, environmental monitoring and impact assessment. However, in the Himalaya, gauging station networks are still very sparse and most catchments are ungauged (Chalise *et al.*, 2003). Himalayan gauging stations are mostly located at low elevations within easy access to human habitation and infrastructure (Shankar, 1990). Very few mountain headwater streams are continuously monitored because their remoteness and inaccessibility makes the logistics of establishing and maintaining gauging stations very challenging and costly. Hydrometrically, it is also difficult to find suitable sites having sufficiently stable cross-sectional areas and necessary downstream hydraulic controls, which are not affected by the high sediment loads that normally are associated with mountain rivers, and are capable of capturing the full range of flows, from low to high.

The locations of the 153 river gauging stations whose data were obtained for this study are shown in Figure 3.19. Of these, 53 have gauged daily flow data, 65 have 10-day data (an aggregation of 10 daily flow values, giving 3 mean flow values per month (WMO, 2008)), and 36 have monthly flow data. Few of these gauging stations, however, were known to have glaciers in their headwaters, and, of those that did, fewer still had a sufficiently complete time-series of long enough duration to form the basis of any meaningful analysis.

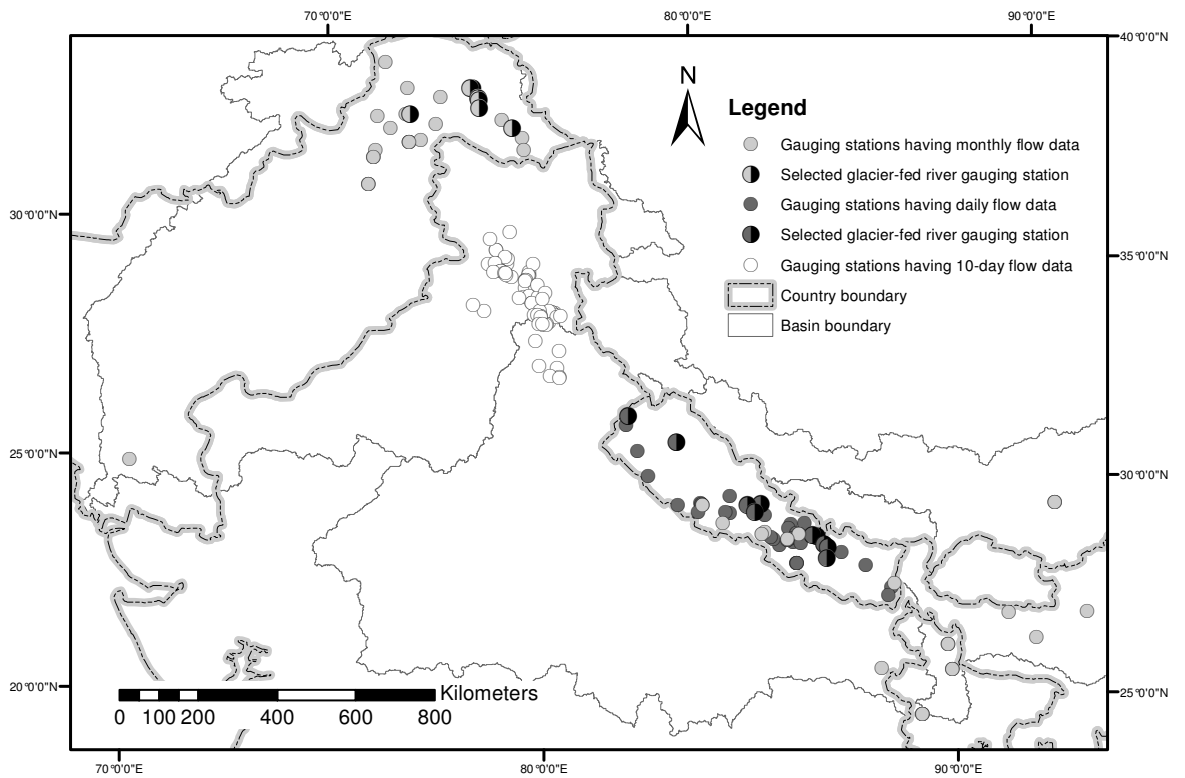


Figure 3.19 Locations of river gauging stations whose data were available to the study, distinguishing between those having monthly (light grey circles), daily (dark grey circles) or 10-daily (white circles) data and showing (half-black circles) the glacier-fed river gauging stations whose data were selected for analysis (details in Table 3.6).

The analysis presented in the following sections, therefore, was based on data from gauging stations having at least 10 years' "complete" records and a percentage glacier cover within the catchment of about 5% or more. A "complete" year's flow record was defined as one in which fewer than 10% of the daily (or monthly) data were missing. Percentage glacier cover, a catchment characteristic not conventionally calculated by the region's hydrometric agencies, was derived by first delineating the catchment area of each gauging station in ArcGIS, using the USGS Hydro1k Digital Elevation Model (USGS, 2001), and, then, overlaying the glacier-cover layer from the Digital Chart of the World (ESRI, 1993) onto each catchment area. Seven gauging stations in the Upper Indus in Pakistan and another ten in the headwaters of the Ganges in Nepal met the basic selection criteria. All 17 catchments have significant glacier cover (3.8% to 40.8%), and reasonably lengthy periods of complete records (from 11 to 31 years). Summary details of the selected gauging stations, their catchment characteristics and data are provided in Table 3.6; their locations are indicated by half-black circles in Figure 3.19. Although limited in number, the seventeen stations provide a useful basis for comparing between glacier-fed flow regimes in the east and west of the region.

3.5.1 General characteristics of glacier-fed flow regimes across the region

Flow regimes characterize the average behaviour of the timing of high and low flows (Krasovskaia *et al.*, 1994). The characterisation of Himalayan river flow regimes has been the subject of several previous studies (e.g. Hannah *et al.*, 2005). Here, descriptions are based on the data of the few selected glacier-fed catchments in Pakistan and Nepal.

The flow regime of a catchment, or any group of catchments in an area or region, is commonly described by a hydrograph of 12 mean monthly flow values, January to December (Krasovskaia *et al.*, 1994). To allow flows from different sized catchments to be compared or combined, areal scale effects need be eliminated from the data. Mean monthly flow values (m^3/s) were calculated for every catchment in both datasets (i.e. the 7 from Pakistan and 10 from Nepal). These values were then converted to mean monthly runoff, mm (i.e. equivalent uniform depth (mm) over the respective catchment area), and normalised as a percentage of the catchment average

annual runoff depth (AARD, mm). Mean monthly runoff values (x12) for each dataset were finally derived by taking the arithmetic mean of the respective catchment normalised mean monthly runoff values. Table 3.7 provides a summary of the average annual runoff and mean monthly runoff data, expressed in absolute terms (mm), for both data sets. The hydrographs of normalised mean monthly runoff values for both data sets are shown in Figure 3.20. Without normalisation, direct visual comparison of the two data sets would have been difficult because the average AARD for the 10 Nepal catchments (2359 mm) is over 20-times that of the 7 Pakistan catchments (117 mm). Such variance in average runoff is consistent with that seen in §3.3, with rain gauge data between east and west, and reflects how little runoff is generated from the glacier free portion of catchments in the Upper Indus.

Despite large differences in absolute runoff values, remarkable similarity is seen between the flow regimes in both regions (Figure 3.20). Flows peak in summer in both regions, albeit a month earlier (July) in Pakistan than in Nepal (August), and then demonstrate classical recession behaviour (Rees *et al.*, 2004) from September through autumn and winter months, finally attaining annual minima in February and/or March. The winter precipitation/rainfall in the west (see §3.3), does not appear to affect winter flows in the selected glacier-fed rivers probably because any winter precipitation is likely to fall as snow in such high elevation catchments. The distinct dry season ends in both areas as flow recovery starts in April, coinciding with increasing spring temperatures. The proportionately higher May, June and July flows in Pakistan are probably due to snow- and ice-melt progressing unabated due to the lack of early summer precipitation, with flow reducing earlier than in Nepal, as solar radiation and temperatures start to decline. The much higher absolute summer runoff totals in Nepal are undoubtedly a consequence of the summer monsoon, and the relative delay of peak flows until August, are thought likely to be a feature of the natural catchment response to the monsoon precipitation.

Table 3.6 Summary of the selected glacier-fed catchments in Nepal and Pakistan, arranged in order of descending percentage glacier cover (% ice) in each country

River	Site	Area ^a (km ²)	Glacier cover ^b (% ice)	Lon (°E)	Lat (°N)	Mean Flow (m ³ /s)	Period of record
Nepal							
Tama Koshi	Busti	2753	28.9	86.09	27.63	145.5	1971-87
Balaphi Khola	Jalbire	629	18.9	85.77	27.81	54.1	1970-95
Madi Khola	Shisa Ghat	858	15.5	84.23	28.10	78.5	1978-93
Seti	Phoolbari	582	15.2	84.00	28.23	53.1	1970-84
Chamelia	Karkale Gaon	1150	13.2	80.56	29.67	54.9	1970-90
Likhu Khola	Sangutar	823	10.7	86.22	27.34	57.6	1970-95
Bhote Koshi	Barabise	2389	9.7	85.89	27.79	69.9	1970-92
Tila Nala	Nagma	1712	5.0	81.92	29.32	42.8	1976-95
Khimti Khola	Rasnalu	333	4.4	86.20	27.58	34.2	1981-93
Mardi Khola	Lahachok	133	3.8	84.35	28.31	15.4	1976-95
Pakistan							
Shigar	Shigar	6927	40.8	75.75	35.33	205.4	1985-97
Hunza	Dainyor	13543	39.5	74.38	35.93	338.5	1966-99
Gilgit	Alam Bridge	28695	24.9	74.60	35.77	644	1966-98
Indus	Partab Bridge	167982	16.0	74.63	35.72	2148.6	1962-96
Indus	Besham Qila	187118	14.6	72.88	34.93	2412.3	1969-97
Gilgit	Gilgit	14138	11.7	74.30	35.93	282	1960-98
Astore	Doyian	3890	4.1	74.70	35.55	136.7	1974-98

Notes:

^a Estimated catchment area, derived from the USGS Hydro1k digital elevation model (USGS, 2001);

^b percentage glacier cover in the catchment, calculated by overlaying the Digital Chart of the World glacier layer (ESRI, 1993) onto the Hydro1k digital elevation model (DEM) (see also Chapter 5).

Table 3.7 Derived average annual and monthly runoff statistics for the 17 selected glacier-fed catchments in Pakistan and Nepal

	Average annual runoff (mm)	Mean monthly runoff (mm)											
		Jan	Feb	Mar	Apr	May	Jun	Jul	Aug	Sep	Oct	Nov	Dec
Pakistan (n = 7)													
Average	117	2	2	2	2	7	20	32	28	12	5	3	2
Minimum	56	1	1	1	1	3	9	15	14	6	2	1	1
Maximum	185	4	3	3	6	20	41	47	45	21	7	5	4
Std Dev	46	1	1	1	2	6	10	13	11	5	2	1	1
Nepal (n = 10)													
Average	2359	48	37	40	44	69	205	555	632	395	186	87	60
Maximum	4633	86	69	75	72	100	474	1310	1341	621	264	129	91
Minimum	779	24	19	20	25	40	54	129	191	143	69	37	28
Std Dev	1179	19	15	17	16	20	114	339	343	172	72	31	21

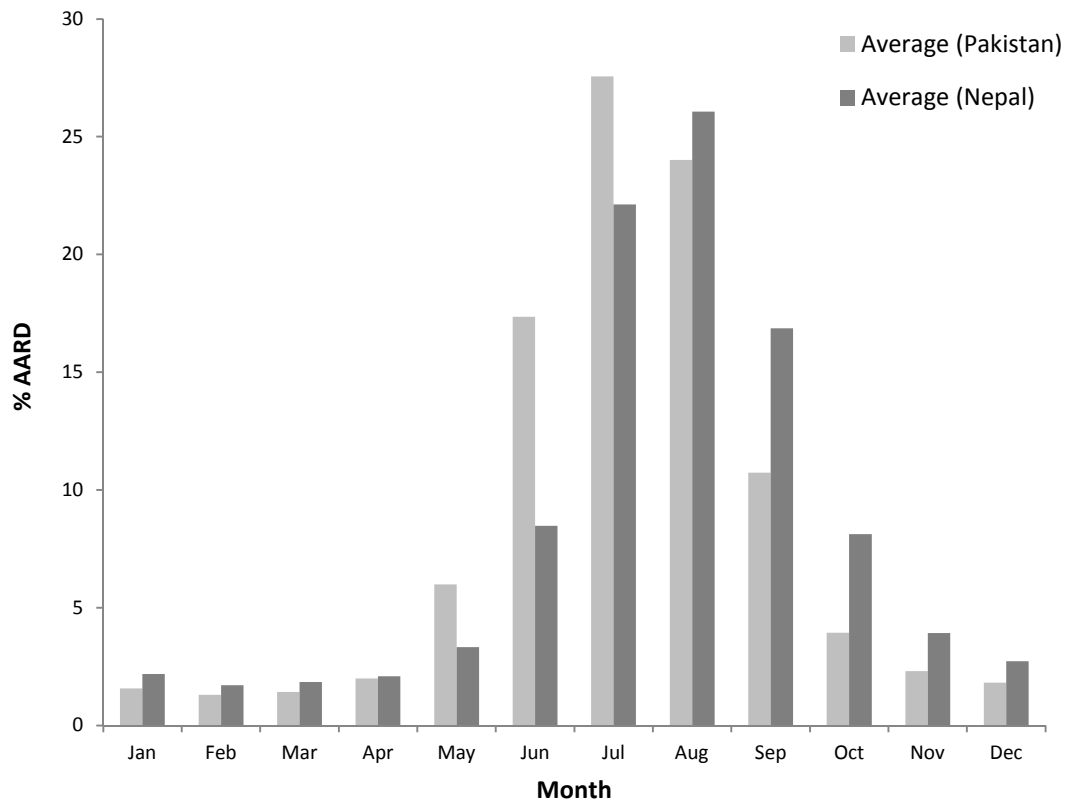


Figure 3.20 Mean monthly runoff, expressed as a percentage of the average annual runoff depth (AARD), for the selected catchments in Pakistan (light grey) and Nepal (dark grey)

3.5.2 Variability of annual runoff in glacier-fed catchments

Several previous studies (e.g. Collins, 1989; 2006; Fountain and Tangborn, 1985) have indicated that the variability of annual runoff in glacier-fed catchments is less than in glacier-free catchments (Singh and Singh, 2001). Variability in the annual runoff of a catchment is conventionally described by the Coefficient of Variation of Annual Runoff (ARCV), defined as the standard deviation of annual runoff expressed as a percentage of the catchment average annual runoff (AARD). The earlier studies showed that in areas of similar annual precipitation, ARCV generally reduces with the percentage glacier-cover within a catchment and attains a minimum value of about 10% at 30-40% of glacier cover.

ARCV values were derived for each of the 17 selected glacier-fed catchments and were plotted against the respective DCW-based percentage glacier cover (Figure 3.21), with the Pakistan data (7 solid circles) presented separately from the Nepalese (10 hollow circles). As the two areas represented by the data receive considerably different amounts of precipitation annually, it is not surprising that the variability of annual runoff in Pakistan, on average, is less than it is Nepal. Both sets of data, however, appear to conform to convention, with lines of best-fit, which describe second-order polynomial (quadratic) equations, showing ARCV minima of about 12% at about 20% glacier-cover (% ice). The best-fit lines show that, statistically, % ice explains 87% of the variance in ARCV in Pakistan and 39% of the variance in ARCV in Nepal.

3.5.3 Exploring trends in glacier-fed river flows

As a key aim of the study was to estimate the effects of climatic warming on future glacier-fed river flows in the Himalaya, it was interesting to explore whether any significant trends or changes were evident in the available data. Annual Mean Flows (AMFs) and period-of-record Mean Flows (MF) and AMFs were calculated from the daily (or monthly) time-series of river flows of each of the 17 selected glacier-fed catchments. Each catchment's AMFs (m^3/s) were normalised by the catchment MF (m^3/s), and then plotted with a linear least-squares trend-line fitted.

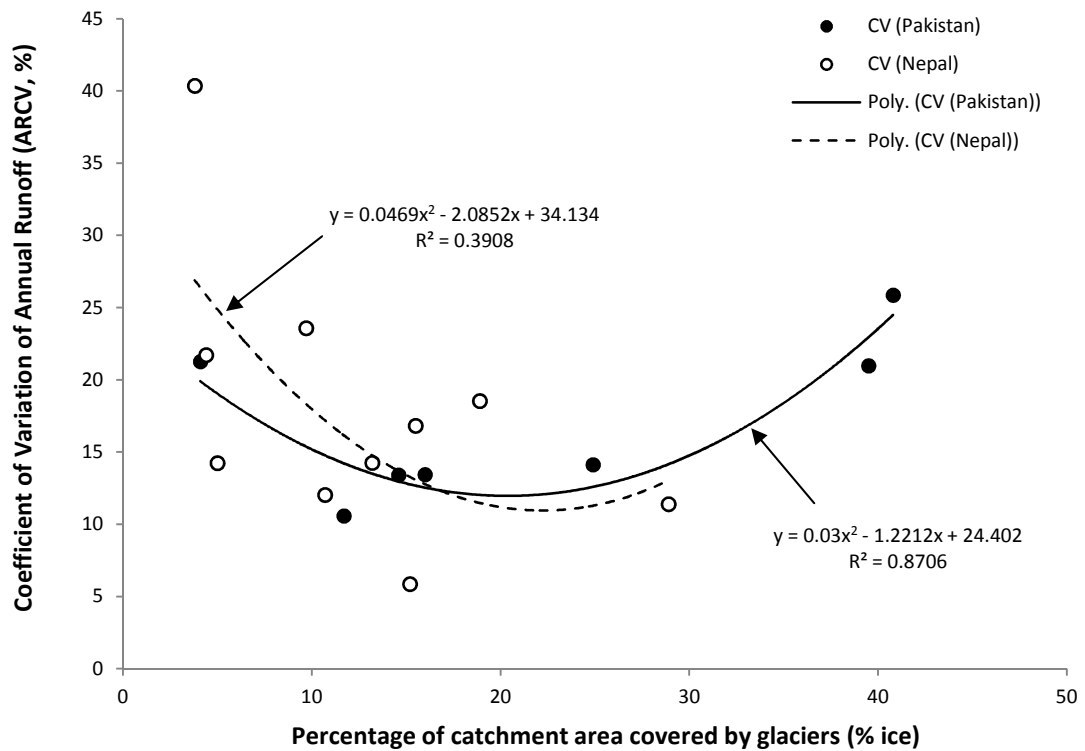


Figure 3.21 Coefficient of Variation of Annual Runoff (ARCV) versus the percentage of glacier area (% ice) for the selected glacier-fed catchments in Pakistan (solid circles) and Nepal (hollow circles); the lines of best fit, which describe second-order polynomial (quadratic) equations, shows that % ice explains 87% of the variance in ARCV in Pakistan and 39% of the variance in ARCV in Nepal

The trend-line (regression) statistics for each catchment in Table 3.8 show there is considerable variability in supposed trends (8 positive, 7 negative and 2 no trend) over the respective periods of record. However, according to Mann-Kendall trend test, statistically significant trends at the 5% significance level were found only in four of the AMF time-series: three in Pakistan (Hunza, Shigar and Astore) and one in Nepal (Bhote Kosi) (Figure 3.22). Of the 3 in Pakistan, Shigar and Astore both show positive trends of flows increasing over time, while the Hunza shows a negative trend of declining flows over time. The greatest rate of change is seen with the Shigar: an increase of over 5% of MF per year from the 11 years of data. Trends in the flows of the Astore and Hunza are comparatively modest at +1.35% and -1.17% of MF per year over their longer 26 and 33 years' records respectively. The one statistically significant trend in Nepal shows flows increasing at a rate of +1.73% of MF per year over the 25 year record.

No conclusions can be drawn from this relatively small sample on whether glacier-fed river flows are generally increasing or decreasing in northern Pakistan or Nepal. The two positive and one negative statistically significant trends in Pakistan, and the one positive trend in Nepal confirm only the inconsistency in trends across the region. Perhaps more telling is the lack of statistically significant trends in the other 14 catchments over the periods of their records, which suggests annual flows of glacier-fed rivers did not change significantly between 1960 and 1999.

Table 3.8 Trend-line (regression) statistics for plots of Annual Mean Flows, expressed as a percentage of the period-of-record Mean Flow (%MF), versus time (years), for the 17 selected glacier-fed catchments; catchments showing significant trends are highlighted in bold.

River	Site	Period of Record ^a	Number of complete years ^b	Slope of trend-line (%MF/yr)	Goodness of fit (R ²)	Significant trend ^c (Y/N)
Nepal						
Tama Koshi	Busti	1971-87	16	-0.90	0.16	N
Balaphi Khola	Jalbire	1970-95	25	+0.18	0.01	N
Madi Khola	Shisa Ghat	1978-93	13	-1.77	0.26	N
Seti	Phoolbari	1970-84	14	-0.40	0.09	N
Chamelia	Karkale Gaon	1970-90	18	-0.57	0.07	N
Likhu Khola	Sangutar	1970-95	19	-0.03	0.00	N
Bhote Koshi	Barabise	1970-92	18	+1.73	0.26	Y
Tila Nala	Nagma	1976-95	18	-0.54	0.07	N
Khimti Khola	Rasnalu	1981-93	11	+2.44	0.23	N
Mardi Khola	Lahachok	1976-95	20	+2.26	0.11	N
Pakistan						
Shigar	Shigar	1985-97	11	+5.08	0.54	Y
Hunza	Dainyor	1966-99	33	-1.17	0.28	Y
Gilgit	Alam Bridge	1966-98	32	-0.61	0.16	N
Indus	Partab Bridge	1962-96	35	+0.36	0.08	N
Indus	Besham Qila	1969-97	29	+0.16	0.01	N
Gilgit	Gilgit	1960-98	32	-0.01	0.00	N
Astore	Doyian	1974-98	26	+1.35	0.24	Y

Notes:

^a Earliest to latest complete year;

^b Complete year, defined as a year in which fewer than 10% of daily (or monthly) flow values are missing;

^c According to the Mann-Kendall trend test (Hirsch *et al.*, 1982).

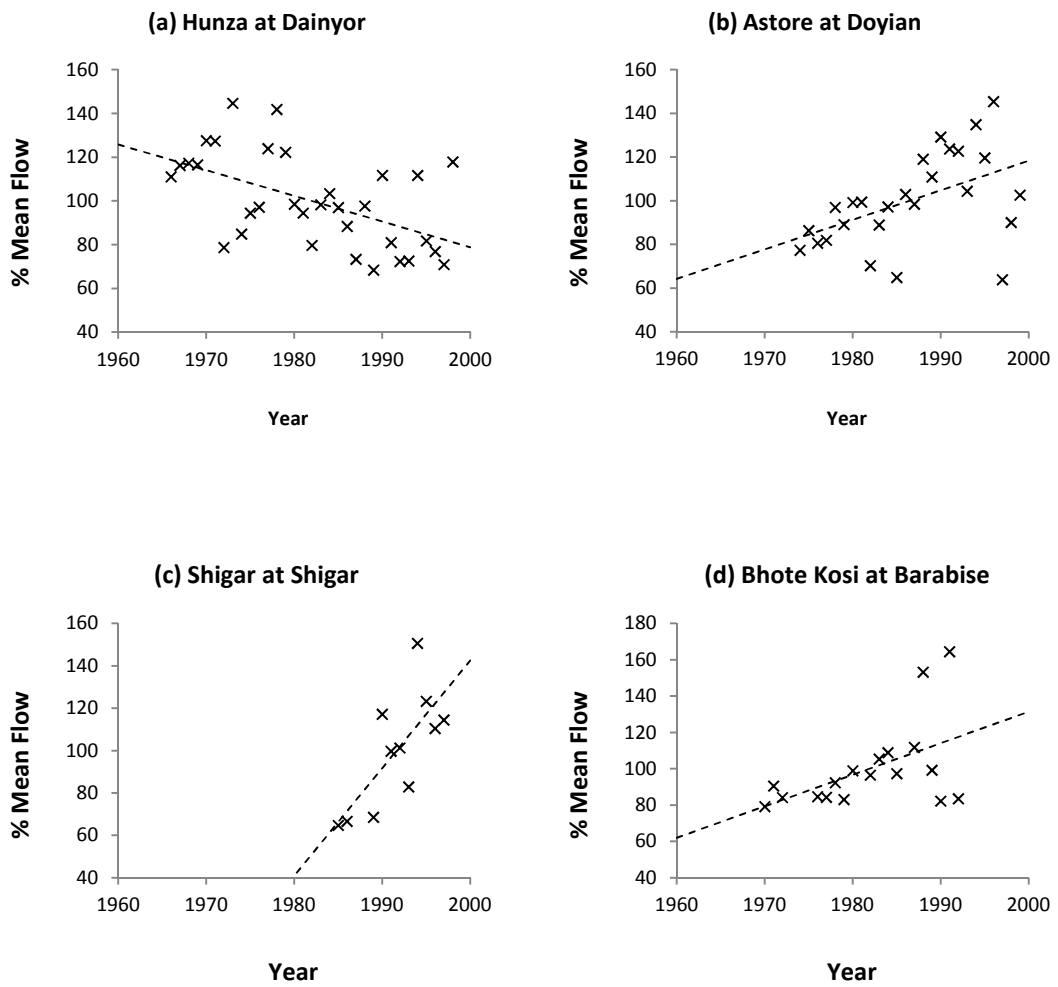


Figure 3.22 The four catchments whose data show statistically significant trends at the 5% significance level according to the Mann-Kendall trend test: (a) the Hunza at Dainyor; (b) the Astore at Doyian; (c) the Shigar at Shigar; and (d) the Bhote Kosi at Barabise; trend-line statistics (slope and R^2) can be found in Table 3.8.

PART 2

4 Model Development

4.1 Introduction

Hydrological models are simplified, conceptual representations of the hydrological cycle and are commonly used to predict conditions where measurements, or data, are unavailable, such as, in ungauged catchments, or for some period of time in the future (Beven, 2012). Models are particularly useful in predicting the hydrological impacts of climate change because they provide an objective means of estimating how possible future climates, applied by simply adjusting model input data according certain climate change scenarios, might affect future catchment response, as represented by corresponding model outputs.

Most hydrological models originally were designed to be applied at the meso-scale, to single catchments or basins having drainage areas in the order of a few 1000 km² or less. Over the last 20 years or so, coinciding with application of Global and Regional Circulation Models (GCMs, RCMs) for climate change studies, there has been a demand for hydrological models capable of being applied at regional scales (>10⁴ km²). Such models, referred to as macro-scale hydrological models (MHMs), resolve precipitation, evapotranspiration and discharge on regular grids spread over large geographical domains, typically to provide estimates of long-term average runoff, at annual, seasonal or monthly timescales. MHMs usually are applied using global or regional data that are consistently available for the entire region of interest and are considered particularly useful where observational data are sparse because they characteristically are applied without calibration at the individual catchment scale (Arnell, 1999b).

The aim of this study, to assess the long-term impact of glacier retreat on the water resources of the Brahmaputra, Ganges, and Indus river basins, required the development of a macro-scale hydrological model specifically for the Himalayan region. However, the application of MHMs in mountain regions is difficult due to the heterogeneity of terrain and climate and because the factors that govern runoff generation operate at much finer scales than those of spatially-averaged MHM input

data (Arnell, 1999b). MHMs also have traditionally ignored glacial melt-water contributions to long-term discharge by assuming no net change in ice volume over time. Clearly such an assumption is inappropriate for the Himalaya, where there are an estimated 54,000 glaciers, having a total glacier area of over 60,000 km² (Bajracharya and Shrestha, 2011), many of which are declining in volume (Miller *et al.*, 2012). The difficulty of representing glaciers in a model of Himalayan basins is further compounded because little is known of the characteristics and geometries of the region's glaciers (e.g. vertical extent, ice-hypsometry and thickness), with only a very small proportion of the total number having been surveyed in any detail (Singh *et al.*, 2011).

This chapter describes the development of a macro-scale hydrological model capable of representing the melt-water contribution from the retreating glaciers of the Himalaya. First, model design is described including an assessment of available data and identification of a suitable candidate model (§4.2). Key features of the selected model are summarised (§4.3) and then details are provided of how the necessary modifications for the Himalaya were implemented (§4.4), the most significant being a new glacier-melt model (§4.5).

4.2 Design of the regional macro-scale hydrological model

Model development requires careful design at the outset, to ensure the model's eventual outputs satisfy the objectives of the study. However, development of a new hydrological model from first principles (conservation of mass or energy) is rarely necessary because existing models are capable of satisfying the majority, if not all, of the requirements of a particular application. Model design followed four distinctive steps (after Beven, 2001):

- (i) define the scope of the model, (i.e. geographical and temporal extents) and its required outcomes;
- (ii) establish a clear understanding of the physical nature and hydrological characteristics of the area to be modelled and identify the key processes that need to be represented;

- (iii) assess the availability of data to drive, calibrate and validate the model, and establish whether such data are readily available, or can be provided within the constraints (time, budget) of the study; and
- (iv) identify a suitable candidate model that could be applied with, or without, modification to produce the desired outputs from the available data.

The following sections elaborate how each of these steps was addressed in the study.

4.2.1 Defining the scope of the macro-scale hydrological model

As stated earlier, the aim of the study was to assess how future climate change and associated glacier retreat might affect future Himalayan river flows. The *geographical extent* of the study was specifically defined as the Indus, Ganges and Brahmaputra rivers basins (Figure 4.1). With drainage basin areas of $1.2 \times 10^6 \text{ km}^2$, $1.1 \times 10^6 \text{ km}^2$ and $0.6 \times 10^6 \text{ km}^2$ respectively (NIH, 2014), and home to over 700 million people (Xu *et al.*, 2007), these are three of the region's largest and most densely populated river basins, of huge importance economically and politically, and representative of the full range of Himalayan glacier-fed flow regimes. However, rather than model all three basins as one single entity, which would have been demanding computationally and difficult to justify hydrologically, the model was designed to be applied to each basin individually. The model was required to provide estimates of river flow at any point along any river in any of the three basins.

To allow an assessment of how glacier-fed river flows might change over time, the model was further required to run over a reasonably long period of up to one hundred years from “present day”. It was decided that the model should provide estimates of the relative changes in average annual- and winter- (October-March) flows at decadal time-steps over the period of interest. Average annual- and winter- (or dry-season) flows are generally considered appropriate proxies for water resource availability in the region. Meanwhile, producing estimates of river flow at decadal time-steps would provide a means of observing how possible changes in climate and glacier-retreat, both of which are progressive in nature, affect changes in water resources availability over time. “Present day” conditions would be represented conventionally by applying

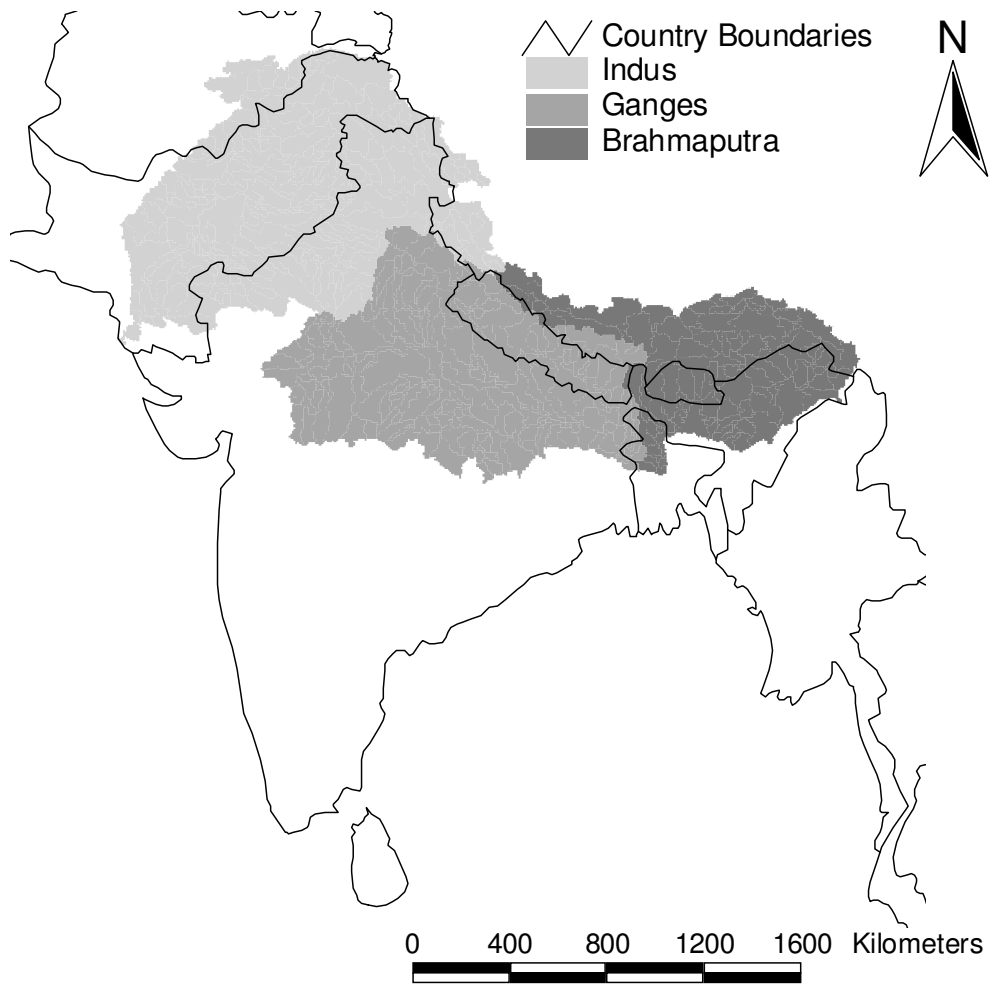


Figure 4.1 Geographical extent of the study: the Indus, Ganges and Brahmaputra river basins

a standard-period, 30-year “normal” climate as the reference baseline. Standard-period baselines are usually used in climate impact studies to represent the sensitivity of future changes, relative to a “normal” (baseline) period. The WMO 1961-90 standard period, a popular baseline for many climate impact studies, was considered appropriate for this study too.

4.2.2 Understanding the physical characteristics of the study area

Understanding the physical nature and hydrological characteristics of the area to be modelled is crucial for model design (Beven, 2012). The Indus, Ganges and Brahmaputra river basins cover a wide range of physical characteristics, from low-lying, sub-tropical plains to high-relief, high-altitude mountains which experience arctic conditions at the highest elevations (Alford, 1992). Although downstream areas of the basins are amongst the most densely populated parts of the world, the behaviour of glaciers high in the headwaters remains predominantly natural. The study, therefore, limited itself to modelling natural conditions throughout, rather than attempting to factor-in artificial influences (e.g. dams, abstractions and discharges, land-use). The modelled impacts correspondingly relate to the theoretical, natural flows and not the actual, artificially influenced flows. Some of the natural processes and features the model would be required to represent are shown in Figure 4.2.

Hydrological models generally aim to resolve the water balance over a certain period, t , deriving estimates of catchment runoff (Q) from the precipitation (P) less losses from actual evapotranspiration (AE) plus (or minus) changes in the water held in storage (ΔS).

$$Q_t = P_t - AE_t \pm \Delta S_t \quad \dots(4.1)$$

Precipitation is a key variable and input for most hydrological models, as are those variables that define “losses” through actual evapotranspiration (e.g. temperature, radiation, wind-speed, cloud-cover). Under natural conditions, the main types of catchment storages are soil moisture, groundwater, lakes, wetlands, snow and ice. Land-cover can significantly affect the catchment water balance, with leaves on trees capable of intercepting precipitation before it reaches the ground, different types of

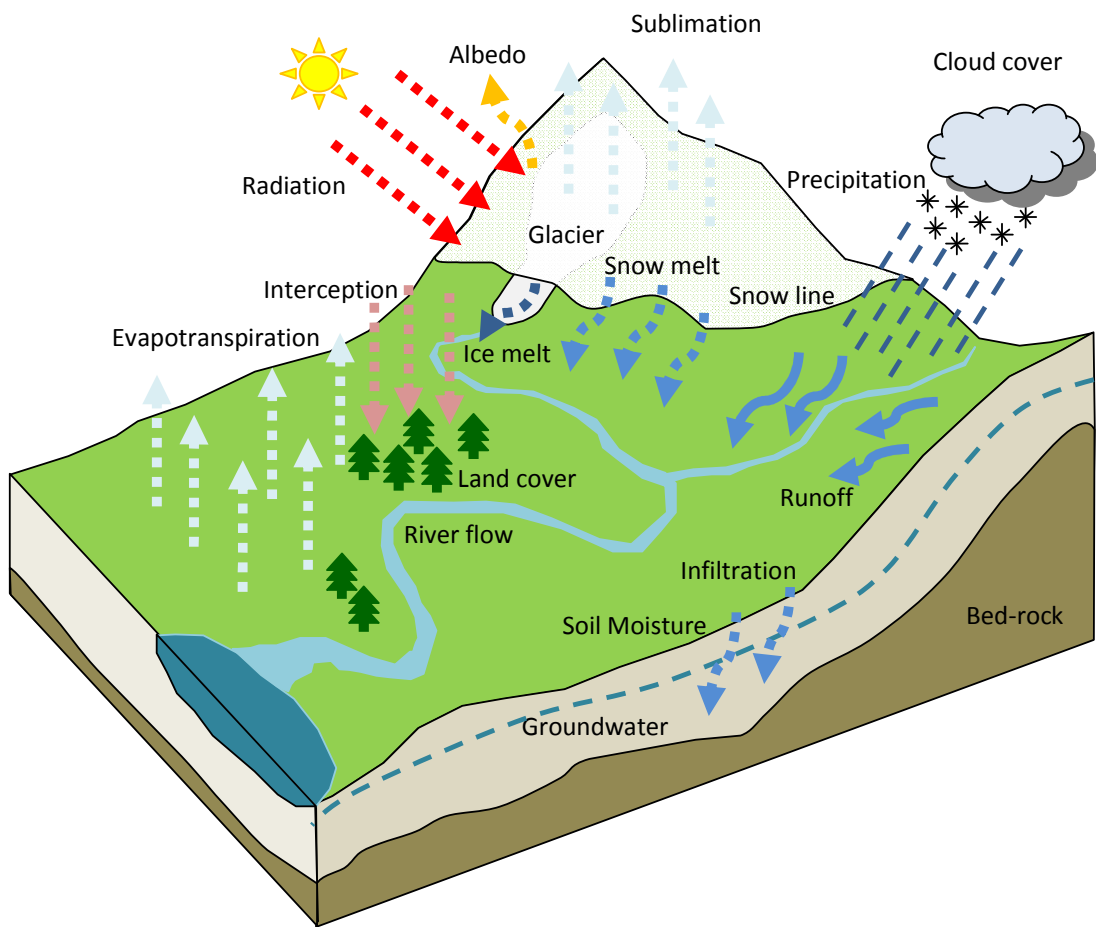


Figure 4.2 Some of the natural features to be represented in the regional model
 (adapted from CSIRO Land and Water, 2010)

vegetation (e.g. grass, forest) transpiring at different rates, depending on the availability of water in the soil, and evaporation occurring from non-vegetated parts (e.g. bare earth, lakes). The porosity and permeability of different types of underlying soils and rocks also strongly influence infiltration and changes in soil moisture and groundwater storage that affect runoff to rivers. In mountainous catchments, temperature, topography (i.e. elevation, slope and aspect) and radiation are important factors because they influence the partitioning of precipitation as snow or rain, the position of the snowline, and the amount of freshwater stored in the snowpack and released as snowmelt. Similarly, where glaciers are present, temperature, radiation, albedo and topography, together with the characteristics of individual glaciers (e.g. areal extent, depth and hypsometry), affect the glacier-melt (ice-melt) contribution to river flow.

4.2.3 Assessing the availability of data

Hydrological modelling in the Himalaya traditionally has been hampered by the limited availability of local hydrometeorological observations to characterise the spatial and temporal distribution of key meteorological and hydrological variables (e.g. precipitation, temperature, river flow) and which normally would be used to calibrate and validate models. Such data, particularly at higher elevations, are generally sparse, of limited duration and are often of inferior quality (Shankar, 1990; Moors and Siderius, 2012; Singh and Singh, 2001). As described in Chapter 3, the study benefitted from a variety of point-measurements of hydrometeorological variables that were obtained from several different sources. Although these data were not well enough distributed across the three basins to define driving data for the model, some (e.g. river flows) would be useful later for model validation.

A key requirement of MHMs is that input data should be uniformly available across the entire area to be modelled (Arnell, 1999b). In the absence of suitable data locally, the study sought to identify those data that were readily available in digital form from wider international sources. The key datasets that were identified are listed in Table 4.1.

Table 4.1 Key datasets readily available from international sources

Data type	Title/Description	Reference
Climate	CRU 1961-90 standard period 0.5° monthly climatological data, 12 average monthly values of for the 1961-90 standard period	New <i>et al.</i> , 1999
Climate projection	UK Met Office Hadley Centre Nested Regional Climate Model HadRM2 outputs for the South Asia, providing forecasts of future climate at a resolution of 0.44° for 2041-2060	Hassell and Jones, 1999
Vegetation	USGS Eurasia Land Cover Characteristics Database, which contains 17 different land-types at a nominal grid resolution of 1 km	USGS, 1997
Soils	FAO Digital Soil Map of the World a 1: 5,000,000 scale vector dataset describing the distribution of 106 soil units (types) globally and their textural classes (i.e. proportion of clay, silt and sand))	FAO, 1995
Topography	USGS Hydro1k digital elevation model, a hydrologically ratified DEM available at a resolution of 1 km globally	USGS, 2001
Glacier cover	Digital Chart of the World (DCW), a vector dataset derived from United States' Defense Mapping Agency 1:1,000,000 Operational Navigation Charts	ESRI, 1993

4.2.4 Identifying a suitable candidate model

Rather than develop a macro-scale hydrological model anew, adaptation of an existing MHM was considered the simplest, and most efficient, way of meeting the objectives of this study. Of the many MHMs in existence (see §2.6), Macro-PDM (Arnell, 1999b), initially developed at the Institute of Hydrology (now the Centre for Ecology & Hydrology), was the most readily available to this study. Having previously been applied in many parts of the world using similar data to those described in the preceding sub-section (e.g. Europe (Arnell, 1999a; Rees *et al.*, 1997), Africa (Meigh *et al.*, 1999; Reynard *et al.*, 1997), Central Asia (Tate and Meigh, 2001)), Macro-PDM was considered suitable, albeit with some modification, for this particular application in the Himalayan region.

4.3 Features of the unmodified Macro-PDM

4.3.1 General features of Macro-PDM

Macro-PDM, an adaptation of the Probability Distributed Moisture model (PDM) (Moore, 1985, 2007), was developed to be applied across large geographical domains, such that its parameters could be defined *a-priori* according to the spatial distribution of vegetation (specifically forest and grass) and soil types. Like PDM, Macro-PDM takes a conceptual water balance approach to rainfall-runoff modelling, based on a soil moisture accounting procedure, and works on a daily time step to transform inputs of precipitation, potential evaporation (PE) and temperature into estimates of runoff. The application of PDM within Macro-PDM has been described previously by others (e.g. Arnell, 1999b; Reynard *et al.*, 1997) and, because it was applied without modification in this study, a more detailed description of its treatment of the different runoff-generating processes within a grid cell is provided for completeness in Appendix A.

A schematic of Macro-PDM is shown in Figure 4.2. As with many MHMs, Macro-PDM is a deterministic, grid-based conceptual rainfall-runoff model that requires, as input, gridded driving- and antecedent-data and various model parameter settings to produce, as output, gridded estimates of runoff. Macro-PDM uses a regular rectilinear grid in which all grid cells are rectangles whose size (resolution) can be modified as

necessary, usually, according to the resolution of available driving- or antecedent data. Grid cell resolutions of previous applications range from 10 km x 10 km (Rees *et al.*, 1997) to 0.5° x 0.5° latitude-longitude (e.g. Reynard *et al.*, 1997; Meigh *et al.*, 1999). Driving data are the meteorological inputs that are necessary to “drive” the model. Antecedent data are data that describe the initial physical characteristics of each grid-cell (e.g. soil type, land-cover, elevation). A requirement of the model is that all input data must be available, or prepared, at the same spatial resolution as the model. As Macro-PDM works on a daily time-step, the driving data must also be converted to daily. Details on how the available data were assessed, prepared and applied to the model are provided in Chapter 5 (Model Application).

The model comprises many sub-components (modules) that individually characterise key physical processes acting within a grid cell and which interact to ultimately provide daily estimates of runoff for every grid cell, the model’s primary output. These daily estimates can then be aggregated at run-time to provide the required long-term (i.e. whole period of the model run) or interim (e.g. decadal) averages of annual- or seasonal-runoff for every grid cell.

Macro-PDM considers each grid-cell as a discrete unit and does not consider the routing of runoff between neighbouring cells. To overcome this limitation, the physical, hydraulic routing of runoff between cells that is required to derive estimates of river flow at specific points along the river network is carried out as a subsequent, post-processing, activity independently of the model.

4.3.2 Snow- and ice-melt modelling within Macro-PDM

Macro-PDM’s treatment of snow and ice is particularly relevant to this study’s application of the model in the Himalaya. Earlier versions of the model assumed input variables to be uniformly distributed across the cell. However, the model was adapted in 2001 for an application in mountainous Central Asia (Tate and Meigh, 2001), to account for altitudinal variations in the three climate input variables. Cells having a maximum elevation of 2000 m or higher were declared “mountain” cells.

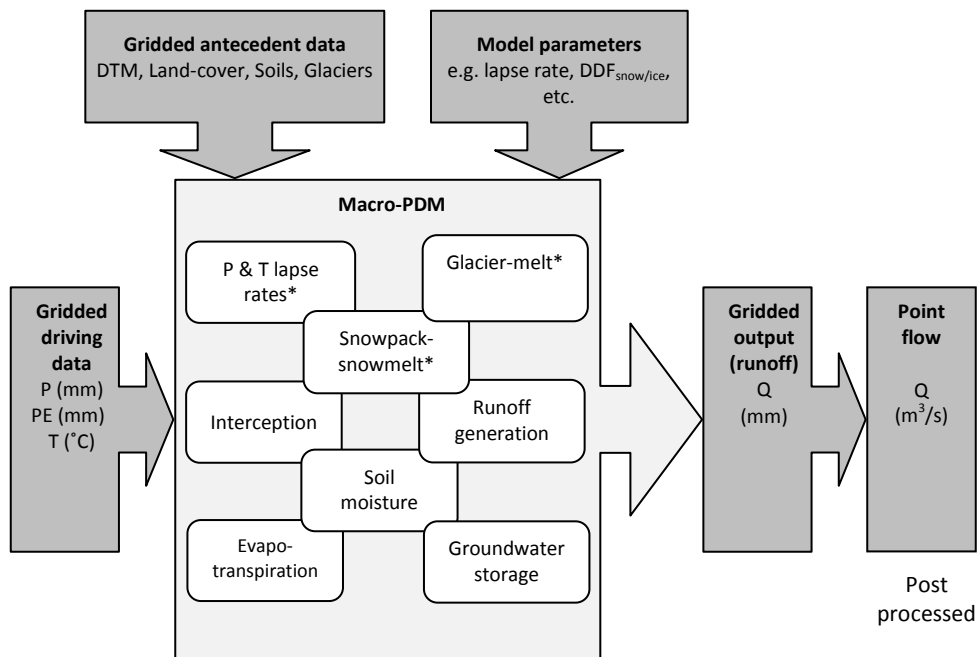


Figure 4.3 A schematic of the macro-scale hydrological model, Macro-PDM, showing the various inputs to, and outputs from, the model and its key modules (* shows those that were new or significantly modified during this study)

Every mountain cell is subdivided (discretized) into a number of discrete elevation bands of equal-height between the vertical extremes of the cell. The distribution of cell area between bands (the cell hypsometry) is determined according to the Pareto distribution, such that $F(z_i)$, the proportion of the cell below the minimum elevation of any band, z_i , is expressed by:

$$F(z_i) = 1 - (1 - f(z_i))^n \quad \dots(4.2a)$$

where

$$n = \frac{1}{f(z_{mean})} \quad \text{and} \quad f(z_{mean}) = \frac{z_{mean} - z_{min}}{z_{max} - z_{min}} \quad \dots(4.2b)$$

and z_{mean} , z_{min} and z_{max} are the mean, minimum and maximum cell elevations respectively, values that usually can be obtained by overlaying the model grid onto a suitable digital elevation model .

The area, A_i , of any band, i , can thus be calculated as:

$$A_i = A (F(z_{i+1}) - F(z_i)) \quad \dots(4.3)$$

where A is the total cell area, in km^2 , and $i = 1$ is the lowermost elevation band.

With the daily temperature for the cell, T_{mean} , ($^{\circ}\text{C}$) assumed to apply at the cell's mean elevation, z_{mean} , the daily temperature in each elevation band, T_i , is calculated according to temperature lapse rate, as follows:

$$T_i = T_{mean} + \alpha(z_{mean} - z_{mid}) \quad \dots(4.4)$$

where z_{mid} is the mid-elevation of the band and α is the temperature lapse rate ($^{\circ}\text{C}/\text{km}$).

Daily precipitation (mm) and potential evaporation (mm) are also allowed to vary with elevation in so-called mountain cells. A simple model is applied to account for orographic increases in precipitation (Equation 4.5), such that the daily precipitation in each elevation band, P_i , increases by a certain percentage (ΔP , %/100 m) of the cell daily precipitation, P , at all elevations above the cell mean elevation.

$$P_i = \begin{cases} P & \text{where } z_{mid} \leq z_{mean} \\ P(1 + \Delta P)^{(z_{mid}-z_{mean})/100} & \text{where } z_{mid} > z_{mean} \end{cases} \quad \dots(4.5)$$

PE can similarly be adjusted (Equation 4.6), reducing exponentially relative to the mean cell elevation and according to a PE lapse rate, ΔPE (/km).

$$PE_i = \begin{cases} PE & \text{where } z_{mid} \leq z_{mean} \\ PE \cdot e^{((\ln \Delta PE) \cdot (z_{mid}-z_{mean})/1000)} & \text{where } z_{mid} > z_{mean} \end{cases} \quad \dots(4.6)$$

Precipitation is considered to reach the ground as snow whenever the band's daily temperature is below a certain threshold temperature, T_{snow} . A snowpack-snowmelt model that couples with the PDM (Bell and Moore, 1999) is applied whenever snow is present in an elevation band. The model represents the accumulation and depletion of the snowpack and the snowmelt contribution to runoff in each elevation band. It uses a temperature index (degree-day) approach to calculate snowmelt and conceptualizes the snowpack (snow storage) as a dry-(snow) store and a wet-(snow) store in series. Any new snow in a band added to the band's dry-store. The wet-store receives water directly as rainfall and, whenever the daily temperature for the band is above a melt threshold (T_{melt}), as snowmelt from the dry-store, at the constant rate of the degree-day-factor for snow, DDF_{snow} . The rate at which melt-water is "released" from the snowpack depends on the wetness of the wet-store, as represented by a model parameter, S_c , the critical liquid water capacity. S_c is the proportion of the wet-store above which fast drainage of melt-water occurs at a rate $k2$. The water content below S_c drains at a slower rate of $k1$. The storage time parameters $k1$ and $k2$ have units of inverse time. Typical values for snowpack model parameters are shown in Table 4.2, at the end of the chapter.

A further key innovation of the 2001 model was the assumption that an inexhaustible supply of permanent snow and ice is available at all elevation bands above 4000 m, with melt-water released from such elevation bands at the same constant rate per degree-day, DDF_{snow} , whenever the daily temperature is above melt threshold, T_{melt} .

Whenever snow or ice are present in an elevation band, the daily melt-water constitute the effective precipitation input to the daily PDM runoff calculations that are applied in the band. The daily cell runoff, Q_t , finally is calculated as the area-weighted total of the daily runoff from all elevation bands, as follows:

$$Q_t = \sum_{i=1}^n (A_i \cdot q_i / A) \quad \dots(4.7)$$

Where A_i is the area of band, i ($i = 1, 2 \dots n$, the number of bands), q_i , the daily runoff from the band, and A is the cell area.

4.4 Modifications required for the application of Macro-PDM in the Himalaya

On assessing Macro-PDM's capabilities against the study's objectives, modifications were considered necessary in the way three key processes were represented: the variation of precipitation with elevation within cells; seasonal variations in temperature lapse rates; and, most importantly, the glacial melt-water contributions from many glaciers to river flows in each study basin. The first two modifications, although potentially significant to the outcomes of the study, were relatively simple programmatically; their implementation is described briefly below. The development of the glacier-melt component, however, was critical to the whole study and its development, therefore, is described fully in §4.5.

4.4.2 Precipitation lapse rate

Many studies have sought to characterise the variation of precipitation with elevation (e.g. Lauer, 1975; Glazirin, 1997). While orographic precipitation usually increases to a maximum at the crests of hills or lesser mountains, maximum precipitation is reached some distance up the windward slopes of the world's highest mountains

(Lauer, 1975; Rakhecha and Singh, 2009). In the Himalaya, orographic precipitation maxima have been observed at elevations of about 2500-5000 m, followed by sharp decreases (e.g. Singh and Kumar, 1997; Putkonen, 2004; Young and Hewitt, 1990).

Equation 4.5 imposes precipitation increases in all elevation bands above the cell mean elevation. This clearly does not reflect Himalayan conditions and could result in an overestimation of precipitation at higher elevations. A modification therefore was applied, whereby the precipitation lapse rate is applied only when the mid elevation of an elevation band, z_{mid} , is within a given range, z_{adjmin} and z_{adjmax} (m ASL). Equation 4.5 thus was revised as shown in Equation 4.8:

$$P_i = \begin{cases} P & \text{where } z_{adjmax} < z_{mid} < z_{adjmin} \\ P(1 + \Delta P)^{z_{adj}/100} & \text{where } z_{adjmin} \leq z_{mid} \leq z_{adjmax} \end{cases} \quad \dots(4.8a)$$

Where P is assumed to apply to the cell's mean elevation, z_{mean} , and z_{adj} is the elevation adjustment for the band, determined as follows:

$$z_{adj} = \begin{cases} z_{mid} - z_{adjmin} & \text{where } z_{mean} \leq z_{adjmin} \\ z_{mid} - z_{mean} & \text{where } z_{mean} > z_{adjmin} \\ 0 & \text{where } z_{mid} \leq z_{mean} \end{cases} \quad \dots (4.8b)$$

Values for parameters ΔP , z_{adjmin} and z_{adjmax} , are set *a-priori*, based on available literature (see Table 4.2).

4.4.3 Seasonally adjusted temperature lapse rate

Following observations made earlier in this study, of lapse rates varying during the year (see §3.4), the model was modified to allow for two seasonal lapse rates over the year: one for winter (October - March), α_{win} , the other, α_{sum} , for summer (April – September). Like many Macro-PDM parameters, these new model parameters were also set *a priori* (see Table 4.2), in this case, based on the empirical data presented in Chapter 3.

4.5 Development of a regional glacier melt model

The development and application of a new model component (module) capable of representing long-term changes in melt-water contributions from retreating glaciers was a core requirement for addressing the objectives of the study. The model was developed following the generic model design steps outlined in §4.2.

4.5.1 Scope of the glacier melt model

With the geographical and temporal extent of the model specified as in §4.2.1, all that was required to be defined in respect of the *scope* of the glacier model were its objectives. Specifically, these somehow were to represent (i) the many glaciers present in each of the three study basins; (ii) possible changes in the dimensions of glaciers under conditions of climatic change, and (iii) the varying and transient glacial melt-water contributions to river flow as glacier dimensions change over time.

4.5.2 Physical processes to be represented by the model

Melt-water from glaciers can contribute significantly to downstream river flows. As outlined in Chapter 2, few hydrological models explicitly consider (if at all) the melt-water contribution from glaciers and fewer still represent the transient nature of the contribution. An understanding of the physical processes and features that affect the dynamics of glaciers and the generation of melt-water is essential for the design of a model. These key processes and features are depicted in Figure 4.4.

Mountain glaciers are formed over many tens or hundreds of years from the annual accumulation of snow at high elevation and the snow's transformation, first, into firn and, ultimately, into ice. Firn is compacted snow left over from previous years' accumulations that has not yet turned into ice. Having formed, a glacier deforms plastically due to its own weight and extends, or moves, down the mountain over the underlying bedrock (Paterson, 1994). The movement to lower elevations increasingly exposes lower parts of the glacier to the factors that induce melting (e.g. solar radiation, warmer air temperatures, rainfall) and other forms of ablation (ways by which mass is lost from a glacier), such as evaporation, sublimation and calving. At the glacier snout, or terminus, rocks and debris picked-up by the glacier over the

course of its travel from a terminal moraine. Melt-water that emerges at or near the glacier terminus arrives directly from the ice surface, through englacial routing via ice-walled conduits (e.g. moulins or crevasses) in the glacial ice, or, more slowly, via subglacial cracks and fissures in the underlying bedrock (Collins, 1978). Melt-water from glaciers largely comprises a mixture of snow- and ice-melt. Some melting also occurs at the base of the glacier (basal melting) due to the pressure of the ice overburden and the friction between the glacier and the bedrock.

The distribution of snow on glaciers has a significant impact on ablation. As well as contributing mass, snow helps to insulate glacier ice from melting. Ice-melt mostly is governed by how much of the glacier's ice surface is free from snow and exposed to melting. The position of the 0 °C isotherm in the atmosphere (i.e. the elevation above which precipitation falls as snow (Collins, 1998b)), the transient snow line (TSL) and the snow covered area (SCA) and are all important factors in determining how much ice is exposed and, hence, the melt from a glacier. As the TSL moves upwards (and SCA reduces) during a melt-season, to reveal more ice, steep increases in ice-melt occur (Collins, 1996). Ice has a lower albedo (radiation reflectance) than snow, which means that radiation is more readily absorbed and melt rates are higher. For example, the degree-day factor for bare ice typically is between 8 to 11 mm/d/°C (Kayastha et al., 2001), about 30% higher than that for clean snow (Singh et al., 2000). Debris cover on glaciers, a common feature of Himalayan glaciers, can also significantly affect ablation rates (Nakawo and Young, 1981; Schaner *et al.*, 2012).

In higher latitude mountains (e.g. in Europe or North America), snow accumulation occurs mainly in winter and the melt season follows in spring and summer. However, in monsoon-affected parts of the central and eastern Himalayas, accumulation- and melt-seasons coincide. The behaviour of the SCA and TSL in this region is less predictable than elsewhere and depends very much on the vagaries of the monsoon, which, not only brings precipitation during summer months but simultaneously suppresses melting by blocking-out solar radiation. In the western Himalayas, where the monsoon influence is weak, snow accumulation is greatest in winter due to moisture-laden westerly winds.

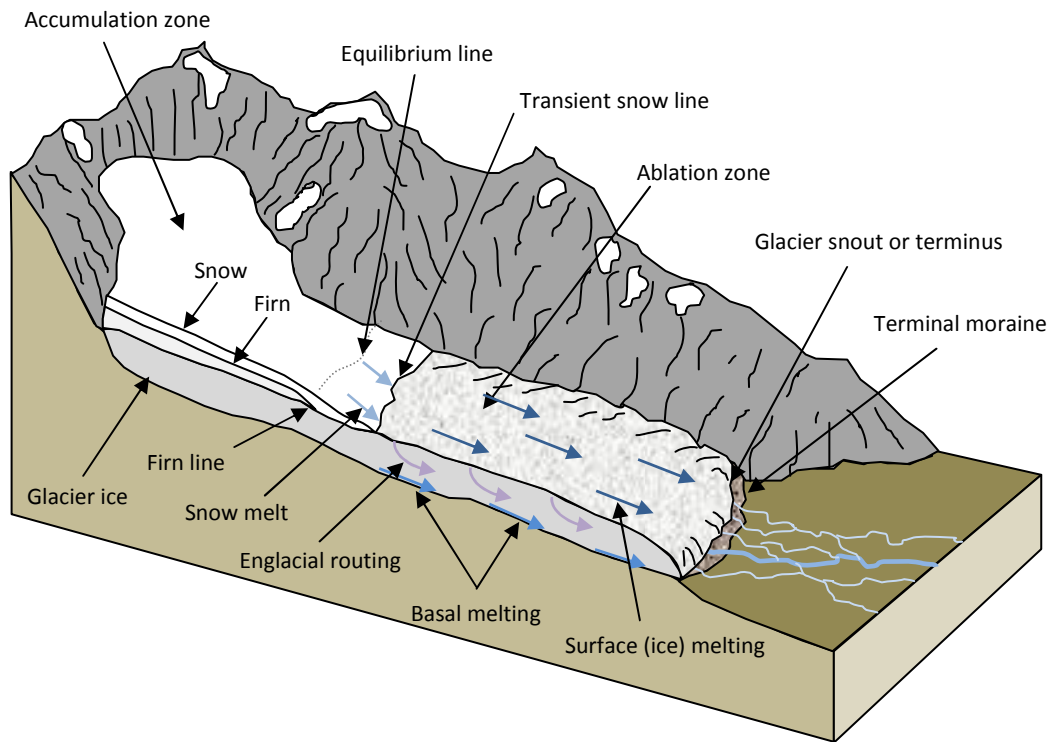


Figure 4.4 Physical features of a glacier to be represented in the glacier-melt model (adapted from Christopherson, 2011)

The maximum elevation of the TSL at the end of the melt-season is referred to as the firn-line. On alpine glaciers, the firn-line approximates to the equilibrium line altitude (ELA) (Hall and Martinec, 1985). Above the ELA, accumulation exceeds ablation and there usually is a net increase of glacier mass over the year. Below the ELA, ablation exceeds accumulation and there is a net loss of mass over the year. Comparing one year's ELA with the average ELA from several years' observations, indicates whether there has been an overall positive or negative mass balance over the year. A rise in the ELA, relative to its average position, reflects a net loss of mass from the glacier, whereas a drop of the firn-line suggests a net gain of glacier mass over the year. Annual mass balance is closely related to the annual runoff (melt-water) from glaciers, with years of negative mass balance resulting in more runoff than years of positive mass balance (Radić and Hock, 2014).

For glaciers in central and eastern Himalaya, the monsoon strongly influences accumulation and ablation and year-to-year variations in mass balance. A strong monsoon typically deposits much snow on glaciers, lowering the TSL, which, along with increased cloud-cover and reduced solar radiation and air temperature, suppresses ablation. Under such conditions, the ELA at the end of the melt season typically is lower than normal, indicating a positive mass balance over the year. A weak monsoon, on the other hand, with little snow deposited, will usually cause the TSL to be higher. More ice would be exposed for longer and an increase in ablation would result. The ELA would finish-up higher than normal at the end of the melt-season, signifying a negative mass-balance year. Over longer timescales, climatic fluctuations correlate with sustained changes in mass balance, which eventually result in variations in glacier extents (Paterson, 1994). Under climatic warming, less snow would be expected to accumulate on glaciers and ice will be exposed longer to higher temperatures, resulting in increased ablation, glaciers having strongly negative mass balances, and termini ultimately retreating.

4.5.3 Data availability

The problem of data availability that traditionally has hampered hydrological modelling in the region is magnified when it comes to the modelling of the region's glaciers. Only ten have been studied in any detail (Singh *et al.*, 2011) and very little still is known of the physical characteristics and dynamic behaviour of the glaciers upon which generalisations can be made. At the time the regional glacier model was being developed in this study, three regional inventories existed: one for the glaciers of Nepal (Mool *et al.*, 2001b), derived from a composite of analogue (paper) maps and remote sensing images; another, similarly derived, for Bhutan (Mool *et al.*, 2001a); and, a third, produced by the Geological Survey of India (GSI) and confined to Indian glaciers only (Kaul and Puri, 1999). The study benefitted from access to the digital maps (arcs and polygons) and the associated feature attribute data that constituted the Nepal and Bhutan inventories. However, requests for the GSI data were turned down because the data were considered classified.

Because the Nepal and Bhutan inventories did not extend to all glaciers in any of the three study basins, it was not possible for these data to be used as the basis for the regional glacier model. Again, the study was required to source data from wider international sources. Two datasets were identified that provided consistent mapping of glacier extents over the entire Himalaya: the ESRI Digital Chart of the World (DCW), which was derived from the Operational Navigation Chart (ONC) 1:1,000,000 vector base map (ESRI, 1993); and the GLIMS (Global Land Ice Measurements from Space) ASTER (Advanced Spaceborne Thermal Emission and reflection Radiometer) acquisition polygons (Raup *et al.*, 2000), compiled from the DCW and data from the World Glacier Monitoring Service's (WGMS) World Glacier Inventory, the National Snow and Ice Data Center's (NSIDC) Eurasian Glacier Inventory. On comparing the datasets in ArcGIS, both plotted glaciers in the same locations but the GLIMS polygons appeared not as well defined as the DCW ones (i.e. fewer points had been used to define the polygons). It was decided, therefore, to use the DCW dataset as the basis for the model.

4.5.4 Identifying a suitable candidate model

With a total of about 30,000 glaciers in the Indus, Ganges and Brahmaputra river basins (Bajracharya and Shrestha, 2011), assessing changes to the combined glacial melt-water contributions to river flows clearly is challenging, particularly when little is known of the glaciers' characteristics. Prior to this study, few MHMs had attempted to represent glaciers at a regional- or global-scale (see §2.6). Meanwhile at the meso-scale, most models of glacierised catchments require detailed information on the distribution of ice within the catchments (e.g. Klok *et al.*, 2001; Verbunt *et al.*, 2003, Huss *et al.*, 2008), which precludes their application at wider scales.

Having few alternatives to consider, the glacier model developed in this study is based on a concept developed by Macdonald (2004), wherein an alpine valley glacier (Findelengletcher) had been represented generically in a catchment-scale hydrological model as a wedge-shaped grid-box in which mass balance was resolved in a distributed manner, for every cell (of the grid-box). In this study, Macdonald's concept was advanced to characterise *all* glaciers in any individual grid cell of Macro-PDM as a single "generic" model glacier.

4.5.5 Defining the model glacier

Macdonald (2004) showed the plausibility of using a generically defined glacier to model daily and sub-daily flows in a small alpine catchment. The novelty of this study was the idea, or hypothesis, that a simple parsimonious model of a single generic glacier could also adequately represent the melt-water contributions from many glaciers in large river basins. Establishing the form the generic glacier would take, and how available regional glacier-cover data might be used to define it, became a fundamental challenge for the study.

To progress the development of the glacier model, a critical decision had to be made on the resolution of the Macro-PDM model grid. Having previously been applied at a range of resolutions (see §4.3.1), any grid cell size theoretically was possible. However, most of the driving data was available at a horizontal resolution of about 0.5°, while antecedent data were available at resolutions upward of 1 km (see Table 4.1). A 0.5° model grid resolution (approximately 48 km x 56 km on the ground at

Himalayan latitudes of around 30 °N) was considered too coarse for the region’s mountainous terrain, but then again it was considered invalid to spatially downscale driving data to too fine a resolution of 10 km or less. A compromise, therefore, was made with the model being arbitrarily defined at a grid resolution 20 km.

Overlaying the Digital Chart of the World (DCW) glacier polygons (ESRI, 1993) onto the 20 km x 20 km grid of each study basin, it was possible to map the proportion of ice, P_{ice} , in any particular grid cell (see Figure 4.5). Rather than simply ascribing the proportion of ice-cover (fractional extent) in each cell as the surface area of the generic model glacier, as adopted more recently by Hirabayashi *et al.* (2010), the study took the more difficult option of considering the surface area of *all* glaciers that contributed melt-water to a cell.

Each individual glacier polygon was given a unique label in ArcGIS and then the glacier coverage was overlaid onto the 1 km USGS Hydro1K DEM in each study basin. The minimum elevation, maximum elevations and location of the minimum elevation were obtained for each individual glacier using ArcGIS zonal tools (ESRI, 2011). Assuming the minimum glacier elevation corresponded to its terminus, it was possible to identify the specific 20 km grid cell that any individual glacier contributed melt-water to. Referring to Figure 4.5, the surface area of the generic model glacier for the central 20 km x 20km cell is defined as the sum of the areas of glaciers A_1 and A_2 , both of which have their minimum elevations in the same cell, but excludes glacier A_3 , which has its minimum elevation in an adjacent cell. The minimum elevation of the central cell’s model glacier, $z_{ice_{min}}$, thus is the minimum elevation of contributing glaciers (i.e. the lowest minimum elevation); its maximum elevation, $z_{ice_{max}}$, is the maximum elevation of all contributing glaciers (the highest maximum elevation).

Written generally, for any n glaciers whose minimum elevations (or termini) occur in a given cell, the defining features of the cells’ model glacier are calculated as follows:

$$A_{ice} = \sum_{i=1}^n A_i \quad \dots(4.7a)$$

where A_{ice} is the area (km^2) of the model glacier and A_i is the surface area of each contributing glacier, i , (also km^2). The minimum and maximum ice elevations of the model glacier, $z_{ice_{min}}$ and $z_{ice_{max}}$ respectively, are:

$$z_{ice_{min}} = \min\{z_{min_i}, i = 1, 2, \dots n\} \quad \dots(4.7b)$$

and

$$z_{ice_{max}} = \max\{z_{max_i}, i = 1, 2, \dots n\} \quad \dots(4.7c)$$

where z_{min_i} is the minimum elevation of a contributing glacier, i , and z_{max_i} is its maximum elevation (both expressed in units of m ASL).

The generic model glacier characteristics, P_{ices} , A_{ices} , $z_{ice_{min}}$, and $z_{ice_{max}}$, were derived for every cell in each basin and eventually supplied as antecedent data to the model.

In contrast to Macdonald's (2004) approach, in which the model glacier was represented as a grid-box of cuboid cells, here each cell's model glacier was given a simple, idealised shape and depth profile, described by 20 contiguous rectangular prisms, or "ice-bands". The upper surface area of each ice-band is defined according to a pre-defined, and adjustable, areal (shape) profile. Various shape profiles were tested (e.g. rectangle, inverted isosceles triangle, rhombus and ellipse), only for a shape that resembles a typical alpine valley glacier (Figure 4.6), from Findelengletscher in the Swiss Alps (Collins, 1998a), to be finally chosen.

Uppermost surfaces of ice-bands are arranged at regular intervals between the vertical extremes of the model glacier, defined by the minimum and maximum elevations, $z_{ice_{min}}$ and $z_{ice_{max}}$, of contributing glaciers. A triangular depth profile is assumed along the thalweg (spine) of each model glacier, with a nominal minimum depth, d_{min} , (m water equivalent (w.e.); 25 m w.e. in this particular application) at ice-bands 1 and 20 and maximum thickness at a pre-set distance up the glacier (halfway, at ice-bands 10 and 11, in this application).

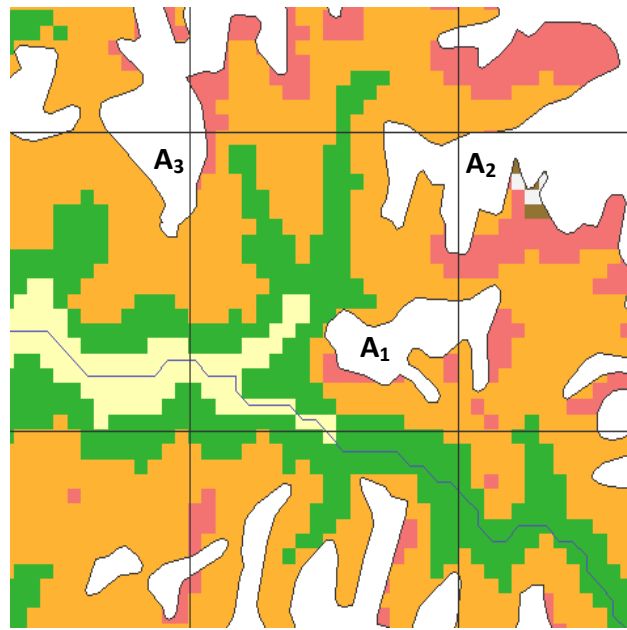


Figure 4.5 Determining the area of the generic model glacier. DCW glacier cover (white polygons) and USGS Hydro1k DEM (coloured grid) mapped onto a 20km Macro-PDM grid cells (thin lines). The termini of glaciers A_1 and A_2 are within the central grid-cell; all melt-water from these glaciers contribute to the runoff of this cell. Although some of glacier A_3 is in the central cell, its melt-water contributes to the runoff of the adjacent cell. The sum of the areas A_1 and A_2 gives the area, A_{ice} , of the model glacier for the central cell.

Maximum thickness, d_{max} (m w.e.), varies for each model glacier according to an empirical relationship (Equation 4.8), derived from glaciers in the Tien Shan mountains of Central Asia, (Liu and Ding, 1986, in Mool *et al.*, 2000), that relates mean ice thickness, d_{mean} (m), to glacier area, A (km²). Maximum thickness is limited to a prescribed value, $maxdepth$, (set as 250 m w.e., in this application, after Müller, 1970), to ensure model glacier thicknesses do not become unrealistically large.

$$d_{mean} = -11.32 + 53.21 \cdot A_{ice}^{0.3} \quad \dots(4.8a)$$

where A_{ice} (km²) is the glacier area, and

$$d_{max} = \begin{cases} (2 \cdot d_{mean}) - d_{min} & \text{where } (2 \cdot d_{mean}) - d_{min} < maxdepth \\ maxdepth & \text{where } (2 \cdot d_{mean}) - d_{min} \geq maxdepth \end{cases} \quad \dots(4.8b)$$

The combination of prescribed shape (Figure 4.6) and depth profiles (Equation 4.8) used in this particular application results in model glacier volumes, V , varying proportionately with surface area, A , with an exponent of 1.33, for glaciers having maximum thicknesses up to 250 m. Thereafter the relationship is linear. Such geometries are not too dissimilar to those described by Bahr *et al.* (1997), who generally predict valley glacier volumes being proportional to surface area with an exponent of 1.375 and report exponents ranging from about 1.3 to 1.4 from studies in the Altai and Tien Shan mountains.

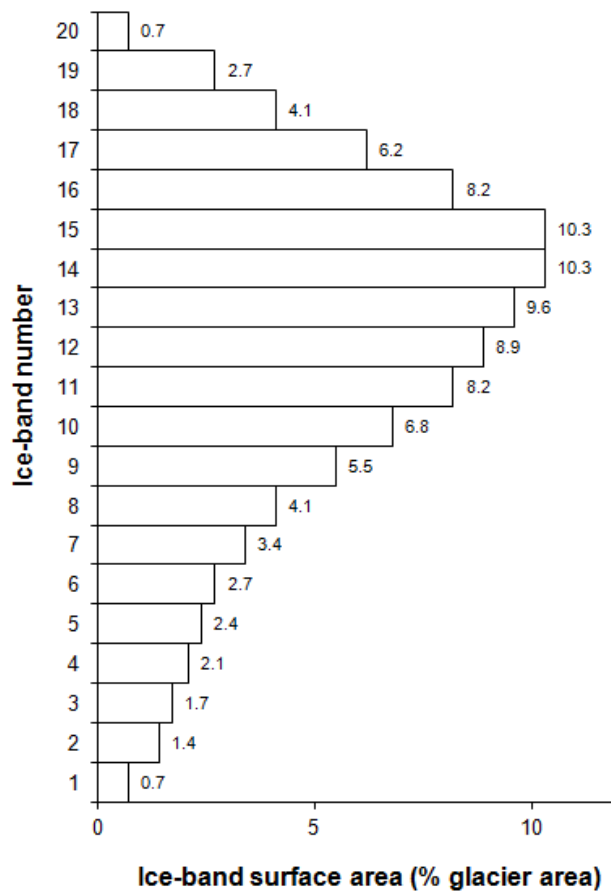


Figure 4.6 Area distribution diagram for the generic glacier, resembling the hypsometry of a typical alpine glacier in the Swiss Alps (Collins, 1998a). The figure shows the percentage of glacier area from lowest to uppermost ice-band (1-20)

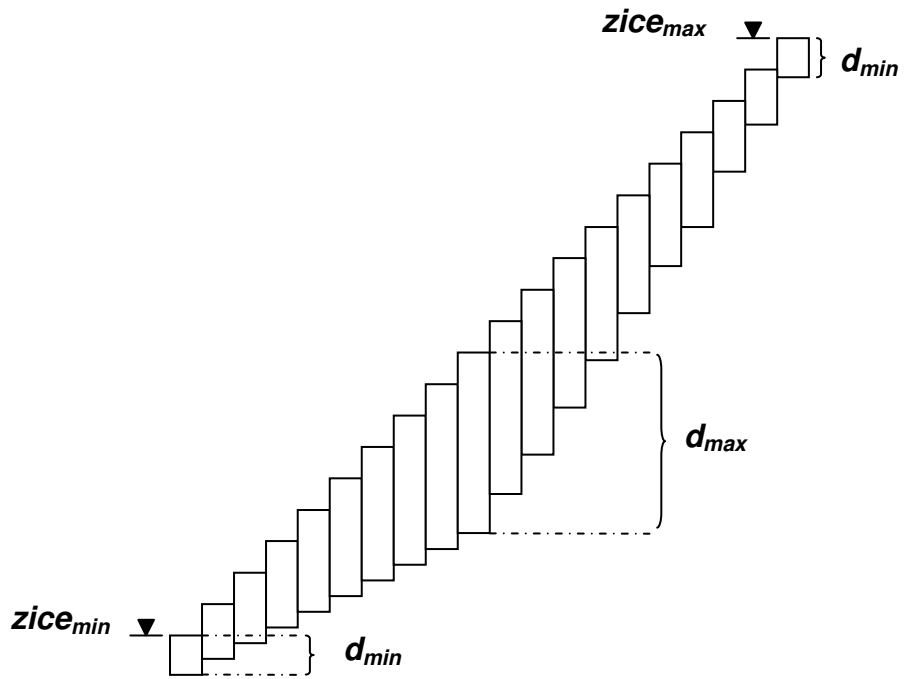


Figure 4.7 A side elevation view of a model glacier having nominal minimum depth, d_{min} , (m w.e.) at ice-bands 1 and 20 and maximum thickness at a pre-set distance up the glacier (at ice-bands 10 and 11, in this example). Maximum thickness, d_{max} (m w.e.), varies according to an empirical relationship (Equation 4.8), derived from Tien Shan glaciers (Liu and Ding, 1986)

4.5.6 Modelling the glacial melt-water contribution to cell runoff

The melt-water that emerges at a glacier terminus usually comprises a mixture, albeit in varying proportions depending on weather conditions, of ice-melt, snowmelt and rain water. In the glacier melt model developed in this study, melt-water generation is calculated independently for every ice-band of the model glacier. Each ice-band is conceptualised as a series of linear storage reservoirs (Figure 4.5). Similarly to the rainfall-runoff part of the model (§4.3.2), daily precipitation and temperature inputs are lapse-rate adjusted to the elevation of the ice-band's upper surface. Accumulation and depletion of the snowpack within an ice-band is also dealt with according the snowpack-snowmelt model (Bell and Moore, 1999), which is applied whenever snow falls on, or is present in, the band. However, with the glacier model, melt-water that is released from the snowpack's wet-store is added to the band's ice-melt store, as opposed to being added the soil moisture store of the rainfall-runoff model. The movement of the transient snow line (TSL) can be tracked daily according to whichever ice-bands have snow present, or absent, in their dry-snow stores.

The ice-melt store is a single linear reservoir representing the englacial and subglacial pathways of melt-water movement through the glacier (Collins, 1979). Its capacity varies according to the ice-depth of the respective ice-band. Water drains slowly from the ice-melt store, at a rate proportional to the depth of water held, until the store reaches capacity, whereupon excess water rapidly drains away (Figure 4.8).

Ice-melt occurs from the upper surface of an ice-band only when the dry-store of the snowpack is empty (i.e. when the ice surface is exposed), the corresponding daily air temperature is above the temperature at which snow begins to melt (T_{melt}), and ice is present in the band. Again, a temperature-index approach is used to calculate the surface ice-melt, with melt-water generated at the constant rate of the degree-day factor for ice, DDF_{ice} (mm/°C/day). Ice-melt, in mm w.e., is added to the ice-melt store, while the band's ice-depth reduces simultaneously by the same amount. Rainfall on exposed ice is added directly to the ice-melt store.

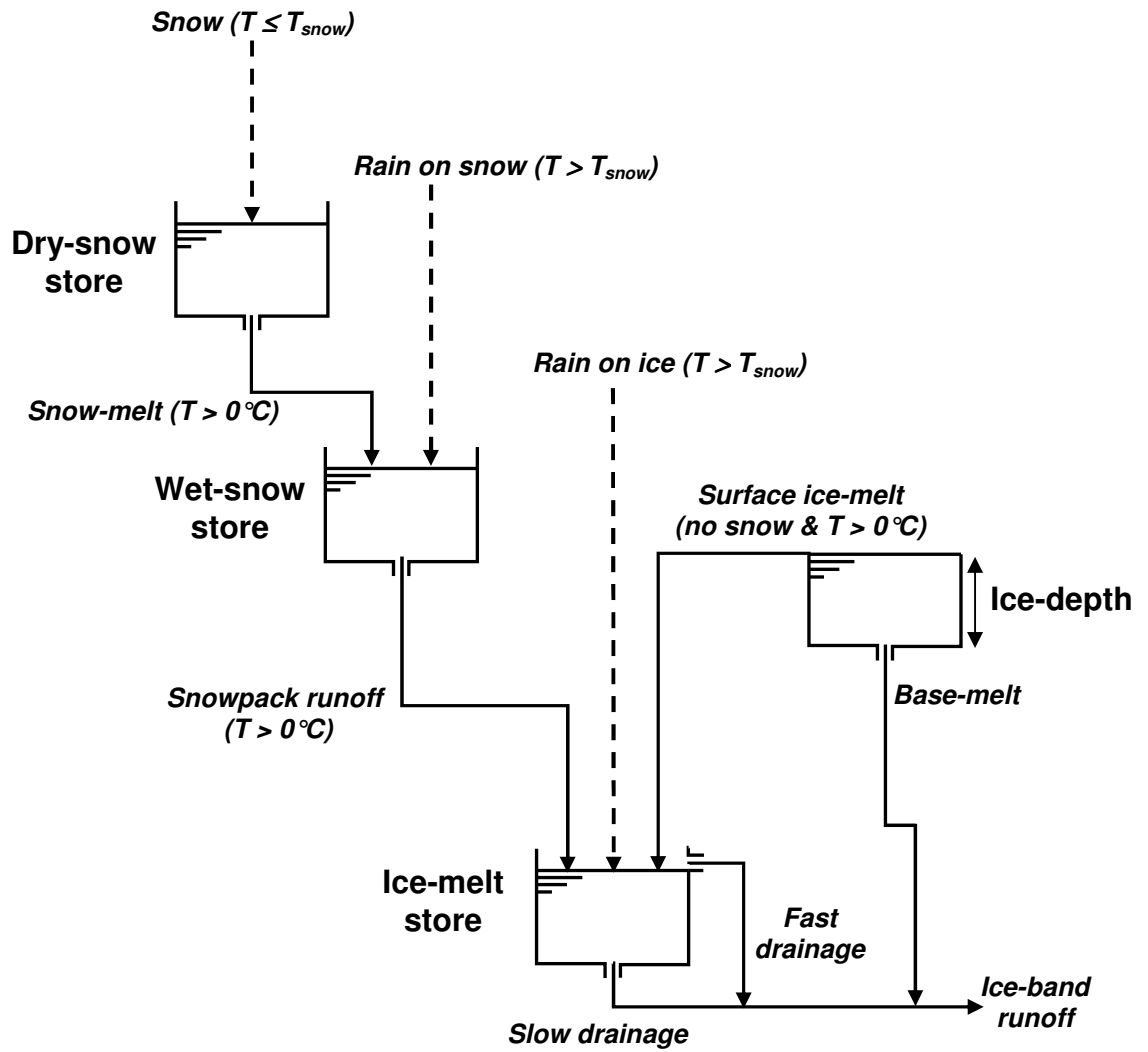


Figure 4.8 Schematic of snow- and ice-stores in an ice-band of the glacier-melt model

The capacity of the ice-melt store (*meltcap*, mm) is proportional to the band's ice-depth. When the ice-melt store is below capacity, water is released slowly, at a rate (k_{slow}) proportional to the depth of water in the store, whereas any water above capacity drains quickly, at a rate (k_{fast}) proportional to amount of excess water. Ablation from the base of the glacier, assumed to be generated by friction between the ice and rock only (geothermal effects are not considered), provides a daily base-melt component that contributes directly to the water emerging from the ice-melt store. Daily base-melt (mm) is assumed to be directly proportional to the band's ice-depth (m), with the proportionality constant, k_{base} , assigned a value of 5×10^{-3} mm/m/day. Such a k_{base} value provides base-melt estimates that are consistent with those found for glaciers in Langtang Khola, Nepal (Braun *et al.*, 1993). Values for the parameters of glacier melt model are shown in Table 4.2 at the end of the chapter.

Hydraulic routing of melt-water between ice-bands is not considered because the timescale of the model application (i.e. daily runoff aggregated to seasonal or annual) negates the need to represent a process that determines melt-water release at the daily or sub-daily scale. Daily runoff from the model glacier (Q_g), thus, is simply calculated as the sum of the daily runoff from all ice-bands, expressed as an uniform depth, in mm, over the 400 km^2 Macro-PDM grid cell (Equation 4.9).

$$Q_g = \frac{\sum_{i=1}^{20} Aband_i \cdot Qband_i}{A} \quad \dots(4.9)$$

where $Aband_i$ is the area (km^2) of each ice-band i ($i = 1, 2, \dots, 20$, the number of ice-bands), $Qband_i$ is the runoff (mm) from each ice-band, A is the cell area (400 km^2).

Combining the glacier runoff (Q_g) with the runoff generated from the glacier-free part of the cell (Q_s), finally gives the total daily cell runoff (Q_t , mm) (Equation 4.10):

$$Q_t = Q_g + (1 - P_{ice}) \cdot Q_s \quad \dots(4.10)$$

where P_{ice} is the proportion of the cell initially covered by ice.

4.5.7 Representation of glacier retreat

The glacier-melt model allows surface area of model glaciers to reduce in-situ, according to their prescribed geometries, as the ice in each ice-band thins through ablation. The dynamic movement, or deformation, of ice, a feature of several meso-scale models (e.g. Huss *et al.*, 2010; Immerzeel *et al.*, 2012; Lüthi, 2009), was not modelled because such sophistication could not be supported by the limited glacier data that were available locally.

For each model glacier, the ice-depth of each ice-band are updated daily. The total volume of “snow” remaining in all ice-band dry-snow stores at the end of each melt season is redistributed evenly as “ice” across remaining bands. As such, the model does not represent the accumulation of firn from year-to-year.

Glacier retreat is represented by the depletion of ice-depth from ice-bands. No further ice-melt can originate from the ice-band once ice-depth in an ice-band has fully depleted (ice-depth = 0). The snowpack model continues to be applied in each ice-band, with any snowmelt that is generated in the ice-band added directly, without routing through the ice-melt store, to the total glacier runoff. Rainfall similarly contributes directly to the total glacier runoff whenever there is no snow present in the fully depleted ice-band.

Table 4.2 Model parameters and typical values they are assigned

Module	Parameter	Typical Value	Definition
<i>Temperature-related parameters (general)</i>	T_{snow}	+2.0 °C	Temperature threshold to discriminate between rain and snow
	T_{melt}	0 °C	Temperature at which snow will begin to melt
	α	±6.0 °C/km	Temperature lapse rate
	DDF_{snow}	4 mm/°C/day	Degree-day-factor for snow, the volume of snowmelt in mm water equivalence per positive degree-day
<i>Snowpack-snowmelt module</i>	S_C	0.5	Critical liquid water capacity, the proportion of the wet-snow store above which fast drainage occurs
	$k1$	0.1/day	Slow drainage constant from the wet-store
	$k2$	0.9/day	Fast drainage from the wet-store surplus
<i>Precipitation lapse rate module</i>	ΔP	5 %/100m	Precipitation lapse rate
	z_{adjmin}	1000 m	Minimum elevation for precipitation adjustment
	z_{adjmax}	3000 m	Maximum elevation for precipitation adjustment
<i>Seasonally adjusted temperature lapse rate</i>	α_{sum}	±6.5 °C/km	Summer temperature lapse rate (April – September)
	α_{winter}	±5.5 °C/km	Winter temperature lapse rate (October – March)
<i>PE lapse rate</i>	ΔPE	0.8/km	Potential Evaporation lapse rate as a proportion per km

Module	Parameter	Typical Value	Definition
<i>Glacier-melt model</i>	d_{min}	25 m w.e.	Minimum initial depth of the model glacier
	$maxdepth$	250 m w.e.	Maximum initial depth of the model glacier
	$wequivk$	1.2048 mm	water equivalence of 1 mm of glacial ice
	DDF_{ice}	9 mm/°C/day	Degree-day-factor for ice, the volume of surface ice-melt in mm water equivalence per positive degree-day
	k_{base}	0.055 mm/m/day	Proportionality constant between depth of ice-band and released basal melt-water
	$Liu-c$	-11.32	Liu and Ding c parameter (see Equation 4.8)
	$Liu-m$	53.21	Liu and Ding m parameter (see Equation 4.8)
	$Liu-e$	0.3	Liu and Ding exponent (see Equation 4.8)
	$meltcap$	20 mm	Ice-melt store capacity (mm)
	k_{slow}	0.01/day	Slow drainage coefficient from ice
k_{fast}	0.9/day	Fast drainage coefficient from the ice-melt store	

5 Application of the regional model

5.1 Introduction

This chapter describes how the regional hydrological model was applied in the three study basins. It first describes how the conceptual model, described in Chapter 4, was translated into an executable computer programme (§5.2) and how the data that were required to run the model in each of the three basins were prepared and conditioned for use (§5.3). Details are then provided (§5.4) of how the model was applied to derive estimates of standard-period average annual and seasonal runoff and how these were transformed into estimates of baseline river flow at any point on any river in each of the three basins. The approach to model tuning and validation is then outlined (§5.5). The penultimate section (§5.6) details the various future climate change “scenarios” that were applied to the model. Section 5.7 finally describes how the resulting model outputs were processed to provide estimates of future decadal changes in glacier-fed river flows, relative to the baseline, over a future time horizon of up to 100 years.

5.2 Software modifications

The previous chapter presented the conceptual design of new model components for the application of Macro-PDM in the Himalaya. Despite Macro-PDM having been applied previously in many parts of the world, some major modifications were necessary to the model code (the program) to incorporate these new capabilities (see §4.4 & §4.5) and enable estimates of river flow to be readily derived from the model’s outputs.

The original, 2001 version of Macro-PDM (Tate and Meigh, 2001) had been written in Fortran 95 to run on PCs running the Microsoft Windows operating system. Fortran is a procedural programming language that is widely used in the hydrological sciences because of its numerical computation capabilities. Fortran programs are made up of statements and procedures (subroutines and functions) that are executed in a specific sequence (Sebesta, 1996). For this study, the Macro-PDM code, including the main program and all subroutines and functions, was brought into the Compaq Visual Fortran (CVF) environment for Windows applications development.

Having imported the code into CVF, one of the first tasks was to assess how data would be input and model results output from the software. In the original 2001 version, all cells were given a label, from which the cell's geographical location could be discerned, and all driving- and antecedent-data were referenced according to this label in two big text files. Model output was similarly referenced. This approach, as well as generating large, unwieldy files, did not lend itself readily to any pre- or post-processing that would be required in ArcGIS.

The input and output subroutines of Macro-PDM, were thus replaced to receive data, and produce results, in ArcGIS ASCII-GRID raster format (ESRI, 2013). Such "grid" files are plain text files in which data are arranged in a rectilinear (orthogonal) grid, in rows and columns. The file header defines the spatial extent of the grid, by specifying the geographic coordinates of the lower left and upper right corners of the grid, the cell size and the number of rows and columns that make up the grid. The location of any grid cell is easily identified by its row and column. As applied in this study, each single grid file contains one static data type (or data layer) only, which means a sequence of gridded data (e.g. a time series of gridded rainfall) would need to be represented by a set of many identically formatted files, with one file (layer) per time-step. Multiple, identically formatted data files (i.e. same header information and number of rows and columns) therefore can be assembled to form a stack of layers, making it possible to drill-down through the stack to obtain sequences or aggregations for any one cell or groups of cells. A major benefit of this approach is that any required input data can easily be manipulated, re-sampled, and prepared to the correct resolution in ArcGIS and applied directly to the program. Output written to files of the format can similarly be applied directly to ArcGIS for post-processing. Examples of these benefits can be seen later in this chapter.

The required model modifications were applied to relevant parts of the Macro-PDM Fortran program. The seasonally adjusted temperature lapse rates (§4.4.3) were applied to the existing lapse rate subroutine, and two completely new subroutines were written to allow for the adjustment of precipitation with elevation (§4.4.2) and to model glacier-melt and retreat (§4.5) respectively. Further minor changes were required to introduce the new model parameters associated with the new model

components and to produce the required long-term average annual- and seasonal-runoff outputs.

The resulting, new version of the Macro-PDM programme comprises over 1,000 lines of executable Fortran code arranged in 28 separate subroutines. Pseudo-code, describing at a high-level, and in an understandable form, the sequence of actions carried out by the new program, is presented in Box 5.1. The many areas where software modifications were applied are highlighted in bold.

5.3 Data Conditioning

As illustrated in Figure 4.3, Macro-PDM requires two main types of gridded input data: climate “driving” data (i.e. precipitation, temperature and potential evaporation); and “antecedent” data that describe the initial state of the catchment and play a major role in controlling and moderating runoff generation (i.e. soils, vegetation, elevation and glacier cover). All gridded input data must be commonly referenced in the same geographical map projection and have the same grid size and resolution (cell size), in this instance 20 km x 20 km. A further condition is that all data be available uniformly, at the specified resolution, over the entire domain of interest (Arnell, 1999). Data that were readily available to the study were identified and are listed in Table 4.1. The following sub-sections outline how these data were prepared (conditioned) for use in the new Macro-PDM program.

5.3.1 Map Projection

With the aim to apply the model separately in each of the three study basins, separate grids (stacks) of data needed to be derived consistently for every basin. All grids that were to be used in the model were defined according to the Lambert Azimuthal Equal-Area (LA) projection (ESRI, 2008), a projection favoured cartographically for preserving the area of polygons with minimal distortion and chosen in this study because its coordinates are expressed conveniently along orthogonal x - and y -axes in units of metres.

Box 5.1: Pseudo Code implementation of the new model

Start: **Open files, read model configuration file, read model parameters, allocate array space**

Read driving data (P, T, PE) and antecedent data (DTM, land-cover, soils, glaciers etc.)

For each row of the model grid...

For each column of the model grid...

If this is a data cell to be modelled...

Disaggregate mean monthly data (P,T,PE) to daily

If mountain cell...

Define elevation bands

If glacier terminus cell, define model glacier ice-bands

For each year...

If change scenario is being applied, update this year's input variables

For each month...

For each day...

For each elevation band

Lapse rate adjust P, T, PE

If below tree-line, calculate interception

If snow if falling or present in band...

Apply snowpack-snowmelt model

Update snow-stores

Calculate snowmelt

End if

Calculate "effective" precipitation

Apply PDM

Update soil- & ground-water stores

Calculate AE

Calculate daily band runoff

Next elevation band

Calculate daily runoff from non-glacier part of cell, Q_s

If glacier terminus cell...

For each ice-band

Lapse rate adjust P, T

If snow if falling or present in ice-band...

Apply snowpack-snow melt model

Update snow-stores

Calculate snowmelt

Else

Apply glacier-melt model

Update ice-stores

Calculate ice-melt

End if

Calculate basal melting

Calculate glacier melt-water from ice-band

Next ice-band

Calculate daily runoff from glacier, Q_g

End if (glacier terminus cell)

Calculate daily cell runoff, $Q_t = Q_g + (1-P_{ice})Q_s$

Next day

Calculate monthly cell runoff

Next month

Calculate annual cell runoff

If glacier terminus cell, calculate annual mass balance and redistribute snow as ice between ice-bands

Next year

(continues next page)

Box 5.1: Pseudo Code implementation of the new Macro-PDM (continued)

(continues from previous page)

```

    Else (mountain cell) ! not a mountain cell!
      For each year...
        If change scenario is being applied, update this year's input variables
        For each month...
          For each day...
            Calculate interception & "effective" precipitation
            Apply PDM
            Update soil- & ground-water stores
            Calculate AE
            Calculate daily cell runoff,  $Q_t$ 
          Next day
          Calculate monthly cell runoff
        Next month
        Calculate annual cell runoff
      Next year
      End if (snow is possible)
      Calculate long-term average annual and seasonal (winter, Oct-Mar) runoff for cell
      Write results to output file(s)
    End if (datal cell)
  Next column
Next row
Close files
Stop
```

5.3.2 Masking Grids

Masking grids were generated for each basin to ensure the model was applied only to valid cells within each study basin. First, the basin boundaries were abstracted from the basin data layer of the Hydro1k dataset (USGS, 2001) and then a basic masking grid was generated at the required 20 km resolution in the LA projection for each basin, such that all cells within the basin boundary were given an integer value of “1” while those outside were given a value of “-9999”, a default “no-data” value. Masking grids similarly were derived at the 0.5° resolution. The basin masking grids would be used subsequently to “pastry-cut” relevant gridded input datasets in advance of being applied in the model.

5.3.3 Climate driving data

Studies to assess the impacts of climate change on long-term water resources are conventionally based on estimates of baseline runoff from trend-free, standard-period climate data. The climate driving data that were used in the study were derived from the CRU 1961-90 standard-period 0.5° global mean monthly climatological dataset (New *et al.*, 1999). This baseline gridded dataset comprises mean monthly values of precipitation, wet-day frequency, mean temperature, diurnal temperature range, vapour pressure, sunshine, cloud cover, ground, frost frequency, and wind speed, derived from a global “dataset of station 1961–90 climatological normals”, in which station data were “interpolated as a function of latitude, longitude, and elevation using thin-plate splines” (New *et al.*, 1999).

Data for the Himalayan region only (broadly defined as 60°-100°E longitude, 20°-40°N latitude) were abstracted from the global CRU dataset. Macro-PDM requires potential evaporation (PE), as well as precipitation and temperature, as basic input data. A Fortran program, used in previous applications of PDM (e.g. Reynard *et al.*, 1997), was applied to the CRU data to derive 0.5° grids of mean monthly Penman-Monteith PE (Monteith, 1965). The Penman-Monteith method for estimating PE is recommended by the United Nations’ Food and Agriculture Organisation (FAO) (Allen *et al.*, 1998) and, of 19 PE estimation methods assessed by Jensen *et al.* (1990), was considered the best performing in humid areas. The 0.5° mean monthly data for

the key climate variables – precipitation and wet-days, temperature and PE – (12 files per variable), were loaded as grids into ArcGIS.

Being such a key input variable for the regional hydrological model, the gridded precipitation data (hereafter considered synonymously with rainfall data) were assessed to see if there was any systematic under- or over-estimation that should be accommodated for in the model. The assessment was made using two sets of observed point rainfall data: the CRU point-rainfall dataset (New *et al.*, 1999) and data from Nepal’s national rain-gauge network. Standard-period grids of average annual rainfall (AAR) and dry-season, or winter (October-March), rainfall (AWR) were derived by simply summing the relevant mean monthly grid values on a cell-by-cell basis in ArcGIS. Grid-based AAR and AWR values were then extracted for every available rain gauge by mapping the rain gauge locations onto the rainfall grids (Figure 5.1). Analysis of the bias between the gridded rainfall data and the CRU point data (Equation 5.1) shows the CRU gridded dataset on average overestimates AAR in all three basins (Table 5.1), particularly in the Brahmaputra, and that AWR tends also to be overestimated in the Indus and Brahmaputra basins but underestimated in the Ganges. However, the variability (standard deviation) in the bias of both AAR and AWR is high in all three basins, suggesting no consistent bias can be attributed to the CRU gridded dataset as far as the CRU point rainfall data is concerned.

$$Bias = 100\% \times \frac{Estimate - Observed}{Observed} \quad \dots(5.1)$$

Similarly comparing CRU gridded data with period-of-record observations from 193 rain gauges of the Nepalese national rain gauge network again shows overestimation on average in the CRU gridded data and a high variability in bias (Table 5.2). Interestingly, the CRU gridded data appears to underestimate AAR but overestimate AWR at higher elevations (> 2000 m) but no consistency can be discerned in the spatial distribution of bias (Figure 5.3). An absence of correlation between raing gauge altitude, latitude and longitude and the biases in AAR and AWR, together with the high variance in biases (Table 5.2), reaffirms there is no consistent over- or under-estimation in the CRU gridded precipitation dataset that could justify corrective adjustment in the model.

The Himalayan-wide 0.5° grids of mean monthly precipitation, wet-days, temperature and PE (x12 per variable) were projected into the Lambert Azimuth Equal-Area (LA) map projection and then re-sampled, using cubic interpolation in ArcGIS (ESRI, 2007), to fit the required model 20 km grid resolution. Cubic interpolation determines the new value of a cell based on a weighted distance average of the 16 nearest cells and is considered the most appropriate for continuous climatic data (ESRI, 2007). The wet-day grids (necessary later for the disaggregation of mean monthly precipitation to a daily time-series (see §5.4.1)), being categorical data (rather than continuous like the other climate variables), were re-sampled according to the nearest cell value. The relevant masking grids (§5.3.2) finally were applied to Himalayan-wide 20km grids to derive the grids that would drive the model in each study basin.

5.3.4 Soils and vegetation data

The necessary soils and vegetation data were obtained from the FAO's Digital Soil Map of the World, (FAO, 1995), and the USGS's Eurasia Land Cover Characteristics Database (USGS, 1997), respectively. Both data sets were imported into ArcGIS and projected into the LA projection. In common with earlier applications of Macro-PDM (e.g. Meigh *et al.*, 1999; Rees *et al.*, 1997), soils were re-classified in ArcGIS into seven texture-based types, while the land-cover data were re-classified simply as either "forest" or "grass". The soils polygons were then gridded at the 1 km resolution before being re-sampled to 20 km and assigned the dominant soil type for the model cell (i.e. an integer value from 1 -7). The re-classified land-cover data, supplied originally at 1 km resolution, was also re-sampled at 20 km resolution and assigned the proportion of forest within the cell (i.e. a real number ranging in value from 0.0 – 1.0). Parameter values for field capacity (FC , the amount of water held in the soil against gravity) and saturation capacity (s_{max} , the amount of water held in the soil when all pore spaces are full), both of which influence soil-water retention within the PDM model (see Appendix A), were set *a priori* according to Vörösmarty *et al.* (1989).

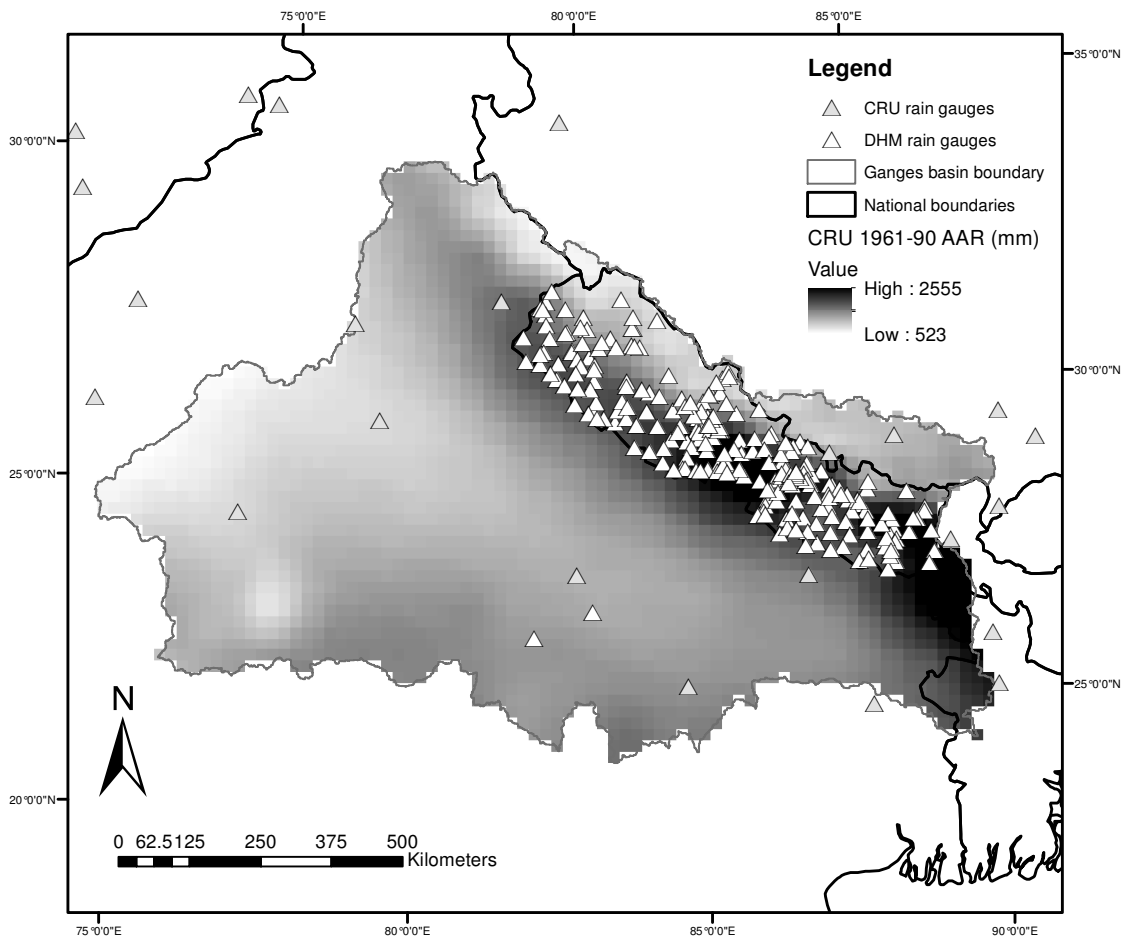


Figure 5.1 Available rain gauges mapped onto the CRU standard-period 1961-90 $0.5^\circ \times 0.5^\circ$ Average Annual Rainfall (AAR) grid for the Ganges basin

Table 5.1 Bias results comparing, in terms of mean bias and the standard deviation (SD) of the bias, Average Annual Rainfall (AAR) and Average Winter Rainfall (AWR) derived from CRU gridded rainfall data with that observed at “CRU” rain gauges in the Indus, Ganges and Brahmaputra basins

Basin	Number of rain gauges	AAR		AWR	
		Mean Bias (%)	SD of Bias (%)	Mean Bias (%)	SD of Bias (%)
Indus	19	+11.3	31.3	+1.2	26.6
Brahmaputra	12	+46.6	81.7	+26.7	101.5
Ganges	8	+7.0	16.6	-14.6	16.5

Table 5.2 Bias results comparing, in terms of mean bias and the standard deviation (SD) of the bias, Average Annual Rainfall (AAR) and Average Winter Rainfall (AWR) derived from CRU gridded rainfall data with that observed at Nepalese rain gauges

Category	Number of rain gauges	AAR		AWR	
		Mean Bias (%)	SD of Bias (%)	Mean Bias (%)	SD of Bias (%)
All Nepal	193	+6.7	34.6	+16.5	28.7
< 1000 m	95	+5.5	32.4	+14.4	27.8
1000–2000 m	70	+2.5	38.5	+7.0	29.4
>2000m	32	-10.9	29.4	+10.2	29.3

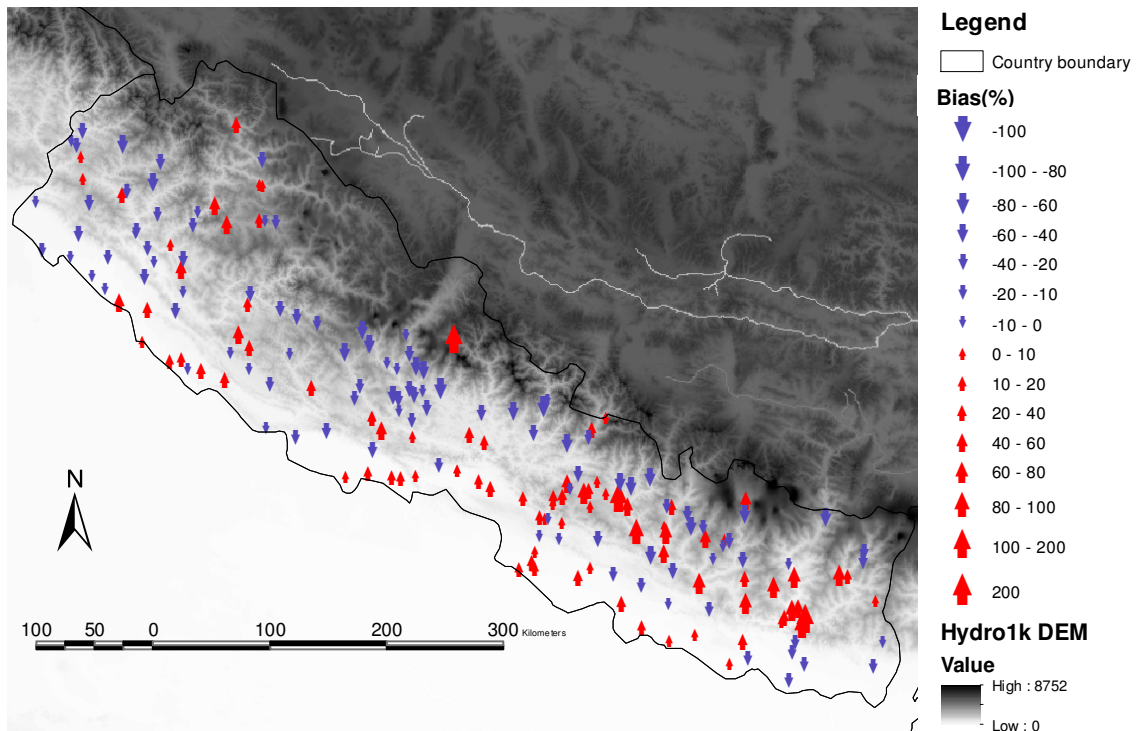


Figure 5.2 Spatial distribution of the bias in Average Annual Rainfall data: CRU gridded data versus DHM observed rain gauge data (red arrows show where CRU data overestimates; blue arrows show where it underestimates)

5.3.5 Digital elevation data

Digital elevation data are essential for the definition and implementation of the regional hydrological model. They are used as antecedent data, to describe the minimum, maximum and mean elevation of each 20 km cell: information that is used within the model to characterise the distribution of elevation within cells. As described in §4.5, they are used in combination with glacier cover data to estimate the initial vertical extents of glaciers and establish which glaciers contribute melt-water to a cell (see also below, §5.3.6). Ultimately, they also are used after model runs to post-process the model output and derive estimates of river flow (see §5.4.3).

The USGS's Hydro1k, a global 1 km resolution digital elevation model (DEM) corrected for known mapped hydrography (i.e. streamlines, drainage basin boundaries, and natural sinks) (USGS, 2001), was identified as the most appropriate DEM for this study. The Hydro1k data for the entire Himalayan region were downloaded and imported as one big grid into ArcGIS. A further 1km resolution DEM was created for each study basin from the big grid. The basin-level DEMs were then overlaid onto the relevant 20 km masking grid and the minimum, maximum and mean elevations for every 20 km cell within each basin were calculated and output as three separate grids, which would later be used as input data to the regional model.

5.3.6 Model glacier-defining data

Chapter 4 (§4.5.5) described how Digital Chart of the World (DCW) glacier polygon data (ESRI, 1993) combined with Hydro1k DEM data to derive the 4 information items needed to define the dimensions of the generic model glacier in every glacier-affected 20 km cell: P_{ice} (the proportion of ice in the cell), A_{ice} (the total area of glaciers that contribute melt-water to the cell), $z_{ice_{min}}$ (the minimum ice elevation of contributing glaciers), and $z_{ice_{max}}$ (the maximum ice elevation of all contributing glaciers). Four grids of these model glacier-defining data were thus derived for each study basin and supplied as antecedent data to the model.

5.4 Model application for the 1961-90 standard-period baseline

Having prepared all necessary data in the correct format, the regional model was applied in each of the three study basins using the CRU 1961-90 standard-period climatology grids (precipitation, rain-days, temperature and PE) for a 30-year model run at the daily time-step. Model results obtained through the application of the standard-period climatology provided the baseline against which the output from future climate scenario runs would be compared.

To run at the required daily time-step, all the mean monthly data that were supplied as input to the model had to be disaggregated to daily at run-time. The approach to the temporal disaggregation of the mean monthly climate data is described below (§5.4.1). The key model outputs at the end of the model run were standard-period estimates of Average Annual- and Average Winter- Runoff Depth (AARD and AWRD respectively) for every 20 km cell in each basin (§5.4.2). These outputs were then transformed, using topographic routing, into estimates of standard-period Mean Flow (MF) and Winter Mean Flow (WMF) for any location along the drainage network of each study basin. Details of the flow derivation are also provided below (§5.4.3).

5.4.1 Temporal disaggregation of the climate driving data

The gridded mean monthly climate input data (i.e. 12 values per variable per cell) were disaggregated at run-time using the same approach described by Arnell (1999) and others (e.g. Meigh *et al.*, 1999). The disaggregation, which is executed within the model at run-time, produces a daily time-series for each of the three essential climate input variables for every cell and for every year of the model-run. However, a different approach is used for each variable:

- Daily *precipitation* data were derived by distributing the mean monthly precipitation total evenly between the number of mean monthly rain-days each month, such that the occurrence of rain-days was arranged randomly every month of the model run.
- Mean daily *temperature* values were derived by linearly interpolating between the mean temperature of the previous and present month (for the first half of the

month) and between the mean temperature of the present and following month (for the second half of the month). A degree of randomness is introduced by adding, or subtracting, a randomly generated value constrained to within ± 1 °C of the original interpolated value.

- Finally, mean monthly values of *PE* were disaggregated to daily simply by applying monthly average value to every day of the respective month.

5.4.2 Average annual- and winter-runoff estimates

The model was applied separately in the Indus, Ganges and Brahmaputra river basins using the CRU 1961-90 climatology data, first for an initial 2-year “warm-up” period, to allow various model stores to fill, or adjust, and then for 30 years, corresponding to the 1961-90 standard period. Daily runoff values, for each day of the 30-year period, were aggregated at run-time to give estimates of standard-period (long-term) average annual and winter (October-March) runoff for every 20 km cell in each of the basins (see Figure 5.3).

5.4.3 Derivation of flow estimates

Estimates of mean- and winter mean-flow for rivers in the three basins finally were derived by re-sampling the 20 km average annual- and winter-runoff grids to 1 km resolution and then applying them (the grids) to the Hydro1k flow-direction grid (USGS, 2001). Previous studies recommend employing higher resolution DEMs for runoff routing because higher resolution drainage networks allow better approximation of actual conditions (e.g. Raje *et al.*, 2013). The resulting flow-accumulation grids, which approximate well to the natural drainage network of the basins, represent the total runoff (annual or winter) accumulated to a single cell from all upstream cells. Further accumulation grids, derived by applying unit weight (cell value = 1) to every cell of the relevant Hydro1k flow-direction grid, provide a measure of upstream catchment area for every 1 km cell. Combining these latter grids with the accumulated annual- and winter-runoff grids provides an estimate of standard-period (baseline) mean- and winter mean-flow (m^3/s) at any location on the derived drainage networks in the study basins. The 1 km flow grids finally were converted to lines (arcs) in ArcGIS,. The result is illustrated in Figure 5.4.

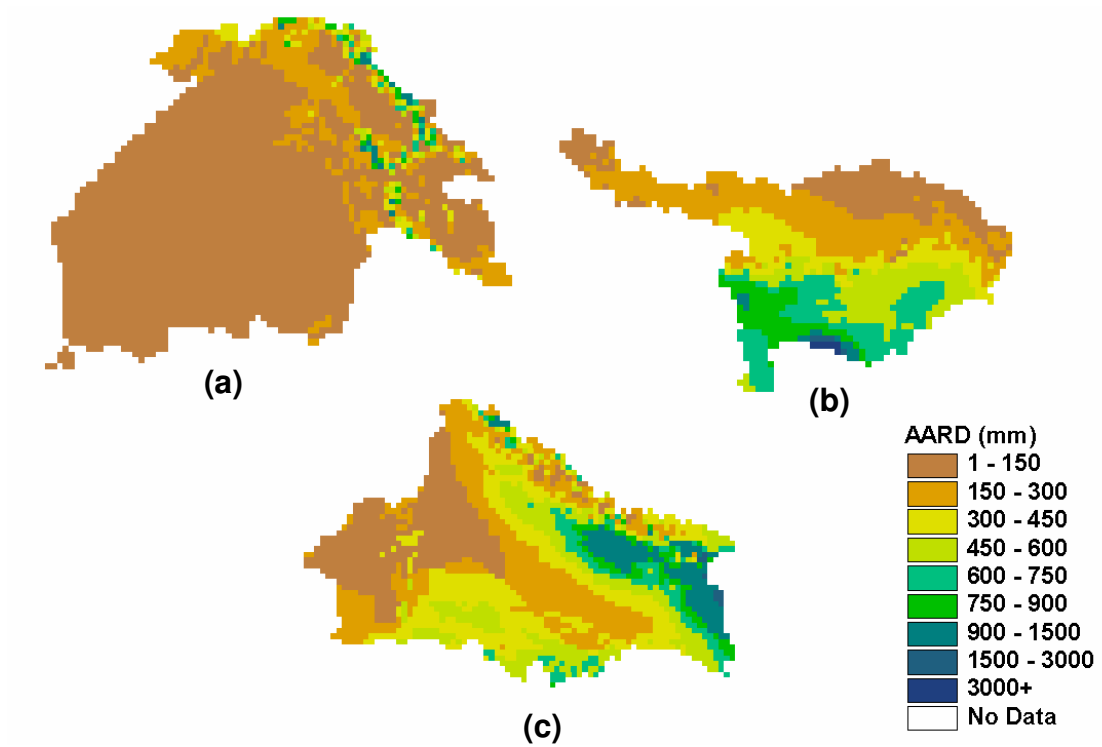


Figure 5.3 Modelled standard-period Average Annual Runoff Depth (AARD) at 20 km resolution for the (a) Indus, (b) Brahmaputra and (c) Ganges basins.

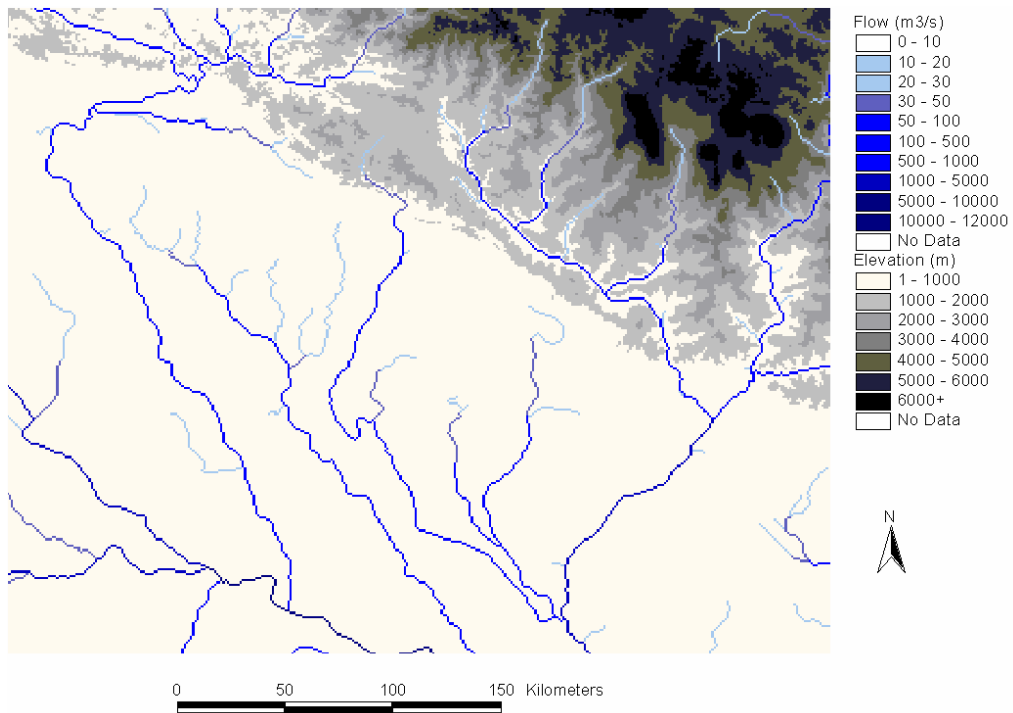


Figure 5.4 An illustration of the drainage network derived from applying the Hydro1k flow direction grid, here showing standard-period mean flow in the upper reaches of the Ganges River basin, derived from model estimates of average annual runoff applied the Hydro1k flow-direction grid

5.5 Model tuning and validation

The conventional method of calibrating catchment-scale models, where parameters are adjusted to optimise a time-series of modelled flows over a calibration period and model performance is then assessed over a separate validation period, is not always appropriate for MHMs, especially when the primary output are singular estimates of long-term mean flow. A process of “tuning”, rather than “calibration”, is commonly undertaken with MHMs (Arnell, 1999), which aims to ensure key model output (long-term average flow or runoff) attain realistic, or plausible, values across the model domain. Results usually are validated against local observations.

In this study, the model was tuned and validated using river flow data from 40 gauging stations in the Upper Indus (Archer, 2003) and Upper Ganges basins (DHM, 1998) whose locations coincided with the derived drainage network of the model. The observed flow data cover a variety of periods, between 1956 (earliest) and 1998 (latest), and durations, from 5 to 40 years. A summary of the stations and their locations are shown in Table 5.3 and Figure 5.5 respectively. Unfortunately, the study was unable to obtain Chinese data for model validation in the Upper Brahmaputra.

Tuning involved repeatedly running the model in either basin, iteratively making manual adjustments to some key model parameters that had greatest influence on output. The values assigned to the majority of parameters, including those characterising the spatially variable soil storages of the rainfall-runoff model (e.g. FC and smax), were set *a-priori*, based on previous applications of Macro-PDM, and remained unaltered for all model runs (Table 4.2). The final chosen values for the few parameters that were adjusted in an effort to improve the baseline flow estimates of the model in the Indus and Ganges river basins are shown in Table 5.5. The values assigned to these parameters are generally consistent with the literature (e.g. Hock, 2003; Singh and Singh, 2001) and earlier Himalayan studies (e.g. Young and Hewitt, 1990; Putkonen, 2004).

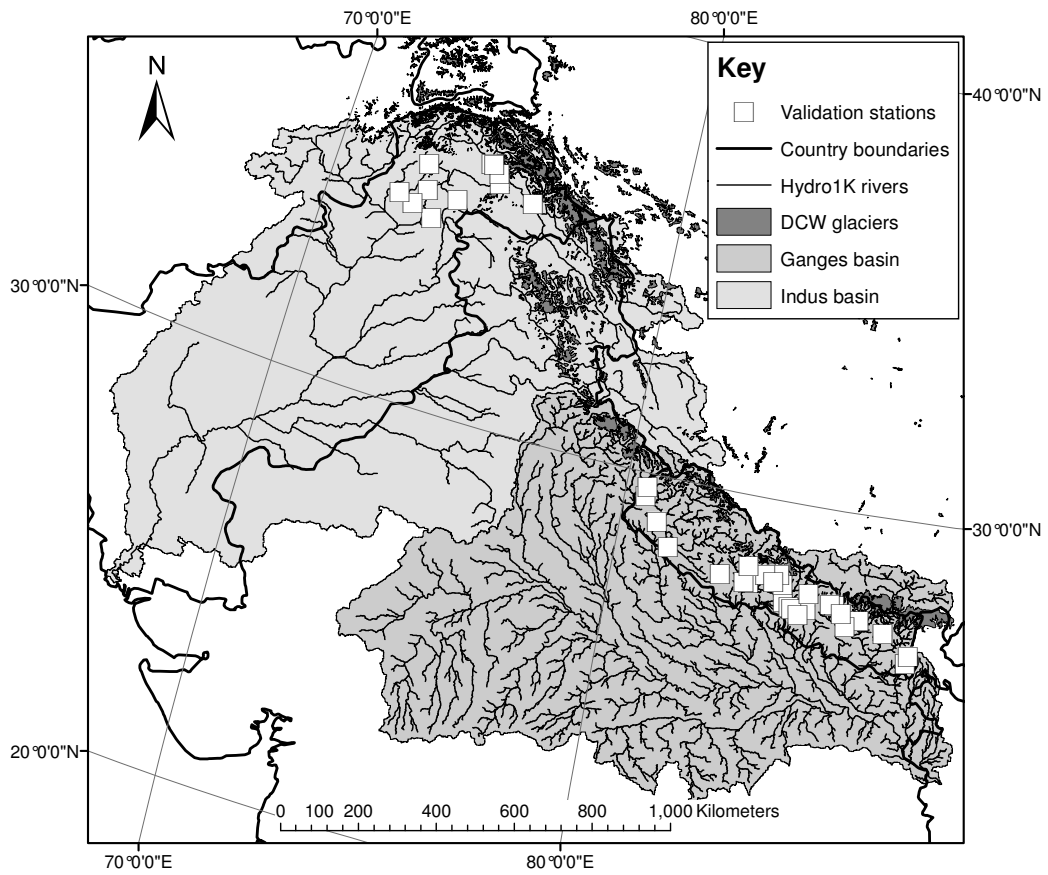


Figure 5.5 Location of stations used for model tuning and validation of the model in the Indus and Ganges river basins

Table 5.3 Summary of the 40 river gauging stations used for model tuning and validation, showing mean, minimum and maximum catchment areas, percentage ice area and period of record for all, glacier-free (no-ice), and glacier-fed (ice) catchments in the Indus and Ganges river basins

Stations	Catchment Area ^a			Percentage ice ^b			Period-of-record ^c		
	<i>n</i>	mean	min	max	mean	min	max	from	to
<i>Indus</i>									
All	11	6870	625	27525				1960	1998
No-ice	4	875	625	1175				1960	1975
Ice	7	10296	2025	27525	15.8	0.5	40.8	1960	1998
<i>Ganges</i>									
All	29	936	80	3000				1964	1995
No-ice	15	752	80	3000				1964	1995
Ice	14	1116	151	2753	10.5	0.1	28.9	1970	1995

Notes:

^a catchment area derived from USGS Hydro1k;

^b percentage of DCW-defined glacier area within a catchment;

^c period-of-record shows earliest (from) and latest (to) year of observed flow data

Table 5.4 Key model parameter values applied in each study basin

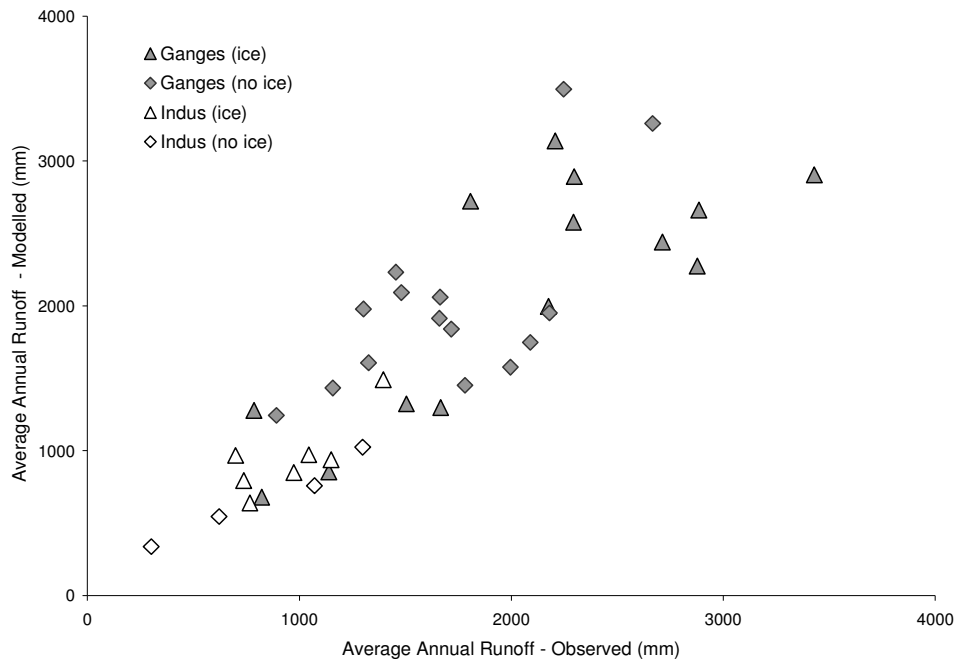
Parameter	Parameter Value			Units
	Indus	Ganges	B'putra	
DDF_{snow}	3	4	3	mm/°C/day
DDF_{ice}	9	12	9	mm/°C/day
α_{win}	±5.5	±5.5	±5.5	°C/km
α_{sum}	±6.5	±6.5	±6.5	°C/km
ΔP	±5	±5	±5	%/km
z_{adjmin}	2500	500	2500	m a.s.l.
z_{adjmax}	5000	3000	5000	m a.s.l.
PE_{adj}	0.5	0.8	0.5	/km
T_{melt}	0	0	0	°C
T_{snow}	+2	+2	+2	°C
k_{base}	5×10^{-3}	5×10^{-3}	5×10^{-3}	mm m ⁻¹ day ⁻¹

Model performance was assessed in terms of bias error, defined as the difference between predicted and observed, expressed as a percentage of the observed (Equation 5.1). Use of a more complex objective function was considered inappropriate given that the observation periods did not correspond exactly with the synthetic 1961-90 model period. For this assessment, both the modelled and observed mean annual and winter (October – March) flows were expressed in terms of the average annual- and winter-runoff depth (AARD and AWRD), as a uniform depth, in mm, over the upstream catchment area. Normalising the flows in this manner eliminates the scaling effect of catchment area on river flows, allowing flow estimates from catchments of different sizes to be directly compared.

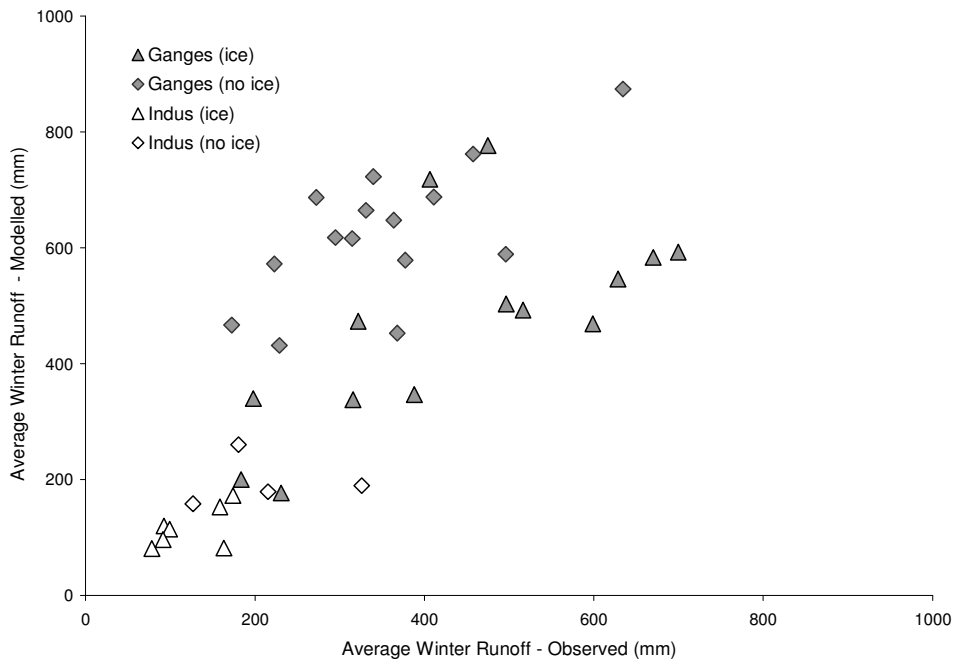
The comparison of model results with observations suggests the model is capable of generating reasonably realistic estimates of catchment long-term average annual runoff depth (mean flow) regionally (Table 5.5). Close inspection (Table 5.5 and Figure 5.6) reveals that Upper Indus mean flows (AARD) generally are underestimated (mean bias of -5), with negative bias values greater on average (mean bias of -13) in glacier-free (no-ice) catchments, while flows in catchments where ice is present, on average, neither are under- nor over-estimated (mean bias of 0). In the Upper Ganges, AARD is generally overestimated (positive bias) for both glacier-free (+19) and glacier-fed catchments (+4). In both basins, bias errors and the variance of bias errors are amplified for estimates of AWRD, presumably because dry-season winter flows are much lower than the annual and can yield proportionally larger (bias) errors. In the Ganges, AWRD is overestimated in all glacier-free catchments. However, further checks for possible systematic errors in model results revealed no significant correlations between bias errors and catchment area, mean elevation, latitude, longitude, or the proportion of ice in catchments.

Table 5.5 Mean, minimum, maximum and standard deviation of bias errors between model estimates and observed Average Annual and Winter Runoff Depth (AARD and AWRD) for glacier-fed (ice) and glacier-free (no-ice) catchments in the upper Indus and Ganges basins

Basin	AARD Bias (%)					AWRD Bias (%)			
	<i>n</i>	mean	min	max	SD	mean	min	max	SD
<i>Indus</i>									
All	11	-5	-29	+38	19	+1	-50	+44	29
No-ice	4	-13	-29	+12	18	+3	-42	+44	39
Ice	7	0	-18	+38	20	0	-50	+29	25
<i>Ganges</i>									
All	29	+12	-25	+63	29	+52	-23	+170	57
No-ice	15	+19	-21	+56	27	+88	+19	+170	47
Ice	14	+4	-25	+63	30	+12	-23	+77	36



(a)



(b)

Figure 5.6 Comparison between model estimates and observations for glacier-fed (ice) and glacier-free (no-ice) catchments in the upper Indus and Ganges basins: (a) average annual runoff; (b) average winter (October-March) runoff

To assess whether the glacier-melt model had a significant bearing on baseline flow estimates, the model was re-applied with the glacier-melt component disabled. Similarly, to examine the importance of the prescribed geometry of the model glaciers, the model was then applied again with the model glacier assigned a rectangular areal profile (i.e. all ice-bands of equal upper surface area). The results for the two additional model runs, using the previous parameter settings (Table 5.4), were compared with the original model estimates of AARD for glacier-fed catchments only (Figure 5.7). The results show that disabling the glacier-melt model reduces model estimates in both basins, with reductions, as expected, greatest in highly glacierised catchments. Mean bias errors in modelled AARD become more negative, by an extra -2% on average for catchments in the Upper Indus basin and by an extra -6% for those in the Upper Ganges. Differences in modelled AARD between either application are significant at the 5% significance level. Changing the shape of the model glacier also significantly affects results, with runoff estimates increasing when the rectangular-shaped glacier is used, probably due to the presence of a higher proportion of glacial ice at lower elevations. Again, effects are most noticeable in highly glacierised catchments. Mean bias errors in AARD become more positive with the rectangular shape, by an extra $+11\%$ and $+5\%$ for catchments in the Indus and Ganges basins respectively.

Modelled annual mass balance estimates, derived by monitoring status of snow- and ice-stores within the model, provide a further plausibility check. Observed annual mass balance data for the Dunagiri ($79^{\circ} 54' E$, $30^{\circ} 33' N$) and Langtang ($85^{\circ} 30' E$, $28^{\circ} 30' N$) glaciers, in the Upper Indus and Ganges basins respectively (Dyrgerov, 2005), were compared with annual mass balance estimates for the model glaciers of corresponding grid-cells. For Dunagiri, observed annual mass balances varied between -945 and -1289 mm/year from 1986 to 1990; the corresponding model glacier had annual mass balances of between -1019 and -1332 mm/year over the 30 years of the model period. Similarly, observed annual mass balance data for Langtang, varied between $+390$ and -700 mm/year from 1987 to 1997, while estimates for the matching model glacier ranged from -13 to -152 mm/year over the longer model period. Although this very limited sample provides no indication of how annual mass balance is captured throughout the model domain (study area), it does infer plausible behaviour.

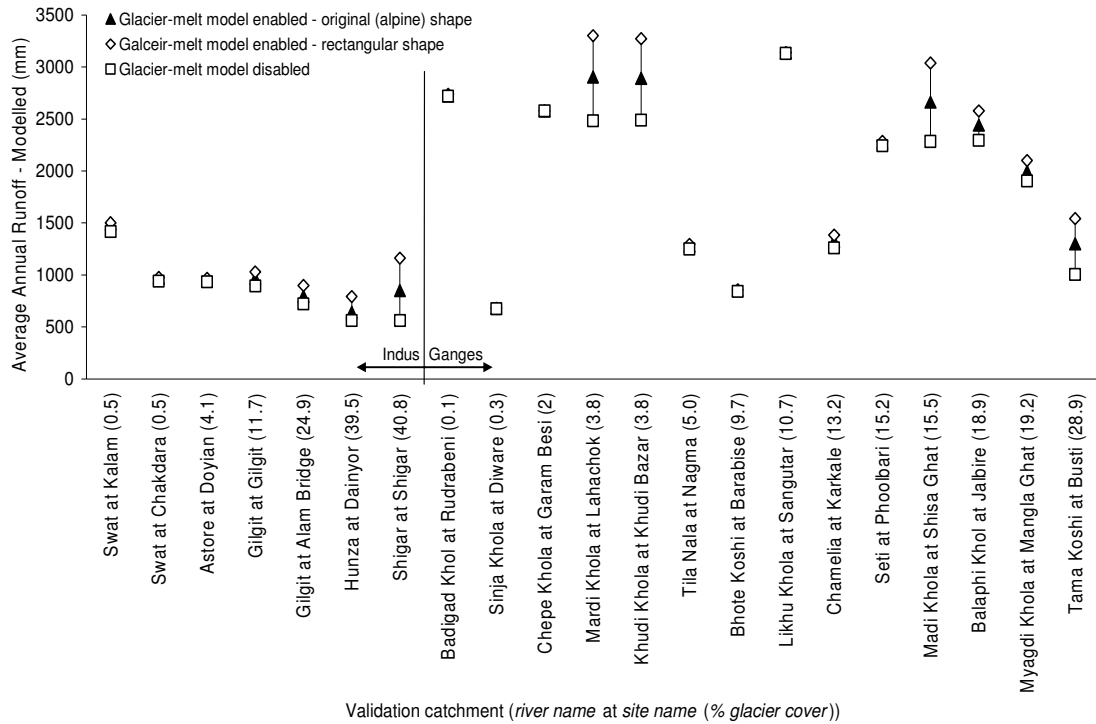


Figure 5.7 Comparison of results for alternative model runs in glacier-fed catchments of both basins: solid black triangles denote the original Average Annual Runoff Depth (AARD) estimate; hollow diamonds show AARD estimates where the model glacier has been ascribed a rectangular shape profile; and hollow squares AARD estimates where the glacier melt model has been disabled. Catchment names are along the x-axis with the percentage ice cover, as defined by DCW, in brackets.

5.6 Future climate representation

A representation of the future climate is necessary to model deglaciation and its effect on Himalayan river flows. Many studies to assess the impact of climate change on the hydrology of catchments represent future climatic conditions according to GCM-based climate change scenarios that are often downscaled (e.g. as RCMs) for the area or region of interest (Prudhomme *et al.*, 2010). Many studies continue to employ the WMO 1961-90 standard period as the baseline (e.g. Immerzeel *et al.*, 2013) and then apply scenarios directly to a hydrological (impact) model to assess the relative changes between the baseline and scenario periods. Despite their popularity, GCM-based scenario approaches often have considerable uncertainties associated with them, which are especially manifest in areas of high topographic variability, such as the Himalayan region (Immerzeel *et al.*, 2013). Although several new RCMs have recently been developed in the region (e.g. Rajbhandari *et al.*, 2014; Moors and Siderius, 2012), projections still show much uncertainty (Moors and Siderius, 2012) with disagreement even in the sign of change (positive or negative) for future precipitation (Rajbhandari *et al.*, 2014).

Such difficulties have resulted in alternative approaches of characterising future conditions gaining traction in climate impact studies. These include (after Carter *et al.*, 2007): artificial experiments, in which unrealistic representations are made of future conditions; analogues, that use similar climatic events in the past as an analogy for the future climate; large-scale singularities, defined as extreme, sudden or irreversible, changes; and sensitivity analyses, in which regularly spaced adjustments (or increments) of important driving variables allow the sensitivity to climatic variations to be assessed. Several such approaches, as well as a GCM-based scenario, were applied in this study in an attempt to gain a comprehensive understanding of the different potential outcomes for varying future climates.

The first, and simplest approach to apply in the model, was an *artificial experiment* (or, arguably, a *large-scale singularity*) in which glacier-cover universally reduced by 50% in each study basin. The reduction was applied at run-time by simply halving the model glacier-defining data P_{ice} (the proportion of ice in the cell) and A_{ice} (the total area of glaciers that contribute melt-water to the cell). The model was run for a

nominal 30-year period with no adjustment of CRU 1961-90 standard-period climate input variables.

Second, the model was run as a *sensitivity analysis*, for a range of incremental adjustments in temperature ($^{\circ}\text{C}/\text{year}$) and precipitation ($\%/ \text{year}$), all but one of which were plausibly defined from observations or previous studies regionally or globally (see Table 5.6). The one exception was an extreme hypothetical incremental adjustment in temperature, an annual increase of $0.15^{\circ}\text{C}/\text{year}$, which may also be described as an *artificial experiment* because such an increase is generally considered unlikely and is beyond the most extreme of GCM-based scenarios in the region (cf. Chaturvedi *et al.*, 2014, Figure 2.2). The regional hydrological model was applied with four incremental adjustments (scenarios) of increasing temperature, two of increasing temperature and increasing precipitation, and two of increasing temperature but decreasing precipitation (Table 5.6). After an initial model “warm-up” period of two years, the increments were applied uniformly to all cells in each respective basin, with the increment being added, or subtracted, annually to the relevant baseline variables at the start of every new year of the 100-year model period. For precipitation, the annual increment ($\%$) was added to each monthly total and then the updated total was distributed between the number of rain-days in the month. The mean monthly number of rain-days, however, remained unchanged over the entire model period. For temperature, the same annual increment ($^{\circ}\text{C}$) was added to each month’s mean monthly temperature each year, with the daily temperature then derived by interpolation, as described earlier (§5.4.1). No attempt was made to vary the incremental increase seasonally.

The third, and final, approach was *climate-scenario* based, using output from the HadRM2 RCM (Hassell and Jones, 1999). At the time the model was being developed and applied, this was the only RCM readily available for the Himalayan region. HadRM2, downscaled from the Hadley Centre’s HadCM2 model, covers the Indian sub-continent at 0.44° resolution for the period 2041-2060 and provides two sets of daily data: a “control” climate, which has evolved from 1991 using fixed present-day carbon dioxide emissions (CO_2) and a “perturbed” climate based on CO_2 concentrations increasing at a rate of 1% per year.

Table 5.6 Sensitivity-analysis increments, showing the annual incremental increases in temperature (*T*) and precipitation (*P*) and the basis of the “scenario”

Annual increment		Basis of the incremental change
T (°C/yr)	P (%/yr)	
0	0	CRU 1961-90 baseline, with no incremental change
+0.03	0	Average global warming predicted by IPCC (2001a)
+0.06	0	Observed warming from temperature gauges in Nepal
+0.10	0	Observed warming from highest 15 gauges in Nepal
+0.15	0	Extreme “hypothetical” scenario or artificial experiment
+0.06	+0.2	High precipitation change scenarios for South Asia, after Giorgi & Francisco (2000) in IPCC (2001a), with medium and high temperature scenarios.
+0.15	+0.2	
+0.06	-0.2	Low precipitation change scenarios for South Asia, after Giorgi & Francisco (2000) in IPCC (2001a), with medium and high temperature scenarios.
+0.15	-0.2	

Some very large and significant inconsistencies were found between the values of the CRU standard-period climate input data and those of the HadRM2 data that meant that the HadRM2 could not be applied directly to the model and its output meaningfully compared with that of the CRU standard-period. Having been re-sampled to the necessary 20km resolution, the HadRM2 data had to be further processed to determine the projected average annual change (Δ) between the perturbed and control monthly precipitation, temperature and PE, for every 20 km cell in each of the study basins (see Figures 5.8 & 5.9, for changes in annual P & T in the Ganges River basin, respectively).

The average annual Δ values were first assigned to the mid-point of the 2041 to 2060 period (year 2050). Assuming the HadRM2 control climate to be equivalent to the CRU standard-period baseline, an annual increment was then calculated for each of the climate variables (P, T and PE) in every cell, corresponding to the annual increase, or decrease, of the variable between 1990 (the end of the period covered by the CRU baseline data) and 2050 (the mid-point of the HadRM2 data). The regional model was then run for 60-years, representing the period 1991 to 2050, with the appropriate annual increment applied each year, as before, to the climate variables in each cell. This approach, illustrated in Figure 5.10, is an adaptation of the “Delta Change”, or “Change Factor”, method (Arnell, 2003; Kay *et al.*, 2009), which is a commonly used approach for dealing with the uncertainties encountered with GCM-based projections (e.g. Lutz *et al.*, 2014; Prudhomme *et al.*, 2010) while preserving the spatial variability of the RCM. This is in contrast to sensitivity-analysis based approaches, which apply changes uniformly over the model domain.

The gradual incremental progression between “present” (1990) and “future” (2050) that was applied in this study diverges for the conventional approach, which applies the Δ instantaneously to baseline over the future RCM-model period (2041-2060, in this case). Conventional application of an instantaneous step-change in climate was considered inappropriate because glacier retreat is progressive and any changes in glacier dimensions and melt-water contributions over the intervening period would not have been captured.

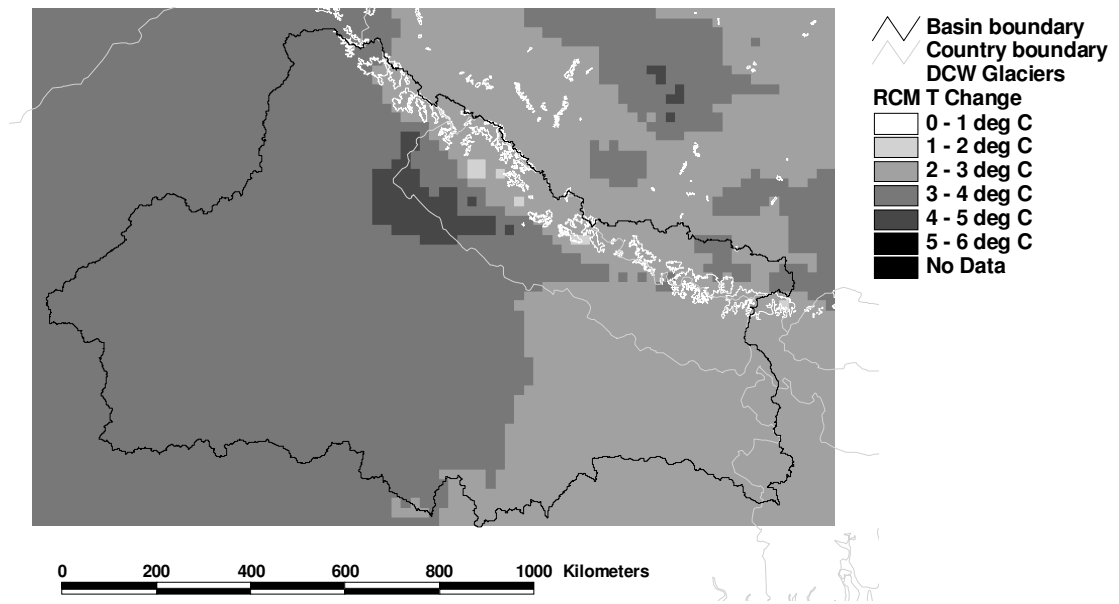


Figure 5.8 Absolute change ($^{\circ}\text{C}$) in average annual temperature (T) between HadRM2 perturbed and control climate for the period 2041- 2060 in the Ganges River basin

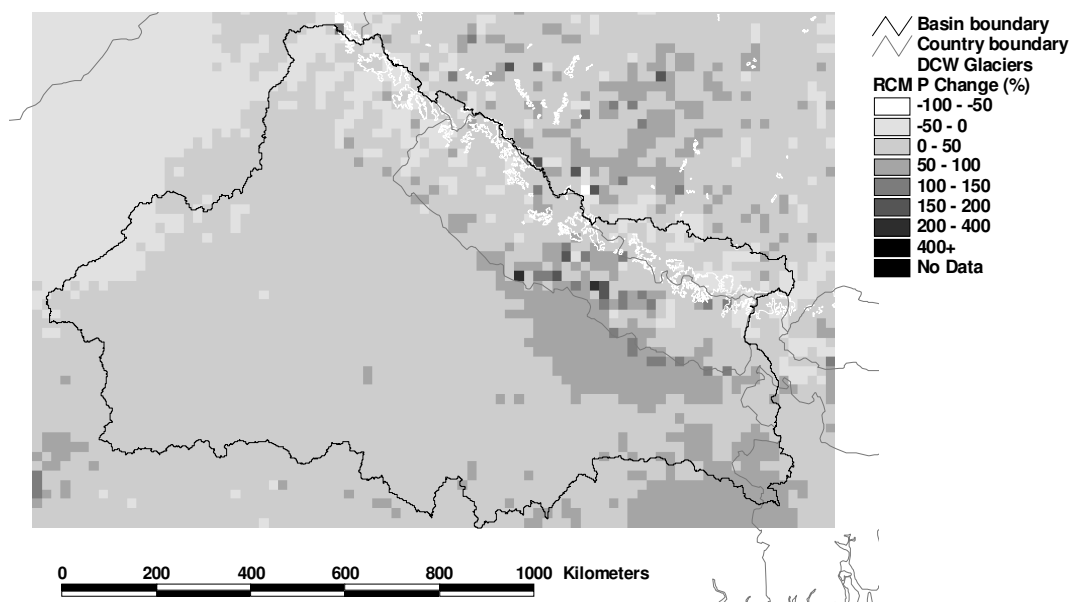


Figure 5.9 Relative change (%) in average annual precipitation (P) between HadRM2 perturbed and control climate for the period 2041- 2060 in the Ganges River basin

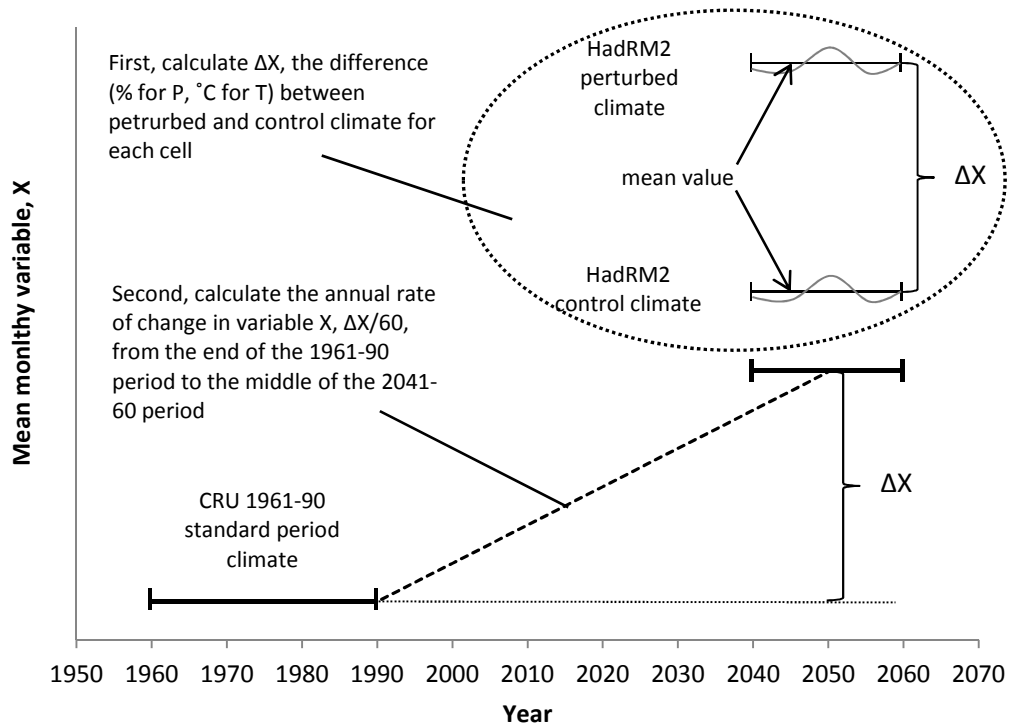


Figure 5.10 Adaptation of the “Delta Change” method that allows a gradual progression of climate input variables between the “present” (1990) and “future”(2050): the mean difference, ΔX , between the HadRM2 perturbed and control climate for monthly variable X , is first calculated for each cell and is assumed to represent how the trend-free 1961-90 standard period climate will have changed by the 2050 mid-point of the 2041-60 RCM period. The annual rate of change in X that needs to be applied to the standard-period baseline in order to attain 2050 values by the end of the 1990 – 2050 period is $\Delta X / 60$.

For all future conditions, or scenarios, the model was applied with the same parameter settings (Table 5.4) that had been used in the standard-period (baseline) model runs for each respective study basin.

5.7 Comparison of predicted flows

In every future climate model run, estimates of annual- and winter-runoff were aggregated at run-time to produce decadal averages (of annual- and winter-runoff). These decadal estimates were output as 20 km grids for post-processing and flow derivation in ArcGIS, as described earlier (§5.4.3). Having derived the 1 km flow grids of average decadal flows in every basin, a comparison of how flows would vary from decade to decade, relative to the baseline, was achieved by overlaying (again in ArcGIS) the decadal grids onto the relevant 1 km baseline grid. Cell values in the resulting “comparison” grids express the change in flow as a percentage (%) of the baseline. Using ArcGIS, the grids can be plotted to provide an overview of how the impacts may vary across the basin, as shown in Figure 5.11, or interrogated cell-by-cell, location-by-location, to see how flows, at specific points, might vary under different future climatic conditions.

The results of the many future climate (scenario) model runs, and how their flow-estimate outputs provide a picture of future decadal changes in glacier-fed river flows, relative to baseline, over a future time horizon of up to 100 years in each basin, are presented and discussed in Chapter 6.

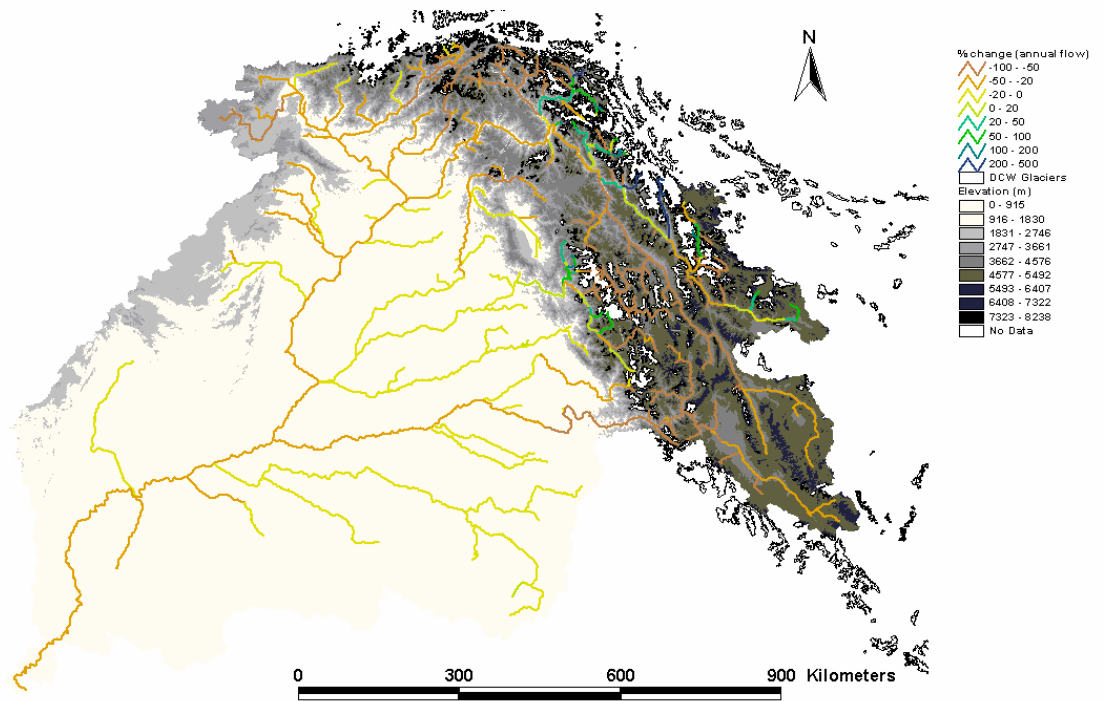


Figure 5.11 Relative changes (%) in mean flows of the Indus River by decade 10, for the +0.1 °C/year incremental temperature scenario

PART 3

6 Results & Discussion

6.1 Introduction

The previous chapter described how the model was implemented and applied, first, for the 1961-90 standard-period baseline and, then, for a range of possible future climates (change scenarios) in each of the three study basins. The outcomes of the many different scenario runs are presented and discussed in this chapter.

As described in Chapter 5, estimates of annual- and winter-runoff were aggregated at run-time to produce decadal averages of annual- and winter-runoff for every future climate model run. These estimates were transformed into 1 km “decadal” flow grids and then compared with the relevant basin baseline, to derive “comparison” grids, which express decadal changes in modelled flow as a percentage (%) of the modelled baseline over the 100-year (60-year for the HadRM2) model run period. Expressing changes in decadal mean flows relative to baseline in this manner allows direct comparison of sites having different catchment areas.

In order to understand how the different change scenarios affected modelled long-term water availability from glacier-fed rivers, and to gain insight on the potential variability of real climate change impacts across the region, the comparison grids were interrogated at specific points in each of the three study basins. Four “focal areas” were selected for scrutiny (Figure 6.1): the Upper Indus (labelled Focal Area A in Figure 6.1); the Upper Ganges (Focal Area B); the Kali Gandaki – Narayani river system in Nepal (Focal Area C), which also is in the headwaters of the Ganges; and the Brahmaputra river (Focal Area D). These focal areas generally cover the full range of conditions along the Himalayan arc, from west-to-east and north-to-south.

Several “study sites” were identified within each focal area (Table 6.1) to reflect the varying changes, or impacts, from upstream to downstream. The sites are located at significant locations in each focal area: at culturally, or economically, important settlements (e.g. Ganges at Haridwar); as pairs of sites immediately upstream or downstream of a confluence (e.g. the Gilgit at Gilgit and Gilgit at Dainyor (downstream of the Gilgit River’s confluence with the Hunza); and the Kali Gandaki

at Kata Gaon and the Narayani at Bharatpur (downstream of the confluence of the Kali Gandaki and Trishuli rivers, from where the river becomes known locally as the Narayani)), to explore the effect of two rivers meeting; or as single sites downstream of major confluences (e.g. Indus at Partab Bridge). Of the 18 selected study sites, 6 are located in India, 5 are in Pakistan, 4 are in Nepal, 2 are in China and 1 is in Bhutan. Basic information describing each site, its catchment area (km^2), initial ice-cover (% ice), modelled baseline (annual) mean flow and winter mean flow (both m^3/s), and its average annual and winter (both in mm) is given in Table 6.1.

Changes in decadal mean flow (DMF) and decadal winter mean flow (DWMF), expressed as a percentage, plus or minus, of baseline, were abstracted for every study site, for every decade of every model scenario run. The results are presented and discussed similarly for every focal area in Sections 6.3 to 6.6. For each focal area, changes in DMF (relative to baseline) for all four temperature scenarios and two precipitation scenarios (see Table 5.5) first are presented in graphs for the uppermost and lowermost study sites only (2 graphs each). Then, three further graphs show results for all sites for the most plausible, $+0.06\text{ }^\circ\text{C}/\text{year}$, temperature scenario, the extreme, $+0.15\text{ }^\circ\text{C}/\text{year}$, scenario, and the HadRM2 RCM-based scenario. In all graphs, the changes are plotted at decadal intervals over the model run period. The selection of graphs, together with the accompanying observations and discussion, convey the salient characteristics of the potential changes to river mean flows in each focal area. The concluding section (§ 6.7) considers key regional messages that can be drawn from the model results.

However, before concentrating of the results of the incremental change scenarios, those from the one “artificial experiment”, an instantaneous and uniform 50% reduction in areal glacier cover, are first presented and discussed in Section 6.2.

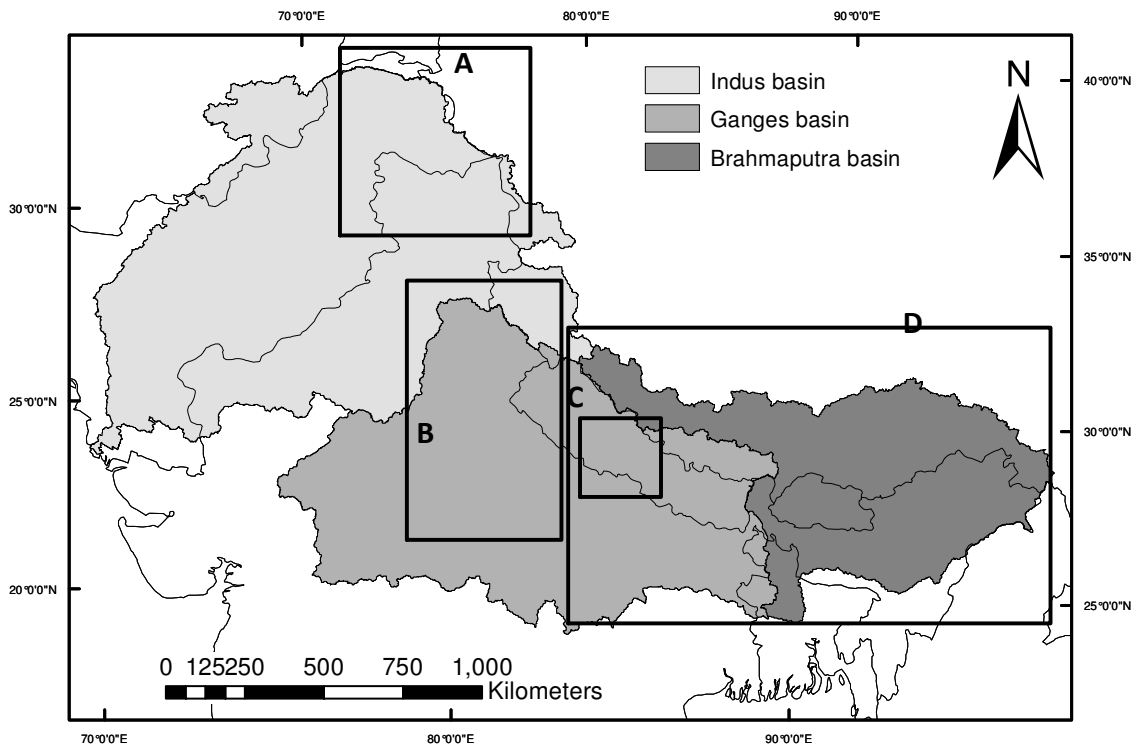


Figure 6.1 Location of the four focal areas: (A) Upper Indus; (B) Ganges; (C) Kali Gandaki-Narayani River System, Nepal; and (D) Brahmaputra

Table 6.1 Selected study sites of the four focal areas, showing site name (river and location), catchment area (km²), percentage initial ice cover (% ice), annual mean flow (AMF, m³/s) and winter mean flow (WMF, m³/s) and average annual rainfall (AAR, mm) and average winter rainfall (AWR, mm).

Site name	Area ^a (km ²)	% ice ^b	Mean flow ^c (m ³ /s)		Rainfall ^c (mm)	
			AMF	WMF	AAR	AWR
Upper Indus (Focal Area A)						
Gilgit at Gilgit	14138	11.7	172	39	365	169
Gilgit at Dainyor	27996	25.2	356	64	331	153
Shyok at Shyok	38312	16.2	333	36	192	91
Indus at Skardu	127099	13.1	1077	162	350	155
Indus at Partab Bridge	167982	16.0	1591	248	402	188
Indus at Besham Qila	187118	14.6	1702	300	889	375
Ganges (Focal Area B)						
Ganges at Uttarkashi	4524	23.4	85	25	982	172
Ganges at Haridwar	23191	16.1	338	108	1044	119
Ganges at Kanpur	89878	4.2	749	345	1447	124
Ganges at Allahbad	424937	0.9	2900	1444	1559	83
Kali Gandaki-Narayani, Nepal (Focal Area C)						
Modi Khola at Kushma	642	16.5	14	7	1646	210
Kali Gandaki at Seti Beni	7104	9.3	82	43	1829	198
Kali Gandaki at Kata Gaon	12235	5.4	214	117	2196	186
Narayani at Bharatpur	32137	9.7	570	292	2154	181
Brahmaputra (Focal Area D)						
Zangpo at Samsang	3784	3.0	22	12	653	162
Zangpo at Xigaze	103612	0.8	1093	591	873	37
Trongsa Chhu at Zhemgang	2755	5.2	161	55	2150	214
Brahmaputra at Tuting	229323	2.1	2077	1114	1131	130

Notes: ^a derived from Hydro1k flow direction grid (USGS, 2001); ^b percentage of glacier cover in catchment, calculated by overlaying DCW (ESRI, 1993) glacier-cover data onto Hydro1k DEM and flow direction grid; ^c model-derived estimates using CRU 1961-90 standard-period climate (New et al., 1999); ^d winter (dry-season) defined as October – March; and ^e at-site rainfall, derived from the CRU 1961-90 standard-period climate

6.2 Artificial Experiment: 50% reduction in glacier cover

This first change “scenario” that was applied, a type of “artificial experiment” (Carter *et al.*, 2007), sought to answer the hypothetical question, “what would happen if there was a 50% reduction in glacier cover?” The model was run for a nominal 30-year period with CRU 1961-90 standard-period climate input variables and a 50% areal reduction in glacier cover applied at run-time by simply halving the model glacier-defining data, P_{ice} (the proportion of ice in a cell) and A_{ice} (the total area of glaciers that contribute melt-water to the cell). The resulting 20 km output grids of average annual runoff were transformed, as described earlier, into 1 km grids of (annual) mean flow and then combined with the corresponding modelled baseline estimates to derive a single grid of relative change in each basin. The resulting change (or comparison) grid for the Indus is shown in Figure 6.2; an extract from the Ganges is provided in Figure 6.3. In both figures, rivers are colour-coded from red through orange, yellow, and green to blue, with red signifying a relatively large reduction of over 40% in mean flow, and blue, a small reduction of between 0% and 10%. The areas covered by the two figures were chosen to illustrate the contrast in impacts between the two basins and, particularly, differences between east and west.

In the Indus basin, the impact of such a large reduction in glacier cover is profound, with significant and widespread reductions in mean flow, of up to 48%, in many headwater rivers (Figure 6.2). The impact persists many hundreds of kilometres downstream, with reductions of between 10% and 20% still apparent at the very lowest reaches of the Indus River. These outcomes, however, should be considered circumspectly because, firstly, the scenario is experimental and, secondly, the model reflects natural conditions when, in reality, the Indus is such a heavily artificially influenced river that mean flows in lower reaches bear little resemblance to the natural.

The impacts in the eastern headwaters of the Ganges in Nepal (Figure 6.3) are in stark contrast to those in the Indus. In the east, the magnitude of the changes are less in most headwaters: only one small glacier-fed tributary in Figure 6.3 has a reduction of 44%, most having reductions of 40% or less. The impacts also appear to diminish

rapidly downstream, reducing by 0% - 10% relative to baseline within a few tens of kilometres in most rivers.

Such differing behaviour is readily explained by our understanding of the different climatic conditions in the two illustrated areas. The windward eastern part of the Himalaya benefits perennially from high monsoonal rainfall during summer months. The proportion of glacial melt-water contribution to river flow diminishes rapidly downstream, the flow increasingly is made up of rainfall-derived runoff from the glacier-free part of the catchment. As shown in Figure 6.3, a significant reduction in glacier cover, therefore, has relatively little impact on river mean flows in this part of the Himalaya.

By contrast, the summer monsoon generally weakens from east to west and usually barely penetrates the headwaters of the Indus. The Indus basin as a whole is much drier than central Nepal, usually having very limited rainfall in downstream parts, beyond the mountains. As glacial melt-water is a significant component of river flow along the entire length of the river, any reduction in the melt-water contribution, as would occur with a 50% reduction on glacier-cover, is likely to have far-reaching impacts, as seen in Figure 6.2.

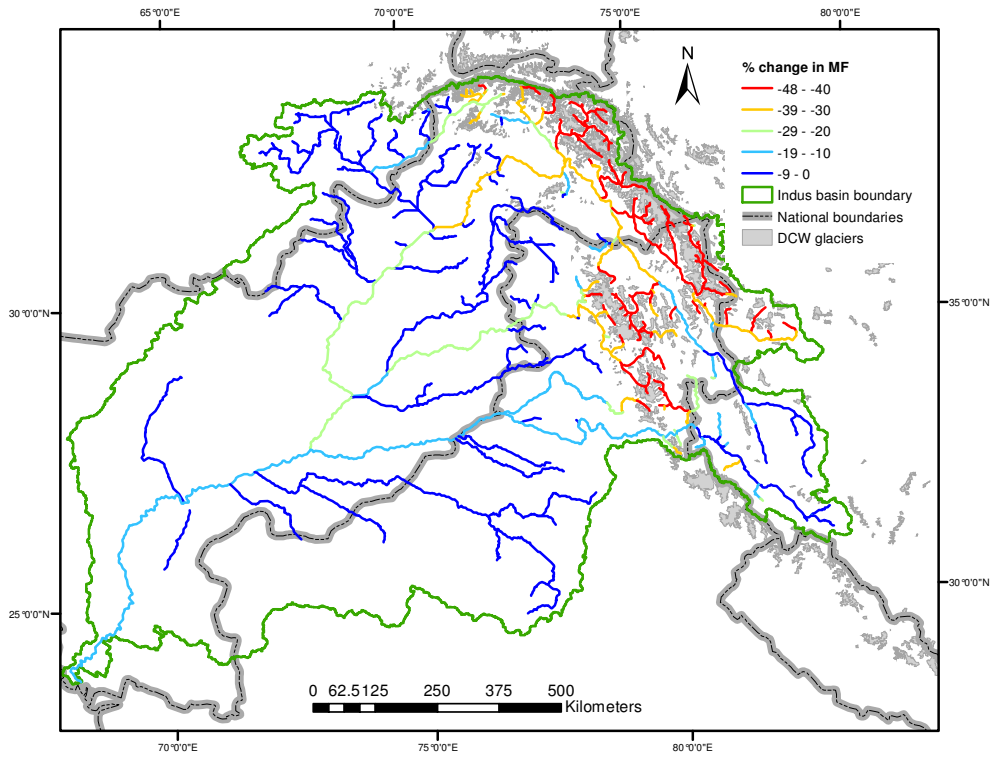


Figure 6.2 Changes in mean flows, relative to the 1961-90 baseline, across the drainage network of the Indus basin for a 50% reduction in glacier cover

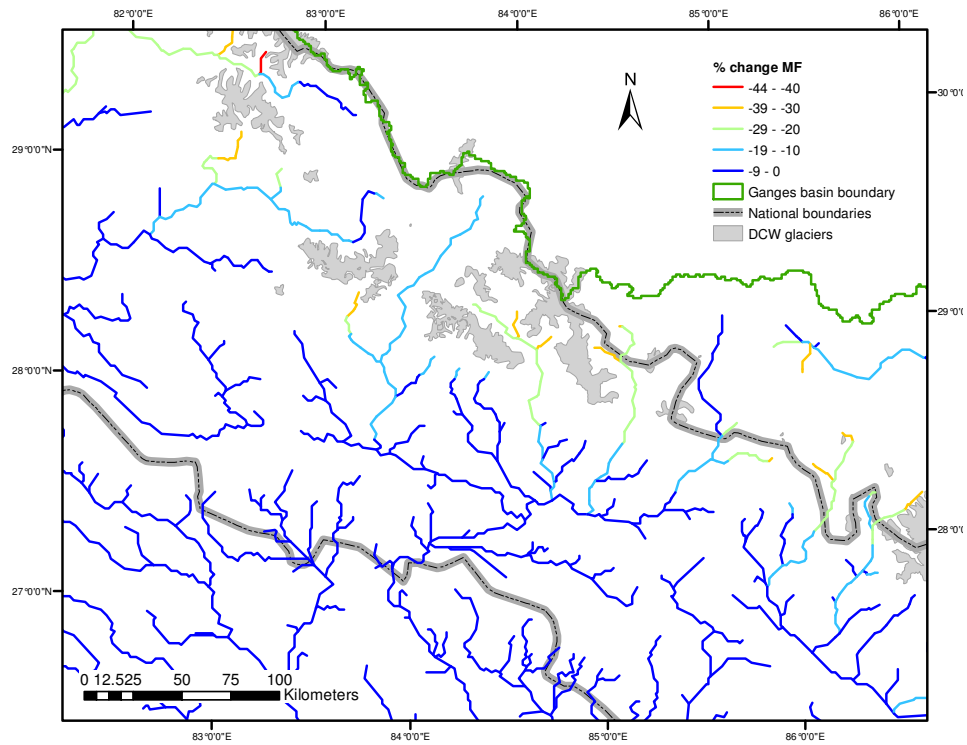


Figure 6.3 Changes in mean flows, relative to the 1961-90 baseline, in the headwaters of the Ganges in Nepal for a 50% reduction in glacier cover

6.3 Analysis of modelled future river flows in the Upper Indus (Focal Area A)

Six sites were selected for investigation in the Upper Indus (Figure 6.4). Decadal mean flow (DMF) results from 100-year model runs for all four incremental temperature increases and two incremental precipitation changes are presented in Figures 6.5 to 6.8 for the Gilgit at Gilgit and the Indus at Bisham Qila. In this one section only, changes in the decadal winter mean flows (DWMF) are presented in Figure 6.9, for the Indus at Bisham Qila. DMF results for all six sites for the +0.06 °C/year , +0.15 °C/year and the HadRM2-based scenario are presented in Figures 6.10 to 6.12.

6.3.1 Gilgit at Gilgit

The Gilgit at Gilgit is a relatively highly glaciated catchment. According to the DCW glacier-cover map (ESRI, 1993) and the Hydro1k flow-direction grid (USGS, 2001), approximately 11.2% of the 14,000 km² catchment area is initially glacier-covered. The river, a tributary of the Indus, rises in the Hindu Kush. Gilgit is the capital city of the Gilgit District in northern Pakistan.

Results for all four incremental increases in temperature are shown in Figure 6.5. An initial increase is seen in the DMFs of all scenarios by Decade 1 (D1). This is a feature common to almost every change scenario that was applied over the course of this study. The initial increase in DMFs is thought to be due to the initial distribution of ice at lower ice-bands of model glaciers generating a surplus of melt-water over the first few years of increasing temperatures.

After the first decade, the DMFs for the two coolest scenarios (+0.03 and +0.06 °C/year) are seen to decline steadily over the 100-year model period, with the rate of the reduction in the DMF (the gradient of the line) of the warmer, +0.06 °C/year, scenario changing gradient and starting to level-out from D8 and ultimately reducing to about -60% of baseline by D10. This gradual reduction with the cooler scenarios presumably is because the rate at which the 0 °C isotherm and the upper limit of transient-snow-line (TSL) rises up the model glaciers, to expose more ice to melting, is insufficient to offset the reduction in melt-water caused by the depletion of ice from lower ice-bands.

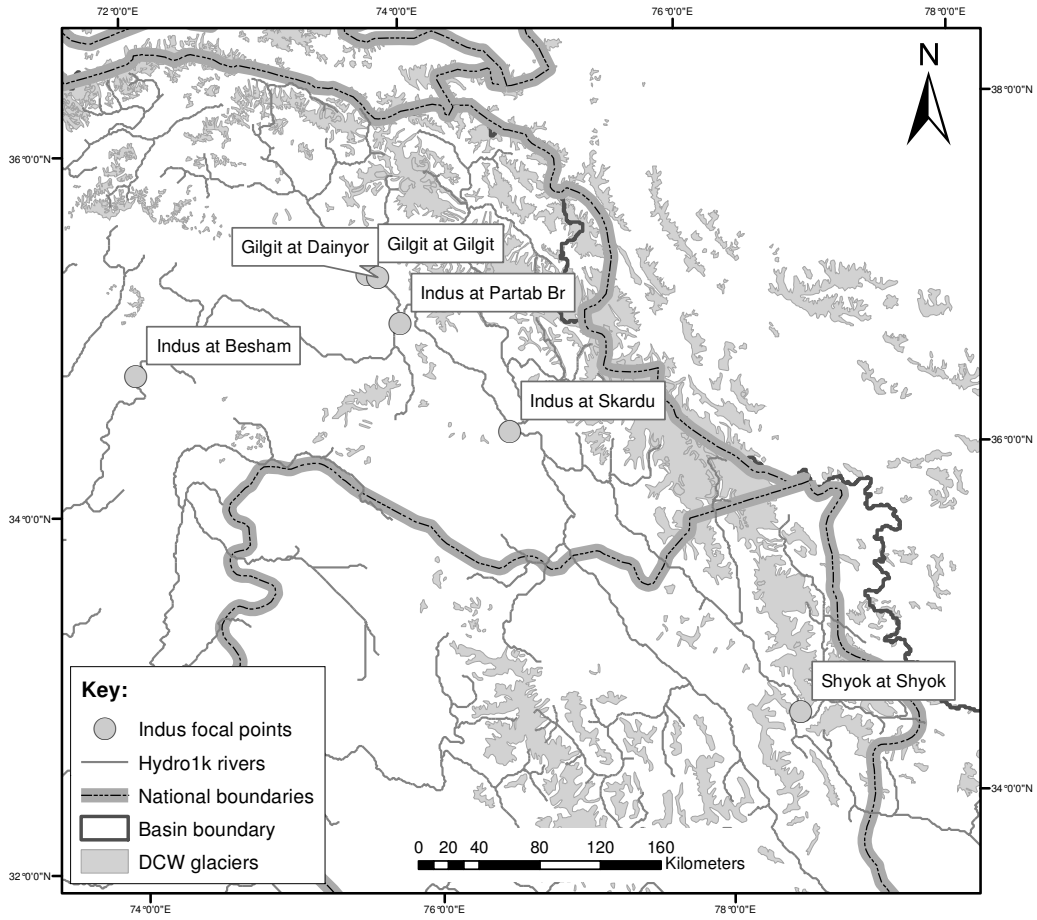


Figure 6.4 Location of the 6 focal area study sites in Upper Indus

With the two warmest scenarios (+0.1 and +0.15 °C/year), further increases in DMFs relative to baseline are seen beyond D1, both peaking at D2. DMFs then decline steadily, albeit at faster rates, until a distinct change of gradient (levelling-out) again occurs at D6 for the warmer +0.15 °C/year scenario and a decade later for the +0.1 °C/year scenario. The DMFs for the two scenarios ultimately reduce to between -60% and -80% of baseline by D10. The initial increases with the warmest scenarios are probably due to the 0 °C isotherm (or TSL) rising up model glaciers and exposing more ice to melting faster than the ice is being extinguished from lower elevations. The rapid decline in DMFs thereafter corresponds to the rate of ice area loss at lower elevations being higher than the rate at which the 0°C isotherm is exposing ice at higher elevations to melting. The asymptotic, levelling-out, behaviour that happens towards the end of the model run periods for the three warmest scenarios is thought to indicate the complete depletion of ice below the 0°C isotherm, which, in some catchments, corresponds to the total extinction of upstream model glaciers. This is possible only when the 0°C isotherm migrates to above the maximum ice elevation of a model glacier.

Application of the two incremental precipitation change scenarios ($\pm 0.2\%$ /year, with +0.06°C/year temperature increases) appears only to have a marginal effect on DMF changes (Figure 6.6), with flows seeming to increase, or decrease, proportionately to the precipitation changes, neither of which significantly affect the glacial melt-water contribution to river mean flow. Such a marginal impact can probably be attributed to the relatively small amount of precipitation the Gilgit catchment receives on an annual basis. The small proportionate incremental increases that are applied in the model would not add much to the annual precipitation total and are unlikely, therefore, to strongly influence model glacier behaviour. A possible underestimation of precipitation at higher elevations, due to the parameter settings of the applied precipitation lapse rate model, could be another reason for the benign response.

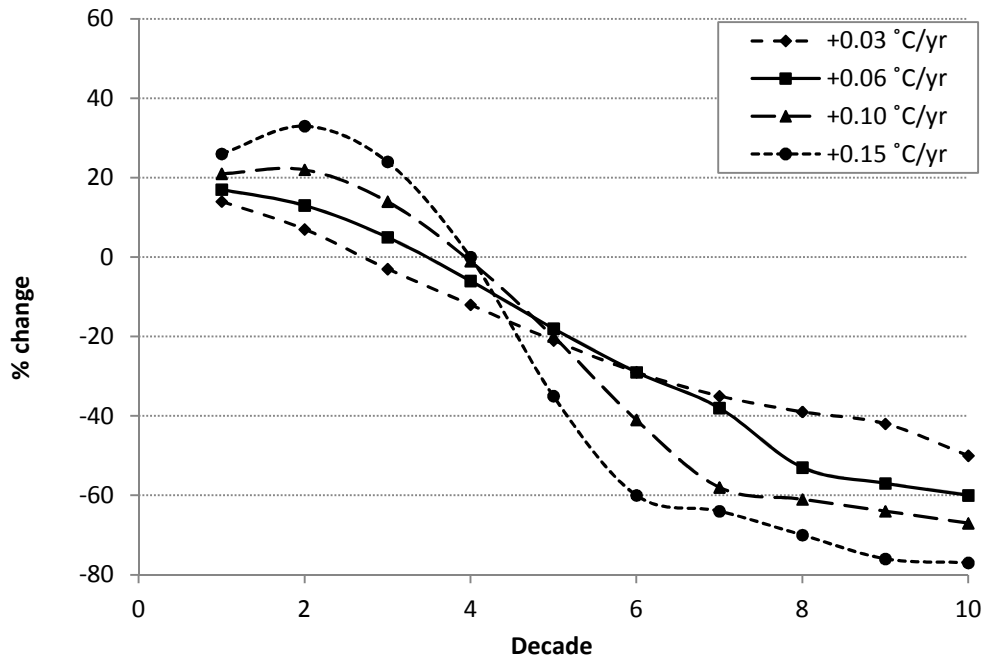


Figure 6.5 Changes in Decadal Mean Flows, relative to baseline, of the Gilgit at Gilgit for the four incremental temperature scenarios (+0.03, +0.06, +0.1 and +0.15 °C/year) over a 100-year period

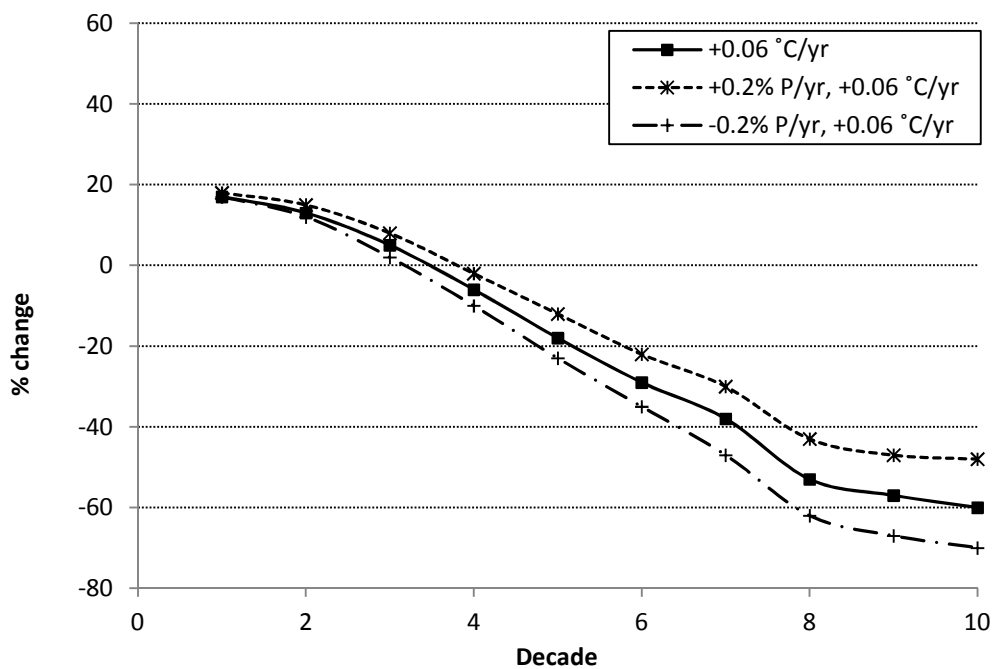


Figure 6.6 Changes in Decadal Mean Flows, relative to baseline, of the Gilgit at Gilgit for two combined incremental precipitation (P) and temperature scenarios (+0.2%P with +0.06 °C/year, -0.2%P with +0.06 °C/year, with the +0.06 °C/year temperature scenario as reference) over a 100-year period

6.3.2 Indus at Besham Qila

Besham Qila is one of the lowermost locations in the Upper Indus, a short distance upstream from the Tarbela Dam, the world's largest earth-filled dam (Tahir, 2011), used for irrigation, hydropower generation, river regulation and flood control and, consequently, of huge economic importance to Pakistan economy. The Indus at Besham Qila drains a catchment area of over 187,000 km², 14.6% of which is glacier-covered, according to the DCW (ESRI, 1993).

The impacts of all four incremental increases in temperature for the Indus at Besham Qila are shown in Figure 6.6. Again, as seen at Gilgit, there is an initial increase in the mean flows by D1 and broadly similar behaviour (to Gilgit) is observed thereafter for all four scenarios. However, unlike Gilgit, the asymptotic behaviour towards the end of the 100-year model period does not appear with any of the scenarios, with DMFs ultimately reducing to about -40% of baseline by D10 for the three coolest scenarios (+0.03, +0.06 and +0.1 °C/year) and to -66% of baseline for the warmest (+0.15 °C/year). This is likely to be a consequence of the greater volume of glacier ice within the catchment, and its probable extension to higher elevations, which ensures a more persistent supply of glacial melt-water, even with the warmest, and arguably most unrealistic, scenario.

The effects of the precipitation scenarios appear (Figure 6.8) more benign at Besham Qila than at Gilgit, again presumably because the relatively small catchment annual precipitation total means the proportionally small incremental precipitation increases are almost insignificant both in absolute terms and when compared with the volume of released melt-water.

Considerable variability is seen (Figure 6.9) in the impact of the four incremental temperature increases on decadal winter (October-March) mean flows (DWMFs). Following the usual increase by D1, DWMFs decrease gradually for all but the warmest, +0.15 °C/year, scenario. Flows for the two coolest scenarios continue to decline and ultimately reduce to about -15% of the baseline winter mean flow by D10. With the +0.1 °C/year scenario, the DWMF appears to increase after D6 and ends up only about -2% of baseline by D10. DWMFs for the warmest scenario never fall below baseline, showing an increase over the first three decades, to a maximum of

just under +15% by D3, but then following a general downward trend, albeit with slight increases at D7 and 8, ultimately to reach +9% of baseline by D10. The gradual reductions of the 2 coolest scenarios appear to reflect the general DMF behaviour, with reductions to the runoff generated during the shoulders of the season (October and March) likely to influence changes in the seasonal mean. In coldest winter months (November – February) snow- and surface ice-melt would not normally be expected to contribute significantly to winter flows, with any runoff probably being generated from glacier basal-melting, groundwater recession and rainfall at lower elevations. However, the vagaries of the results for the two warmest scenarios are thought to be due to the significantly warmer climate reducing winter snow accumulation and affecting snow- and glacier-melt during winter months.

6.3.3 All sites for the +0.06 °C/year, +0.15 °C/year and RCM-based scenarios

Considering results of the +0.06 °C/year scenario at all study sites together (Figure 6.10), it is seen that impacts for the Gilgit at Dainyor and the Indus at Skardu are similar to those at Bisham Qila, with DMFs reducing to -33% and -38% of baseline by D10. The Indus at Skardu, behaves similarly initially but diverges from the Bisham Qila behaviour from D6, with the DMFs ultimately reducing to -47% of baseline by D10. The two most noticeable departures are the Gilgit at Gilgit (discussed earlier) and the Shyok at Shyok. The Shyok, having a catchment area of 38,312 km² and ice cover of 16%, is downstream of the confluence with the Nubra River, which drains the Rimo Glacier, which is a tongue of the Siachen Glacier, one of the largest Karakoram glaciers (Ahmad and Rais, 1998; Kaul, 1998). At this site, the DMFs continue to increase to +27% of baseline by D3 and then decline steadily over the next seven decades, eventually reducing to -40% of baseline by D10. Although the proportion of ice in this catchment is similar to other sites, the larger increase in DMFs is considered likely a result of the catchment having large glaciers in its headwaters, with a greater volume of ice available at all elevations ensuring slower depletion and, thus sustaining glacial melt-water contributions to river flow for longer. In contrast to the Gilgit at Gilgit, the Shyok does not demonstrate, for this scenario at least, the asymptotic levelling-out of DMFs that signifies the total extinction of model glacier ice below the 0 °C isotherm.

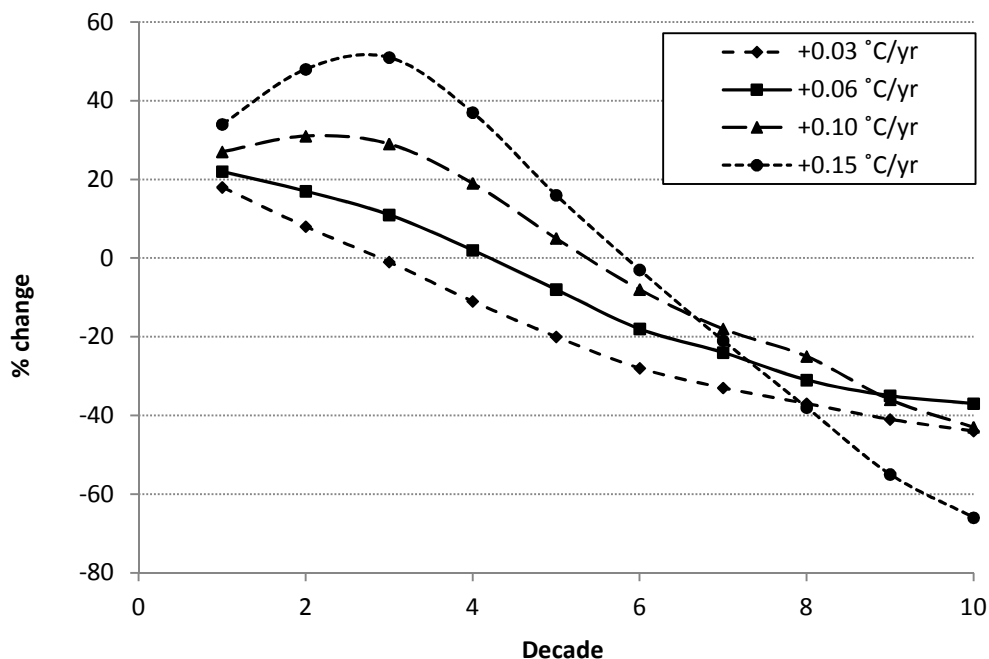


Figure 6.7 Changes in Decadal Mean Flows, relative to baseline, of the Indus at Besham Qila for the four incremental temperature scenarios (+0.03, +0.06, +0.1 and +0.15 °C/year) over a 100-year period

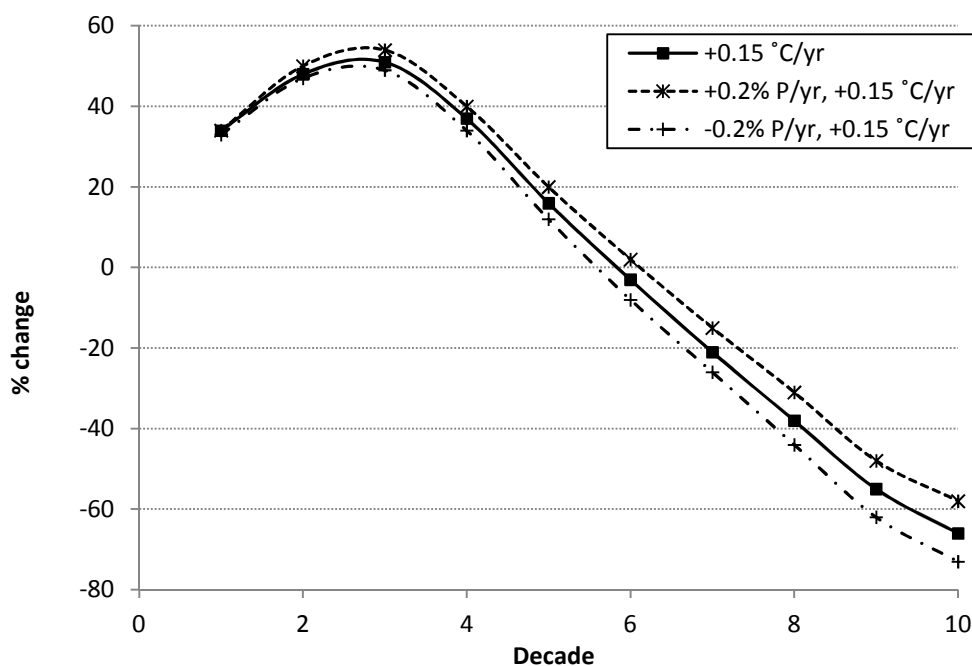


Figure 6.8 Changes in Decadal Mean Flows, relative to baseline, of the Indus at Besham Qila for two combined incremental precipitation (P) and temperature scenarios (+0.2%P with +0.156 °C/year, -0.2%P with +0.15 °C/year, with the +0.15 °C/year temperature scenario as reference) over a 100-year period

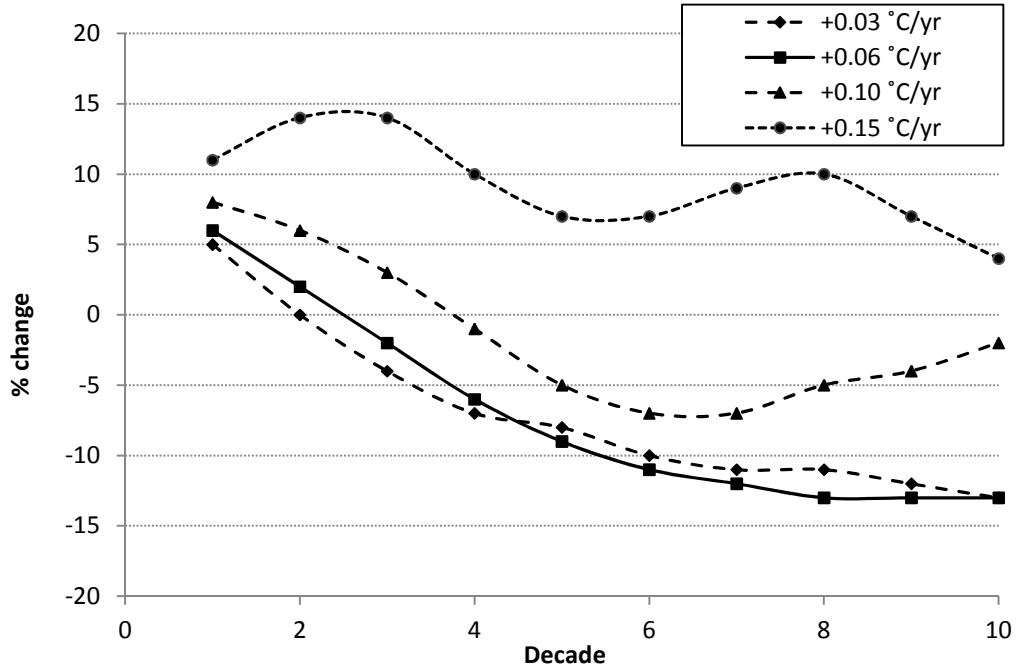


Figure 6.9 Changes in Decadal Winter Mean Flows, relative to baseline, of the Indus at Besham Qila for the four incremental temperature scenarios (+0.03, +0.06, +0.1 and +0.15 °C/year) over a 100-year period

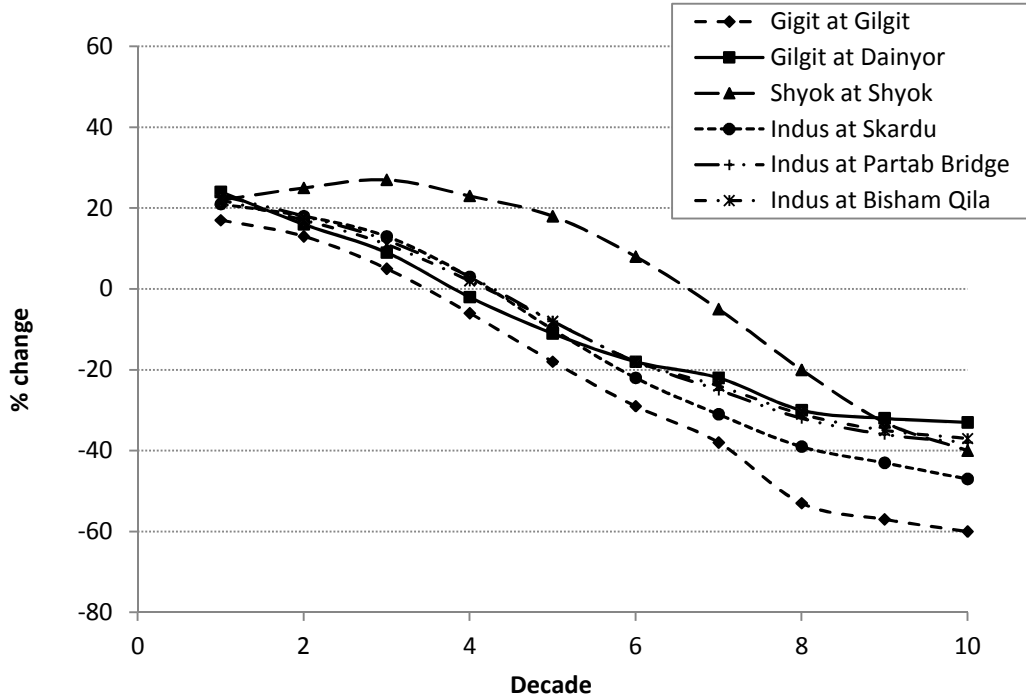


Figure 6.10 Changes in Decadal Mean Flows, relative to baseline, of the Indus and its tributaries at all six study sites for the +0.06 °C/year incremental temperature scenario over a 100-year period

A similar picture emerges when considering results for the extreme $+0.15\text{ }^{\circ}\text{C}/\text{year}$ incremental scenario together (Figure 6.11), with the impacts at Gilgit and Shyok again departing notably from others'. At all sites, DMFs continue to increase beyond D1. The Gilgit at Gilgit and the Gilgit at Dainyor peak with increases of $+33\%$ and $+48\%$ of baseline at D2. The four other sites peak at D3: the three Indus River sites (Skardu, Partab Bridge and Bisham Qila) with values of between $+55\%$ and $+51\%$ of baseline, and the Shyok with a huge $+91\%$ increase. All DMFs decline thereafter, reducing to between -62% (Hunza) and -88% (Shyok) of baseline by D10. The steepest decline, is seen with the Shyok, which also shows asymptotic levelling-out only in D9, four decades later than at Gilgit. No such asymptotic behaviour is apparent with the four other sites. The results for the Shyok indicate that the large ice-reserves in the catchment fully deplete by the end of the model run for this extreme temperature scenario. That flows, however, are sustained at the four other sites (albeit with much-reduced DMFs) suggests these catchments benefit from the presence of ice at higher elevations that has yet to be depleted by D10 with this scenario.

Results at all sites for the HadRM2 RCM-based scenario (Figure 6.12) are quite neutral, compared with those from the earlier incremental temperature scenarios. Initial increases are again seen at D1, with DMFs for all sites, apart from the Shyok, declining steadily to between -8% and -16% of baseline by the end of the 60-year model run at D6. Comparing with the plausible $+0.06\text{ }^{\circ}\text{C}/\text{year}$ scenario, DMFs for the same five sites had reduced to between -18% and -29% by D6. Shyok, again, is the exception, with DMFs peaking at $+37\%$ at D2, sustained at $+36\%$ for the next two decades, and then declining to $+21\%$ of baseline by D6. This behaviour reinforces the earlier supposition that the Shyok benefits from greater ice-reserves at low- and mid-elevations than other sites. These results also clearly indicate that the HadRM2 RCM-based scenario in the Upper Indus is considerably more conservative than any of the sensitivity-analysis-based scenarios that were considered in this study

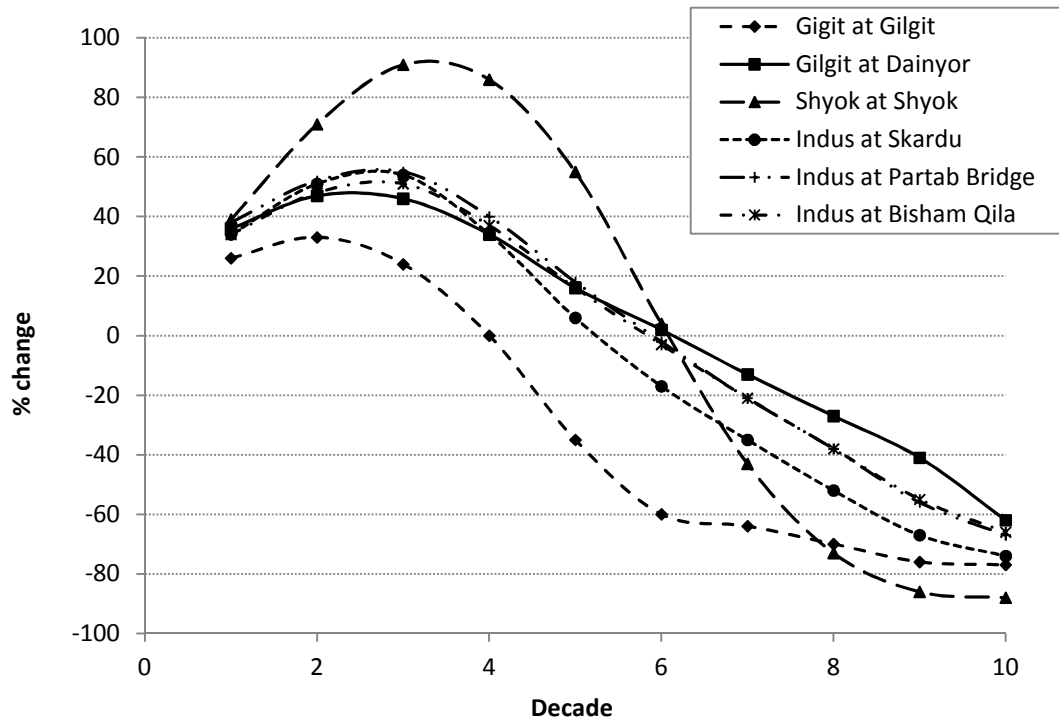


Figure 6.11 Changes in Decadal Mean Flows, relative to baseline, of the Indus and its tributaries at all six study sites for the +0.15 °C/year incremental temperature scenario over a 100-year period

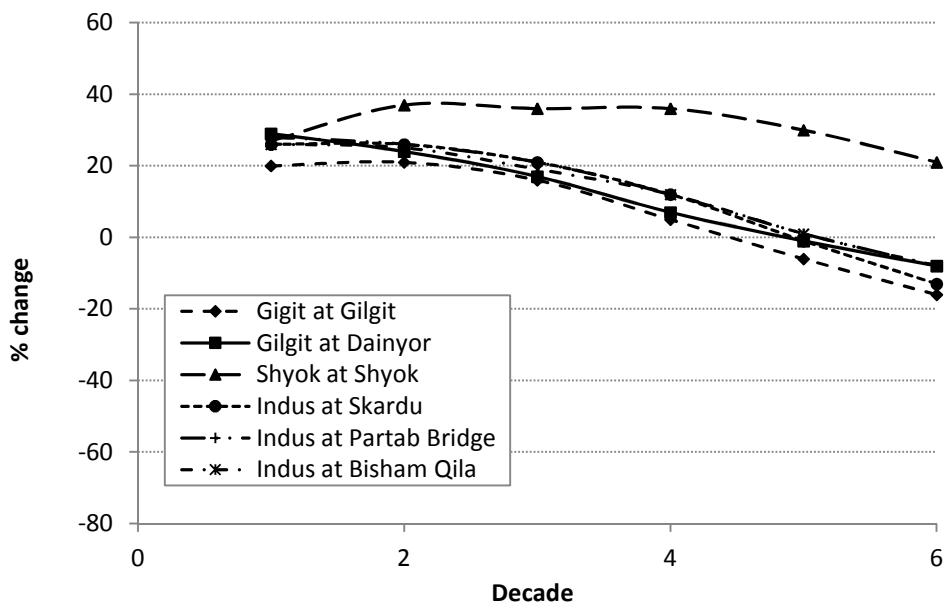


Figure 6.12 Changes in Decadal Mean Flows, relative to baseline, of the Indus and its tributaries at all six study sites, for the HadRM2-based scenario over a 60-year period

6.4 Analysis of modelled future river flows of the Ganges River (Focal Area B)

The four study sites in this focal area (Figure 6.13) were selected to illustrate the potential impacts of future climate change along the upper half of the Ganges River in India, from its headwaters to major cities on the Gangetic plain. The Ganges is the holiest of rivers in the Hindu culture and, as a source of water for irrigation, hydropower, and public water supply, is also vitally important to India's economy. As in the previous section, results from 100-year model runs for all four incremental temperature increases and two incremental precipitation changes are presented in graphs (Figures 6.14 to 6.17) for the uppermost and lowermost sites respectively (i.e. Uttarkashi and Allahbad). Then, three further graphs present results for all four sites from the 100-year model runs for the +0.06 °C/year and +0.15 °C/year increasing temperature scenarios (Figure 6.18 and 6.19) and the 60-year run of the HadRM2 RCM-based scenario (Figure 6.20). The same order of presentation is repeated in subsequent sections for both Focal Areas C and D.

6.4.1 Ganges (*Bhagirathi*) at Uttarkashi

One of the smallest and highly glacierised catchment areas of all the sites considered (4524 km²; 23.4% ice), Uttarkashi is only about 60 kilometres from the Gangotri glacier (Google Earth, 2013), the source of the Ganges. Locally, at this location, the river is called the Bhagirathi.

Results for all four incremental increases in temperature are shown in Figure 6.14. After the usual initial increase in D1, the DMFs for all scenarios reduce, with the rate of reduction greater the warmer the scenario. Asymptotic (levelling-out) behaviour is seen within the 100-year model run for the 3 warmest scenarios, at D6 for the +0.1 and +0.15 °C/year scenarios and at D8 for the +0.06 °C/year scenario. This graph appears to confirm the association between asymptotic behaviour and model glacier extinction. In this particular catchment, the asymptote is clearly seen at about -54% of baseline and, because very little further variation of DMFs is seen once this level is attained, total extinction of all model glaciers upstream can be assumed. This indicates also the level at which river flows are likely to be determined exclusively by contemporary precipitation.

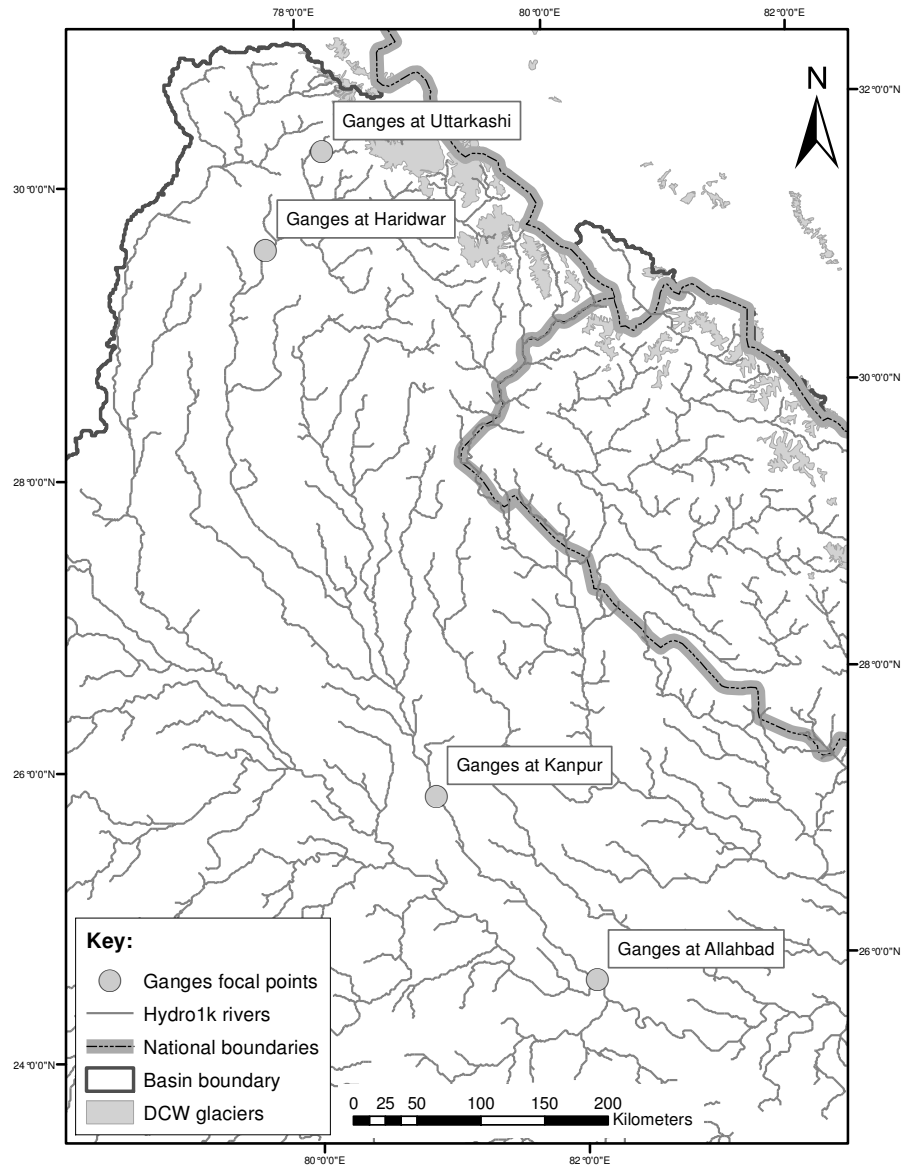


Figure 6.13 Location of the 4 focal area study sites in the Ganges

As in the Upper Indus (Gilgit and Besham Qila), application of the two incremental precipitation change scenarios (Figure 6.15) appears only to have a marginal effect on DMFs, with flows seeming to increase, or decrease, proportionately to the precipitation change, rather than being affected by any changes to glacial melt-water contributions. Although the average annual precipitation total is higher near Uttarkashi than at Gilgit, it is still relatively small, which means the small proportionate incremental increases that are applied in the model have little influence on model behaviour. It is interesting to note the slight increases and decreases in DMFs once the model glaciers have depleted from D8 onwards, as flows become determined exclusively by precipitation.

6.4.2 Ganges at Allahbad

Allahbad is a major city in the north Indian state of Uttar Pradesh, having a population of over 1.2 million, and located at the confluence of the Ganges and Yamuna Rivers. The study site is immediately downstream of the confluence, giving a catchment area of about 425,000 km² and a percentage glacier cover of only 0.9%.

As can be seen (Figure 6.16), the impact of all four incremental temperature scenarios on modelled DMFs at Allahbad is minimal, with only small reductions seen in every case over the entire 100-year model period. For all scenarios, DMFs peak at D1 at under +5% of baseline and reduce to less than -5% of baseline by D10. This is because glacier-melt is such a very small proportion of the river flow at this location, the vast majority of which is derived from rainfall over the glacier-free parts of the catchment.

As a predominantly rain-fed catchment it is not surprising then to see (Figure 6.17) that small incremental increases or decreases in precipitation applied uniformly upstream can dramatically augment or attenuate DMFs at Allahabad.

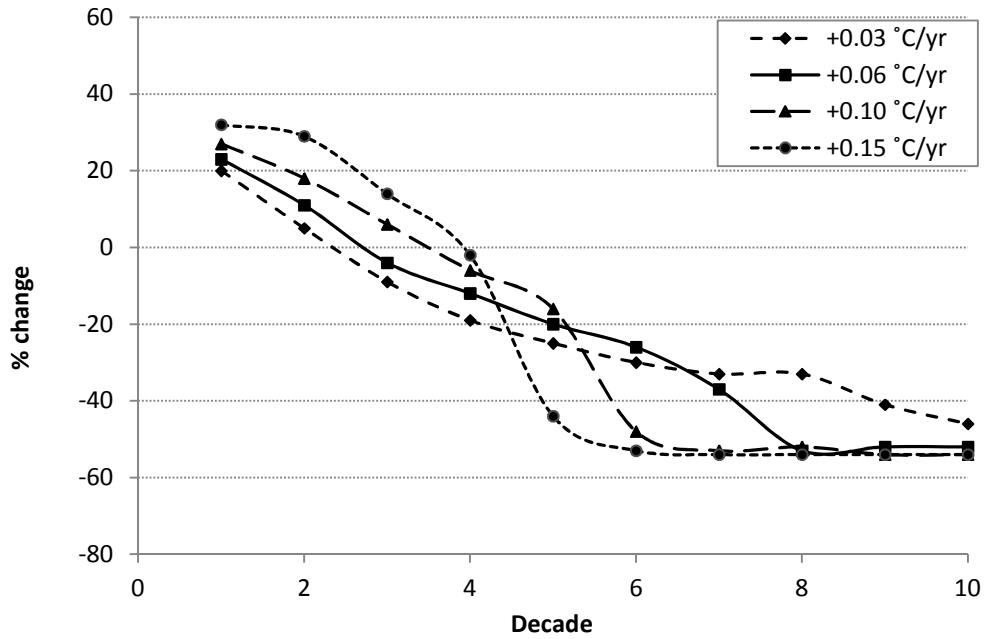


Figure 6.14 Changes in Decadal Mean Flows, relative to baseline, of the Ganges at Uttarkashi for the four incremental temperature scenarios (+0.03, +0.06, +0.1 and +0.15 °C/year) over a 100-year period

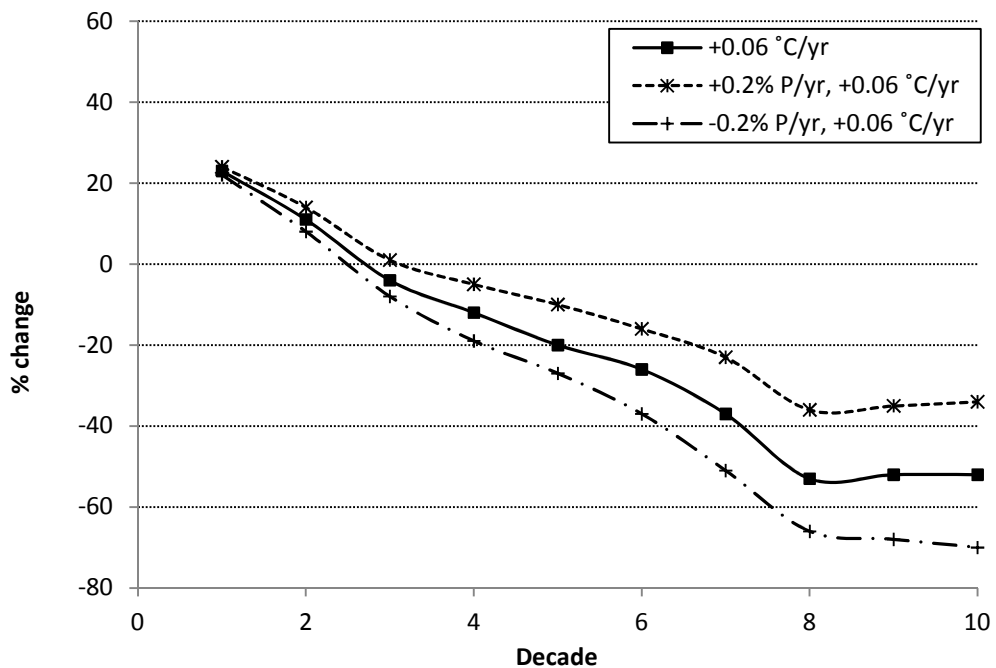


Figure 6.15 Changes in Decadal Mean Flows, relative to baseline, of the Ganges at Uttarkashi for two combined incremental precipitation (P) and temperature scenarios (+0.2% P with +0.06 °C/year, -0.2% P with +0.06 °C/year, with the +0.06 °C/year temperature scenario as reference) over a 100-year period

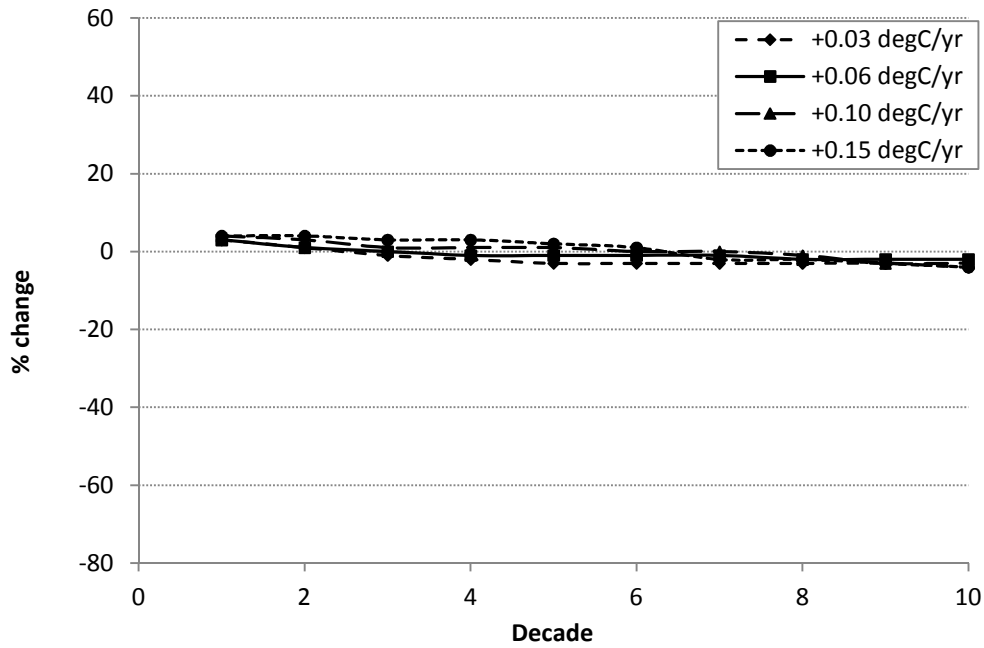


Figure 6.16 Changes in Decadal Mean Flows, relative to baseline, of the Ganges at Allahabad for the four incremental temperature scenarios (+0.03, +0.06, +0.1 and +0.15 °C/year) over a 100-year period

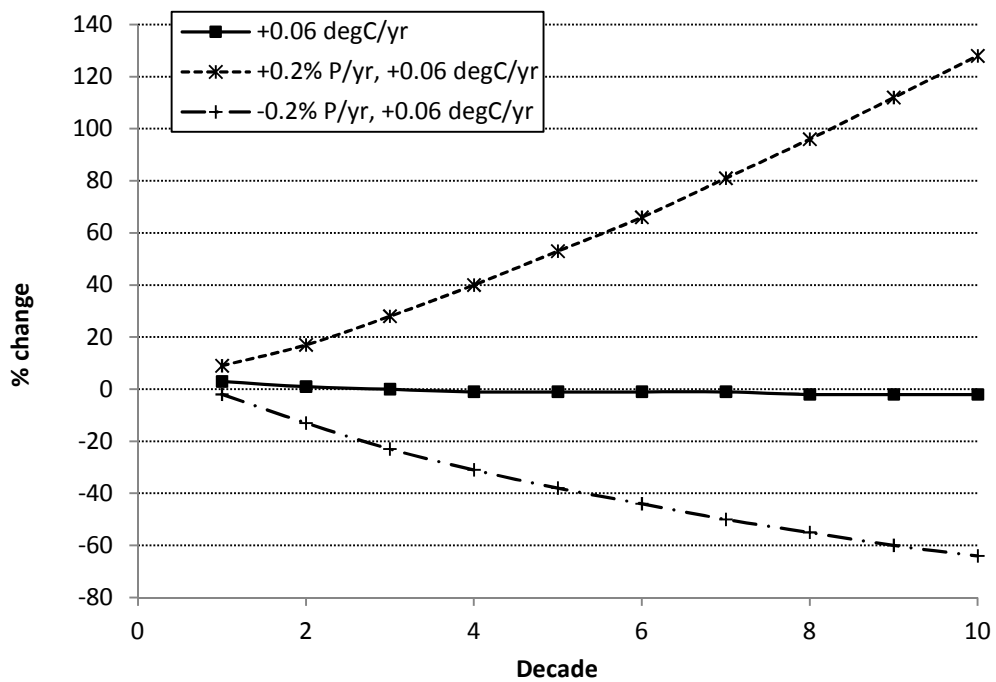


Figure 6.17 Changes in Decadal Mean Flows, relative to baseline, of the Ganges at Allahabad for two combined incremental precipitation (P) and temperature scenarios (+0.2% P with +0.06 °C/year, -0.2% P with +0.06 °C/year, with the +0.06 °C/year temperature scenario as reference) over a 100-year period

6.4.3 All sites for the +0.06 °C/year, +0.15 °C/year and RCM-based scenarios

Figure 6.18 presents results of the +0.06 °C/year scenario for all four Ganges study sites. Changes to DMFs are broadly similar at Kanpur and Allahabad, those at Kanpur being greater because its upstream glacier cover, at 4.2%, is more than double Allahabad's 1.9%. The most interesting feature of this graph is the result for Haridwar, Although 16% of the 23,000 km² upstream catchment area is glacier-covered, the impacts of this temperature scenario appear limited, having an initial peak of +19% relative to baseline at D1 and diminishing to only -5% of baseline by D10. This contrasts with changes seen for the same scenario at Uttarkashi, less than 200 km upstream and whose percentage glacier-cover contributes over a quarter of the ice cover of the Haridwar catchment. As annual precipitation at Haridwar (1044 mm) is not much higher than at Uttarkashi (982 mm), it is assumed that the distribution of ice with elevation elsewhere in the catchment, possibly in the headwaters of the Gangotri-fed Bhilangna River (another tributary of the Ganges), is sufficient in volume and extends sufficiently high to sustain flows longer over the duration of the model run.

This logic seems valid also when inspecting the results for the extreme +0.15 °C/year scenario at all sites (Figure 6.20). DMFs at both Haridwar and Kanpur continue to increase, relative to the baseline, until D3, with peaks of +41% and +18% respectively, but then are sustained above baseline for a further three decades until D7, finally resulting in reductions of -21% and -10% of baseline respectively by D10. Apart from at Uttarkashi, none of the asymptotic behaviour that is characteristic of model glacier extinction is seen. Such sustained flows are likely when sufficient volumes of ice are present in ice-bands of upstream model glaciers and when the upper extremities of model glaciers are high enough to prevent their total depletion.

Results for the HadRM2-based scenario (Figure 6.20) show DMFs at all sites reducing (relative to baseline), after initial peaks of between +29% and +5% of baseline in D1, almost linearly to between -6% and -22% in D6. The rate of change is greatest at Uttarkashi, from +29% in D1 to -22% in D6. This is consistent with the results for other scenarios at the site, which suggests the characteristics of this particular catchment make it particularly sensitive to changes in climate input variables.

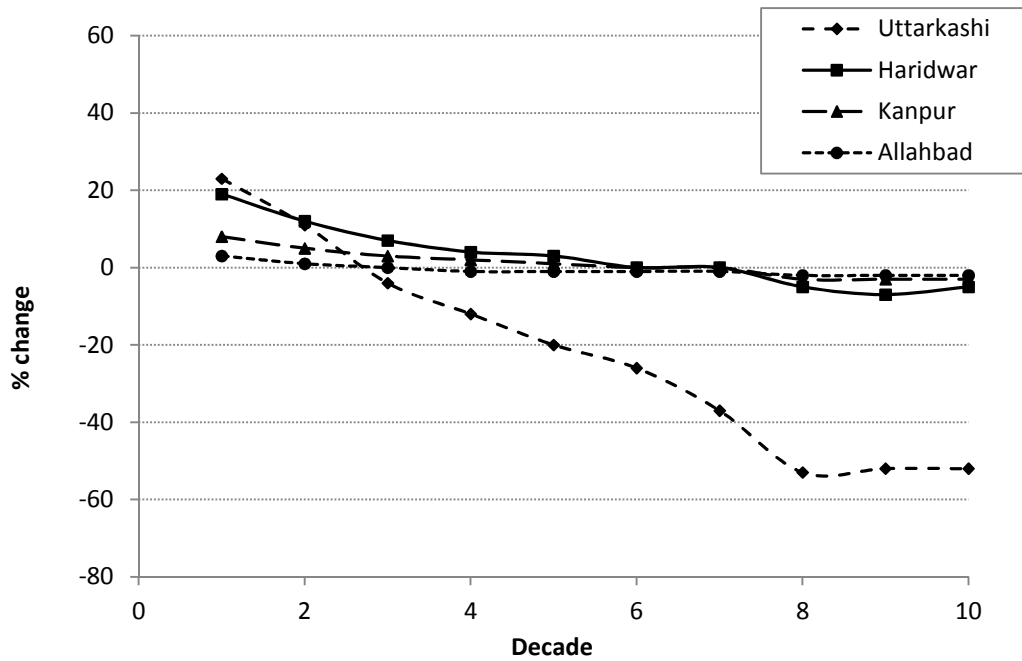


Figure 6.18 Changes in Decadal Mean Flows, relative to baseline, of the Ganges at all four study sites for the +0.06 °C/year incremental temperature scenario over a 100-year period

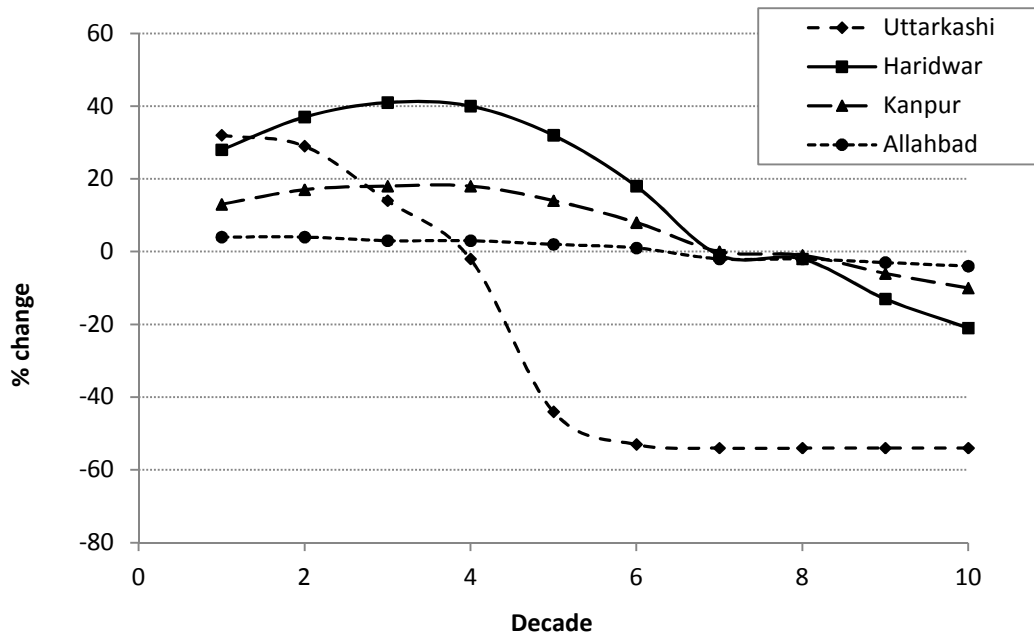


Figure 6.19 Changes in Decadal Mean Flows, relative to baseline, of the Ganges at all four study sites for the +0.15 °C/year incremental temperature scenario over a 100-year period

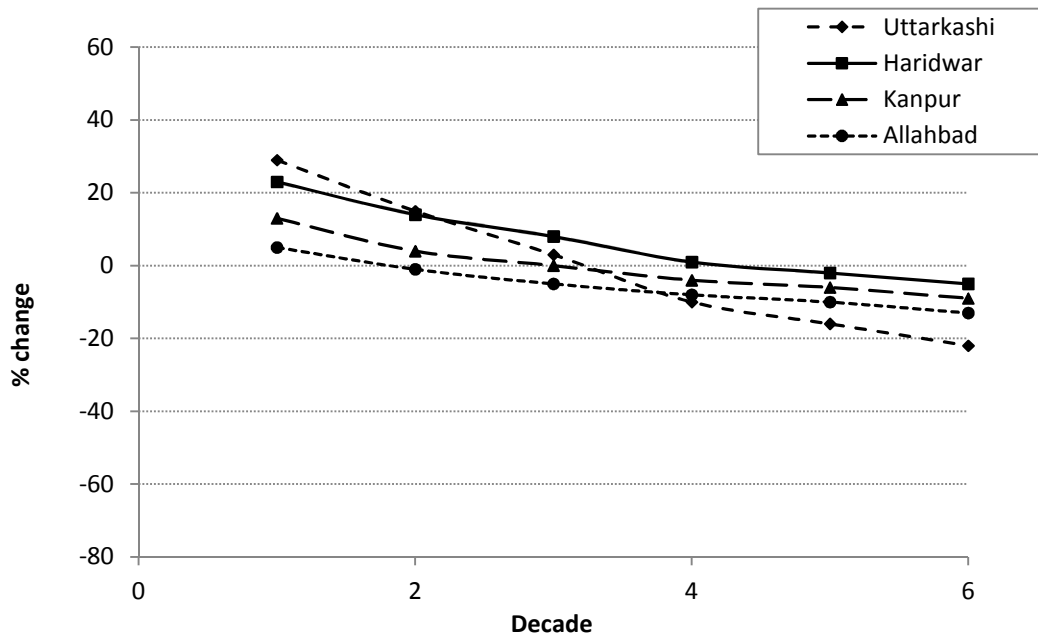


Figure 6.20 Changes in Decadal Mean Flows, relative to baseline, of the Ganges at all four study sites for the HadRM2-based climate change scenario over a 60-year period

6.5 Analysis of modelled future river flows in the Kali Gandaki-Narayani River, Nepal (Focal Area C)

The Kali Gandaki-Narayani River in central Nepal (Figure 6.21) was chosen as a focal area because it was considered indicative of summer monsoon-affected, eastern Himalayan conditions. The drainage basin includes the Annapurna, Dhaulagiri, Langtang and Manaslu mountain massifs. It is one of the most economically important glacier-fed rivers in the country, vital for hydropower generation, tourism and, in its lower reaches in Nepal, agriculture and industry. The Narayani River, which is named the Gandak River in India, is a tributary of the Ganges. Annual rainfall totals for the four selected study sites (Table 6.1) are around 2000 mm, almost double the rainfall totals for the upstream sites of the Ganges focal area (Uttarkashi and Haridwar), and about five-times higher than the totals of some Upper Indus (Focal Area A) sites.

Results for all four incremental temperature increases and two incremental precipitation changes are presented (Figures 6.22 to 6.28) for the Modi Khola at Kushma and the Narayani at Bharatpur. Three further graphs present results for all four sites for the +0.06 °C/year, +0.15 °C/year and HadRM2-based scenarios (Figures 6.29 to 6.31).

6.5.1 Modhi Khola at Kushma

The Modi Khola is fed by melt-water from glaciers of the Annapurna Himal. It is a major tributary of the Kali Gandaki, which it meets at the village of Kushma. At Kushma, the catchment area for the Modi Khola is 642 km², about 16.5% of which is glacier covered. A 14 megawatt (MW) run-of-river hydropower scheme has been installed on the river and a further two schemes, in the middle and upper reaches of the river, with a planned installed capacity of 15 and 25 MW respectively, are under construction (Himal Hydro, 2014; The Kathmandu Post, 2012). The river is also a popular tourist destination for rafting and kayaking.

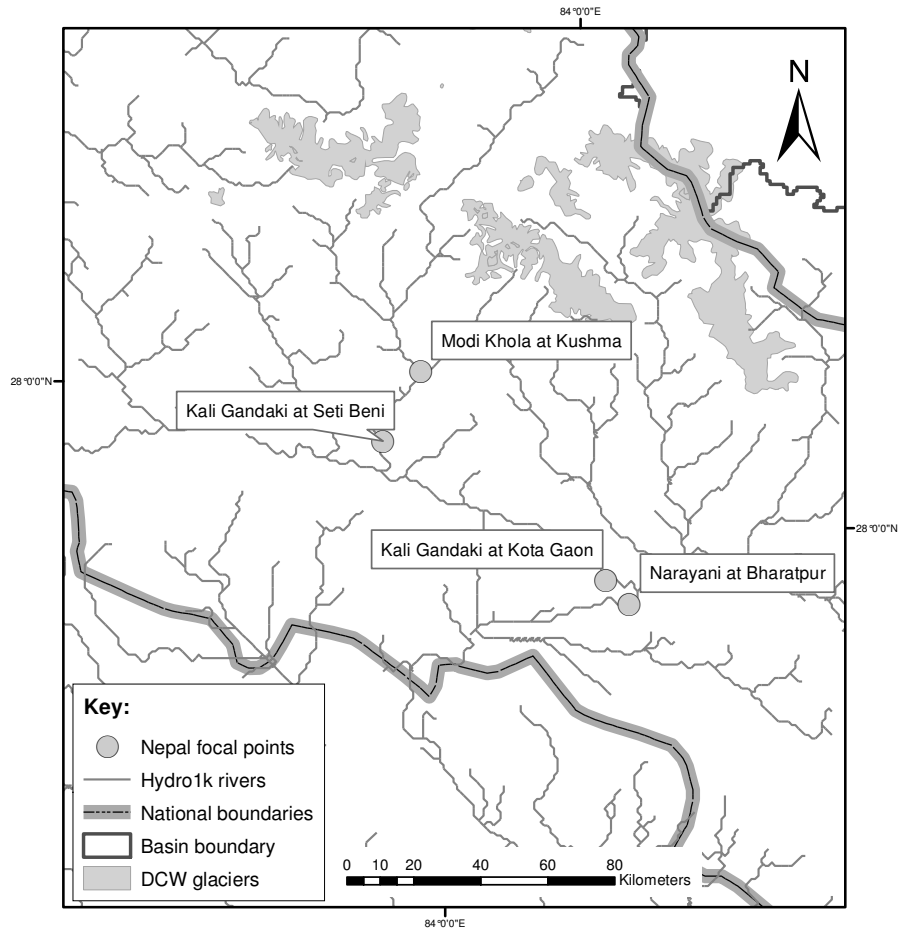


Figure 6.21 Location of the 4 study sites in Kali Gandaki-Narayani river system (headwaters of the Ganges) in Nepal

Results for the Modi Khola (Figure 6.22) contrast starkly with those seen for similarly glacier-covered upstream sites (e.g. Gilgit at Gilgit (Figure 6.5) and Ganges at Uttakshi (Figure 6.14)) in the more westerly focal areas. For all four increasing temperature scenarios, changes in DMFs relative to baseline continue to increase for several decades more. Maxima (peaks) are only seen with the two warmest, +0.1 and +0.15 °C/year, scenarios at +48% and +62% of baseline in D8 and D5 respectively. As seen with the upstream study sites of Focal Areas A and B, DMFs appear to reduce rapidly after peaking. With the warmest, +0.15 °C/year, scenario, a change of gradient and levelling-out (asymptotic behaviour) then is seen at D8, and flows eventually reduce to near baseline levels (-1% of baseline) at D10. Such asymptotic behaviour is not seen with the +0.1 °C/year scenario over the model period. DMFs continue to rise for the two coolest, +0.06 and +0.03 °C/year, scenarios for the entire 100-year model run, reaching +32% and +13% of baseline by D10 respectively, and following a trajectory that would suggest the increases would continue for a considerable period beyond the 100 years.

The results for the two coolest scenarios suggest that, as warming continues, the rise of the 0 °C isotherm is exposing ice at a higher rate than that at which ice is being depleted from lower elevations for the entire model period. Clearly, the differential is greater the warmer the scenario. The persistence of ice at lower elevations, a feature not seen earlier in either of the two western focal areas, can probably be attributed to the higher summer monsoonal precipitation that the catchment's glaciers benefit from every year. As described in §4.5.2, summer precipitation falling as snow both contributes to the accumulation of mass on glaciers and suppresses melting by blocking-out solar radiation until snow-cover is depleted. The model replicates this behaviour by preventing surface ice melting in an ice-band until the band's snow store is depleted. The model's redistribution of accumulated snow as ice between remaining ice-bands of model glaciers at the end of every year (see §4.5.7) probably also contributes to the persistence of ice in the catchment, especially as the volume of accumulated snow that would be available for annual redistribution is likely to be much higher here than in western catchments.

The peaks at D5 and D8 for the two warmest scenarios represent the point at which the rate of ice depletion exceeds the rate of ice exposure. As in other focal areas, the change of gradient and onset of asymptotic behaviour that is seen later at D8 with the warmest, +0.15% C/year, scenario is likely to correspond with the total depletion of some, but not all, of the catchment's model glaciers. However, the level at which the asymptotic behaviour begins (i.e. at or about baseline) is much higher here than in western catchments. This, again, probably is due to the high precipitation over the non-glacier part of the catchment, which contributes so significantly to river flow that the depletion of upstream glaciers has a relatively small effect. The same limited effect of deglaciation in the eastern Himalaya was illustrated earlier in §4.5.2, with the experimental 50% reduction in glacier cover.

The results of two precipitation change scenarios - incremental $\pm 0.2\%$ /year changes in precipitation coupled with incremental temperature increases of +0.15% °C/year - are shown in Figure 6.23. For the increasing precipitation scenario, DMF changes, relative to baseline, peak a decade later, in D6, than the temperature only scenario, and then reduces for two decades only (D7 & D8), before a second turning point is seen at D8, when flows start increasing gradually to D10. The delay in the peak possibly can be attributed to the increased precipitation "protecting" the glacier for longer. The second turning point, which coincides with the onset of the asymptotic behaviour characteristic of glacier depletion, suggests river flows thereafter are being determined predominantly by the increasing precipitation over the rest of the catchment. For the decreasing precipitation scenario, DMF changes relative to baseline are increasingly more negative (or less positive) for the entire model period. The timing of the peak at D5, and change in gradient at D8, coincide with those of the unadjusted temperature scenario, which suggests, somewhat unexpectedly, that the reducing precipitation, in contrast to the increasing, has relatively little influence on model glacier behaviour. A possible explanation for this is that the decrease in precipitation, at only -10% of baseline by D5, is insufficient to significantly affect the rate of depletion of model glacier ice in the catchment, whereas a +10% increase in precipitation contributes just enough to delay a decline in DMF by a single decade.

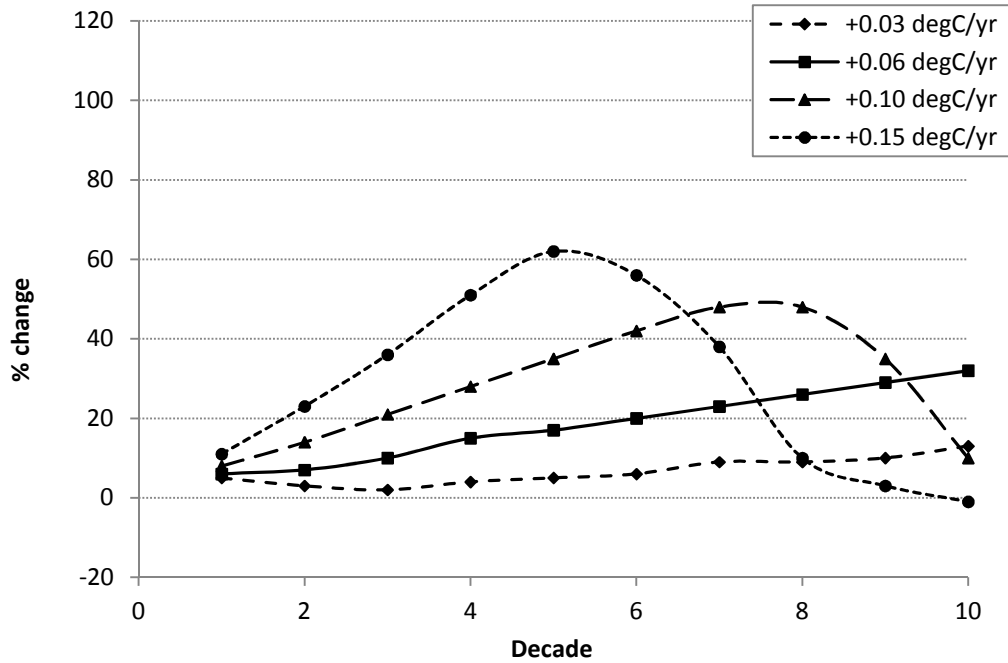


Figure 6.22 Changes in Decadal Mean Flows, relative to baseline, of the Modhi Khola at Kushma for the four incremental temperature scenarios (+0.03, +0.06, +0.1 and +0.15 °C/year) over a 100-year period

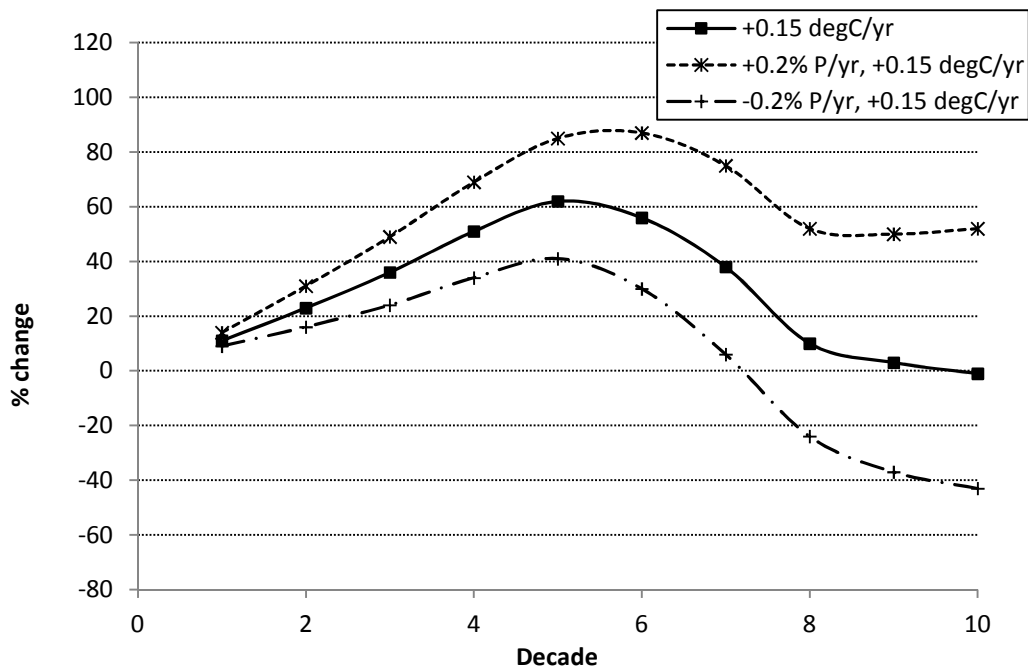


Figure 6.23 Changes in Decadal Mean Flows, relative to baseline, of the Modhi Khola at Kushma for two combined incremental precipitation (P) and temperature scenarios (+0.2%P with +0.15 °C/year, -0.2%P with +0.15 °C/year, with the +0.15 °C/year temperature scenario as reference) over a 100-year period

6.5.2 Narayani at Bharatpur

Bharatpur is Nepal's fifth largest city with a population of over 142,000 (NPCS-CBS, 2012) and is a centre of commerce in central southern Nepal. It is a short distance downstream of the confluence of the Kali Gandaki and Trisuli Rivers, which form the Narayani River. The upstream catchment area of the Narayani at Bharatpur is over 32,000 km², about 10% of which originally is glacier-covered, according to the DCW.

Model results for the four temperature scenarios (Figure 6.24) show DMFs increasing relative to baseline over the entire 100-year model period for all but the warmest, +0.15 °C/year, scenario, reaching +48%, +27% and +9% of baseline by D10 for the +0.03, +0.06 and +0.1 °C/year scenarios respectively. The +0.15 °C/year scenario peaks at +60% of baseline at D8 and only reduces to +52% by D10. As discussed for the Modi Khola, the steadily increasing flows are probably sustained because of the persistence of glacial ice, which is a consequence of summer monsoon precipitation. The changes in DMFs are more gradual at Bharatpur due to the integrating effect of more contributing glaciers upstream, which would equate to a greater volume of ice distributed, and persisting, across a wider range of elevations.

The precipitation change scenarios, seen in Figure 6.25 coupled with an incremental temperature increase of +0.06 °C/year, seem to have little effect on glacial melt-water contributions to river flow, with the changes in DMFs relative to baseline appearing almost proportional to the increase or decrease in precipitation inputs. The results do, however, indicate the sensitivity of the catchment's response to precipitation changes. For example, for the 20% difference in precipitation that is attained between the two scenarios by D5, there is a difference of over 50% in the DMFs (relative to baseline); by D10, the 40% precipitation difference is amplified to a 114% difference in DMFs.

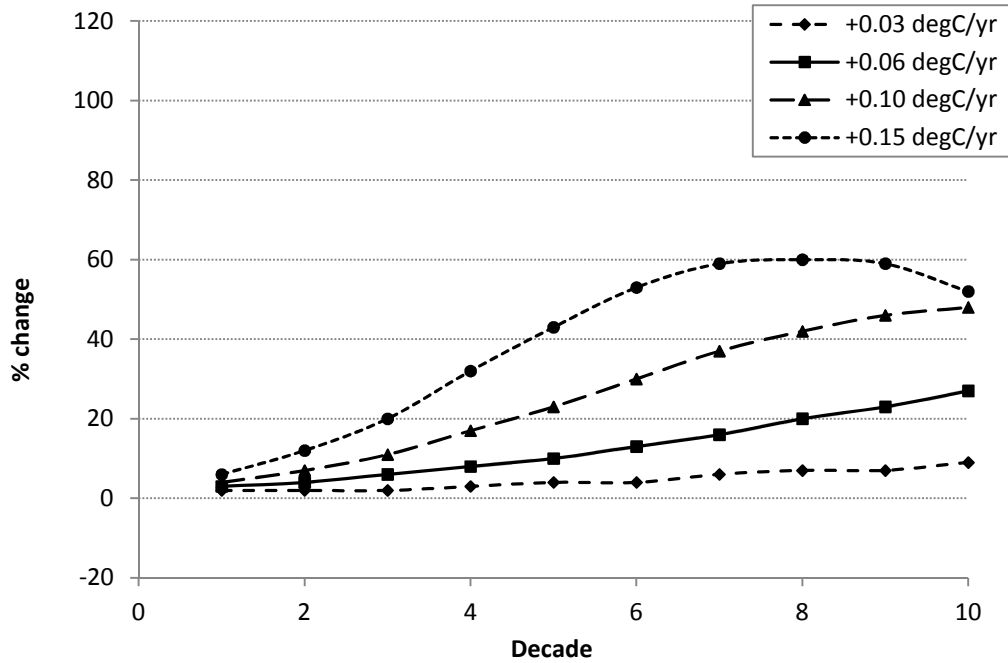


Figure 6.24 Changes in Decadal Mean Flows, relative to baseline, of the Narayani at Bharatpur for the four incremental temperature scenarios (+0.03, +0.06, +0.1 and +0.15 °C/year) over a 100-year period

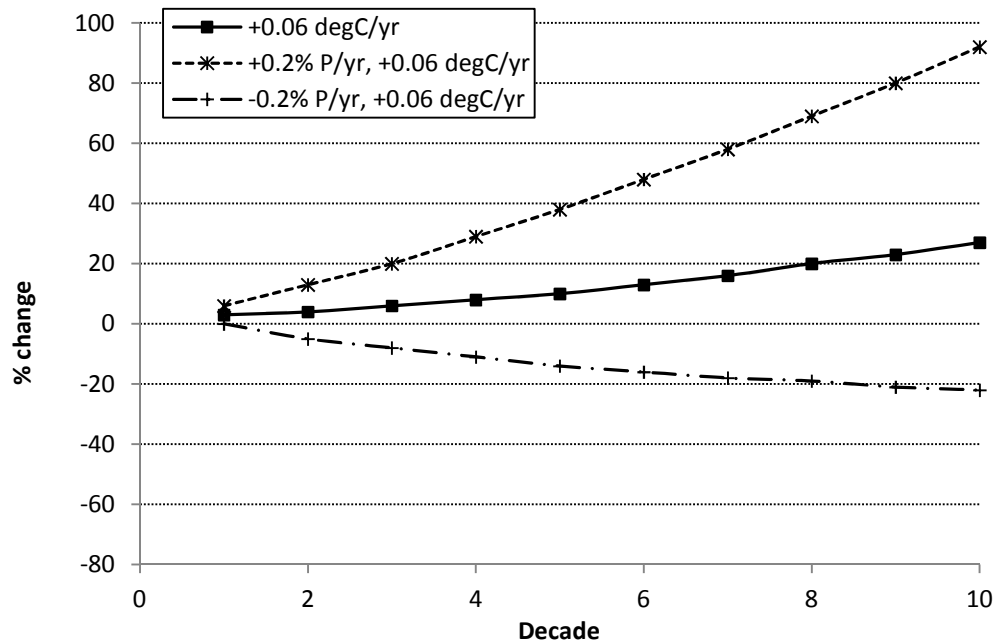


Figure 6.25 Changes in Decadal Mean Flows, relative to baseline, of the Narayani at Bharatpur for two combined incremental precipitation (P) and temperature scenarios (+0.2%P with +0.06 °C/year, -0.2%P with +0.06 °C/year, with the +0.06 °C/year temperature scenario as reference) over a 100-year period

6.5.3 All sites for the +0.06 °C/year, +0.15 °C/year and RCM-based scenarios

Changes to the DMFs at all four sites in Focal Area C for the +0.06 °C/year scenario appear similar (Figure 6.26), with the DMFs increasing, relative to baseline, decade by decade over the entire 100-year model run period, to reach between +47% (Kali Gandaki at Seti Beni) and +9% (Kali Gandaki at Kata Gaon) of baseline by D10. All seem to follow a trajectory that suggests river flows would continue to increase well beyond the 100 years for this plausible change scenario.

Similar behaviour is seen at all four sites for the warmest, experimental, +0.15 °C/year scenario (Figure 6.27). DMFs at all sites continue to increase relative to baseline for several decades, albeit at different rates, and peak at different times. DMFs peak earliest at Kushma with a +62% increase in DMF relative to baseline at D5, then at Seti Beni (+87% of baseline) and Kata Gaon (+32%) at D6 and at Bharatpur at D8 (+60%). Differences in the time-to-peak are thought likely to be dependent on the total volume of ice at higher elevations and the vertical range, or extent, of the ice. For example, the Modi Kholā at Kushma, which peaks first, being the smallest catchment, is likely to have the lesser volume of ice occupying a narrow vertical range than the largest catchment, the Narayani at Bharatpur, which peaks latest. The differences in the magnitude of DMF changes between Seti Beni and Kata Gaon are simply because of the different proportion of glacier-cover in either catchment: both are fed by the same glaciers and, thus, the glacier-melt contribution to river flow at Kata Gaon is proportionately less than at Seti Beni, resulting in smaller changes in DMFs relative to baseline.

Results from the application of the 60-year model run of the HadRM2-scenario (Figure 6.28) appear similar to some of the more plausible incremental scenarios, showing steady increases at all four sites over the model period and reaching between +54% of baseline at Kushma and +20% at Kata Gaon by D6. This suggests a degree of consistency between the two scenario types in this part of the Himalaya.

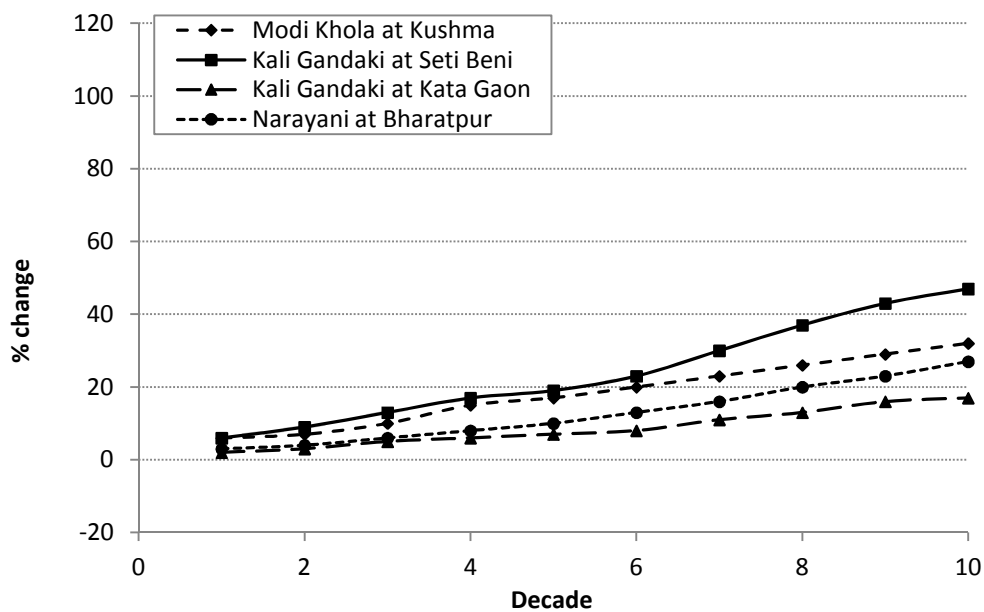


Figure 6.26 Changes in Decadal Mean Flows, relative to baseline, of the Kali Gandaki-Narayani river system at all four study sites for the +0.06 °C/year incremental temperature scenario over a 100-year period

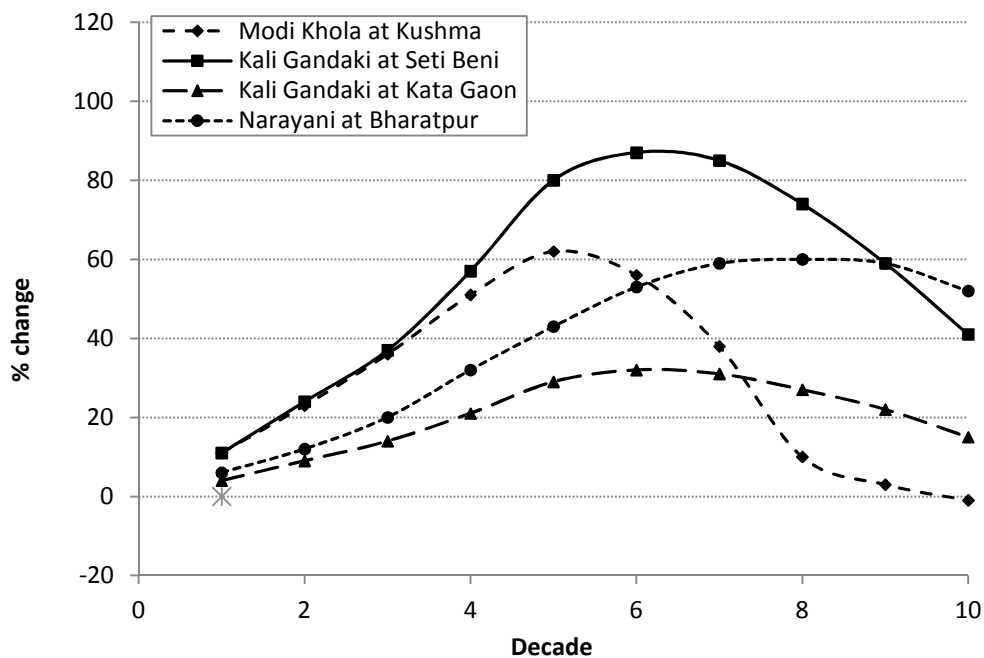


Figure 6.27 Changes in Decadal Mean Flows, relative to baseline, of the of the Kali Gandaki-Narayani river system at all four study sites for the +0.15 °C/year incremental temperature scenario over a 100-year period

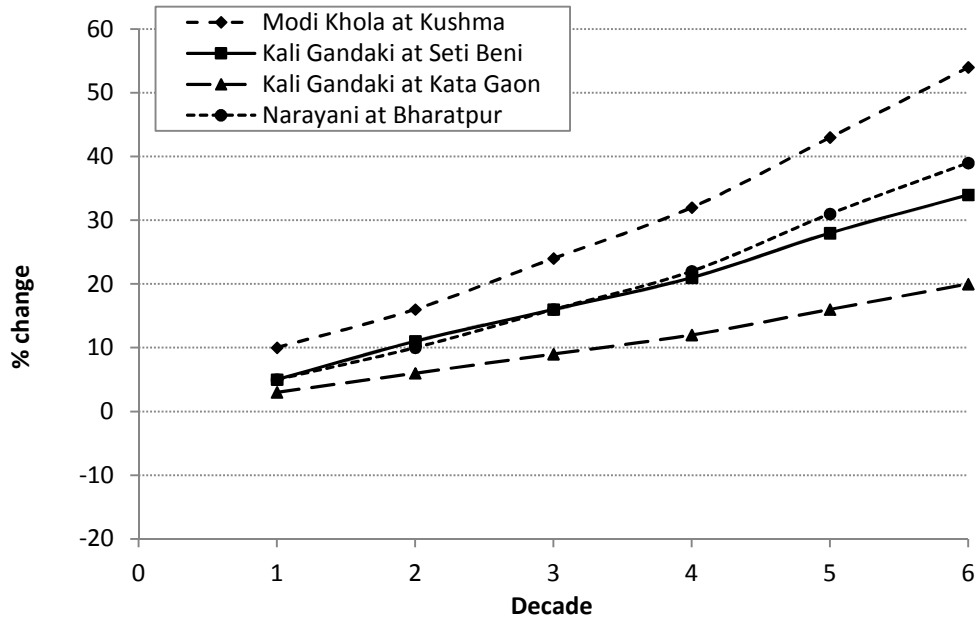


Figure 6.28 Changes in Decadal Mean Flows, relative to baseline, of the Kali Gandaki-Narayani river system at all four study sites for the HadRM2-based climate change scenario over a 60-year period

6.6 Analysis of modelled future river flows in the Brahmaputra (Focal Area D)

The study sites for the Brahmaputra focal area (Figure 6.29) were selected to demonstrate potential impact of climatic changes along the main river (named Zangpo or Tsangpo in China) from its source, the Angsi Glacier on the northern side of the Himalaya in Tibet (IRSA, 2010), to where it enters the north eastern Indian state of Arunachal Pradesh, at the city of Tuting. The river in China is on the northern, leeward side of the Himalaya and annual rainfall totals for the selected study sites, Samsang (653 mm) and Xigaze (873 mm), are less than half that experienced by the Kali Gandaki-Narayani study sites of on the south-facing windward side in Nepal (see Table 6.1). One site, however, was selected from one of the many tributaries of the Brahmaputra that drain the southerly windward slopes of the Himalaya: at the town of Zhemgang on the Trongsa Chhu river in Bhutan, which, in contrast to the Chinese sites, receives about 2150 mm rainfall annually.

Similarly to all other focal areas considered in this chapter, results are presented for all four incremental temperature increases and two incremental precipitation changes (Figures 6.30 to 6.33) for the uppermost (Zangpo at Samsang) and lowermost (Brahmaputra at Tuting) main river sites. Three further graphs present results for all four study sites for the +0.06 °C/year, +0.15 °C/year and HadRM2-based scenarios (Figures 6.34 to 6.36).

6.6.1 Zangpo at Samsang

Samsang is a small, remote village in Tibet, one of the closest settlements to the source of the Brahmaputra and a staging post for trans-Himalayan-Tibetan trekkers. The catchment area for the Zangpo at Samsang is 3784 km², and despite its proximity to the source of the river, according to the DCW (ESRI, 1993) only 3% of the catchment is glacier-covered.

Results for all four incremental temperature scenarios at Samsang (Figure 6.30) demonstrate a general downward trend in DMFs relative to baseline over the entire 100-year model run, the rate of decline being greater the warmer the scenario.

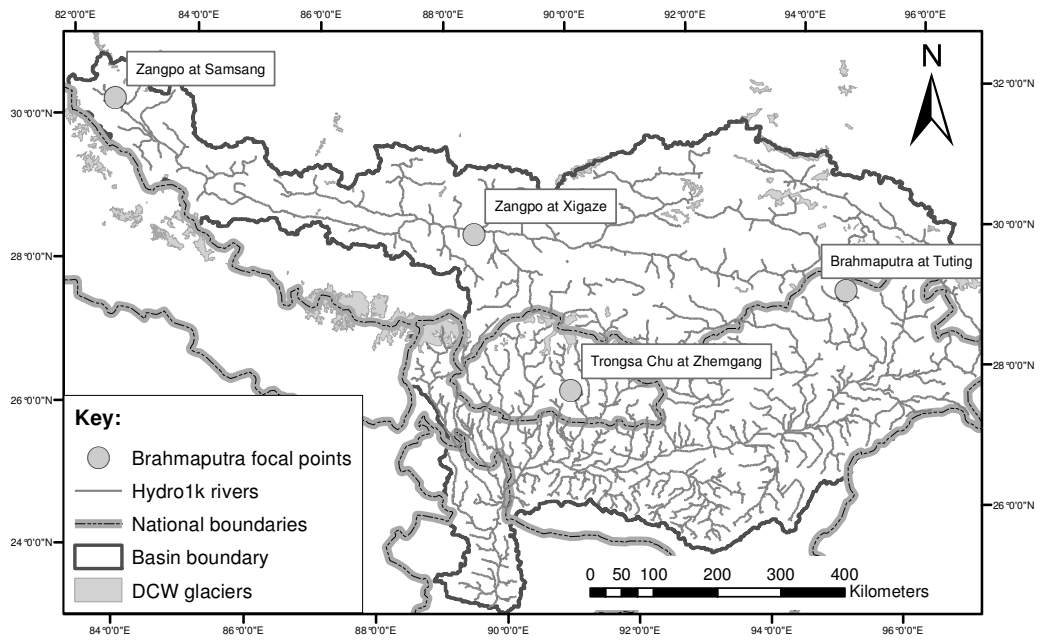


Figure 6.29 Location of the 4 study sites in the Brahmaputra focal-area

After only a very small initial increase at D1, DMFs ultimately reduce to between -17% and -71% of baseline by D10. The behaviour is indicative of glacial ice being depleted at a faster rate at lower elevations than it is being exposed to melting by the upward migration of the 0 °C isotherm. The absence of asymptotic behaviour with any of the scenarios suggests that, despite the limited glacier cover, ice continues to be present in the catchment over the whole model period, possibly because the ice extends to sufficiently high elevations to persist throughout.

As seen elsewhere, the precipitation change scenarios, shown in Figure 6.31 coupled with an incremental temperature increase of +0.15 °C/year, have little effect on glacial melt-water contributions to river flow, with the DMF changes appearing proportional to the changes in precipitation inputs.

6.6.2 Brahmaputra at Tuting

The Brahmaputra locally is referred to as the Siang River as it enters India. At Tuting, its catchment area is over 229,000 km², 2.1% of which is glacier-covered. It is near here that the west-east traversing main Brahmaputra river abruptly turns south and cuts a deep gorge through the mountains (the Tsangpo Canyon), before emerging into India (near Tuting), flowing south west along the Assam Valley, and eventually meeting the Ganges in Bangladesh, to form the Maghna River.

Results (Figure 6.32) show all incremental temperature increases only have a limited effect on DMFs at Tuting. As seen at Samsang, some 1600 km upstream (Google Earth, 2013), there is a general trend for the DMFs to reduce gradually over the model period for all scenarios, with flow reducing by a greater amount the warmer the scenario. DMF estimates at D10 are only between -10% and -26% of baseline. Asymptotic levelling-out occurs with the warmest, +0.15 °C/year, scenario at D9 and D10, both decades having DMF values of -26% relative to baseline.

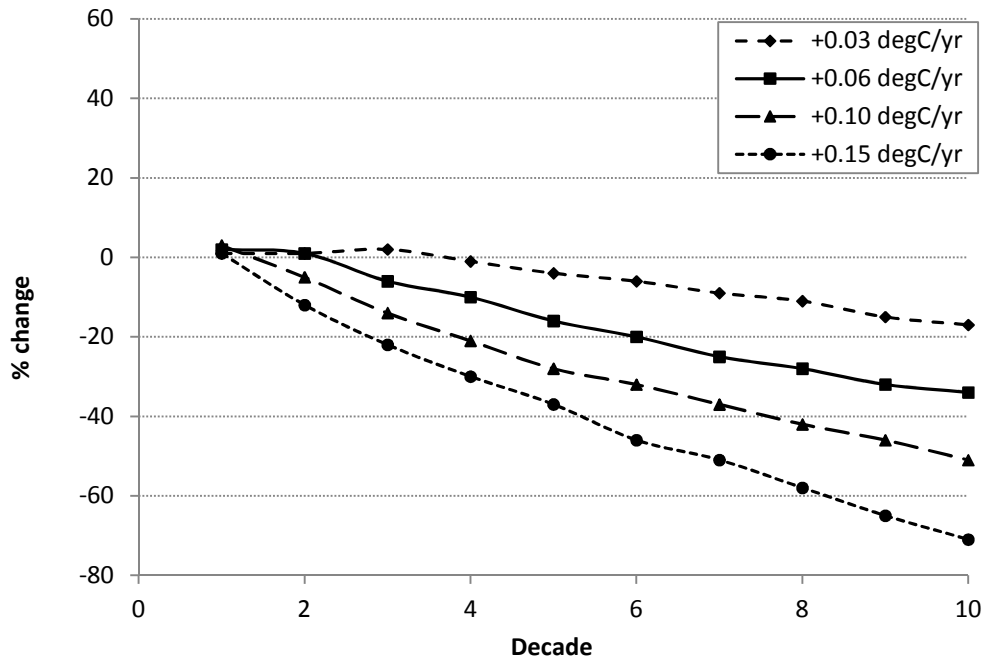


Figure 6.30 Changes in Decadal Mean Flows, relative to baseline, of the Zangpo at Samsang for the four incremental temperature scenarios (+0.03, +0.06, +0.1 and +0.15 °C/year) over a 100-year period

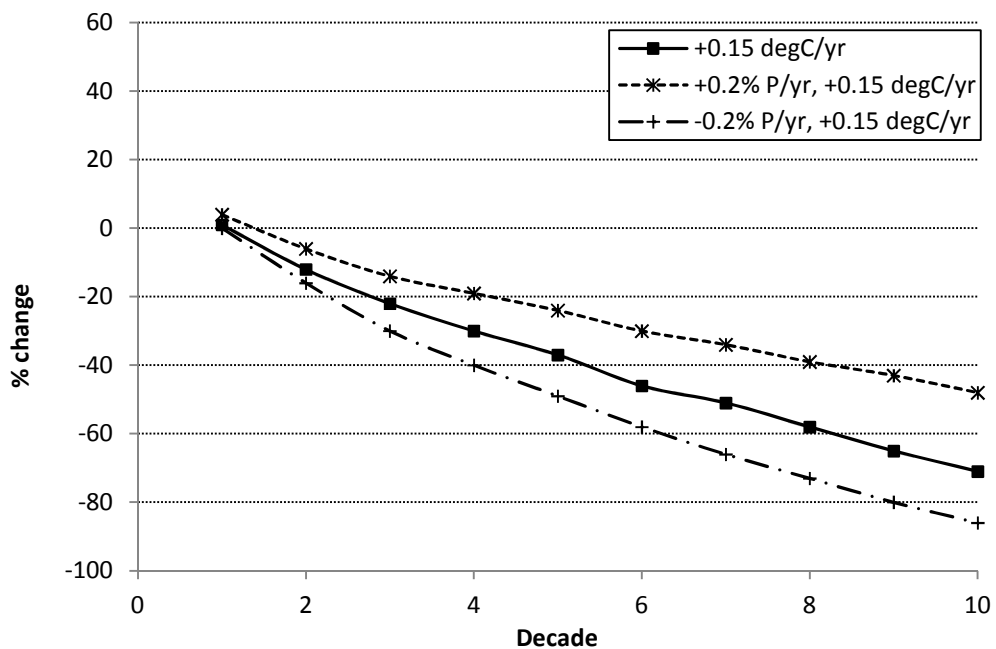


Figure 6.31 Changes in Decadal Mean Flows, relative to baseline, of the Zangpo at Samsang for two combined incremental precipitation (P) and temperature scenarios (+0.2%P with +0.15 °C/year, -0.2%P with +0.15 °C/year, with the +0.15 °C/year temperature scenario as reference) over a 100-year period

The precipitation change scenarios, shown in Figure 6.33 coupled with an incremental temperature increase of $+0.15\text{ }^{\circ}\text{C}/\text{year}$, again appear to have little effect on glacial melt-water contributions to river flow, with the DMF changes seemingly proportional to the changes in precipitation inputs. In this particular graph, it is interesting to note the upward trajectory from D9 with the positive precipitation change scenario, as river flows become determined by the contemporary precipitation.

6.6.3 All sites for the $+0.06\text{ }^{\circ}\text{C}/\text{year}$, $+0.15\text{ }^{\circ}\text{C}/\text{year}$ and RCM-based scenarios

With all three graphs in this sub-section (Figure 6.34 to 6.36), the immediate and most noticeable feature is the considerable difference in results for the Trongsa Chhu at Zhamgang (Bhutan) compared to those of the three study sites on the main Brahmaputra River. The three main river sites appear to be similarly affected by all change scenarios, whereas Trongsa Chhu (2755 km^2 ; 5.2% ice), not surprisingly, given its location on the southern, windward side of the eastern Himalaya, presents results that resemble those of the Kali Gandaki-Narayani focal area in Nepal (Focal Area C). Similarly to the Nepalese sites, a general upward trend is seen with the “plausible” $+0.06\text{ }^{\circ}\text{C}/\text{year}$ warming scenario (Figure 6.34), while with the extreme $+0.15\text{ }^{\circ}\text{C}/\text{year}$ scenario (Figure 6.35) DMFs peak at +35% of baseline at D4 and 5 and then reduce sharply to reach a level asymptote at -6% of baseline by D8. The difference is particularly evident with the HadRM2-based scenario (Figure 6.36), in which the DMFs for main river sites all peak at below +10% of baseline at D2 and then hover around baseline for the remainder of the 60-year model run; DMFs at Zhemgang however generally increase from about +20% in D1 and D2 to over +45% of baseline by D6.

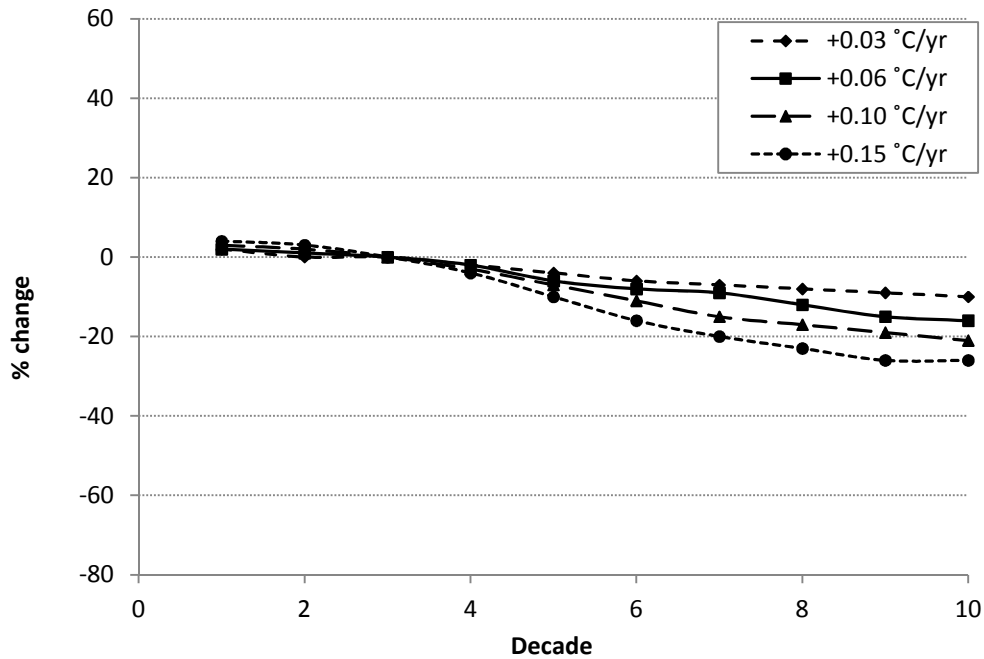


Figure 6.32 Changes in Decadal Mean Flows, relative to baseline, of the Brahmaputra at Tuting for the four incremental temperature scenarios (+0.03, +0.06, +0.1 and +0.15 °C/year) over a 100-year period

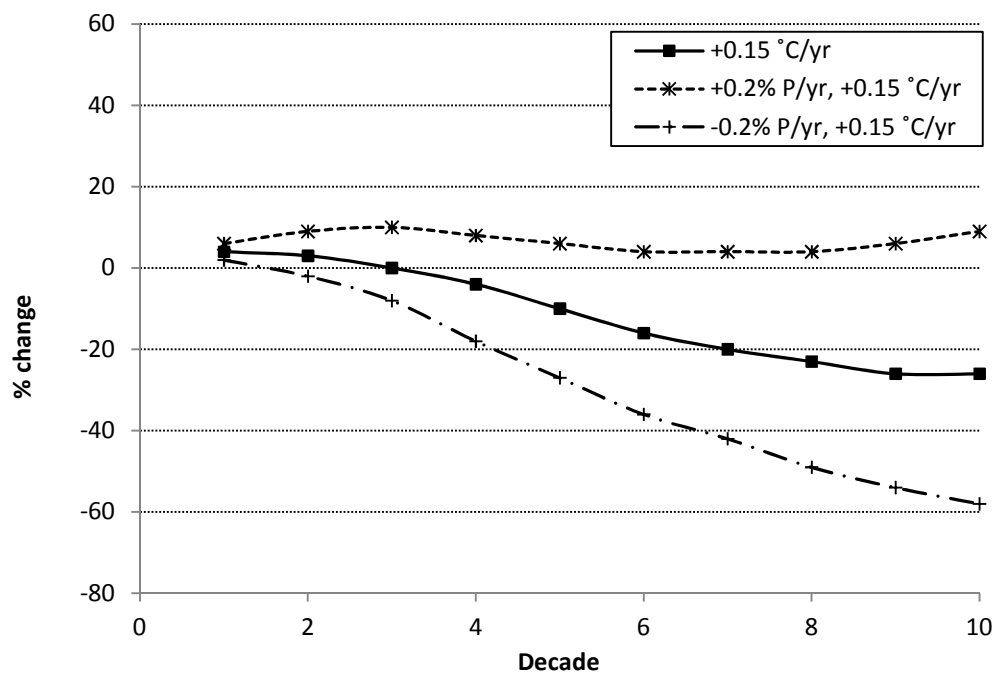


Figure 6.33 Changes in Decadal Mean Flows, relative to baseline, of the Brahmaputra at Tuting for two combined incremental precipitation (P) and temperature scenarios (+0.2%P with +0.15 °C/year, -0.2%P with +0.15 °C/year, with the +0.15 °C/year temperature scenario as reference) over a 100-year period

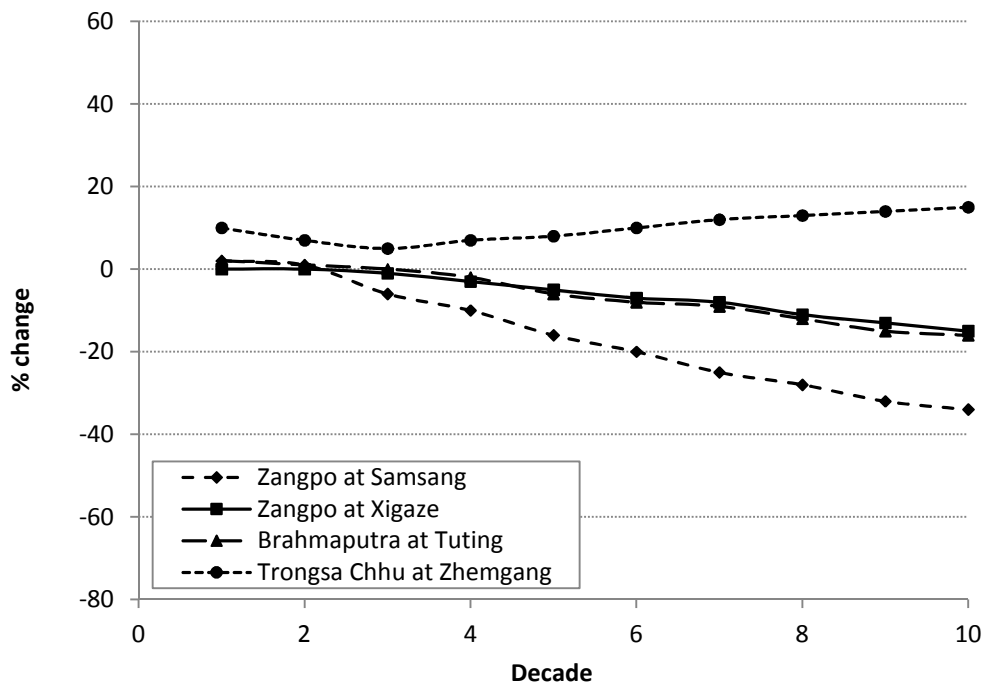


Figure 6.34 Changes in Decadal Mean Flows, relative to baseline, of the Brahmaputra and tributaries at all four study sites for the +0.06 °C/year incremental temperature scenario over a 100-year period

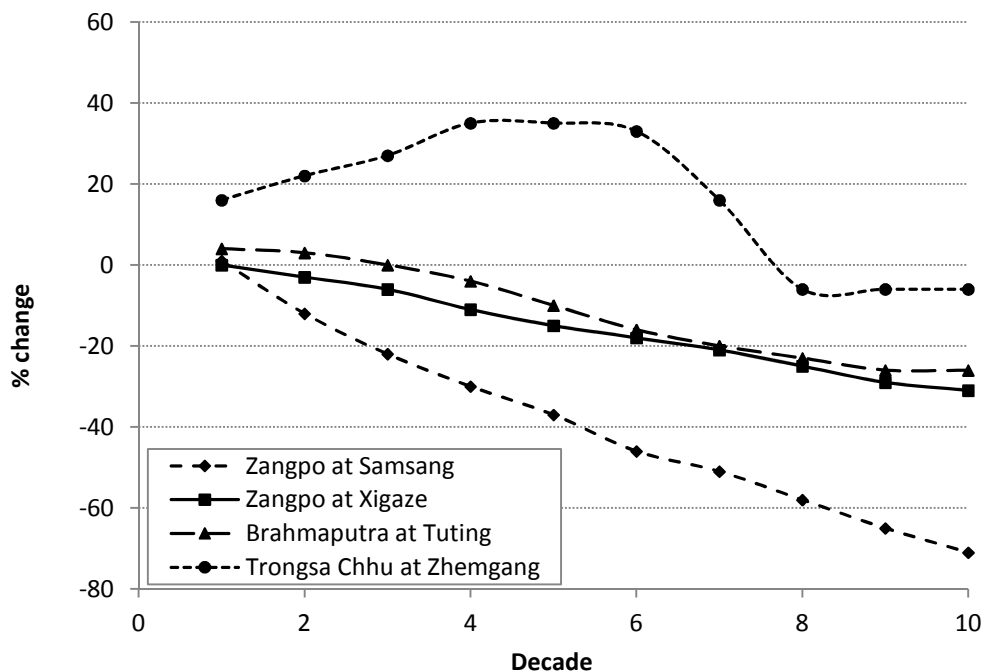


Figure 6.35 Changes in Decadal Mean Flows, relative to baseline, of the Brahmaputra and tributaries at all four study sites for the +0.15 °C/year incremental temperature scenario over a 100-year period

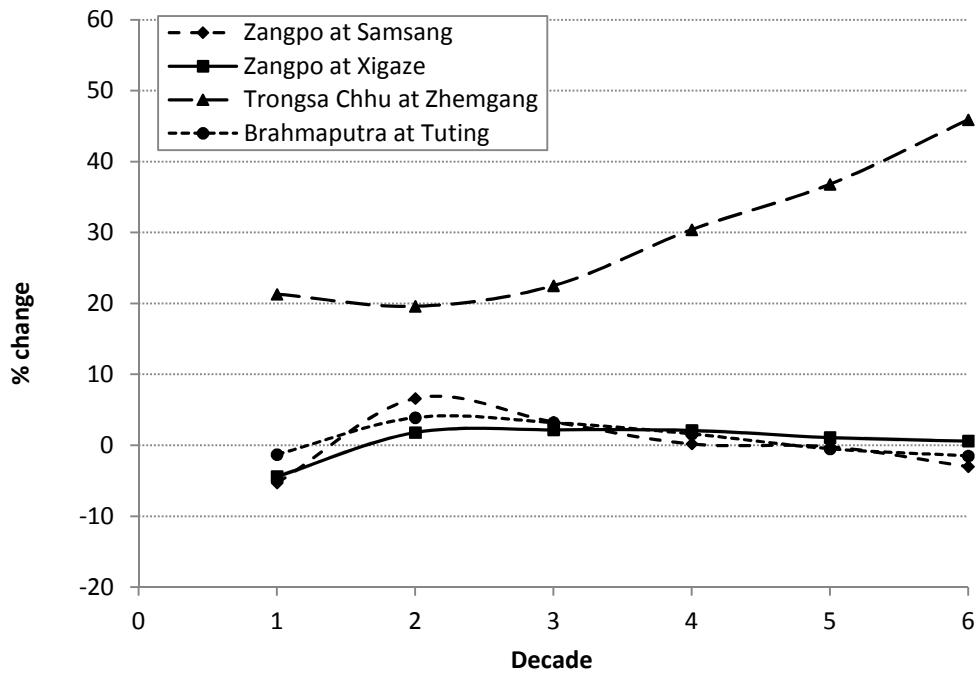


Figure 6.36 Changes in Decadal Mean Flows, relative to baseline, of the Brahmaputra at all four study sites for the HadRM2-based climate change scenario over a 100-year period

6.7 Discussion on model results

This Section distils the key messages that emerge from the model results. Discussion on the approach, the model and its implementation and application, is deferred to the final, concluding chapter, Chapter 7.

6.7.1 The East-West divide and the influence of the summer monsoon

The modelled results clearly show impacts of climatic change on glaciers and glacial melt-water contributions to river flows are likely to vary considerably across the region and within catchments. Analysis of the results from the different focal areas indicates the very important role precipitation, and the summer monsoon in particular, plays in influencing the direction, rate and magnitude of changes to river flow. A clear gradient in impacts is seen from west to east.

The summer monsoon usually does not penetrate strongly to the headwaters of the Indus and, as consequence of the limited precipitation, early increases in Upper Indus flows that result from climatic warming are soon followed by steep reductions, corresponding to the rapid loss of ice from lower elevations. The lack of precipitation contributes to retreat in two ways: limited summer precipitation allows ablation to continue unabated while the amount of winter snowfall is inadequate to offset loss of ice in summer. The impacts of the changes, as illustrated both in §6.1 and §6.2, persist for considerable distances downstream because so little of the river flow is derived from the small amount of rainfall over the glacier-free parts of catchments that the glacier-melt component of flow remains dominant throughout.

By contrast, high monsoonal precipitation in the east (e.g. Focal Area C), which occurs as snow at higher elevations, both protects glaciers from ablation during key summer months and helps to offset the loss of ice mass by snow accumulation. Under climatic warming, flows initially are augmented as increasing temperatures raise the 0 °C isotherm and the limits of the transient snow-line (TSL) to higher elevations, to expose more ice to melting, while the annual redistribution of accumulated snow delays retreat. Flows starts to reduce once the rate at which ice is exposed to melting no longer offsets the area of ice lost around the glacier terminus. Flows in the east only appear to reduce under the warmest change scenarios. However, in catchments

where precipitation is high, the impacts of glacier retreat are clearly seen to diminish rapidly downstream, as the runoff contribution from rainfall over the glacier-free parts of catchments quickly swamps the glacial melt-water contribution.

It is probably safe to deduce, therefore, that catchments in the eastern Himalaya, which benefit from the high precipitation of the summer monsoon every year, are less susceptible to the impacts of glacier retreat than those in the west, where the monsoon is very much weaker.

6.7.2 Effects of the assumed distribution of glacial ice

The assumed initial distribution of glacial ice and its mapping onto individual grid cells within the model inevitably will affect results. The initial increases in DMFs over D1, a feature seen under almost every change scenario, is thought to be a consequence of a surplus of ice at lower elevation ice bands of model glaciers melting rapidly as temperatures begin to rise.

Results thereafter, though also dependent on the assumed initial geometries of model glaciers, appear consistent with our understanding of local conditions. The initial geometries, which are unique to every grid cell, affect the rate of change of increases (and decreases) in catchment DMFs and the timing of turning points but are unlikely to influence the general direction of responses. That different study sites in the same focal areas (e.g. Gilgit at Gilgit, Shyok at Shyok in the Upper Indus) show similar responses lends weight to this assertion.

It should be noted that the results that were presented were for specific catchments and not individual grid cells. In every case, the site results represent an integrated response, not of one model glacier in a single grid cell only, but of many model glaciers in many grid cells in the upstream catchment. Clearly, the larger the catchment, the greater the likelihood is of there being more model glaciers upstream and, consequently, a more integrated catchment response may be expected. As in reality, the smallest catchments appear most sensitive to changes in climate. This is seen in the model results for the majority of near-headwater study sites (Gilgit at Gilgit, Shyok at Shyok, Ganges at Uttarkashi, Modi Khola at Kushma and Trongsa

Chuu at Zhemgang), all of which demonstrate the characteristic hydrological response expected of glaciers under climatic warming: as ice area declines, flows initially increase and then decrease, over variable timescales, until the glaciers eventually disappear (cf. Stahl and Moore, 2006; Ye *et al.*, 2003). Absolute timings of changes in flow and recession are strongly dependent on ice thickness and area and the range of elevation within which glaciers exist. Such classical responses are delayed in larger highly glaciated catchments (e.g. Indus at Bisham Qila, Narayani at Bhratpur) because of the integrating effect of many model glaciers upstream, which means larger volumes of ice are available over wider elevation ranges.

The effect is illustrated in Figure 6.37, for two model glaciers having identical geometries but differing vertical extents. Glacier A represents the model glacier of a small catchment, Glacier B another's. As climatic warming causes the 0 °C isotherm in the atmosphere to rise, Glacier A's ice will be exposed to melting earlier and for longer than Glacier B's. Glacier A's ice will deplete quicker from successive ice-bands, flows will peak earlier, and total extinction will occur much sooner than with Glacier B. Considering then a larger catchment downstream benefitting from both glaciers in its headwaters: with a greater volume of ice available for melting over a wider elevation range, peak flows will be delayed, as it takes longer to deplete ice from elevation bands, as will total depletion, until the 0 °C isotherm reaches the upper limit of Glacier B. This simple illustration also demonstrates how river flows in larger catchments are likely to be more resilient to changes in glacier cover brought about by climatic warming.

Another interesting feature of the results, seen mainly with the warmer change scenarios is the asymptotic, levelling-out, of DMFs over latter decades in some of the smaller catchments. Such behaviour is an indication of the complete depletion of model glaciers in the respective catchments, and the asymptote represents the level, relative to baseline, at which river flows (in the absence of glaciers upstream) are determined solely from contemporary precipitation. That the behaviour is seen only in smaller catchments in itself reaffirms the resilience of larger catchments generally to

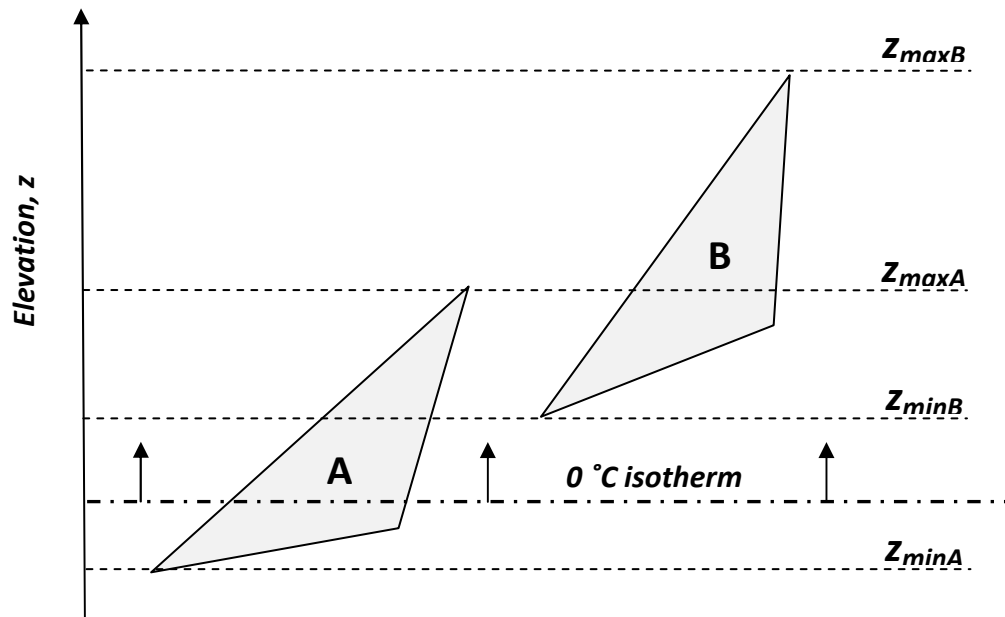


Figure 6.37 The importance of model glacier vertical extents on results: two identically shaped model glaciers (A and B, seen here from the side) but having different elevation ranges, $z_{\min A}$ to $z_{\max A}$, for Glacier A and $z_{\min B}$ to $z_{\max B}$, for Glacier B; as the 0 °C isotherm moves up with climatic warming, the ice of Glacier A is exposed earlier and longer to melting than that of Glacier B; total depletion will happen much earlier with Glacier A than B.

glacier retreat. The behaviour appears also to reiterate the east-west differential, as the level of the asymptote can be seen to decline from east to west: from -26% of baseline at Tuting in the east, to -54% at Uttarkashi, and -78% at Shyok in the far west.

Total glacier depletion is only apparent at a few upstream study sites and usually only then after several decades of the warmest temperature scenarios. This would suggest the imminent disappearance of Himalayan glaciers that had been suggested by some commentators is unlikely to happen within the foreseeable future. Undoubtedly there will be extinctions of some smaller glaciers having narrow vertical extents as temperature continue to rise, but for many larger glaciers the prospect of total depletion over coming decades appears remote.

6.7.3 Comparison with other studies

Results compare favourably with other modelling studies in the region that have considered glacier melt-water contributions to river flows (see Table 2.1). The characteristic responses reported by Stahl and Moore (2006) and Ye *et al.* (2003) are seen within the simulation period for the smaller, more highly-glacierised, catchments under the warmest scenarios, and the extent of the changes (as a % of the baseline) are of the same order reported by others, e.g. the 91% increase in DMF at Shyok under the most extreme +0.15°C/year incremental scenario is close to what Akhtar *et al.* (2008) predicted for the Hunza using the PRECIS RCM under the SRES A2 emission scenario. Ultimate reductions in the modelled flows of the Upper Indus under the +0.15 °C/year scenario (-62 to -88% of baseline by D10) are remarkably similar to Akhtar's (-65 to -94% by 2100). Modelled increases in the eastern Himalaya, under the more plausible +0.03, +0.06 and +0.1 °C/year scenarios of +9, +27 and +48% , respectively, by D10 for the Narayani at Bharatpur, compare well to results from recent model studies of the upstream Langtang catchment (Immerzeel *et al.*, 2012; Immerzeel *et al.*, 2013), which predicted increases of between +31 and +88%, relative to the same 1961-90 baseline, by 2100 using CMIP3 SRES A1B and CMIP5 RCP4.5 and RCP8.5 scenarios.

6.7.4 Plausibility of results

The physical explanation that can be proffered for the majority of results confirms that this new regional model provides a reasonably plausible representation of how climatic changes might affect future glacier retreat and glacial melt-water contributions to Himalayan river flows. The results broadly demonstrate consistency with our understanding of reality across the region, capturing nuances between east and west and from upstream to downstream, as the proportion of glacier cover within catchments diminishes.

The results, however, should be considered as indicative only. The synthetically disaggregated climate input data that correspond to a supposed trend-free standard period, together with global antecedent data, were nominally assumed to be representative of existing baseline conditions in the region. Changes in decadal mean flows relative to the baseline were charted for a nominal period of up to 100 years. The study deliberately did not ascribe dates in the presentation of these results because to do so would infer a forecast of conditions at specific future dates. The nominal nature of the method and approach simply does not warrant such specificity. The model described is also most reliably used in comparative, or differential, mode, showing differences in future river flows between existing (baseline) climate continuing and a climatic warming scenario being applied. In differential mode also, future differences in response between two or more areas can be discerned.

The results present potential changes to long-term annual and seasonal mean flows, which are useful measures of future water resources availability. They should not, however, be used to infer changes in frequency and magnitude of future hydrological extremes such, as floods or droughts. The broad spatial and temporal scales of the macro-scale hydrological models do not support assessment of extremes. Alternative approaches, probably using meso-scale catchment models, should be used for if changes in extremes are of interest.

Site-specific results should also only be considered indicative of regional behaviour. They should not form the basis of decisions for any single catchment in isolation. Applying locally derived climate data and catchment characteristics to a local catchment-scale hydrological model is likely to yield considerably different results

from those obtained by applying regionally aggregated data to the macro-scale model developed in this study. Moreover, the utility of this study's outcomes is to provide those responsible for large-scale policy and planning decision with an appreciation of possible changes that will help them mitigate the potential impacts of climatic warming on future Himalayan water resources.

7 Conclusions and future research directions

7.1 Introduction

Preceding chapters have set the context of this PhD study (Chapters 1-3) and charted the development of a new model for assessing melt-water contributions from many retreating glaciers on a regional-scale, from its initial design (Chapter 4), through its implementation within an existing MHM (Chapter 5), to its eventual application with a range of different climate change scenarios to provide estimates of potential changes to future river flows in the Indus, Ganges and Brahmaputra river basins (Chapter 6). This concluding chapter sums up the outcomes of the study and is framed around four simple questions: (1) were the objectives of the study met; (2) what are the impacts of the study; (3) how might the approach and method of the study be improved; and (4) what future research and development needs and opportunities has the study identified?

7.2 Meeting the aims and objectives of the study

To recap from Chapter 1, the primary aim of this study was “*to develop a novel parsimonious grid-based macro-scale hydrological model (MHM) for the Indus, Ganges and Brahmaputra basins that, in order to represent transient melt-water contributions from retreating glaciers, innovatively allowed glacier dimensions to change over time*”, with the specific objectives:

- 1) To develop a new method of representing mountain glaciers in MHMs that is capable of accounting for the varying melt-water contributions from many retreating glaciers in a large river basin, or region;
- 2) To incorporate the method into an MHM, with the resulting, combined, hydro-glaciological model tested in the region against observed river flow data;
- 3) To apply the new model with a range of different climate-change scenarios, with view to assessing how ensuing glacier-retreat might affect spatial and temporal variations in mean annual and winter flows of the Indus, Ganges and Brahmaputra rivers, and their tributaries, several decades into the future.

It is clear that the original aims and objectives of the study were fully met, with the ultimate outcomes of the study showing, as detailed in Chapter 6: how the impacts of future climatic change on glaciers and glacial melt-water contributions to river flows are likely to vary considerably across the region and within catchments; the important role precipitation, the summer monsoon in particular, plays in influencing changes to glacier-fed river flows; and that a clear gradient in impacts is seen from west to east, such that catchments in the east appear much less susceptible to the impacts of glacier retreat than those in the west. The ability to provide a physical explanation to the majority of results, together with the results' consistency with those of other studies in the region (e.g. Ye *et al.*, 2003; Immerzeel *et al.*, 2013), lends considerable weight to the plausibility of the model.

The adopted approach certainly was *novel* at the outset of the study and arguably still is. Few hydrological models, whether applied at the meso- or macro-scale, even now account for the transient behaviour of glaciers. Of the few that do allow for changing glacier dimensions at the individual catchment (meso-) scale, most are highly data intensive (e.g. Huss *et al.*, 2010) and are not well suited to widespread application, particularly in regions where data are sparse or little is known of local glacier dynamics. Approaches that require fewer data and are applicable at broader spatial scales, have recently been developed (e.g. Hirabayashi *et al.*, 2010; Stahl *et al.*, 2008; Lutz *et al.*, 2013) but none to-date are known to have been used in regional applications of existing MHMs.

The model developed in this study undoubtedly is highly *parsimonious*, capable of being applied with climate and physiographical data that are readily and universally available (i.e. CRU climate input data; glacier cover data from the Digital Chart of the World; DTM, soils and land-use data from the USGS) and calibrated with parameters whose range of acceptable values (e.g. degree-day factors; lapse rates) are easily obtained from literature. The model also catered for the two approaches most commonly used for representing future conditions in climate impact studies (Carter *et al.*, 2007): a sensitivity analysis based approach, with incremental adjustments to key driving variables, and a climate-model scenario based approach, as exemplified by the study's use of the HadRM2 RCM. As such, the model's application for climate impact studies in other glacier-fed regions would be undemanding.

7.3 Impacts of the study

Outcomes of the study have had impact both scientifically and, more widely, on how climate-change Himalayan glacier retreat is perceived in the media and by policy makers. Two first-authored peer-reviewed science papers were published (Rees and Collins, 2006a; Rees and Collins, 2006b), which outlined spatial and temporal variations glacier-fed river flows across the region under varying future climatic conditions (see Annex B). To-date, the one paper (Rees and Collins, 2006b) has been cited 67 times in other peer-reviewed journal papers, with the majority of citations occurring over the last three years: 14 citations in 2012, 16 in 2013, and 15, so far, in 2014 (Web of Science, 2014). The general approach, method and outputs have also been presented at several international conferences, workshops and seminars in Asia, Europe and South America (e.g. Collins *et al.*, 2010; Coudrain *et al.*, 2005; Singh *et al.*, 2011) over the course of the study, quite possibly prompting others (e.g. Immerzeel *et al.*, 2012; Kotlarski, 2007; Stahl *et al.*, 2008) to consider glacier dynamics in the development and application of their own models.

The key scientific messages presented are summarised in the previous section: that such a parsimonious approach is capable, with limited data, to derive plausible predictions of the future state of Himalayan glacier-fed rivers, and that precipitation plays a vital role in influencing changes to glacier-fed river flows from east to west. Another major outcome of the study was the realisation that, under all but the most extreme (and unrealistic) climate change scenarios, river flows in most glacier-fed rivers in the Himalaya are likely to be sustained by ice-melt from glaciers for the foreseeable future, thus dispelling alarmist predictions of imminent catastrophic water shortages. Care has always been taken, however, to issue caveats about the study's findings: as mentioned in §6.7, due to the limitations of input data and synthetic nature of the approach, results should only be considered indicative of regional behaviour and not form the basis of local, catchment-scale decisions.

Scientific impacts were realised with early versions of the study's regional-glacier melt model being applied in two DFID-funded regional climate impact studies, "Snow and Glacier Aspect of Water Resources Management in the Himalaya" (Rees *et al.*, 2004) and "Impact of Climate and Sea Level Change in part of the Indian Sub-

Continent” (Farquharson *et al.*, 2007). Interim findings also led to several new DFID-funded initiatives, including “A review of current knowledge of Himalayan and Andean glacier melting” (Rees, 2008), then a more formal, systematic review of Himalayan glacier melt (Miller *et al.*, 2013), and a “Precipitation study - Calibrating above and below snow line precipitation as inputs to mountain hydrology models”, undertaken by the University of Utrecht in The Netherlands (Immerzeel *et al.*, 2013). The EU’s funding of the recent High Noon project (Moors and Stoffel, 2013), a study into adaptations to climate change in the Ganges basin in northern India, can also be traced back to this study.

The study has attracted worldwide media attention over the years. In 2008, filming was conducted for the national Japanese broadcaster, NHK, as a contribution to a documentary on climate change effects on glaciers and water resources (NHK, 2008), and an interview on Himalayan deglaciation was conducted for national German radio (Deutsche Radio, 2008). Following the revelation that the IPCC Fourth Assessment Report (Cruz *et al.*, 2007; IPCC, 2007) had apparently overlooked publications that contradicted its claims that Himalayan glaciers could vanish within 25 years (e.g. Rees and Collins, 2004; 2006b), articles referring to the study were published in The Sunday Times (Leake, 2010) and the Daily Mail (Derbyshire, 2010).

7.4 Possible improvements to the approach and method

The approach to the application of the Macro-PDM macro-scale hydrological in this study, its adaptation to Himalayan conditions, and the wholly new glacier-melt model that was developed, while providing reasonably plausible results that generally meet the aims and objectives of the project, leave many areas for possible improvement. Some of the identified improvements relate fundamentally to the approach, while others have emerged over time (since the study began), as new science discoveries, improved data (e.g. from remote sensing), and technological advances (e.g. high performance computing) offer better alternatives than were originally available. The most significant improvement areas can be grouped under four headings: (i) data availability; (ii) treatment of climate input variables; (iii) glacier-melt modelling; and (iv) model application. Thoughts on each area are presented in the following subsections.

7.4.1 Data availability

The gridded driving data used in this study were derived from the CRU 1961-90 0.5° global mean monthly climatological data set (New *et al.*, 1999). New higher spatial and temporal resolution regional and global gridded climate products are now available, including the TRMM (Huffman *et al.*, 2007), APHRODITE (Yatagai *et al.*, 2012), HadCRUT3 (Brohan *et al.*, 2006), the GHCN monthly mean temperature data set (Lawrimore *et al.*, 2011), or NOAA's 20th century data reanalysis product (Compo *et al.*, 2011), that probably would provide a better representation of baseline climate were they to be applied to the model.

Improved, more comprehensive, glacier cover data based on standardised analysis of satellite images from, for example, the Landsat ETM+ instrument, combined with SRTM digital terrain data (Bajracharya and Shrestha, 2011), are now available for the region, contributing to the new global Randolph Glacier Inventory (Arendt *et al.*, 2012). The Digital Chart of the World (DCW) glacier-cover data used in the study, having a reference date of 1992, were derived from ONC 1:1,000,000 scale paper maps that had been collated from the mid-1960s to the early 1990s (ESRI, 2007). Schaner *et al.* (2012) had recently used DCW glacier-cover data in their global application of VIC model. Clearly, application of the new regional dataset to this study's model, instead of the DCW, would yield more contemporary-relevant results.

Only one climate-model based scenario, HadRM2 RCM (Hassell and Jones, 1999), was applied to the model over the course of the study. Application of HadRM2 usefully demonstrated the model's ability to deal with climate-model based output using the "delta change" approach (Kay *et al.*, 2009). In the early- to mid-2000s, few other RCM outputs were available in the region. Recently, however, many more RCMs are available (e.g. HadRM3, PRECIS (Jones *et al.*, 2004), REMO (Jacob, 2001), cf. Biemans *et al.*; Kumar *et al.*, and Mathison *et al.*, (all 2013), Rajbhandari *et al.*, 2014), derived from CMIP3 GCMs under various SRES emission scenarios (see §2.4.3). A range of new CMIP5 RCP-based projections (cf. Chaturvedi *et al.*, 2014) is now available. Applying the model with ensembles of such climate-model based projections, directly or indirectly (i.e. with a delta change approach), would provide further insight to the range, and uncertainty, of potential future outcomes.

7.4.2 Treatment of climate input variables

Precipitation (P), temperature (T) and potential evaporation (PE) data, derived from the CRU 1961-90 0.5° global mean monthly climatological data set (New *et al.*, 1999) were resampled to the required 20 km model grid resolution. The mean monthly data (12 values per variable per cell) were disaggregated to daily at run-time using rudimentary algorithms (§5.4.1) and then adjusted, or distributed, within each mountain grid cell according to an assumed hypsometry and different lapse rates (§4.3.2). Such approaches have been used for many years, in previous model applications of Macro-PDM (see §4.2.4).

The model's basic subdivision of mountain cells into elevation bands, upon which the lapse rate adjustments to daily P, T and PE are made, is based on the Pareto distribution function (see §4.3.2). Whilst being computationally efficient, this approach of characterising meteorological conditions over the glacier-free portion of grid cells probably could be improved by using a hypsometric curve derived from the observed elevation distribution of USGS Hydro1k 1km grid cells. Such a change however would require considerable re-processing of “antecedent” input data (see §4.3.1) and significant changes to the original model code: effort that was considered tangential to the aims of the study.

The “rudimentary” temporal disaggregation of mean monthly climate variables, clearly is another area of potential improvement. More sophisticated algorithms (e.g. to allow clustering of rain days around storm events, or variable increments according to season) should be considered. The newer continuous, higher temporal resolution datasets listed in the previous sub-section (e.g. HadCRUT3) probably would provide a better representation of contemporary climatic variability but, again, would require substantial modification to the original code.

Initial input data processing aside, improvements could also be made to the subsequent spatial adjustment within the model of the three climate variables (P, T and PE), both over the glacier-covered and glacier-free portion of mountain cells. A relatively simple elevational adjustment to precipitation is made, in which precipitation increases linearly by a percentage, the precipitation lapse rate (ΔP ,

%/100 m), of the cell daily P within a certain elevation range (z_{adjmin} , z_{adjmax}) (see Equation 4.8 in §4.4.2). In the model application (§5.4), these model parameters are justifiably constrained by values from the scientific literature (e.g. Putkonen, 2004). However, there is still much uncertainty over how precipitation varies with elevation and location in the Himalaya (partly because there are so few continuous measurements of precipitation at high elevation), and, so, the model's characterisation of precipitation variation could be a source of major error. Furthermore, the same precipitation lapse is applied uniformly to all cells in a basin, with no adjustment made for local relief (slope, aspect), possible rain-shadow effects, which results in increased precipitation on windward slopes and less on the leeward sides of mountains and hills (Rakhecha and Singh, 2009), or the time of year (winter, pre- or post-monsoon, monsoon) (Singh and Singh, 2001). With precipitation having such a strong influence on the mass balance and response of glaciers to climate change, a much better understanding of precipitation at high elevation in the Himalaya is crucial if studies such as this are to make an accurate and reliable assessment of potential climate change impacts in future.

Following observations made in Chapter 3, regarding temporal variations in temperature lapse rates, the model was adapted to allow two different lapse rates over the year, α_{win} and α_{sum} , for the winter (October-March) and summer (April-September) periods respectively (see §4.4.3). Few other modelling studies have employed variable lapse rates (notable exceptions being Chiu *et al.*, 2014; Komatsu *et al.*, 2010) and, whilst it was difficult to discern any significant benefit in this study from applying seasonal lapse rates, possibly greater improvements might be realised from adjusting them on a monthly basis, as in Chiu *et al.* (2014). As with the precipitation lapse rate, the temperature lapse rates were applied uniformly in each basin, with no adjustment for local topography (i.e. slope, aspect, shading). Some snow- and ice-melt models account for such effects by modifying the degree-day factor (DDF) as a function of the potential direct solar radiation (Hock, 2003, 2005). Similar approaches ought to be considered in the model's snow- and ice-melt calculations.

The model's treatment of snow, whereby the snow-pack is adjusted daily in every cell elevation band and ice-band according to the modelled daily precipitation and temperature, could also be looked at. Presently, the snowpack (dry- and wet-snow

stores) initially is built-up over a model “warm-up” period. No calibration is made in respect of observed snow covered area (SCA) either at the beginning of the simulation period or at any time subsequently. With contemporaneous climate input and satellite-derived SCA data now available (e.g. from MODIS), it may be possible to use SCA data to validate or constrain model estimates.

The Macro-PDM’s elevation adjustment of PE remained unaltered in this study (see Equation 4.6, §4.4.3). Further research into the applicability/validity, of the adjustment in Himalayan conditions, and in comparison with other methods (e.g. the Blaney-Cridle method, suitable for estimating PE when only air temperature data is available for a site), might offer further improvements to the original model.

7.4.3 Possible improvements to the regional glacier-melt model

The regional glacier-melt model that was developed over the course of the study was completely novel. Building on a generic glacier concept developed by Macdonald (2004) for a small alpine catchment, no previous climate impact studies had attempted to use such an approach to represent the transient melt-water contributions from retreating glaciers on a regional (macro-) scale. Only a very few have attempted to do so in any way since (see §2.5.3). As with every innovation of this kind, there is always considerable scope for improvement.

One key area identified for improvement is the approach to the definition of a single model glacier for every cell within which a glacier terminus occurred. In contrast to recent methods that consider only the fractional extent of glacier ice within grid cells (e.g. Hirabayashi *et al.*, 2010; Kotlarski, 2007; Lutz *et al.*, 2013; Lutz *et al.*, 2014), this study’s model uniquely accounts for the melt-water contribution from the portion of a glacier’s area that overlaps onto neighbouring cells. As described in §4.5.5, the dimensions of a cell’s model glacier are defined by the total area of all “contributing” glaciers and a pre-determined areal (shape) and depth profile. Testing of the model under baseline conditions (§5.5) illustrated the model’s sensitivity to varying shape profiles: with little information of the hypsometry of the region’s glaciers, a more representative shape was difficult to define. Maximum ice thickness meanwhile varies for each model glacier according to an empirically derived relationship between

glacier area and ice depth (Liu and Ding, 1986), albeit constrained by a maximum depth parameter. Defining the model glacier in such a way could result in the maximum ice depth being artificially large and a possible overestimation of ice volume in some ice bands of the single model glacier. An alternative approach, which could be applied without compromising the generic model glacier concept, would be to consider (and model) each contributing glacier individually. Ice-depths would thus be kept at realistic levels (although determining what are realistic ice depths is itself problematic, because very little is known of how ice-depth varies in the Himalaya). With the improved remote-sensing derived glacier inventories (e.g. Bajracharya and Shrestha, 2011) that are now available, it may also be possible to dispense with the generic areal profile and derive unique shape and elevation (hypsometric) profiles for every individual glacier, combining the glacier area data with high resolution DTMs (e.g. SRTM), and incorporate these in the model. This could address another identified limitation of the existing model: of accounting for multi-tongued/multi-tributary glaciers (*pers. comm.* Andy Barrett, NSIDC, 2007). Larger glaciers often have more than one terminus (e.g. Gangotri, which is the source of both the Bhagirathi and Bhilanga Rivers) and may, in the model context, contribute melt-water to more than one cell. Better, higher resolution, information on the distribution of ice with elevation would allow the drainage path (directional routing) of any glacier's melt-water to be properly defined.

Another area of likely improvement for the glacier melt model is its representation of glacier dynamics. Presently, the model glaciers fundamentally are considered static, declining in-situ as ice from ice-bands is allowed ablate daily (according to the daily air temperature and whether there a covering of snow is present or absent) or accumulate annually (depending on the volume of surplus snow over the entire glacier at the end of each year (see §4.5.7)). Retreat, represented by the depletion of ice-depth from lowermost ice bands, is the only permissible mode of areal change. Ice-flow dynamics, and the possibility of glacier expansion and advances, are not considered and, clearly, this is a deficiency of the model. Adoption of volume-area scaling (Bahr *et al.*, 1997), as applied by Hirabayashi *et al.* (2010), Lutz *et al.* (2013) and Stahl *et al.* (2008), would allow for glacier expansion and shrinkage within the model. However, as Bolch *et al.* (2012) point out, “for any given area... measured thicknesses vary widely, and so volume-area scaling is highly uncertain for individual

glaciers... this is in particular the case for glaciers... in the Himalaya”. It is considered that some representation of ice-flow, such as that applied by Ye *et al.* (2003), in Tien Shan, or Immerzeel *et al.* (2012), in the Langtang catchment in Nepal, may also be applicable at the regional scale, given the improved glacier cover and high-resolution DTM data that are now available.

The suggestion of applying varying degree day factors (DDFs), to account for slope, aspect and shade in snow- and ice-melt calculations (after Hock, 2003), was made in the previous sub-section. Consideration should also be given in the model for the effect of debris cover on glacier-melt. Scherler *et al.* (2011) highlight the importance of debris cover on Himalayan glacier retreat, and assert “the effect [of debris cover] has so far been neglected in predictions of future water availability”. Dust and debris cover is a common feature of Himalayan glaciers: a thin covering of dust (of just a few centimetres (5-10 cm) in depth can significantly enhance melting, whereas thicker debris tends to insulate the ice and retards ablation (Nakawo and Young, 1981).

Other, perhaps more minor, areas of potential improvement for the regional glacier-melt model include: the modelling of firn and firn-melt (the DDF for firn typically is higher than that of snow, but lower than that of ice, (Singh and Singh, 2001)); the modelling of englacial and sub-glacial drainage; and the routing of melt-water between model glacier ice bands (the latter two probably would be more relevant if the model were to be applied over shorter timescales).

7.4.4 Improvements to model application

Despite its simplicity, this modified version of the Macro-PDM still requires many model parameters to be defined. Incorporation of the new regional glacier-melt model added several to the list. As described in §5.5, a process of model tuning rather than calibration is commonly undertaken with MHMs, with the modest aim of attaining plausible results over the model domain (Arnell, 1999). Model tuning in this study was undertaken by manually adjusting the few model parameters that were considered to have greatest influence on model output (the majority of parameter settings were assigned a-priori, based on previous applications). A more systematic, automated, sweep of all conceivable values (e.g. a Monte-Carlo simulation) was not possible

because of the computational constraint of running the model, and subsequently deriving (post-processing) the 1km flow grids (of decadal mean flows) in ArcGIS, on a single PC. Migration of the model onto a high-performance computing platform, and incorporation of the hydraulic routing of runoff between cells (crucial to avoid manual post-processing intervention), clearly is necessary to allow better calibration (or tuning) of the model and to develop understanding of the sensitivity of the model to different parameter settings and, hence, the uncertainty of its predictions.

Such modifications would also allow model output (1km flow estimates) to be generated at finer temporal resolutions, as daily or monthly means, instead of decadal averages. Modifications to cater for the new continuous global and regional climate input data mentioned in §7.2, at daily or monthly time-steps, would yield continuous output at the same resolution, thus enabling analyses of potential changes in flow frequencies (both high- and low-flows) and hydrological extremes (floods and drought). Ensembles of GCM and RCM model outputs could also be applied directly to the model to give a more comprehensive indication of the range of possible future outcomes.

7.5 Future research directions

The improvement areas identified in the previous section provide ample scope for future research. To summarise, some of the most tractable, listed in no particular order, include:

1. Investigation into the accuracy of contemporary climatological datasets (e.g APHRODITE) and their applicability for climate-impact studies using MHMs in the Himalayan region;
2. Development of improved methods for the temporal disaggregation of mean monthly climate variables that consider vagaries in local climatic conditions (e.g. clustering of rainfall events) and adjust to future changes in climate;
3. Further research into methods for accurately extrapolating daily values of key climatological variables (P, T and PE) to higher elevations in Himalayan

catchments, accounting for observed variations in horizontal location (east-west/north-south) and local topography (e.g. slope, aspect);

4. Exploration of ways to employ contemporary satellite-derived snow cover data (e.g. MODIS) to calibrate, validate or constrain the build-up and depletion of the snowpack within the model (e.g. application of slow-depletion curves, as used in the SRM);
5. Investigation into the best approaches for calculating snow- and ice-melt in macro-scale models of the region (e.g. modified temperature-index, variable DDFs (cf. Hock, 2003)) that account for variations in local climatic and physiological conditions (e.g. slope, aspect, glacier debris cover)
6. Research into temporal and spatial variations in evapotranspiration in mountainous Himalayan catchments (comparatively little is presently known to inform hydrological model development);
7. Redefinition of model glaciers using recent satellite-derived glacier inventory data (e.g. the Randolph Glacier Inventory), with view to attaining better characterisation of ice-area and -depth variation with elevation (i.e. improved shape and depth profiles), e.g. applying high-resolution pixel-based approaches to defining individual model glaciers;
8. Development of improved methods for representing the dynamics (growth and shrinkage) of glaciers in MHMs (e.g. application of volume-area scaling (cf. Stahl *et al.*, 2008) in combination with a generic ice-flow model);
9. Reconfiguration of the model to allow its implementation on high-performance or cloud computing infrastructures, to allow full Monte-Carlo-style parameter sweeps and application of multi-climate model ensembles, to enable better measures of uncertainty in model predictions to be derived; and
10. Subject to some of the above, adaptation and application of the model to investigate potential inter-annual changes in flow regimes, and the frequency and magnitude of extreme hydrological events (floods and drought).

Over the course of the study, however, it has become apparent that many problems of a more general nature have yet to be overcome and, thus, are a barrier to understanding climate change impacts in the Himalaya. The inadequacy of hydro-meteorological monitoring at high elevations in the region remains a major challenge. Little still is known of how meteorological variables, precipitation in particular, vary spatially across the region, and very few glacier-fed rivers close to source are monitored. Whilst satellite-derived products (e.g. TRMM, MODIS), have helped in mapping the distribution of precipitation and snow cover across the region, there is a general lack of in-situ measurements to validate their estimates. More extensive and spatially representative networks of meteorological (weather) and river gauging stations at high elevations would help considerably. Research should be conducted to determine optimal network designs that would deliver the required representativeness in a pragmatic, and cost-effective manner.

Despite the recent compilation of new glacier inventories (e.g. Bajracharya and Shrestha, 2011), information is scant on how the dimensions of Himalayan glaciers (area, depth and volume) and the extent and thickness of debris cover (cf. Scherler *et al.*, 2011) vary with elevation or location. Such information is vital to improve predictions of the timing and magnitude of hydrological regime change. Further use of satellite imagery, high-resolution DTMs (e.g. SRTM), backed-up by ground-truthing campaigns, is needed. Few glaciers in the region are monitored routinely (Singh *et al.*, 2011). A well-coordinated, and sustained, programme of mass-balance monitoring on a few benchmark glaciers from across the region would provide categorical indications of glacier fluctuations and climate change and information on snow-ice-atmospheric feedbacks.

Significant improvements to the region's hydrometeorological and glaciological networks, and the data they generate, inevitably will require substantial financial investment by the national governments of the region, development banks and foreign aid agencies. Not only should the investment be on equipment and infrastructure but it should also be channelled towards developing the skills base within the region, to ensure sufficient numbers of suitably qualified staff are well enough equipped to conduct the monitoring and to process and analyse the resulting data. Initial capital

investment should be supported by commitments to sustain monitoring over the long-term.

Practical difficulties, due to remoteness, inaccessibility and harsh high-mountain conditions, will always hamper environmental monitoring in the region. One of the biggest challenges, however, is the reluctance between agencies to share data. Support to regional initiatives must continue in order to break down the prevailing mistrust, to demonstrate the benefits of cooperation and data sharing, and, ultimately, to develop appropriate adaptation strategies to mitigate the impacts of climate change on the region's water resources.

References

- Abdulla, F.A., Lettenmaier, D.P. (1997) Development of regional parameter estimation equations for a macroscale hydrologic model. *Journal of Hydrology*, 197(1-4), 230-257.
- Adam, J.C., Clark, E.A., Lettenmaier, D.P., Wood, E.F. (2006) Correction of global precipitation products for orographic effects. *Journal of Climate*, 19(1), 15-38.
- Ageta, Y., Naito, N., Nakawo, M., Fujita, K., Shankar, K., Pokhrel, A.P., Wangda, D. (2001) Study project on the recent rapid shrinkage of summer-accumulation type glaciers in the Himalayas, 1997-1999. *Bulletin of Glaciological Research*, 18, 45-49.
- Ahmad, N., Rais, S. (1998) *Himalayan Glaciers*. APH Publishing, New Delhi, India, pp. 150.
- Akhtar, M., Ahmad, N., Booij, M.J. (2008) The impact of climate change on the water resources of Hindukush–Karakorum–Himalaya region under different glacier coverage scenarios. *Journal of Hydrology*, 355(1–4), 148-163.
- Alcamo, J., Döll, P., Henrichs, T., Kaspar, F., Lehner, B., Rösch, T., Siebert, S. (2003) Global estimates of water withdrawals and availability under current and future “business-as-usual” conditions. *Hydrological Sciences Journal*, 48(3), 339-348
- Alford, D. (1992) *Hydrological aspects of the Himalayan region*, ICIMOD, Kathmandu, Nepal, pp. 68.
- Alford, D., Armstrong, R. (2010) The role of glaciers in stream flow from the Nepal Himalaya. *The Cryosphere Discuss.*, 4(2), 469-494.
- Allen, R.G., Pereira, L.S., Raes, D., Smith, M. (1998) *Crop Evapotranspiration – Guidelines for Computing Crop Water Requirements*. FAO Irrigation and Drainage Paper 56. Food and Agriculture Organization of the United Nations, Rome, Italy.
- Archer, D. (2003) Contrasting hydrological regimes in the upper Indus Basin. *Journal of Hydrology*, 274(1-4), 198-210.

Archer, D.R., Fowler, H.J. (2004) Spatial and temporal variations in precipitation in the Upper Indus Basin, global teleconnections and hydrological implications. *Hydrology and Earth System Sciences*, 8(1), 47-61.

Arendt, A., Bolch, T., Cogley, J.G., Gardner, A., Hagen, J.O., Hock, R., Kaser, G., Pfeffer, W.T., Moholdt, G., Paul, F., Radić, V. (2012) Randolph Glacier Inventory – A Dataset of Global Glacier Outlines: Version 3.2, Global Land Ice Measurements from Space (GLIMS) - Digital Media, Boulder, Colorado, USA.

Arnell, N.W. (1999a) Climate change and global water resources. *Global Environmental Change*, 9, S31-S49.

Arnell, N.W. (1999b) The effect of climate change on hydrological regimes in Europe: a continental perspective. *Global Environmental Change*, 9(1), 5-23.

Arnell, N.W. (1999c) A simple water balance model for the simulation of streamflow over a large geographic domain. *Journal of Hydrology*, 217(3-4), 314-335.

Arnell, N.W. (2003a) Effects of IPCC SRES emissions scenarios on river runoff: a global perspective. *Hydrology and Earth System Sciences*, 7(5), 619-641.

Arnell, N.W. (2003b) Relative effects of multi-decadal climatic variability and changes in the mean and variability of climate due to global warming: future streamflows in Britain. *Journal of Hydrology*, 270(3-4), 195-213.

Arnold, J.G., Fohrer, N. (2005) SWAT2000: current capabilities and research opportunities in applied watershed modelling. *Hydrological Processes*, 19(3), 563-572.

Arnold, N., Richards, K., Willis, I., Sharp, M. (1998) Initial results from a distributed, physically based model of glacier hydrology. *Hydrological Processes*, 12(2), 191-219.

Bahr, D.B., Meier, M.F., Peckham, S.D. (1997) The physical basis of glacier volume-area scaling. *Journal of Geophysical Research*, 102(B9), 20355-20362.

Bajracharya, S.R., Mool, P.K., Shrestha, A.B. (2007) Impact of climate change on Himalayan glaciers and glacial lakes. Case studies of GLOF and associated hazards in Nepal and Bhutan. ICIMOD/UNEP, Kathmandu, Nepal, June 2007, pp. 119, pp. 119.

- Bajracharya, S.R., Shrestha, B. (2011) The status of glaciers in the Hindu-Kush Himalayan Region, ICIMOD, Kathmandu, Nepal, pp. 140.
- Barnett, T.P., Adam, J.C., Lettenmaier, D.P. (2005) Potential impacts of a warming climate on water availability in snow-dominated regions. *Nature*, 438(7066), 303-309.
- Barry, R.G. (2006) The status of research on glaciers and global glacier recession: a review. *Progress in Physical Geography*, 30(3), 285-306.
- Barry, R.G. (2008) *Mountain Weather and Climate*. Cambridge University Press, July 2008, pp. 532, pp. 532.
- Basistha, A., Arya, D.S., Goel, N.K. (2009) Analysis of historical changes in rainfall in the Indian Himalayas. *International Journal of Climatology*, 29(4), 555-572.
- Batura Glacier Investigation Group (1979) The Batura glacier in the Karakoram Mountains and its variations. *Scientia Sinica*, 22, 958-974.
- Bell, V.A., Moore, R.J. (1999) An elevation-dependant snowmelt model for upland Britain. *Hydrological Processes*, 13, 1887-1903.
- Belò, M., Mayer, C., Smiraglia, C., Tamburini, A. (2008) The recent evolution of Liligo glacier, Karakoram, Pakistan, and its present quiescent phase. *Annals of Glaciology*, 48(1), 171-176.
- Benn, D.I., Owen, L.A. (1998) The role of the Indian summer monsoon and the mid-latitude westerlies in Himalayan glaciation: review and speculative discussion. *Journal of the Geological Society*, 155(2), 353-363.
- Bergström, S., Forsman, A. (1973) Development of a conceptual deterministic rainfall-runoff model. *Nordic Hydrology*, 4, 147-170.
- Berthier, E., Arnaud, Y., Kumar, R., Ahmad, S., Wagnon, P., Chevallier, P. (2007) Remote sensing estimates of glacier mass balances in the Himachal Pradesh (Western Himalaya, India). *Remote Sensing of Environment*, 108(3), 327-338.
- Beven, K.J. (2001) *Rainfall-Runoff Modelling: The Primer*. John Wiley & Sons Ltd., pp. 352.

Beven, K.J. (2012) *Rainfall-Runoff Modelling: The Primer*. Second Edition. John Wiley & Sons Ltd., pp. 457.

Bhutiyani, M. (1999) Mass balance studies on Siachen Glacier in the Nubra valley, Karakoram Himalaya, India. *Journal of Glaciology*, 45(149), 112-118.

Bhutiyani, M., Kale, V., Pawar, N. (2008) Changing streamflow patterns in the rivers of northwestern Himalaya: Implications of global warming in the 20th century *Current Science*, 95(5), 616-626.

Bhutiyani, M.R., Kale, V., Pawar, N.J. (2007) Long-term trends in maximum, minimum and mean annual air temperatures across the Northwestern Himalaya during the twentieth century. *Climatic Change*, 85(1-2), 159-177.

Biemans, H., Speelman, L.H., Ludwig, F., Moors, E.J., Wiltshire, A.J., Kumar, P., Gerten, D., Kabat, P. (2013) Future water resources for food production in five South Asian river basins and potential for adaptation — A modeling study. *Science of The Total Environment*, 468–469, Supplement(0), S117-S131.

Blandford, T.R., Humes, K.S., Harshburger, B.J., Moore, B.C., Walden, V.P., Ye, H. (2008) Seasonal and Synoptic Variations in Near-Surface Air Temperature Lapse Rates in a Mountainous Basin. *Journal of Applied Meteorology and Climatology*, 47(1), 249-261.

Bolch, T., Kulkarni, A., Käab, A., Huggel, C., Paul, F., Cogley, J.G., Frey, H., Kargel, J.S., Fujita, K., Scheel, M., Bajracharya, S., Stoffel, M. (2012) The State and Fate of Himalayan Glaciers. *Science*, 336(6079), 310-314.

Bookhagen, B., Burbank, D.W. (2010) Toward a complete Himalayan hydrological budget: Spatiotemporal distribution of snowmelt and rainfall and their impact on river discharge. *Journal of Geophysical Research: Earth Surface*, 115(F3), F03019.

Braithwaite, R.J., Zhang, Y. (2000) Sensitivity of mass balance of five Swiss glaciers to temperature changes assessed by tuning a degree-day model. *Journal of Glaciology*, 46(152), 7-14.

Braun, L.N., Grabs, W., Rana, B. (1993) Application of a conceptual precipitation-runoff model in the Langtang Khola Basin, Nepal Himalaya. In Proc: Snow and Glacier Hydrology, Kathmandu Symposium, November 1992. IAHS, 218, pp 221-237.

Brohan, P., Kennedy, J.J., Harris, I., Tett, S.F.B., Jones, P.D. (2006) Uncertainty estimates in regional and global observed temperature changes: A new data set from 1850. *Journal of Geophysical Research: Atmospheres*, 111(D12), D12106.

Brookfield, M.E. (1998) The evolution of the great river systems of southern Asia during the Cenozoic India-Asia collision: rivers draining southwards. *Geomorphology*, 22(3-4), 285-312.

Burbank, D.W., Blythe, A.E., Putkonen, J., Pratt-Sitaula, B., Gabet, E., Oskin, M., Barros, A., Ojha, T.P. (2003) Decoupling of erosion and precipitation in the Himalayas. *Nature*, 426(6967), 652-655.

Burbank, D.W., Leland, J., Fielding, E., Anderson, R.S., Brozovic, N., Reid, M.R., Duncan, C. (1996) Bedrock incision, rock uplift and threshold hillslopes in the northwestern Himalayas. *Nature*, 379(6565), 505-510.

Carter, T.R., Jones, R.N., Lu, X., Bhadwal, S., Conde, C., Mearns, L.O., O'Neill, B.C., M.D.A., R., Zurek, M.B. (2007) New Assessment Methods and the Characterisation of Future Conditions. In: *Climate Change 2007: Impacts, Adaptation and Vulnerability. Contribution of Working Group II to the Fourth Assessment Report of the Intergovernmental Panel on Climate Change*. Parry, M.L., *et al.* (eds). Cambridge University Press, Cambridge, UK, pp. 133-171.

Chalise, S.R., Kansakar, S.R., Rees, G., Croker, K., Zaidman, M. (2003) Management of water resources and low flow estimation for the Himalayan basins of Nepal. *Journal of Hydrology*, 282(1-4), 25-35.

Chalise, S.R., Khanal, N.R. (eds) (1996) *Hydrology of the Hindu Kush-Himalayas - Report of the Regional Workshop, 23-24 March 1996, Kathmandu, Nepal*. Organised by UNESCO and ICIMOD, in collaboration with DHM/HMG/N and the German

IHP/OHP Committee. International Centre for Integrated Mountain Development, pp. 45.

Chaturvedi, R., Kulkarni, A., Karyakarte, Y., Joshi, J., Bala, G. (2014) Glacial mass balance changes in the Karakoram and Himalaya based on CMIP5 multi-model climate projections. *Climatic Change*, 123(2), 315-328.

Chen, J., Ohmura, A. (1990) Estimation of Alpine glacier water resources and their change since 1870s. In Proc: Hydrology in Mountainous Regions, IAHS Symposium, Lausanne, Switzerland. IAHS, 193(127-135).

Chiu, C.-A., Lin, P.-H., Tsai, C.-Y. (2014) Spatio-Temporal Variation and Monsoon Effect on the Temperature Lapse Rate of a Subtropical Island. *Terrestrial Atmospheric and Oceanic Sciences*, 25(2), 203-217.

Christensen, J.H., K. Krishna Kumar, E. Aldrian, S.-I. An, I.F.A. Cavalcanti, M. de Castro, W. Dong, P. Goswami, A. Hall, J.K. Kanyanga, A. Kitoh, J. Kossin, N.-C. Lau, J. Renwick, D.B. Stephenson, S.-P. Xie and T. Zhou (2013) Climate Phenomena and their Relevance for Future Regional Climate Change. In: *Climate Change 2013: The Physical Science Basis. Contribution of Working Group I to the Fifth Assessment Report of the Intergovernmental Panel on Climate Change*, 10.1017/CBO9781107415324.028. Stocker, T.F., D. Qin, G.-K. Plattner, M. Tignor, S.K. Allen, J. Boschung, A. Nauels, Y. Xia, V. Bex and P.M. Midgley (ed). Cambridge University Press, Cambridge, United Kingdom and New York, NY, USA, pp. 1217–1308.

Christopherson, R.W. (2011) *Geosystems: An Introduction to Physical Geography* Prentice Hall, January 8, 2011 pp. 688.

Cogley, J.G., Kargel, J.S., Kaser, G., van der Veen, C.J. (2010) Tracking the Source of Glacier Misinformation. *Science*, 327(5965), 522.

Collins, D.N. (1978) Hydrology of an Alpine glacier as indicated by the chemical composition of melt water. *Z. Gletscherkd. Glazialgeol.*, 13, 219-238.

Collins, D.N. (1979) Quantitative determination of the subglacial hydrology of two alpine glaciers. *Journal of Glaciology*, 23, 347-362.

- Collins, D.N. (1989) Influence of glacierisation on the response of runoff from Alpine basins to climate variability. In Proc: Conf. Climate and Water 1, pp 319-328.
- Collins, D.N. (1996) Sediment transport from glacierized basin in the Karakoram mountains. In Proc: Erosion and Sediment Yield: Global and Regional Perspectives, Exeter Symposium. IAHS, 236, pp 85-96.
- Collins, D.N. (1998a) Outburst and rainfall-induced peak runoff events in highly glacierized Alpine basins. *Hydrological Processes*, 12(15), 2369-2381.
- Collins, D.N. (1998b) Rainfall-induced high-magnitude runoff events in highly-glacierized Alpine basins. In Proc: HeadWater'98 Conference: Hydrology, Water Resources and Ecology in Headwaters Meran/Merano, Italy, April 1998. IAHS, 248, pp 69-78.
- Collins, D.N. (2006) Variability of runoff from Alpine basins. In Proc: Fifth FRIEND World Conference: Climate variability and change - hydrological impacts, Havana, Cuba, November 2006. IAHS, 308, pp 466-472.
- Collins, D.N. (2008) Climatic warming, glacier recession and runoff from Alpine basins after the Little Ice Age maximum. *Journal of Glaciology*, In-press accepted.
- Collins, D.N., Davenport, J.L., Stoffel, M. (2013) Climatic variation and runoff from partially-glacierised Himalayan tributary basins of the Ganges. *Science of The Total Environment*, 468–469, Supplement(0), S48-S59.
- Collins, D.N., Moors, E.J., Rees, G. (2010) Variations in runoff from partially-glacierised basins along the Himalayan arc. In Proc: EGU General Assembly 2010, Vienna, Austria, 2-7 May, 2010 Geophysical Research Abstracts, 12, pp 14562.
- Compo, G.P., Whitaker, J.S., Sardeshmukh, P.D., Matsui, N., Allan, R.J., Yin, X., Gleason, B.E., Vose, R.S., Rutledge, G., Bessemoulin, P., Brönnimann, S., Brunet, M., Crouthamel, R.I., Grant, A.N., Groisman, P.Y., Jones, P.D., Kruk, M.C., Kruger, A.C., Marshall, G.J., Mauerer, M., Mok, H.Y., Nordli, Ø., Ross, T.F., Trigo, R.M., Wang, X.L., Woodruff, S.D., Worley, S.J. (2011) The Twentieth Century Reanalysis Project. *Quarterly Journal of the Royal Meteorological Society*, 137(654), 1-28.

Coudrain, A., Francou, B., Kundzewicz, Z.W. (2005) Glacier shrinkage in the Andes and consequences for water resources—Editorial. *Hydrological Sciences Journal*, 50(6), 925-932.

Cruz, R.V., Harasawa, H., Lal, M., Wu, S., Anokhin, Y., Punsalmaa, B., Honda, Y., Jafari, M., Li, C., Huu Ninh, N. (2007) Asia. In: *Climate Change 2007: Impacts, Adaptation and Vulnerability. Contribution of Working Group II to the Fourth Assessment Report of the Intergovernmental Panel on Climate Change*. Parry, M.L., *et al.* (eds). Cambridge University Press, Cambridge, UK, pp. 469-506.

Derbyshire, D. (2010) The Great Lie over Melting Glaciers; Climate Change Chief Says Sorry for Alarmist Claim. *Daily Mail*, London, 22 January 2010.

Deutsche Radio (2008) Himalayan deglaciation and impacts on water resources. *Radioeutschlandfunk - Wissenschaft im Brennpunkt - Tauwetter über den Gipfeln der Welt*. Radio broadcast, <http://www.dradio.de/dlf/sendungen/wib/871924/>. 23 November 2008.

Dey, B., Sharma, V.K., Rango, A. (1989) A test of Snowmelt-Runoff Model for a major river basin in Western Himalayas. *Nordic Hydrology*, 20, 167-178.

DFID (2006) *Eliminating world poverty: making governance work for the poor*, Department for International Development, London, UK, London, UK, 13 July 2006, pp. 91.

DHM (1998) *Hydrological records of Nepal – Streamflow Summary*. Department of Hydrology and Meteorology of Nepal, Kathmandu, pp. 264.

Dickinson, R.E., Oleson, K.W., Bonan, G., Hoffman, F., Thornton, P., Vertenstein, V., Yang, Z.L., Zeng, X. (2006) The Community Land Model and its climate statistics as a component of the Community Climate System Model. *Journal of Climate*, 19, 2302-2324.

Döll, P., Kaspar, F., Lehner, B. (2003) A global hydrological model for deriving water availability indicators: model tuning and validation. *Journal of Hydrology*, 270(1-2), 105-134.

Duan, K., Yao, T. (2003) Monsoon variability in the Himalayas under condition of global warming. *Journal of the Meteorological Society of Japan*, 81(2), 251-257.

Dyurgerov, M.B. (2005) Mass balance of mountain and sub-polar glaciers outside the Greenland and Antarctic ice sheets. Supplement to Occasional Paper No. 55, Institute of Arctic and Alpine Research, University of Colorado, Boulder.

Dyurgerov, M.B., Meier, M.F. (2000) Twentieth century climate change: Evidence from small glaciers. *PNAS*, 97(4), 1406-1411.

ESRI (1993) Digital Chart of the World for use with ARC/INFO: data dictionary. ESRI, Redlands, California.

ESRI (2007) Cell size and resampling in analysis. ESRI, Redlands, California, <http://webhelp.esri.com/arcgisdesktop/9.2>

ESRI (2008) Lambert Asimuthal Equal-Area Projection. ESRI Inc., http://webhelp.esri.com/arcgisdesktop/9.3/index.cfm?TopicName=Lambert_Azimuthal_Equal_Area, 21 October 2008

ESRI (2011) An overview of the Zonal tools. ESRI Inc., <http://webhelp.esri.com/arcgisdesktop/9.3>. 7 September 2011

ESRI (2013) ESRI Grid Format. ESRI Inc., <http://help.arcgis.com/en/arcgisdesktop/10.0/help/index.html>

FAO (1995) The Digital Soil Map of the World (CD-ROM), 1: 5 000 000 scale. Food and Agriculture Organization of the United Nations, Rome.

Farquharson, F.A.K., Fung, F., Chowdhury, J.U., Hassan, A., Horsburgh, K., Lowe, J. (2007) Impact of CLimate And Sea Level Change in part of the Indian Sub-Continent (CLASIC) - Final Report. KAR Project R8038, Department for International Development, Centre for Ecology & Hydrology, Wallingford, UK, February 2007, pp. 139.

Fekete, B.M., Vörösmarty, C.J., Grabs, W. (1999) Global, Composite Runoff Fields on Observed River Discharge and Simulated Water Balances. , Global Runoff Data Centre, Federal Institute of Hydrology, Koblenz, Germany, April 1999, pp. 113.

- Fekete, B.M., Vörösmarty, C.J., Lammers, R.B. (2001) Scaling gridded river networks for macroscale hydrology: development, analysis and control of error. *Water Resources Research*, 37(7), 1955-1967.
- Fountain, A.G., Tangborn, W.V. (1985) Effect of Glaciers on Streamflow Variations. *Water Resources Research*, 21(4), 579-586.
- Fowler, H.J., Archer, D.R. (2006) Conflicting signals of climatic change in the Upper Indus Basin. *Journal of Climate*, 19(17), 4276-4293.
- Fujita, K., Kadota, T., Rana, B., Kayastha, R.B., Ageta, Y. (2001) Shrinkage of Glacier AX010 in Shorong region, Nepal Himalayas in 1990s. *Bulletin of Glaciological Research*, 18, 51-54.
- Fujita, K., Nakawo, M., Fujii, Y., Paudyal, P. (1997) Changes in glaciers in Hidden Valley, Mukut Himal, Nepal Himalayas, from 1974 to 1994. *Journal of Glaciology*, 43(145), 583-588.
- Fukushima, Y. (1988) A model for river flow forecasting for a small forested catchment. *Hydrological Processes*, 2, 167-185.
- Fukushima, Y., Watanabe, O., Higuchi, K. (1991) Estimation of streamflow change by global warming in a glacier-covered high mountain area of the Nepal Himalaya. In *Proc: International Symposium Vienna, 11 - 24 August 1991*. IAHS Press, IAHS Publication No. 205.
- Gardelle, J., Berthier, E., Arnaud, Y. (2012) Slight mass gain of Karakoram glaciers in the early twenty-first century. *Nature Geosci*, 5(5), 322-325.
- Gardner, A.S., Moholdt, G., Cogley, J.G., Wouters, B., Arendt, A.A., Wahr, J., Berthier, E., Hock, R., Pfeffer, W.T., Kaser, G., Ligtenberg, S.R.M., Bolch, T., Sharp, M.J., Hagen, J.O., van den Broeke, M.R., Paul, F. (2013) A Reconciled Estimate of Glacier Contributions to Sea Level Rise: 2003 to 2009. *Science*, 340(6134), 852-857.
- Glazirin, G.E. (1997) Precipitation distribution with altitude. *Theoretical and Applied Climatology*, 58(3-4), 141-145.

Google Earth (2013) Google Earth - Ruler - Path tool, 7.1.2.2041. Google Inc., 7 October 2013.

Gore, A. (2006) *An Inconvenient Truth: The Planetary Emergency of Global Warming and What We Can Do About It*. Bloomsbury Publishing, pp. 336.

Gosain, A., Rao, S., Basuray, D. (2006) Climate change impact assessment on hydrology of Indian river basins. *Current Science*, 90(3), 346-353.

Gosling, S.N., Arnell, N.W. (2011) Simulating current global river runoff with a global hydrological model: model revisions, validation, and sensitivity analysis. *Hydrological Processes*, 25(7), 1129-1145.

Grabs, W.E., Pokhrel, A.P. (1993) Establishment of a Measuring Service for Snow and Glacier Hydrology in Nepal – Conceptual and Operational Aspects. In Proc: Kathmandu Symposium, November 1992. IAHS, I218, pp 3–16.

Grove, J.M. (1988) *The Little Ice Age*. Methuen, pp. 498.

Gurung, D.R., Kulkarni, A.V., Giriraj, A., Aung, K.S., Shrestha, B., Srinivasan, J. (2011) Changes in seasonal snow cover in Hindu Kush-Himalayan region. *The Cryosphere Discuss.*, 5(2), 755-777.

Haerberli, W. (1996) Fluctuations of mountain glaciers. In: *Variations of snow and ice in the past and at present on a global and regional scale*, International Hydrological Programme IHP-IV Project H-4.1. Kotlyakov, V.M. (ed). UNESCO, Paris, pp. 35-43.

Haerberli, W., Hoelzle, M. (2001) *The World Glacier Monitoring Service*, <http://www.nerc-bas.ac.uk/public/icd/icsi/WGMS.html> Accessed: 20 September 2014

Haerberli, W., Hoelzle, M., Paul, F., Zemp, M. (2007) Integrated monitoring of mountain glaciers as key indicators of global climate change: the example of the European Alps. In Proc: *The International Symposium on Cryospheric Indicators of Global Climate Change*, Cambridge, UK, 21-25 August, 2006, pp 150-160.

Hamilton, A., Hutchinson, D., Moore, R. (2000) Estimating Winter Streamflow Using Conceptual Streamflow Model. *Journal of Cold Regions Engineering*, 14(4), 158-175.

- Hannah, D.M., Kansakar, S.R., Gerrard, A.J., Rees, G. (2005) Flow regimes of Himalayan rivers of Nepal: nature and spatial patterns. *Journal of Hydrology*, 308(1-4), 18-32.
- Harding, R., Best, M., Blyth, E., Hagemann, S., Kabat, P., Tallaksen, L.M., Warnaars, T., Wiberg, D., Weedon, G.P., Lanen, H.v., Ludwig, F., Haddeland, I. (2011) WATCH: Current Knowledge of the Terrestrial Global Water Cycle. *Journal of Hydrometeorology*, 12(6), 1149-1156.
- Hasnain, S.I. (1999) Report on Himalayan Glaciology. Unpublished minutes of the Bureau of the International Commission for Snow and Ice, July 1999.
- Hassell, D., Jones, R.G. (1999) Simulating climatic change of the southern Asian monsoon using a nested regional climate model (HadRM2), Hadley Centre for Climate Prediction and Research, Bracknell, UK.
- Herschy, R.W. (1995) Streamflow measurement. E & FN Spon, London, pp. 524.
- Hewitt, K. (2005) The Karakoram Anomaly? Glacier Expansion and the 'Elevation Effect,' Karakoram Himalaya. *Mountain Research and Development*, 25(4), 332-340.
- Hewitt, K. (2007) Tributary glacier surges: an exceptional concentration at Panmah Glacier, Karakoram Himalaya. *Journal of Glaciology*, 53(181), 181-188.
- Hewitt, K., Young, G.J. (1993) The Snow and Ice Hydrology Project; a Pakistan-Canada Research and Training Programme. In Proc: Snow and Glacier Hydrology, Kathmandu Symposium, November 1992. IAHS, 218, pp 49-58.
- Hidalgo, H.G., Das, T., Dettinger, M.D., Cayan, D.R., Pierce, D.W., Barnett, T.P., Bala, G., Mirin, A., Wood, A.W., Bonfils, C., Santer, B.D., Nozawa, T. (2009) Detection and Attribution of Streamflow Timing Changes to Climate Change in the Western United States. *Journal of Climate*, 22(13), 3838-3855.
- Higuchi, K. (1993) Nepal-Japan Cooperation in Research on Glacier and Climates of the Nepal Himalaya. In Proc: Snow and Glacier Hydrology, Kathmandu Symposium, November 1992. IAHS, 218, pp 29-36.

Himal Hydro (2014) Himal Hydro & General Construction Ltd. - Projects, Kathmandu, Nepal, <http://www.himalhydro.com.np/projects.html>.

Hirabayashi, Y., Döll, P., Kanae, S. (2010) Global-scale modeling of glacier mass balances for water resources assessments: Glacier mass changes between 1948 and 2006. *Journal of Hydrology*, 390(3–4), 245-256.

Hirsch, R.M., Slack, J.R., Smith, R.A. (1982) Techniques of trend analysis for monthly water quality data. *Water Resources Research*, 18(1), 107-121.

Hock, R. (2003) Temperature index melt modelling in mountain areas. *Journal of Hydrology*, 282(1-4), 104-115.

Hock, R. (2005) Glacier melt: a review of processes and their modelling. *Progress in Physical Geography*, 29(3), 362-391.

Huffman, G.J., Bolvin, D.T., Nelkin, E.J., Wolff, D.B., Adler, R.F., Gu, G., Hong, Y., Bowman, K.P., Stocker, E.F. (2007) The TRMM Multisatellite Precipitation Analysis (TMPA): Quasi-Global, Multiyear, Combined-Sensor Precipitation Estimates at Fine Scales. *Journal of Hydrometeorology*, 8(1), 38-55.

Huss, M., Farinotti, D., Bauder, A., Funk, M. (2008) Modelling runoff from highly glacierized alpine drainage basins in a changing climate. *Hydrological Processes*, 22(19), 3888-3902.

Huss, M., Joutet, G., Farinotti, D., Bauder, A. (2010) Future high-mountain hydrology: a new parameterization of glacier retreat. *Hydrol. Earth Syst. Sci.*, 14(5), 815-829.

Immerzeel, W., van Beek, L.P.H., Konz, M., Shrestha, A.B., Bierkens, M.F.P. (2012) Hydrological response to climate change in a glacierized catchment in the Himalayas. *Climatic Change*, 110(3-4), 721-736.

Immerzeel, W.W., Bierkens, M.F.P. (2012) Asia's water balance. *Nature Geosci.*, 5(12), 841-842.

Immerzeel, W.W., Droogers, P., de Jong, S.M., Bierkens, M.F.P. (2009) Large-scale monitoring of snow cover and runoff simulation in Himalayan river basins using remote sensing. *Remote Sensing of Environment*, 113(1), 40-49.

Immerzeel, W.W., Pellicciotti, F., Bierkens, M.F.P. (2013) Rising river flows throughout the twenty-first century in two Himalayan glacierized watersheds. *Nature Geosci*, 6(9), 742-745.

Immerzeel, W.W., van Beek, L.P.H., Bierkens, M.F.P. (2010) Climate Change Will Affect the Asian Water Towers. *Science*, 328(5984), 1382-1385.

IPCC (2007) *Climate Change 2007: The Physical Science Basis. Contribution of Working Group I to the Fourth Assessment Report of the Intergovernmental Panel on Climate Change* [Solomon, S., D. Qin, M. Manning, Z. Chen, M. Marquis, K.B. Averyt, M. Tignor and H.L. Miller (eds.)]. Cambridge University Press, Cambridge, United Kingdom and New York, NY, USA, pp. 996.

IPCC (2013a) *Climate Change 2013: The Physical Science Basis. Contribution of Working Group I to the Fifth Assessment Report of the Intergovernmental Panel on Climate Change*. 10.1017/CBO9781107415324. Cambridge University Press, Cambridge, United Kingdom and New York, NY, USA, pp. 1535.

IPCC (2013b) *Summary for Policymakers*. In: *Climate Change 2013: The Physical Science Basis. Contribution of Working Group I to the Fifth Assessment Report of the Intergovernmental Panel on Climate Change* Stocker, T.F., *et al.* (eds). Cambridge University Press, Cambridge, United Kingdom and New York, NY, USA, pp. 28.

IPCC (2013c) *What is a GCM?* Intergovernmental Panel on Climate Change - Data Distribution Centre, http://www.ipcc-data.org/guidelines/pages/gcm_guide.html. 18 June 2013, Accessed: 5 September 2014

IRSA (2010) *Four Great Rivers' Source Pinpointed*. Institute of Remote Sensing Applications (IRSA), Chinese Academy of Sciences, Beijing, China, http://english.irsa.cas.cn/ns/Researchnews/201011/t20101109_61089.html, 09 November 2010

- Ives, J.D., Messerli, B. (1989) *The Himalayan Dilemma: Reconciling Development and Conservation*. Routledge, pp. 336.
- Jacob, D. (2001) A note to the simulation of the annual and inter-annual variability of the water budget over the Baltic Sea drainage basin. *Meteorology and Atmospheric Physics*, 77, 61-73.
- Jain, S.K., Kumar, N., Ahmad, T., Kite, G.W. (1998) SLURP model and GIS for estimation of runoff in a part of Satluj catchment, India. *Hydrological Sciences Journal*, 43(6), 875-884.
- Jain, S.K., Storm, B., J.C., B., Refsgaard, J.-C., Singh, R.D. (1992) Application of the SHE to catchments in India: Part 2. Field experiments and simulation studies with the SHE on the Kolar sub-catchment of the Narmada River. *Journal of Hydrology*, 140, 25-47.
- Jakeman, A.J., Littlewood, I.G., Whitehead, P.G. (1990) Computation of the instantaneous unit hydrograph and identifiable component flows with application to two small upland catchments. *Journal of Hydrology*, 117(1-4), 275-300.
- Jansson, P., Hock, R., Schneider, T. (2003) The concept of glacier storage: a review. *Journal of Hydrology*, 282(1-4), 116-129.
- Jensen, M.E., Burman, R.D., Allen, R.G. (1990) *Evapotranspiration and Irrigation Water Requirement*. ASCE Manuals and Reports on Engineering Practices, 70. American Society of Civil Engineers, New York, NY.
- Jones, R., Noguera, M., Hassell, D., Hudson, D., Wilson, S., Jenkins, G., Mitchell, J. (2004) *Generating High Resolution Climate Change Scenarios using PRECIS*. Met Office Hadley Centre, Exeter, UK, April 2004, pp. 40.
- Kääb, A., Berthier, E., Nuth, C., Gardelle, J., Arnaud, Y. (2012) Contrasting patterns of early twenty-first-century glacier mass change in the Himalayas. *Nature*, 488(7412), 495-498.

Kansakar, S.R., Hannah, D.M., Gerrard, J., Rees, G. (2004) Spatial pattern in the precipitation regime of Nepal. *International Journal of Climatology*, 24(13), 1645-1659.

Kaser, G., Cogley, J.G., Dyurgerov, M.B., Meier, M.F., Ohmura, A. (2006) Mass balance of glaciers and ice caps: Consensus estimates for 1961-2004. *Geophysical Research Letters*, 33(19).

Kaser, G., Fountain, A.G., Jansson, P. (2003) A manual for monitoring the mass balance of mountain glaciers with particular attention to low latitude characteristics - a contribution from the

International Commission on Snow and Ice (ICSI) to the UNESCO HKH-Friend program. *IHP-VI - Technical Documents in Hydrology*, 59. UNESCO, Paris, France, pp. 137.

Kattelman, R. (1993) Role of snowmelt in generating streamflow during spring in East Nepal. In *Proc: Kathmandu Symposium, November 1992*. IAHS Press, IAHS Publication No. 218, pp 103-111.

Kaul, H.N. (1998) *Rediscovery of Ladakh*. Indus Publishing Company.

Kaul, M.K., Puri, V.M.K. (eds) (1999) *Inventory of the Himalayan Glaciers*. Geological Survey of India Special Publication 34. Geological Survey of India, pp. 165.

Kay, A.L., Davies, H.N., Bell, V.A., Jones, R.G. (2009) Comparison of uncertainty sources for climate change impacts: flood frequency in England. *Climatic Change*, 92(1-2), 41-63.

Khanal, N.R., Chalise, S.R., Pokhrel, A.P. (1998) Ecohydrology of river basins of Nepal. In *Proc: International Conference on Ecohydrology of High Mountain Areas, Kathmandu, Nepal, 24-28, March, 1996*. International Centre for Integrated Mountain Development, pp 49-61.

Khattak, M.S., Babel, M.S., Sharif, M. (2011) Hydro-meteorological trends in the upper Indus River basin in Pakistan. *Climate Research*, 46(2), 103-119.

Klok, E.J., Jasper, K., Roelofsma, K.P., Gurtz, J., Badoux, A. (2001) Distributed hydrological modelling of a heavily glaciated Alpine river basin. *Hydrological Sciences Journal-Journal Des Sciences Hydrologiques*, 46(4), 553-570.

Komatsu, H., Hashimoto, H., Kume, T., Tanaka, N., Yoshifuji, N., Otsuki, K., Suzuki, M., Kumagai, T.o. (2010) Modeling Seasonal Changes in the Temperature Lapse Rate in a Northern Thailand Mountainous Area. *Journal of Applied Meteorology and Climatology*, 49(6), 1233-1246.

Konz, M., Grabs, W., Shrestha, A.B., Uhlenbrook, S. (2006) Runoff from Nepalese Headwater Catchments - Measurements and Modelling. IHP/HWRP-Sekretariat Bundesanstalt für Gewässerkunde, Koblenz, Germany, pp. 160.

Kotlarski, S. (2007) A Subgrid Glacier Parameterisation for Use in Regional Climate Modelling. PhD, Max Planck Institut für Meteorologie - Universität Hamburg, Hamburg, Germany, 4 April 2007, pp. 179.

Krasovskaia, I., Arnell, N.W., Gottschalk, L. (1994) Flow regimes In northern and western Europe: development and application of procedures for classifying flow regimes. In Proc: FREIND: Flow Regimes from International Experimental and Network Data, Braunschweig, Germany, October 1993. IAHS Press Ltd., IAHS Publication No. 221, pp 185-192.

Kulkarni, A.V., Bahuguna, I.M., Rathore, B.P., Singh, S.K., Randhawa, S.S., Sood, R.K., Dhar, S. (2007) Glacial retreat in Himalaya using Indian Remote Sensing satellite data *Current Science*, 92(1), 69-74.

Kulkarni, A.V., Rathore, B., Mahajan, S., Mathur, P. (2005) Alarming retreat of Parbati glacier, Beas basin, Himachal Pradesh. *Current Science*, 88(11), 1844.

Kumar, K., Dumka, R.K., Miral, M., Satyal, G., Pant, M. (2008) Estimation of retreat rate of Gangotri glacier using rapid static and kinematic GPS survey. *CURRENT SCIENCE-BANGALORE-*, 94(2), 258.

Kumar, P., Wiltshire, A., Mathison, C., Asharaf, S., Ahrens, B., Lucas-Picher, P., Christensen, J.H., Gobiet, A., Saeed, F., Hagemann, S., Jacob, D. (2013) Downscaled climate change projections with uncertainty assessment over India using a high

resolution multi-model approach. *Science of The Total Environment*, 468–469, Supplement(0), S18-S30.

Kumar, V.S., Haefner, H., Seidel, K. (1991) Satellite snow cover mapping and snowmelt runoff modelling in Beas basin. In Proc: Vienna Symposium, August 1991. IAHS Press, IAHS Publication No. 205, pp 101-109.

Kumar, V.S., Paul, P.R., Rao, C.L.V.R., Haefner, H., Seidel, K. (1993) Snowmelt runoff forecasting studies in Himalayan basins. In Proc: Kathmandu Symposium, November 1992. IAHS Press, IAHS Publication No. 218, pp 85-94.

Kundzewicz, Z.W., Mata, L.J., Arnell, N.W., Döll, P., Kabat, P., Jiménez, B., Miller, K.A., Oki, T., Sen, Z., Shiklomanov, I.A. (2007) Freshwater resources and their management. In: *Climate Change 2007: Impacts, Adaptation and Vulnerability. Contribution of Working Group II to the Fourth Assessment Report of the Intergovernmental Panel on Climate Change*. Parry, M.L., *et al.* (eds). Cambridge University Press, Cambridge, UK, pp. 173-210.

Lambrecht, A., Mayer, C. (2009) Temporal variability of the non-steady contribution from glaciers to water discharge in western Austria. *Journal of Hydrology*, 376(3–4), 353-361.

Lauer, W. (1975) Klimatische Grundzüge der Höhenstufung tropischer Gebirge. Tagungsbericht und wissenschaftliche Abhandlungen, Deutscher Geographentag, 40, 76-90.

Lawrimore, J.H., Menne, M.J., Gleason, B.E., Williams, C.N., Wuertz, D.B., Vose, R.S., Rennie, J. (2011) An overview of the Global Historical Climatology Network monthly mean temperature data set, version 3. *Journal of Geophysical Research: Atmospheres*, 116(D19), D19121.

Leake, J. (2010) Panel ignored warnings on glacier error. *The Sunday Times*, London, 31 January 2010.

Liang, X., Lettenmaier, D.P., Wood, E.F., Burges, S.J. (1994) A simple hydrologically based model of land surface water and energy fluxes for general circulation models. *Journal of Geophysical Research*, 99(D7), 14,415-414,428.

- Liu, C., Ding, L. (1986) The Newly Progress of Glacier Inventory of Tianshan Mountains. *Journal of Glaciology and Geocryology*, 8(2), 168-169.
- Lüthi, M.P. (2009) Transient response of idealized glaciers to climate variations. *Journal of Glaciology*, 55(193), 918-930.
- Lutz, A.F., Immerzeel, W.W., Gobiet, A., Pellicciotti, F., Bierkens, M.F.P. (2013) Comparison of climate change signals in CMIP3 and CMIP5 multi-model ensembles and implications for Central Asian glaciers. *Hydrol. Earth Syst. Sci.*, 17(9), 3661-3677.
- Lutz, A.F., Immerzeel, W.W., Shrestha, A.B., Bierkens, M.F.P. (2014) Consistent increase in High Asia's runoff due to increasing glacier melt and precipitation. *Nature Clim. Change*, 4(7), 587-592.
- Macdonald, O.G. (2004) Coupling glacier mass balance and meltwater yield in the European Alps with future climate change: downscaling from integrations of the HadCM model. PhD, School of Environment and Life Sciences, University of Salford, Salford, UK, December 2003, pp. 226.
- Martinec, J. (1975) Snowmelt-runoff model for streamflow forecasts. *Nordic Hydrology*, 6, 145-154.
- Marzeion, B., Cogley, J.G., Richter, K., Parkes, D. (2014) Attribution of global glacier mass loss to anthropogenic and natural causes. [Science10.1126/science.1254702](https://doi.org/10.1126/science.1254702).
- Mathison, C., Wiltshire, A., Dimri, A.P., Falloon, P., Jacob, D., Kumar, P., Moors, E., Ridley, J., Siderius, C., Stoffel, M., Yasunari, T. (2013) Regional projections of North Indian climate for adaptation studies. *Science of The Total Environment*, 468–469, Supplement(0), S4-S17.
- Mayekwski, P.A., Jeschke, P.A. (1979) Himalayan and Trans-Himalayan Glacier Fluctuations since AD 812. *Arctic and Alpine Research*, 11(3), 267-287.

Meigh, J.R., McKenzie, A.A., Sene, K.J. (1999) A Grid-Based Approach to Water Scarcity Estimates for Eastern and Southern Africa. *Water Resources Management*, 13(2), 85-115.

Microsoft (2014) Microsoft Office - Excel Help - Use the Analysis ToolPak to perform complex data analysis. Microsoft Corporation.

Miller, J.D., Immerzeel, W.W., Rees, G. (2012) Climate Change Impacts on Glacier Hydrology and River Discharge in the Hindu Kush–Himalayas. *Mountain Research and Development*, 32(4), 461-467.

Miller, J.D., Rees, G., Warnars, T., Young, G.J., Collins, D.N., Shrestha, A.B. (2013) What is the evidence of glacial shrinkage across the Himalayas - Systematic Review. CEE Review 10-008. Collaboration for Environmental Evidence, pp. 97.

Molnar, P. (1986) The Geologic History and Structure of the Himalaya. *American Scientist*, 74, 144-154.

Molnar, P. (1993) Mantle dynamics, uplift of the Tibetan Plateau and the Indian Monsoon. *Review of Geophysics*, 31(4), 357-396.

Monteith, J.L. (1965) Evaporation and environment In Proc: Symposia of the Society for Experimental Biology, 19, pp 205-224.

Mool, P.K., Bajracharya, S.R., Joshi, S.P. (eds) (2000) Inventory of Glaciers, Glacial Lakes and Glacial Lake Outburst Floods – Monitoring and Early Warning Systems in the Hindu Kush-Himalayan Region - Nepal. International Centre for Integrated Mountain Development, Kathmandu, Nepal, pp. 363.

Mool, P.K., Joshi, S.P., Bajracharya, S.R. (2001a) Inventory of Glaciers, Glacial Lakes and Glacial Lake Outburst Floods: Monitoring and Early Warning Systems in the Hindu Kush-Himalayan Region - Nepal. ICIMOD, Kathmandu, Nepal.

Mool, P.K., Wangda, D., Bajracharya, S.R., Joshi, S.P., Kunzang, K., Gurung, D.R. (2001b) Inventory of Glaciers, Glacial Lakes and Glacial Lake Outburst Floods: Monitoring and Early Warning Systems in the Hindu Kush-Himalayan Region - Bhutan ICIMOD, Kathmandu, Nepal.

- Moore, R.J. (1985) The probability-distributed principle and runoff production at point and basin scales. *Hydrological Sciences Journal*, 30, 273-297.
- Moors, E.J., Siderius, C. (2012) *Adaptation to Climate Change in the Ganges Basin, Northern India: A Science and Policy Brief*. Alterra, Wageningen UR, Wageningen, The Netherlands, pp. 48.
- Moors, E.J., Stoffel, M. (2013) Changing monsoon patterns, snow and glacial melt, its impacts and adaptation options in northern India: Setting the stage. *Science of The Total Environment*, 468–469, Supplement(0), S1-S3.
- Müller, F. (1970) Pilot study for an investigation of the glaciers in the Eastern Himalayas. Inventory of glaciers in the Mount Everest Region. In: *Perennial Ice and Snow Masses*. Technical Papers in Hydrology No. 1. UNESCO/IAHS, pp. 47-59.
- Nakawo, M., Young, G.J. (1981) Field experiments to determine the effect of a debris layer on ablation of glacier ice. *Annals of Glaciology*, 2, 85-91.
- Nepal, S., Krause, P., Flügel, W.A., Fink, M., Fischer, C. (2013) Understanding the hydrological system dynamics of a glaciated alpine catchment in the Himalayan region using the J2000 hydrological model. *Hydrological Processes*, 28(3), 1329-1344.
- New, M.G., Hulme, M., Jones, P.D. (1999) Representing twentieth century space-time climate variability. Part 1: development of a 1961-90 mean monthly terrestrial climatology. *Journal of Climate*, 12, 829-856.
- NHK (2008) *Himalayan deglaciation - contribution to documentary on climate change effects on glaciers and water resources*. Kimura, H. Television programme, Japan Broadcasting Corporation (NHK), Tokyo, Japan. 7 June 2008.
- NIH (2014) *Hydrology Information System of India*. National Institute of Hydrology, Roorkee, India.
- Nijssen, B., O'Donnell, G.M., Hamlet, A.F., Lettenmaier, D.P. (2001a) Hydrologic sensitivity of global rivers to climate change. *Climatic Change*, 50(1-2), 143-175.

- Nijssen, B., O'Donnell, G.M., Lettenmaier, D.P., Lohmann, D., Wood, E.F. (2001b) Predicting the discharge of global rivers. *Journal of Climate*, 14(15), 3307-3323.
- NPCS-CBS (2012) National Population and Housing Census 2011 (National Report), Volume 01. Government of Nepal: National Planning Commission Secretariat, Central Bureau of Statistics, Kathmandu, Nepal, November, 2012, pp. 262.
- Oerlemans, J. (1988) Simulation of historic glacier variations with a simple climate-glacier model. *Journal of Glaciology*, 34, 333-341.
- Oerlemans, J. (1994) Quantifying Global Warming from the Retreat of Glaciers. *Science*, 264(5156), 243-245.
- Oerlemans, J. (1998) Modelling glacier fluctuations. In: Into the second century of worldwide glacier monitoring. *Studies and Reports in Hydrology*. Haeberli, W., *et al.* (eds). UNESCO, pp. 85–96.
- Oerlemans, J. (2005) Extracting a Climate Signal from 169 Glacier Records. *Science*, 308(5722), 675-677.
- Oki, T., Kanae, S. (2006) Global Hydrological Cycles and World Water Resources. *Science*, 313(5790), 1068-1072.
- Papola, T.S. (2002) Poverty in Mountain Areas of the Hindu Kush-Himalayas. Some basic issues in measurement, diagnosis and alleviation, International Centre for Integrated Mountain Development, Kathmandu, Nepal, March 2002, pp. 31.
- Paterson, W.S.B. (1994) *The Physics of Glaciers*. 3rd Edition. Elsevier Science Ltd., pp. 481.
- PCMDI (2014) CMIP - Coupled Model Intercomparison Project - Overview. PCMDI - Program for Climate Model Diagnosis and Intercomparison, Lawrence Livermore National Laboratory, San Francisco, CA, <http://cmip-pcmdi.llnl.gov/>. Accessed: 5 September 2014
- Pearce, F. (1999) Flooded out: retreating glaciers spell disaster for valley communities. *New Scientist*, 2189, 5 June 1999 pp. 18.

Philip, A.J. (2003) Cherrapunji no longer wettest. Challenge comes from nearby village. *Tribune On-line News Service*, Sunday, August 24, 2003.

Prudhomme, C., Wilby, R.L., Crooks, S., Kay, A.L., Reynard, N.S. (2010) Scenario-neutral approach to climate change impact studies: Application to flood risk. *Journal of Hydrology*, 390(3–4), 198-209.

Putkonen, J.K. (2004) Continuous Snow and Rain Data at 500 to 4400 m Altitude near Annapurna, Nepal, 1999-2001. *Arctic, Antarctic, and Alpine Research*, 36(2), 244-248.

Quick, M.C., Pipes, A. (1977) UBC watershed model. *Hydrological Sciences Bulletin*, 22, 161-253.

Radić, V., Hock, R. (2014) Glaciers in the Earth's Hydrological Cycle: Assessments of Glacier Mass and Runoff Changes on Global and Regional Scales. *Surveys in Geophysics*, 35(3), 813-837.

Raina, V.K. (2009) Himalayan Glaciers: A State-of-Art Review of Glacial Studies, Glacial Retreat and Climate Change. MoEF Discussion Paper. Ministry for Environment and Forests, Government of India, pp. 56.

Rajbhandari, R., Shrestha, A.B., Kulkarni, A., Patwardhan, S.K., Bajracharya, S.R. (2014) Projected changes in climate over the Indus river basin using a high resolution regional climate model (PRECIS). *Climate Dynamics* 10.1007/s00382-014-2183-8, 1-19.

Raje, D., Priya, P., Krishnan, R. (2013) Macroscale hydrological modelling approach for study of large scale hydrologic impacts under climate change in Indian river basins. *Hydrological Processes*, 28(4), 1874-1889.

Rakhecha, P.R., Singh, V.P. (2009) *Applied Hydrometeorology*. Springer, pp. 350.

Raup, B.H., Kieffer, H.H., Hare, T.M., Kargel, J.S. (2000) Generation of Data Acquisition Requests for the ASTER Satellite Instrument for Monitoring a Globally Distributed Target: Glaciers. *IEEE Transactions On Geoscience and Remote Sensing*, 38(2), 1105-1112.

Ravallion, M., Chen, S., Sangraula, P. (2007) New Evidence on the Urbanization of Global Poverty, April 2007, pp. 48.

Rees, G. (2008a) Hydrological Data. In: Manual on Low-flow Estimation and Prediction, Operational Hydrology Report No. 50, WMO-No. 1029. World Meteorological Organization, Geneva, pp. 22-35.

Rees, G. (2008b) A review of current knowledge on Himalayan and Andean glacier melting. DFID Contract Number: W/S011, Centre for Ecology & Hydrology, Wallingford, 30 September 2008, pp. 25.

Rees, H.G., Collins, D.N. (2004) SAGARMATHA - Snow and Glacier Aspects of Water Resources Management in the Himalayas – Final Technical Report: Volume 2, An assessment of the impacts of deglaciation on the water resources of the Himalaya. Client Report for DFID KAR Project No. 7980. CEH, Wallingford, pp. 54.

Rees, H.G., Collins, D.N. (2006a) An assessment of the potential impacts of climatic warming on glacier-fed river flow in the Himalaya. In Proc: Fifth FRIEND World Conference, Havana, Cuba, November 2006. IAHS Press, IAHS Publication No. 308, pp 473-478.

Rees, H.G., Collins, D.N. (2006b) Regional differences in response of flow in glacier-fed Himalayan rivers to climatic warming. *Hydrological Processes*, 20(10), 2157-2169.

Rees, H.G., Croker, K.M., Reynard, N.S., Gustard, A. (1997) Estimation of renewable water resources in the European Union. In Proc: Third International Conference on FRIEND, Postojna, Slovenia, 30 September - 4 October 1997. IAHS Press, IAHS Publication No. 246, pp 31-38.

Rees, H.G., Croker, K.M., Zaidman, M., Cole, G.A., Kansakar, S.R., Kumar, A., Saraf, A., Singhal, M.K. (2002) Application of the regional flow estimation method in the Himalayan region. In Proc: FRIEND 2002 – 4th International Conference on FRIEND UNESCO International Hydrology Programme, Cape Town, South Africa, 18-22 March 2002. IAHS Press, IAHS Publication No. 274, pp 425-432.

Rees, H.G., Holmes, M.G.R., Young, A.R., Kansakar, S.R. (2004a) Recession-based hydrological models for estimating low flows in ungauged catchments in the Himalayas. *Hydrology and Earth System Sciences*, 8(5), 891-902.

Rees, H.G., Sullivan, C.A., O'Regan, D. (2004b) SAGARMATHA - Snow and Glacier Aspects of Water Resources Management in the Himalayas – Final Technical Report: Volume 1, Project Overview. Client Report for DFID KAR Project No. 7980. CEH, Wallingford, pp. 75.

Refsgaard, J.-C., Seth, S.M., Bathurst, J.C., Erlich, M., Storm, B., Jogenson, G.H., Chandra, S. (1992) Application of the SHE to catchments in India: Part 1. General Results. *Journal of Hydrology*, 140, 1-23.

Reynard, N.S., Andrews, A., Arnell, N.W. (1997) The derivation of a runoff grid for southern Africa for climate impact analyses. In Proc: Third International Conference on FRIEND, Postojna, Slovenia, 30 September - 4 October 1997. IAHS Press, IAHS Publication No. 246, pp 23-30.

Rolland, C. (2003) Spatial and Seasonal Variations of Air Temperature Lapse Rates in Alpine Regions. *Journal of Climate*, 16(7), 1032-1046.

Samuel, E. (2001) Total Meltdown. *New Scientist*, 2294, 9 June 2001 pp. 13.

Schaner, N., Voisin, N., Nijssen, B., Lettenmaier, D. (2012) The contribution of glacier melt to streamflow. *Environmental Research Letters*, 7(3), 034029.

Scherler, D., Bookhagen, B., Strecker, M.R. (2011) Spatially variable response of Himalayan glaciers to climate change affected by debris cover. *Nature Geosci*, 4(3), 156-159.

Schiermeier, Q. (2010) Glacier estimate is on thin ice - IPCC may modify its Himalayan melting forecasts. *Nature*, 463, 276-277.

Schmeits, M.J., Oerlemans, J. (1997) Simulation of the historical variations in length of the Unterer Grindelwaldgletscher. *Journal of Glaciology*, 43(143), 152-164.

Sebesta, R.W. (1996) *Concepts of Programming Languages*, 3rd Edition. Addison-Wesley Publishing Company, Reading, Mass.

Seeber, L., Gornitz, V. (1983) River profiles along the Himalayan arc as indicators of active tectonics. *Tectonophysics*, 92(4), 335-337.

Shankar, K. (1990) Mountain hydrology in reference to the Hindu Kush - Himalayan region. Working paper prepared for the Regional working Group (RWG) meeting on Mountain Hydrology, Kathmandu. October 24-26, 1990. ICIMOD, U.-I.a. (ed), Kathmandu, Nepal, August 1990, pp. 29.

Sharma, C.K. (1977) *River Systems of Nepal*, Kathmadu, Nepal, pp. 214.

Sharma, K.P. (1993) Role of meltwater in major river systems of Nepal. In Proc: Kathmandu Symposium, November 1992. IAHS Press, IAHS Publication No. 218, pp 113-122.

Sharma, K.P., Vörösmarty, C.J., Moore, B. (2000) Sensitivity of the Himalayan hydrology to land-use and climatic changes. *Climatic Change*, 47, 117-139.

Shrestha, A., Aryal, R. (2011) Climate change in Nepal and its impact on Himalayan glaciers. *Regional Environmental Change*, 11(1), 65-77.

Shrestha, A.B., Wake, C.P., Mayewski, P.A., Dibb, J.E. (1999) Maximum temperature trends in the Himalaya and its vicinity: an analysis based on temperature records from Nepal for the period 1971-94. *Journal of Climate*, 12, 2775-2786.

Shrestha, M.L., Shrestha, A.B. (2004a) Recent trends and potential climate change impacts on glacier retreat/galcier lakes in Nepal and potential adaptation measures. In Proc: Global Forum on Sustainable Development, Paris, 11-23 November 2004. OECD, Environment Directorate, Environment Policy Committee, pp 23.

Shrestha, M.L., Shrestha, A.B. (2004b) Recent trends and potential climate change impacts on glacier retreat/glacier lakes in Nepal and potential adaptation measures. In Proc: OECD Global Forum on Sustainable Development: Development and Climate Change, Paris, 11-12 November 2004. OECD, pp 23.

Singh, P., Arora, M., Goel, N.K. (2006a) Effect of climate change on runoff of a glacierized Himalayan basin. *Hydrological Processes*, 20(9), 1979-1992.

- Singh, P., Bengtsson, L. (2004) Hydrological sensitivity of a large Himalayan basin to climate change. *Hydrological Processes*, 18(13), 2363-2385.
- Singh, P., Bengtsson, L. (2005) Impact of warmer climate on melt and evaporation for the rainfed, snowfed and glacierfed basins in the Himalayan region. *Journal of Hydrology*, 300(1-4), 140-154.
- Singh, P., Haritashya, U.K., Kumar, N., Singh, Y. (2006b) Hydrological characteristics of the Gangotri Glacier, central Himalayas, India. *Journal of Hydrology*, 327(1-2), 55-67.
- Singh, P., Jain, S.K. (2003) Modelling of streamflow and its components for a large Himalayan basin with predominant snowmelt yields. *Hydrological Sciences Journal*, 48(2), 257-276.
- Singh, P., Kumar, N. (1997a) Effect of orography on precipitation in the western Himalayan region. *Journal of Hydrology*, 199, 183-206.
- Singh, P., Kumar, N. (1997b) Impact assessment of climate change on the hydrological response of a snow and glacier melt runoff dominated Himalayan river. *Journal of Hydrology*, 193, 316-350.
- Singh, P., Quick, M.C. (1993) Streamflow simulation of Satluj River in the Western Himalayas. In Proc: Kathmandu Symposium, November 1992. IAHS Press, IAHS Publication No. 218, pp 261-271.
- Singh, P., Singh, V.P. (2001) *Snow and Glacier Hydrology*. Water Science and Technology Library, 37. Kluwer Academic Publishers, Dordrecht/Boston/London, pp. 742.
- Singh, S.P., Bassignana-Khadka, I., Karky, B.S., Sharma, E. (2011) *Climate change in the Hindu Kush-Himalayas: The state of current knowledge*, ICIMOD, Kathmandu, Nepal, pp. 88.
- Singh, V.P. (1995) *Computer Models of Watershed Hydrology*. Water Resource Publications, Highlands Ranch, CO.

Stahl, K., Moore, R.D. (2006) Influence of watershed glacier coverage on summer streamflow in British Columbia, Canada. *Water Resources Research*, 42(W06201).

Stahl, K., Moore, R.D., Shea, J.M., Hutchinson, D., Cannon, A.J. (2008) Coupled modelling of glacier and streamflow response to future climate scenarios. *Water Resources Research*, 44(W02422), 13.

Stern, N. (2007) *The Economics of Climate Change - The Stern Review*. Cabinet Office - HM Treasury. Cambridge University Press, pp. 579.

Su, Z., Shi, Y. (2002) Response of monsoonal temperate glaciers to global warming since the Little Ice Age. *Quaternary International*, 97-98, 123-131.

Sullivan, C.A., Rijal, S.P., Shrestha, M., Khanal, N.R., O'Regan, D.P. (2004) *SAGARMATHA - Snow and Glacier Aspects of Water Resources Management in the Himalayas – Final Technical Report: Volume 3: An assessment of the potential impacts of climate-change induced deglaciation on communities and their livelihoods in the Hindu Kush Himalaya*. Client Report for DFID KAR Project No. 7980. CEH, Wallingford, pp. 185.

Tahir, A.A. (2011) Impact of climate change on the snow covers and glaciers in the Upper Indus River Basin and its consequences on the water reservoirs (Tarbela Dam) – Pakistan, *Universtie Montpellier 2 Science et Techniques du Languedoc*, 21 September 2011, pp. 233.

Tahir, A.A., Chevallier, P., Arnaud, Y., Neppel, L., Ahmad, B. (2011) Modeling snowmelt-runoff under climate scenarios in the Hunza River basin, Karakoram Range, Northern Pakistan. *Journal of Hydrology*, 409(1–2), 104-117.

Tate, E., Farquharson, F.K. (2000) Simulating Reservoir Management under the Threat of Sedimentation: The Case of Tarbela Dam on the River Indus. *Water Resources Management*, 14(3), 191-208.

Tate, E., Meigh, J.R. (2001) *Grid-based model of the Caspian Sea Basin: Phase II Report*, Centre for Ecology and Hydrology, Wallingford, UK, December 2001, pp. 40.

Thayyen, R.J., Gergan, J.T. (2010) Role of glaciers in watershed hydrology: a preliminary study of a "Himalayan catchment". *The Cryosphere*, 4(1), 115-128.

Thayyen, R.J., Gergan, J.T., Dobhal, D.P. (2005) Monsoonal control on glacier discharge and hydrograph characteristics, a case study of Dokriani Glacier, Garhwal Himalaya, India. *Journal of Hydrology*, 306(1-4), 37-49.

The Kathmandu Post (2012) Construction of Upper Modi Khola project begins. *The Kathmandu Post*, Kathmandu, Nepal, 29 December 2012.

Trenberth, K.E., Chen, S.-C. (1988) Planetary Waves Kinematically Forced by Himalayan Orography. *Journal of the Atmospheric Sciences*, 45(20), 2934-2948.

Trenberth, K.E., Jones, P.D., Ambenje, P., Bojariu, R., Easterling, D., Tank, A.K., Parker, D., Rahimzadeh, F., Renwick, J.A., M. Rusticucci, Soden, B., Zhai, P. (2007) Observations: Surface and Atmospheric Climate Change In: *Climate Change 2007: The Physical Science Basis. Contribution of Working Group I to the Fourth Assessment Report of the Intergovernmental Panel on Climate Change*. Solomon, S., *et al.* (eds). Cambridge University Press, Cambridge, United Kingdom and New York, NY, USA, pp. 235-336.

Uhlenbrook, S., Roser, S., Tilch, N. (2004) Hydrological process representation at the meso-scale: the potential of a distributed, conceptual catchment model. *Journal of Hydrology*, 291(3-4), 278-296.

UNEP (2007) *Global Outlook for Ice and Snow*. United Nations Environment Programme, Nairobi, Kenya, pp. 235.

USGS (1997) Eurasia Land Cover Characteristics Data Base Version 1.2. Land Processes Distributed Active Archive Center (LPDAAC), U.S. Geological Survey (USGS) Center for Earth Resources Observation and Science (EROS) <http://LPDAAC.usgs.gov>.

USGS (2001) United States Geological Survey Hydro1k Elevation Derivative Database (Asia). Land Processes Distributed Active Archive Center (LPDAAC), at the USGS EROS Data Center.

Valdiya, K.S. (2002) Emergence and evolution of Himalaya: reconstructing history in the light of recent studies. *Progress in Physical Geography*, 26(3), 360-399.

Vaughan, D.G., Comiso, J.C., Allison, I., Carrasco, J., Kaser, G., Kwok, R., Mote, P., Murray, T., Paul, F., Ren, J., Rignot, E., Solomina, O., Steffen, K., Zhang, T. (2013) Observations: Cryosphere. In: *Climate Change 2013: The physical science basis. Contribution of Working Group I to the Fifth Assessment Report of the Intergovernmental Panel on Climate Change*, <http://nora.nerc.ac.uk/506740/>. Stocker, T.F., *et al.* (eds). Cambridge University Press, Cambridge, pp. 317-382.

Verbunt, M., Gurtz, J., Jasper, K., Lang, H., Warmerdam, P., Zappa, M. (2003) The hydrological role of snow and glaciers in alpine river basins and their distributed modeling. *Journal of Hydrology*, 282(1-4), 36-55.

Verdhen, A., Prasad, T. (1993) Snowmelt runoff simulation models and their suitability in Himalayan conditions. In *Proc: Kathmandu Symposium*, November 1992. IAHS Press, IAHS Publication No. 218, pp 239-248.

Vörösmarty, C.J., Fekete, B.M., Meybeck, M., Lammers, R.B. (2000a) Geomorphometric attributes of the global system of rivers at 30-minute spatial resolution. *Journal of Hydrology*, 237(1-2), 17-39.

Vörösmarty, C.J., Green, P., Salisbury, J., Lammers, R.B. (2000b) Global Water Resources: Vulnerability from Climate Change and Population Growth. *Science*, 289(5477), 284-288.

Vörösmarty, C.J., Moore, B., Grace, A.L., Gildea, M.P., Melillo, J.M., Peterson, B.J., Rasetter, E.B., Steudler, P.A. (1989) Continental scale models of water balance and fluvial transport: an application to South America. *Global Biogeochemical Cycles*, 3, 241-265.

Wanchang, Z., Ogawa, K., Besheng, Y., Yamaguchi, Y. (2000) A monthly stream flow model for estimating the potential changes of river runoff on the projected global warming. *Hydrological Processes*, 14, 1851-1868.

WCRP (2014) World Climate Research Programme, <http://www.wcrp-climate.org/>. Accessed: 5 Spetember 2014

Web of Science (2014) Web of Science Citation Report for "Regional differences in response of flow in glacier-fed Himalayan rivers to climatic warming" (by Rees, H.G. and Collins, D.N.). Thomson Reuters. Accessed: 6 September 2014

Wilby, R.L., Wigley, T.M.L., Conway, D., Jones, P.D., Hewitson, B.C., Main, J., Wilks, D.S. (1998) Statistical downscaling of general circulation model output: A comparison of methods. *Water Resources Research*, 34, 2995-3008.

WMO (2008) Guide to Hydrological Practices, Volume I, Hydrology – From Measurement to Hydrological Information, WMO-No. 168. World Meteorological Organization, Geneva, Switzerland, pp. 273.

WMO (2014) Emission Scenarios. World Meteorological Organisation, Geneva, Switzerland, http://www.wmo.int/pages/themes/climate/emission_scenarios.php. Accessed: 31 August 2014

Wood, E.F., Lettenmaier, D., Liang, X., Nijssen, B., Wetzel, S.W. (1997) Hydrological modeling of continental-scale basins. *Annual Review of Earth and Planetary Sciences*, 25, 279-300.

WWF (2003) Going, going, gone! Climate change and global glacier decline, World Wildlife Fund Climate Change Programme, pp. 6.

WWF (2005) An overview of glaciers, glacier retreat, and subsequent impacts in Nepal, India and China, World Wildlife Fund Nepal Program, March 2005, pp. 70.

Xu, J., Shrestha, A.B., Vaidya, R., M., E., Hewitt, K. (2007) The Melting Himalayas - Regional Challenges and Local Impacts of Climate Change on Mountain Ecosystems and Livelihoods, International Centre for Integrated Mountain Development (ICIMOD), Kathmandu, Nepal, June, 2007, pp. 15.

Yang, D.W., Musiak, K. (2003) A continental scale hydrological model using the distributed approach and its application to Asia. *Hydrological Processes*, 17(14), 2855-2869.

- Yatagai, A., Kamiguchi, K., Arakawa, O., Hamada, A., Yasutomi, N., Kito, A. (2012) APHRODITE: Constructing a Long-Term Daily Gridded Precipitation Dataset for Asia Based on a Dense Network of Rain Gauges. *Bulletin of the American Meteorological Society*, 93(9), 1401-1415.
- Yates, D.N. (1997) Approaches to continental scale runoff for integrated assessment models. *Journal of Hydrology*, 201(1-4), 289-310.
- Ye, B., Ding, Y., Liu, F., Liu, C. (2003) Responses of various-sized alpine glaciers and runoff to climatic change *Journal of Glaciology*, 49(164), 1-7.
- Young, G.J., Hewitt, K. (1990) Hydrology research in the upper Indus basin, Karakoram Himalaya, Pakistan. In *Proc: Hydrology of Mountainous Areas, Štrbské Pleso*, June 1988. IAHS Press, IAHS Publication No. 190, pp 139-152.
- Young, G.J., Neupane, B. (1996) Bibliography on the Hydrology of the Himalaya-Karakoram Region. *Glaciological Data Report GD-29*. World Data Centre-A for Glaciology (Snow and Ice), Boulder, Colorado.
- Zemp, M., Haberli, W. (2007) *Glaciers and Ice Caps*. In: *Global Outlook for Ice and Snow*. United Nations Environment Programme, Nairobi, Kenya, pp. 115-152.
- Zemp, M., van Woerden, J., Roer, I. (2008) *Global Glacier Changes : Facts and Figures*. United Nations Environment Programme (UNEP), Geneva, Switzerland, pp. 88.
- Zhao, F., Chiew, F.H.S., Zhang, L., Vaze, J., Perraud, J.-M., Li, M. (2012) Application of a Macroscale Hydrologic Model to Estimate Streamflow across Southeast Australia. *Journal of Hydrometeorology*, 13(4), 1233-1250.
- Zhao, Q., Ye, B., Ding, Y., Zhang, S., Yi, S., Wang, J., Shangguan, D., Zhao, C., Han, H. (2013) Coupling a glacier melt model to the Variable Infiltration Capacity (VIC) model for hydrological modeling in north-western China. *Environmental Earth Sciences*, 68(1), 87-101.

Ziegler, A.D., Sheffield, J., Maurer, E.P., Nijssen, B., Wood, E.F., Lettenmaier, D.P. (2003) Detection of Intensification in Global- and Continental-Scale Hydrological Cycles: Temporal Scale of Evaluation. *Journal of Climate*, 16(3), 535-547.

Appendix A

The Probability Distributed Moisture model (PDM)

The Probability Distributed Moisture model (PDM)

The Probability Distributed Moisture model (PDM) is a conceptual rainfall-runoff model, first developed at CEH in 1985 (Moore, 1985, 2007). Within Macro-PDM the original PDM model was adapted to be applied across a large geographical domain, such that, its parameters could be defined *a-priori* according to the spatial distribution of vegetation and soil types. The model regards each grid cell as an individual catchment, with no routing of runoff between cells. It takes a conceptual water balance approach to rainfall-runoff modelling, based on a soil moisture accounting procedure, and works at the daily time using daily rainfall and potential evaporation (PE) data as inputs to the model to derive estimated of daily runoff.

The model also requires information on soil properties and vegetation within each cell. Vegetation data are required by the model to determine evaporation and soil moisture characteristics. The land cover data was also used to calculate the percentage cover of forest in each cell, while the soils information was used to calculate both the soil field capacity (the amount of water held in the soil against gravity) and soil saturation capacity (the amount of water held in the soil when all the pore spaces are full) (Vorosmarty *et al.*,1989). The PDM assumes a soil moisture store, with a capacity that varies across each cell, and a groundwater store. The parameters describe the size of these stores and the rate of removal of water from them. The soil moisture capacity (c) is assumed to be spatially variable across each cell and is represented by the following power distribution:

$$F(c) = 1 - \left[1 - \frac{c}{c_{\max}} \right]^b \quad 0 \leq c \leq c_{\max} \quad \dots(\text{A.1})$$

where the parameter, b , reflects the degree of spatial variability of the maximum storage capacity in the cell. A value of 0.0 would imply a constant capacity, with 1.0 representing a uniform variation. The c_{\max} parameter is the maximum storage capacity within a cell. The amount of water that may be held in storage in the soil is represented by the integral of the above equation between 0.0 and c_{\max} :

$$S_{\max} = \frac{c_{\max}}{(1+b)} \quad \dots(\text{A.2})$$

The PDM works through a simple accounting procedure as follows:

$$S_t = S_{t-1} + P_t - AE_t - Q_t - D_t \quad \dots(\text{A.3})$$

The soil moisture content (S_t) in the current period (day) is calculated as a function of the soil moisture content of the previous period (S_{t-1}), the rainfall (P_t) and the actual evaporation (AE_t). The soil moisture content is also reduced by direct runoff (Q_t) and the drainage of water from the soil into the groundwater store (D_t). The final runoff is determined as a function of Q_t and D_t , such that when the entire cell has reached capacity, direct runoff is:

$$Q_t = (P_t - AE_t - D_t) - (s_{\max} - S_t) \quad \dots(\text{A.4})$$

It is assumed that all the water content in the soil above field capacity drains away in one day, so that the drainage term is:

$$D_t = S_t - FC \quad \dots(\text{A.5})$$

where FC is the field capacity in millimetres.

The AE_t is calculated as a function of the daily PE_t , which is an input to the model, and the field capacity. It is assumed that AE_t continues at the potential rate until field capacity is reached, thereafter it declines linearly to zero:

$$\frac{AE_t}{PE_t} = 1 \quad \text{where } S_t \geq FC \quad \text{and} \quad \dots(\text{A.6})$$

$$\frac{AE_t}{PE_t} = \frac{S_t}{FC} \quad \text{where } S_t \leq FC \quad \dots(\text{A.7})$$

The model distinguishes between two vegetation types: grass and forest. The PE is assumed to be greater over forest than over grass, according to the ratio FPE (see Table A.1). In addition to this distinction, the rainfall over the forest regions is assumed to be intercepted and subsequently evaporated. The daily interception model was developed by Calder (1990):

$$I_d = \gamma(1 - e^{-\delta P}) \quad \dots(\text{A.8})$$

where I_d is the daily interception, and γ and δ are parameters that are held constant across the entire study area.

Runoff is routed within cells according to two parameters, S_{rout} and G_{rout} . The S_{rout} parameter determines the direct routing of runoff through two linear reservoirs and occurs once the entire catchment is saturated. The delayed runoff, or baseflow, is determined by the Q_{rout} parameter. The model, therefore, depends on 8 parameters as defined above and listed in Table A.1. The s_{max} and FC parameters vary between cells, as defined by the spatial distribution of soils and vegetation data. The remaining 6 parameters are assigned values *a-priori*, based on previous applications of Macro-PDM.

Table A.1 Parameters that define Macro-PDM and typical values they are assigned

Parameter	Value	Definition
B	0.25	Defines the variability in soil moisture capacity across cells
S_{\max}	Varies between cells	Total saturation capacity
FC	Varies between cells	Cell field capacity
S_{rout}	1	Direct runoff routing coefficient
G_{rout}	0.1	Delayed (baseflow) routing coefficient
Γ	2.5	Maximum daily interception loss
Δ	0.1	Parameter of the interception model, defined empirically
FPE	1.1	Ratio of forest to grass PE

References

Calder, I.R. (1990) Evaporation in the uplands. John Wiley & Sons Ltd., Chichester, England, pp. 148.

Moore, R.J. (1985) The probability-distributed principle and runoff production at point and basin scales. *Hydrological Sciences Journal*, 30, 273-297.

Moore, R.J. (2007) The PDM rainfall-runoff model. *Hydrol. Earth Syst. Sci.*, 11(1), 483-499.

Appendix B

Publications Associated with this Study

Publications Associated with this Study

The following two first-authored, peer-reviewed papers were published as a result of this study and are included in this Appendix:

- Rees, H.G., Collins, D.N. (2006) An assessment of the potential impacts of climatic warming on glacier-fed river flow in the Himalaya. In Proc: Fifth FRIEND World Conference, Havana, Cuba, November 2006. IAHS Press, IAHS Publication No. 308, 473-478.
- Rees, H.G., Collins, D.N. (2006) Regional differences in response of flow in glacier-fed Himalayan rivers to climatic warming. *Hydrological Processes*, 20(10), 2157-2169.

Other relevant papers and technical reports that the author produced, or contributed to, over the period, are as follows:

- Chalise, S.R., Kansakar, S.R., Rees, G., Croker, K., Zaidman, M. (2003) Management of water resources and low flow estimation for the Himalayan basins of Nepal. *Journal of Hydrology*, 282(1-4), 25-35.
- Collins, D.N., Macdonald, O.G., Reynolds, A.C., Rees, H.G. (2002) Climatic variation, mass balance and runoff from European glacierised mountain basins. In Proc: Eighth National Hydrology Symposium, University of Birmingham, 8-11, September, 2002. British Hydrological Society.
- Collins, D.N., Moors, E.J., Rees, G. (2010) Variations in runoff from partially-glacierised basins along the Himalayan arc. In Proc: EGU General Assembly 2010, Vienna, Austria, 2-7 May, 2010 *Geophysical Research Abstracts*, 12, pp 14562.
- Hock, R., Rees, G., Williams, M.W., Ramirez, E. (2006) Contribution from glaciers and snow cover to runoff from mountains in different climates. *Hydrological Processes*, 20(10), 2089-2090.

- Kansakar, S.R., Hannah, D.M., Gerrard, J., Rees, G. (2004) Spatial pattern in the precipitation regime of Nepal. *International Journal of Climatology*, 24(13), 1645-1659.
- Miller, J.D., Immerzeel, W.W., Rees, G. (2012) Climate Change Impacts on Glacier Hydrology and River Discharge in the Hindu Kush–Himalayas. *Mountain Research and Development*, 32(4), 461-467.
- Miller, J.D., Rees, G., Warnars, T., Young, G.J., Collins, D.N., Shrestha, A.B. (2013) What is the evidence of glacial shrinkage across the Himalayas - Systematic Review. *CEE Review 10-008. Collaboration for Environmental Evidence*, pp. 97.
- Rees, G. (2008) A review of current knowledge on Himalayan and Andean glacier melting. DFID Contract Number: W/S011, Centre for Ecology & Hydrology, Wallingford, 30 September 2008, pp. 25.
- Rees, H.G., Collins, D.N. (2004) SAGARMATHA - Snow and Glacier Aspects of Water Resources Management in the Himalayas – Final Technical Report: Volume 2, An assessment of the impacts of deglaciation on the water resources of the Himalaya. Client Report for DFID KAR Project No. 7980. CEH, Wallingford, pp. 54.

An assessment of the potential impacts of climatic warming on glacier-fed river flow in the Himalaya

H. GWYN REES^{1,2} & DAVID N. COLLINS²

¹ Centre for Ecology and Hydrology, Wallingford, Oxfordshire OX10 8BB, UK
hgrees@ceh.ac.uk

² Alpine Glacier Project, University of Salford, Greater Manchester M5 4WT, UK

Abstract A regional hydro-glaciological model has been developed to assess the potential impacts of climatic warming on glacier-fed river flows in the Indus and Ganges basins. The model, applied at a 20 km × 20 km grid resolution, considers glaciers contributing runoff to a cell as a single idealized glacier that is allowed to recede through time. Using 1961–1990 climate data as input, “baseline” flow estimates were derived for every stretch of river in either basin. A transient warming scenario of +0.06°C year⁻¹ was then imposed for 100 years from an arbitrary start-date of 1991. Comparison of results at 10 sites in two representative areas suggest the impacts of such climatic warming are similar regionally, with estimates of future decadal mean flows continually increasing at 1–4% per decade, relative to baseline, at most sites considered. Flows peaked at only two of the sites several decades into the model run.

Key words regional hydro-glaciological model; climatic warming; river flow; Himalaya

INTRODUCTION

Mountain glaciers are considered sensitive indicators of climate change, and measurements taken over the last century reveal a “general shrinkage of mountain glaciers on a global scale” (Haerberli *et al.*, 1999). In the Himalayan region, there is particular concern about glacier recession because of the potential consequences downstream for the 500 million inhabitants of the Indus, Ganges and Brahmaputra basins, as river flows are first expected to increase but then decline. It has been said that Himalayan glaciers will vanish within 40 years, leading to drastic reductions in river flow and widespread water shortages (Pearce, 1999; WWF, 2005).

There have been few studies of the impact of climatic warming on glacier-fed river flows in the Himalaya (e.g. Singh & Kumar, 1997a; Singh & Bengtsson, 2005; Sharma *et al.*, 2000). Most have involved the application of models in specific catchments where instantaneous step-changes in temperature were imposed for simulation periods of less than a decade, with glacier dimensions time-invariant. Climatic warming is, however, progressive and glacier volume and area change continually. The intensive data requirements of many of the models, together with their inability to consider transient conditions, preclude their application at a broad, regional-scale over longer timescales. A simple temperature-index-based hydro-glaciological model was therefore developed with a view to assessing, in a region where data measurements are sparse, how gradual changes in climate will affect glacier-fed river flows. The model, applied at a 20 km × 20 km grid-resolution, considers glaciers contributing to runoff in a cell as a single generic glacier whose dimensions are allowed to vary through time. Designed for glaciers in recession, the model generates estimates of long-term variation in river flows, as glacier thickness and area deplete.

The model was applied separately to the entire Indus and Ganges river basins, first with standard-period (1961–1990), or “baseline”, climate data, and, then, with a transient climatic warming scenario of +0.06°C year⁻¹ for a period of 100 years from an arbitrary start-date of 1991, with precipitation maintained at baseline levels. Estimates of future decadal mean flow were derived by routing the runoff generated in each 400 km² grid-cell through a digital elevation model (DEM). These were combined with similarly derived baseline flow estimates to provide estimates of future proportional changes in mean flow for every stretch of river in either basin. Results from 10 sites in two representative areas in the upper reaches of the two basins were analysed to show how the impacts of climatic warming on glacier-fed river flows might vary regionally.

THE HYDRO-GLACIOLOGICAL MODEL

The regional hydro-glaciological model developed in this study was a conceptual, physically-based semi-distributed model, in which the relevant river basin was subdivided into grid-cells at a

20 km × 20 km resolution. Runoff is calculated for each cell independently. The model comprises: a rainfall–runoff model, operating in the ice-free portion of the cell; a glacier-melt model for estimating melt from glaciers; and a snowpack module, to represent the accumulation and melting of snow.

Rainfall–runoff model

Each grid-cell was subdivided into 20 equal-height elevation bands, and the distribution of cell area between bands was allocated according to the Generalized Pareto Distribution, in which the shape and scale parameters were defined by the mean, minimum and maximum elevation of each 20-km cell, as described by the HYDRO1k DEM (USGS, 2001). The model runs at a daily time step, and requires, as input to each cell, daily values of precipitation, potential evaporation and temperature. These were derived by disaggregation of the 1961–1990 standard-period 0.5° global mean monthly climatology from Climatic Research Unit (CRU; New *et al.*, 2000). The input data were further adjusted for elevation within cells using lapse rates. Precipitation increased linearly (P_{lapse}) by 50 mm 100 m⁻¹ year⁻¹ within a specified elevation range of 2500–5000 m ($z_{adj_{min}}$, $z_{adj_{max}}$) in the Indus, and by 90 mm 100 m⁻¹ year⁻¹ from 1500–4000 m in the Ganges. Outside these ranges, precipitation remained constant. An air temperature lapse rate (T_{lapse}) of –6°C km⁻¹ was applied in each band. Precipitation in a band was considered to fall as snow when the air temperature of the band ($T_{snow-rain}$) was ≤ +2°C. Daily runoff generated was aggregated at runtime to provide estimates of annual and seasonal runoff for each cell.

The rainfall–runoff calculations are based on the Probability Distribution Model (PDM) (Moore, 1985). Runoff from both rainfall and snowmelt in each band were routed through two parallel storage reservoirs, representing rapid runoff and baseflow. Daily runoff from a band was calculated as the sum of the water released from both stores each day, and cell runoff as the sum of the area-weighted runoff from all bands.

Snowpack module

Accumulation and melting of snow in an elevation band was represented in the snowpack module by a dry- and wet-store in series (Bell & Moore, 1999). New snowfall was added to the dry-store. Melt from the dry- enters the wet-store when daily air temperature for a band exceeds 0°C (T_{melt}), at a rate of 4 mm C⁻¹ day⁻¹, the degree-day factor for snow (DDF_{snow}). Rain on snow contributes directly to the wet-store. Daily release from the wet-store is proportional to the water depth in the store.

Glacier-melt model

The model assumes that the meltwater contribution from a glacier can be adequately estimated by representing the glacier generically, as having an idealized shape and depth. In this study, glaciers contributing runoff to a 20-km cell (i.e. those with the terminus falling within a cell) were considered as a single “generic” glacier. The total surface area of contributing glaciers, obtained from the Digital Chart of the World (DCW) (ESRI, 1993), defines the initial surface area of the generic glacier (Fig. 1). Each generic glacier was given a simple shape and depth profile, described by 20 contiguous rectangular prisms, or “ice-bands”. The horizontal elevations of the top surfaces of the ice bands were arranged at regular intervals between the minimum and maximum elevations of the generic glacier, which were determined as the minimum and maximum elevations, respectively, of all contributing glaciers. A wedge-shaped depth profile was assumed for the *thalweg* of each generic glacier, with a nominal minimum depth of 25 m set at both extremes and a maximum thickness halfway up the glacier. The maximum thickness varied according to the glacier’s area, up to a maximum of 250 m (Liu & Ding, 1986). The area of each ice-band was defined according to a pre-defined shape profile that was considered typical of alpine valley glaciers.

Uniquely, the glacier-melt component allows the surface area of the generic glacier to reduce according to the prescribed geometry as the receding ice thins. The snowpack module was applied to ice-bands whenever daily precipitation fell as snow or if snow remained in a band. Ice-melt occurred in a band only when ice was exposed (i.e. when the snowpack dry- and wet-store were

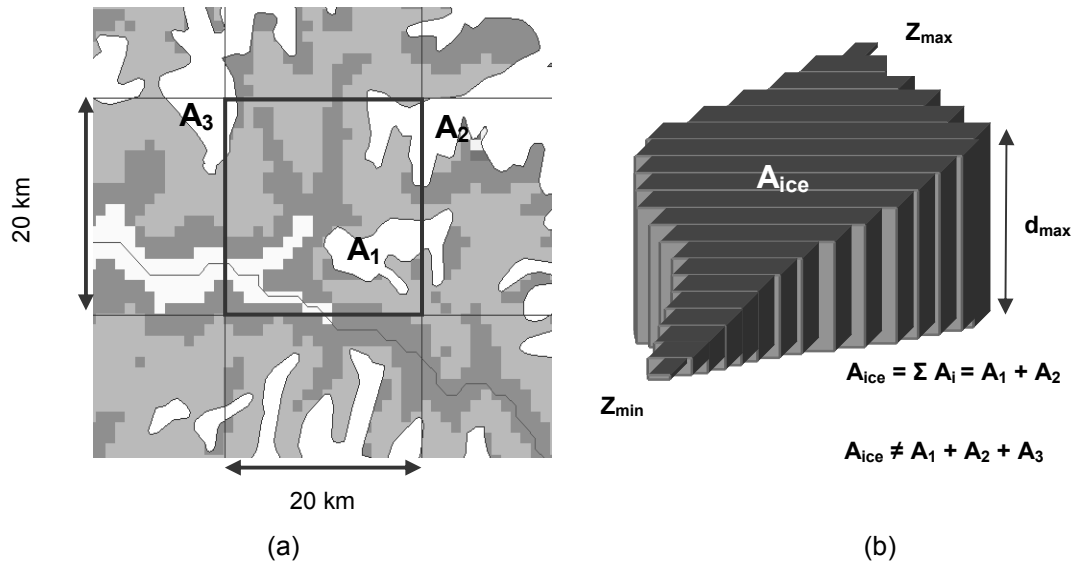


Fig.1 Defining a generic glacier: (a) identify contributing glaciers from DCW (polygons) and HYDRO1k (shaded); (b) conceptual representation of the glacier

both empty) and the air temperature at that elevation was $>0^{\circ}\text{C}$. Ice-melt was calculated using a degree-day factor for ice (DDF_{ice}) of $12 \text{ mm } ^{\circ}\text{C}^{-1} \text{ day}^{-1}$. Total discharge from the glacier was the sum of the runoff generated from all ice-bands. Once ice-depth depleted to zero the rainfall–runoff model was activated to calculate generate runoff in a band. At the end of each calendar year, accumulated snow was redistributed uniformly as ice over the remaining ice-bands.

MODEL APPLICATION

Baseline flows and model calibration

The model was applied in both basins at the daily time-step for a 10-year period using the CRU 1961–1990 climatology. The daily runoff output (mm) was aggregated at run-time to give estimates of standard-period average annual runoff for each cell. The runoff grids were then converted to river flows ($\text{m}^3 \text{ s}^{-1}$) in GIS: the grids were first re-sampled to a 1-km resolution and overlaid onto the HYDRO1k flow-direction grid to derive a flow-accumulation grid; the accumulated average annual runoff of every 1-km cell was then converted to provide a grid of baseline mean flow in each basin.

Key model parameters were calibrated by an iterative process of comparing modelled baseline flows, derived from a variety of sensible parameter settings, with discharge measurements for 40 gauging stations in either basin (from Archer, 2003, and DHM, 1998). The aim of the calibration was not to achieve absolute accuracy for any particular catchment but simply to ensure that reasonably realistic estimates of flow were generated by the model. The final chosen parameter values, as stated in the previous section, were consistent with published data (e.g. Singh & Kumar, 1997b) and gave mean bias errors for modelled average annual runoff of +6% in the Upper Indus (no. 11, bias range: -47% to $+93\%$, standard deviation: 38%) and -2% in the Upper Ganges (no. 29, bias range: -41% to $+87\%$, standard deviation: 29%).

Climatic warming scenario

Next, the model was applied in both basins for 100 years from an arbitrary start-date of 1991 with a transient climatic warming scenario of $+0.06^{\circ}\text{C year}^{-1}$ applied, but maintaining standard period precipitation. This scenario is realistic against reported values of $+0.06$ to $+0.12^{\circ}\text{C year}^{-1}$ in Nepal (Shrestha *et al.*, 1999). Daily runoff outputs were aggregated at run-time to provide estimates of average decadal runoff for each 20-km cell in the respective basins. These too were converted to provide ten 1-km grids of decadal mean flow. A comparison of how flows vary from decade to decade, relative to baseline, could thus be made by overlaying the decadal flow grids onto the baseline flow grid. Resulting grids express future changes as a percentage (%) of baseline.

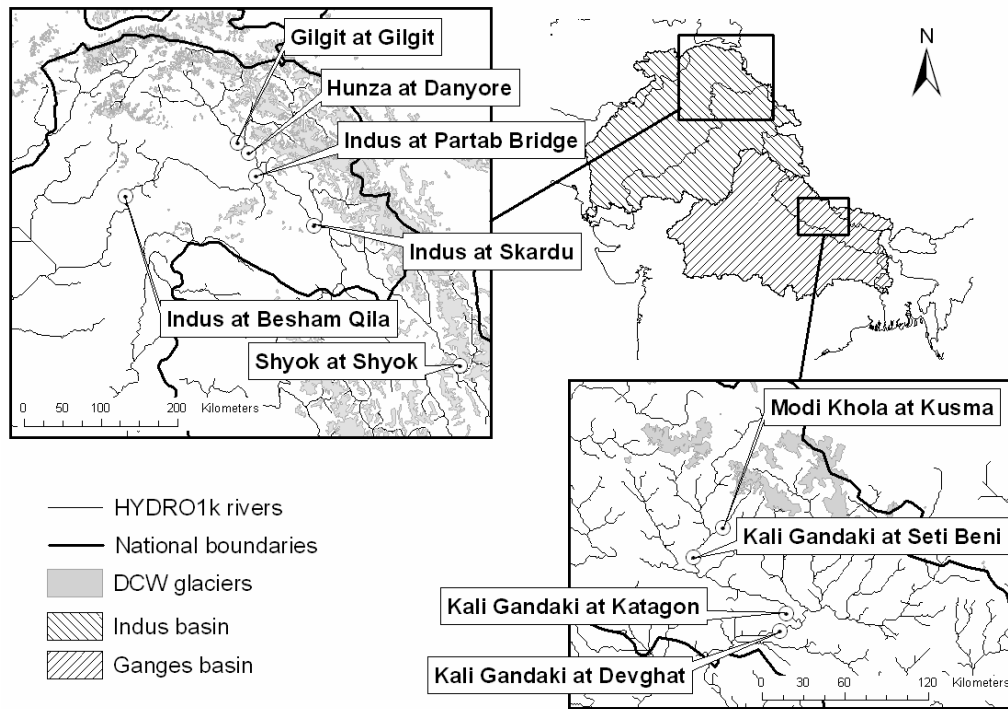


Fig. 2 Kali Gandaki and Upper Indus focal areas.

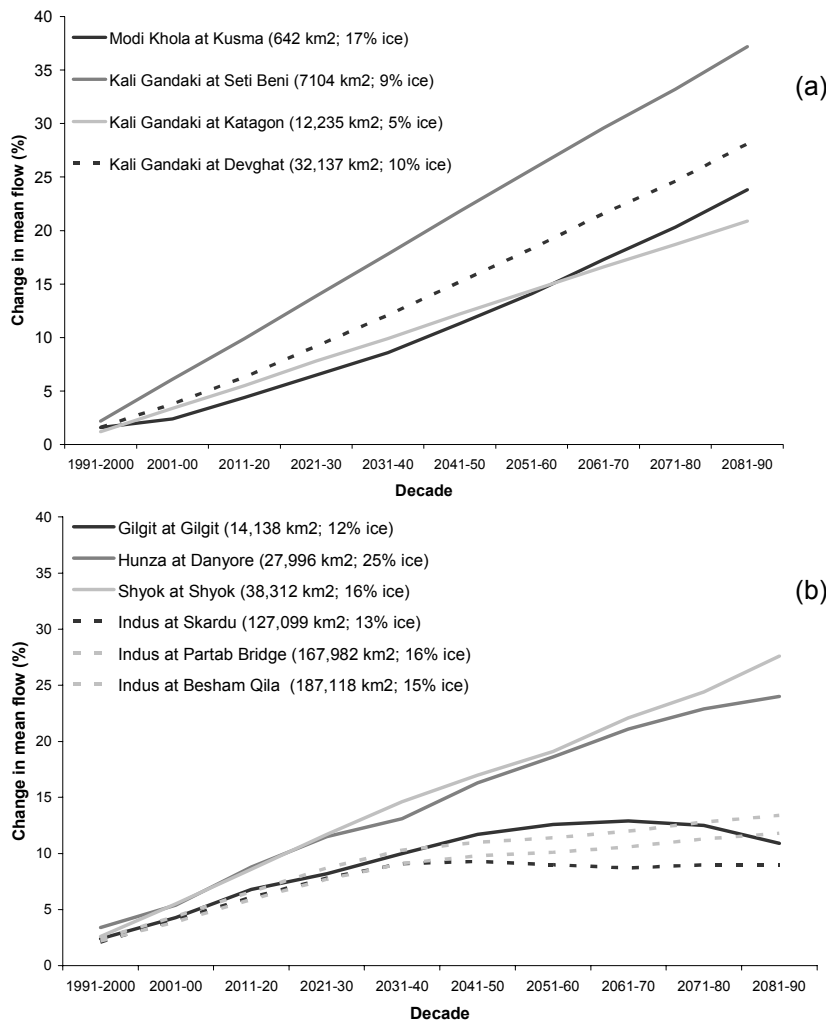


Fig. 3 Changes in decadal mean flows, relative to baseline, in the (a) Kali Gandaki and (b) Upper Indus basins.

RESULTS ANALYSIS

To assess the regional impact of glacier retreat on future river flows, changes in decadal mean flows were studied at 10 separate locations in two representative focal areas: the Upper Indus; and the Kali Gandaki River in the Upper Ganges in Nepal (Fig. 2). Under climatic warming, river flows in glacier-fed catchments are expected to show initial increases, as the area of exposed ice increases with rising temperature, followed, ultimately, by a reduction, once ice area begins to diminish. Model results from the two focal areas (Fig. 3) show decadal mean flows continually increasing at most sites at rates of around 1–4% per decade, relative to baseline, over the 100-year model run. Flows appear to peak at two of the sites in the Upper Indus only: for the Gilgit River at Gilgit, at about +13% of baseline in decade 2061–1970, and for the Indus River at Skardu, at +9.3% of baseline in decade 2041–1960. The results suggest that, under this particular warming scenario and for all but two of the selected catchments, headwater glaciers are exposed at a rate which exceeds that of ice area loss (due to recession) at their termini for the entire period, such behaviour being sustained by a sufficient volume of ice at high elevation. Different rates of flow increases reflect local variations in precipitation, the proportion of glacial ice within catchments, and the distribution of the ice with elevation. For the Indus at Skardu and the Gilgit at Gilgit, peak flows denote the moment the rate of ice loss from headwater glacier termini exceeds the rate at which ice is being exposed at higher elevations; flows reduce thereafter as ice area declines.

CONCLUSIONS

Developing an understanding of how glacier-fed rivers respond to climatic warming is difficult in the Himalaya because little is known of the hydrology and glaciology of the region and records of mountain climatic variables and runoff are sparse and short. To overcome this problem a simple temperature-index based macro-scale hydro-glaciological model was developed with parameter values consistent with the literature. Comparison between the observations and baseline model output show reasonably realistic estimates of mean flow being obtained, suggesting that the model provides an adequate basis for assessing the potential impacts of climatic warming. However, there is scope for improving the model, such as, through the use of more representative input data, better characterization of ice with elevation, and improved interpretation of glacier dynamics. Sensitivity analyses for the major parameters would also improve confidence in the forecasts, and may also have effect the timings and scales of river responses. Despite this, the results were plausible and indicated that the impacts of climatic warming on glacier-fed river flows are broadly similar across the region, with the feared widespread water shortages appearing unlikely for many decades.

Acknowledgements The study was funded by the UK Department for International Development and the Centre for Ecology and Hydrology (CEH). The authors are most grateful for the support provided by: Heather Musgrave and Alan Gustard, CEH; Adarsha Pokhrel and Arun Shrestha, Department of Hydrology and Meteorology, Kathmandu; and Rajesh Kumar and Syed Hasnain, Jawaharlal Nehru University, New Delhi.

REFERENCES

- Archer, D. R. (2003) Contrasting hydrological regimes in the Indus Basin. *J. Hydrol.* **74**, 198–210.
- Bell, V. A. & Moore, R. J. (1999) An elevation-dependant snowmelt model for upland Britain. *Hydrol. Processes* **13**, 1887–1903.
- DHM (1998) *Hydrological records of Nepal – Streamflow Summary*. Department of Hydrology and Meteorology of Nepal, Kathmandu, Nepal.
- ESRI (1993) *Digital Chart of the World for use with ARC/INFO: data dictionary*. ESRI, Redlands, California, USA.
- Haeberli, W., Hoelzle, M. & Frauenfelder R. (1999) *Glacier mass balance bulletin. Bulletin no. 5 (1996–1997)*. IAHS-UNEP-UNESCO.
- Liu C. & Ding L. (1986) The Newly Progress of Glacier Inventory in Tianshan Mountains. *J. Glaciol. Geocryol.* **8**(2), 168–169.
- Moore, R. J. (1985) The probability-distributed principle and runoff production at point and basin scales. *Hydrol. Sci. J.* **30**, 273–297.
- New, M. G., Hulme, M. & Jones, P. D. (2000) Representing twentieth-century space-time climate variability. Part II: Development of 1901–1996 monthly grids of terrestrial surface climate. *J. Climate* **13**, 2217–2238.
- Pearce, F. (1999) Flooded out: retreating glaciers spell disaster for valley communities. *New Scientist* **162**(2189), 18.
- Sharma, K. P., Vorosmarty, C. J. & Moore, B. (2000) Sensitivity of the Himalayan hydrology to land-use and climatic changes. *Climatic Change* **47**, 117–139.

- Shrestha, A. B., Wake, C. P., Mayewski, P. A. & Dibb, J. E. (1999) Maximum temperature trends in the Himalaya and its vicinity: an analysis based on temperature records from Nepal for the period 1971–94. *J. Climate* **12**, 2775–2786.
- Singh, P. & Bengtsson, L. (2005) Impact of warmer climate on melt and evaporation for the rainfed, snowfed and glacierfed basins in the Himalayan region. *J. Hydrol.* **300**, 140–154.
- Singh, P. & Kumar, N. (1997a) Impact assessment of climate change on the hydrological response of a snow and glacier melt runoff dominated Himalayan river. *J. Hydrol.* **193**, 316–350.
- Singh, P. & Kumar, N. (1997b) Effect of orography on precipitation in the western Himalayan region. *J. Hydrol.* **199**, 183–206.
- USGS (2001) United States Geological Survey HYDRO1k Elevation Derivative Database (Asia).
- WWF (2005) *An Overview of Glaciers, Glacier Retreat, and Subsequent Impacts in Nepal, India and China*. World Wildlife Fund, Nepal Program.

Regional differences in response of flow in glacier-fed Himalayan rivers to climatic warming

H. Gwyn Rees^{1,2*} and David N. Collins²

¹ Centre for Ecology and Hydrology, Maclean Building, Crowmarsh Gifford, Wallingford, Oxfordshire OX10 8BB, UK

² Alpine Glacier Project, School of Environment & Life Sciences, University of Salford, Salford Crescent, Manchester M5 4WT, UK

Abstract:

River flow from glacierized areas in the Himalaya is influenced both by intra-annual variations in precipitation and energy availability, and by longer term changes in storage of water as glacier ice. High specific discharge from ice melt often dominates flow for considerable distances downstream, particularly where other sources of runoff are limited, providing a major water resource. Should Himalayan glaciers continue to retreat rapidly, water shortages might be widespread within a few decades. However, given the difference in climate between the drier western and monsoonal eastern ends of the region, future warming is unlikely to affect river flow uniformly throughout.

A simple temperature-index-based hydro-glaciological model, in which glacier dimensions are allowed to decline through time, has been developed with a view to assessing, in data-sparse areas, by how much and when climate warming will reduce Himalayan glacier dimensions and affect downstream river flows. Two glaciers having the same initial geometries were located (one each) in the headwaters of two identical nests of hypothetical catchments, representing contrasting climates in the west and east of the region. The hypothetical catchments were nested such that percentage ice cover declined with increasing basin area. Model parameters were validated against available but limited mass-balance and river flow measurements. The model was applied for 150 years from an arbitrary start date (1990), first with standard-period (1961–1990) climate data and then with application of a $0.06\text{ }^{\circ}\text{C year}^{-1}$ transient climatic warming scenario.

Under this warming scenario, Himalayan rivers fed by large glaciers descending through considerable elevation range will respond in a broadly similar manner, except that summer snowfall in the east will suppress the rate of initial flow increase, delay peak discharge and postpone eventual disappearance of the ice. Impacts of declining glacier area on river flow will be greater in smaller and more highly glacierized basins in both the west and east, and in the west, where precipitation is scarce, for considerable distances downstream. © Crown Copyright 2006. Reproduced with the permission of Her Majesty's Stationery Office. Published by John Wiley & Sons, Ltd.

KEY WORDS glacier recession; climatic warming; river flow; Himalaya

Received 6 April 2005; Accepted 19 October 2005

INTRODUCTION

During periods of climatic warming and glacier decline, melting from ice adds a component of flow to runoff from glacierized basins in excess of that related to contemporary precipitation. This additional component cannot be sustained indefinitely because, should the warming continue, glaciers will ultimately disappear and runoff will reduce to levels simply reflecting precipitation. The Intergovernmental Panel on Climate Change (IPCC) suggested that up to a quarter of the total global mountain glacier mass could disappear by 2050 and up to half by 2100 (Watson *et al.*, 1996). In the Himalayan region, there is particular concern about glacier recession because of potential consequences downstream for the 500 million inhabitants of the Indus, Ganges and Brahmaputra basins, as river flows will first increase but then decline. It has been said that Himalayan

* Correspondence to: H. Gwyn Rees, Centre for Ecology and Hydrology, Maclean Building, Crowmarsh Gifford, Wallingford, Oxfordshire OX10 8BB, UK. E-mail: hgrees@ceh.ac.uk

glaciers will vanish within 40 years, leading to drastic reductions in river flow and widespread water shortages (Pearce, 1999; WWF, 2005).

The Himalayan region extends across the north of the Indian subcontinent, in a broad arc from northwest to southeast (70–105 °E, 40–25 °N) over a distance of some 3000 km. The region includes the Hindu Kush, Karakoram and Greater Himalaya mountain ranges, *inter alia*. Glaciers in the region occupy an area of over 55 000 km² (Dyurgerov and Meier, 1997), the most highly glacierized area outside the polar regions (Dyurgerov, 2005). Accelerated glacier retreat has occurred in Nepal and Bhutan over the last 20 years of the 20th century (e.g. Kadota *et al.*, 2000; Ageta *et al.*, 2001; Fujita *et al.*, 2001), and, in India, one of largest glaciers in the region, i.e. Gangotri, has retreated approximately 850 m out of a total of 2 km over the last 200 years (Naithani *et al.*, 2001).

Climatic controls on Himalayan river flow and glacier mass balance vary considerably from west to east. In summer months, the monsoon from the Bay of Bengal produces heavy precipitation, intensified on windward slopes, predominantly in the southeast of the region. The monsoon weakens from east to west, rarely penetrating as far as the Karakoram, so that summer precipitation declines in the same direction. Although westerly winds bring precipitation in the west (and at higher elevations throughout the Himalaya) in winter, the total annual precipitation generally increases from west to east. Arid conditions exist at lower elevations in the west; hence, melt water from glacierized mountains remains the major component of runoff for great distances downstream, whereas monsoonal precipitation in the more humid east contributes much of the flow at all elevations. Glaciers experience winter accumulation and summer ablation in the west, but there is predominantly synchronous summer accumulation and summer melt in the east. This paper examines the potential effects of such regionally differing climatic controls on the hydrological response of glacier-fed rivers in the Himalaya to climatic warming.

Studies to determine the impact of future climatic warming on river flows derived from snow- and ice-melt typically require application of physically based models to represent the various hydro-glaciological processes controlling catchment response. Such models generally treat glaciers as stationary elements, the dimensions of which remain constant through time. Several models have been used to assess the impact of climatic warming on river flows in the Himalaya. Singh and Kumar (1997a) used the UBC watershed model (Quick and Pipes, 1977) to model a sub-basin of the Satluj River in northwest India and indicated annual increases in runoff of up to 18% from snowmelt and 38% from glacier melt for a 2 °C rise in air temperature. Singh and Bengtsson (2003, 2005) used the SNOWMOD model of Singh and Jain (2003) also in the Satluj, suggesting faster depletion of snow, earlier exposure of glacier ice and enhanced melting at higher elevations, such that temperature increases of 1–3 °C would reduce snow melt by 11–23% but increase glacier melt by 16–50%. In the eastern Himalaya, an application of the Water Balance Model (Vorosmarty *et al.*, 1989) indicated an annual runoff decrease of 9% for a temperature increase of 5 °C (Sharma *et al.*, 2000). Other models, used in Langtang Khola basin in Nepal (Fukushima *et al.*, 1991; Braun *et al.*, 1993), suggested increased summer discharge of between 50 and 100% for a 2 °C temperature increase. The range of variability of predictions results from use of different models under varying warming scenarios. In all these forecasts, instantaneous step changes in temperature were imposed for simulation periods of less than a decade, with glacier area being time invariant. Climatic warming is, however, progressive and glacier dimensions change gradually. The inability of the above models to consider transient conditions precludes their application at longer time-scales. All the models were used on selected individual catchments only, making interpretation difficult at the Himalayan regional scale.

A simple temperature-index-based hydro-glaciological model, in which glacier dimensions are allowed to vary through time, has been developed with a view to assessing, in an area in which climatic, glaciological and hydrological data are sparse, by how much and when climate warming will reduce Himalayan glacier dimensions and increase or decrease downstream river flows. This model was applied to two identical nests of hypothetical glacierized catchments, one located in the west and one in the east of the Himalayan arc (Figure 1), in order to assess differentially how rivers experiencing contrasting climatic controls might respond differently to the same global warming signal. In terms of comparison between west and east, differences in

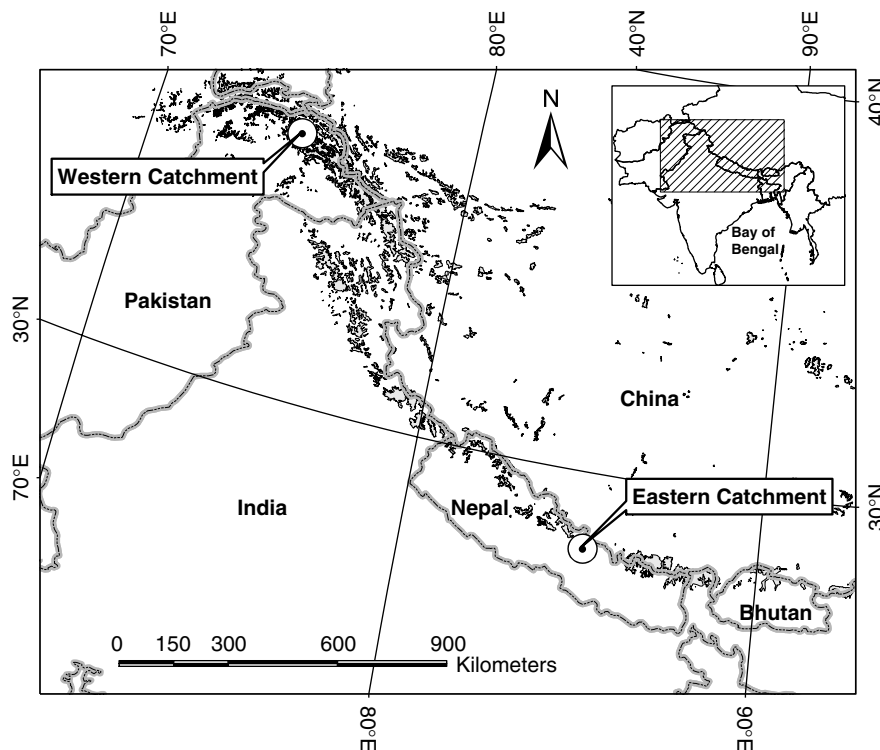


Figure 1. Locations of the two nests of hypothetical catchments (circled), the western catchment in the Karakoram Mountains and the eastern in the Greater Himalaya, together with the overall distribution of glaciers in the Himalayan arc (grey polygons), as indicated on the *Digital Chart of the World* (ESRI, 1993)

behaviour were thought to be more important than absolute accuracy of results. Each set of catchments was nested such that percentage ice cover declined with increasing basin area. Glaciers with the same prescribed initial geometry were located (one each) in the headwaters of each nest of catchments. The model is designed specifically to deal with glaciers in recession. It generates estimates of long-term variation in downstream runoff, as glacier thickness and area deplete with climatic warming, and, hence, indicates how long it will take for the hypothetical glaciers to disappear. The model was applied to each catchment for a period of 150 years from an arbitrary start date of 1990, first with standard-period (1961–1990), or ‘baseline’, climate data, and then with a transient climatic warming scenario of $0.06\text{ }^{\circ}\text{C year}^{-1}$. Precipitation was maintained at baseline levels. Potential differences in response of glacier-fed rivers to climatic warming between west and east were thus differentiated.

CHARACTERISTICS AND CLIMATE OF THE HYPOTHETICAL CATCHMENTS

The two nests of hypothetical catchments were located so that one was approximately coincident with Batura Glacier in the Karakoram in the west ($75^{\circ}00'\text{E}$, $36^{\circ}24'\text{N}$) and one with Langtang Glacier in the east ($85^{\circ}30'\text{E}$, $28^{\circ}30'\text{N}$) in the Nepal Himalaya (Figure 1). The largest basin in each nest of catchments was 5000 km^2 in area. Both possessed identical physiographical characteristics: each had a glacier of 50 km^2 in its headwaters, had minimum, mean and maximum catchment elevations of 1000 m, 2000 m and 6000 m a.s.l. respectively, with grass the sole land cover and lithosols the dominant soil type in both. Elevations were consistent with US Geological Survey HYDRO1k digital elevation data in the vicinities

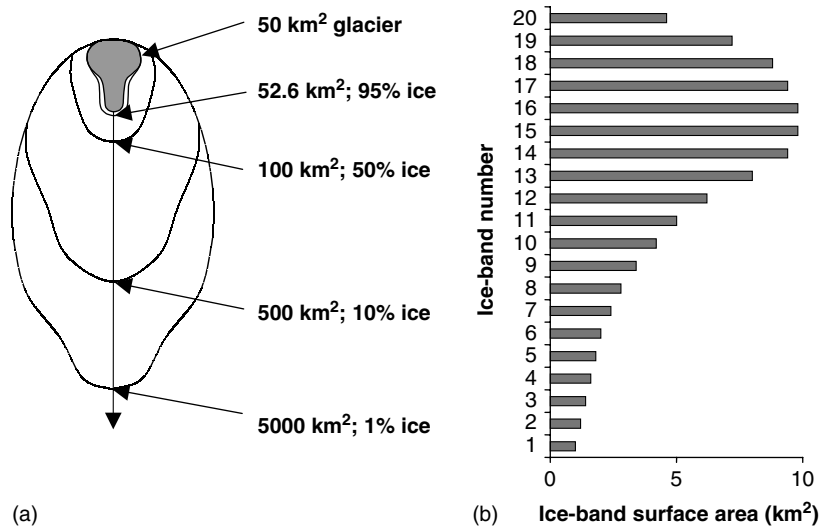


Figure 2. (a) Conceptual representation of a nest of hypothetical catchments (not to scale); (b) distribution of ice surface area to ice bands for a hypothetical glacier

of respective sites (USGS, 2001). Distribution of land surface elevation within the catchments was described by the generalized Pareto distribution. Nested subcatchments were assigned areas of 52.6 km², 100 km², and 500 km², corresponding to initial glacier cover of 95%, 50% and 10% respectively, with the overall large catchment having 1% glacierization (Figure 2a).

The hypothetical glacier was given a simple shape and depth profile, described by a finite number of contiguous rectangular prisms, referred to as 'ice bands'. The 50 km² glaciers were both subdivided into 20 ice bands, the horizontal elevations of the top surfaces of which were arranged at 100 m intervals in the elevation range 4000–6000 m, typical of many Himalayan glaciers (Kaul, 1999; ICIMOD, 2000). The distribution of ice surface area to bands (Figure 2b) approximates to the shape of a typical alpine valley glacier (e.g. Collins *et al.*, 2002). A wedge-shaped depth profile was assumed for the *thalweg* of each glacier, with a nominal minimum thickness of 25 m at both extremes and a maximum thickness of 250 m halfway up the glacier. The maximum thickness is consistent with previously reported values from the region (e.g. Müller *et al.*, 1977).

Relevant local climatic data, giving only the initial difference between the two catchments, were taken from the appropriate 0.5° × 0.5° grid square of the Climatic Research Unit (CRU) 1961–1990 standard-period climatology (New *et al.*, 2000). Mean monthly values of precipitation, rain-days, temperature and potential evaporation were obtained for 2000 m elevation (Figure 3). These data were disaggregated to provide the daily input necessary for the model.

THE HYDRO-GLACIOLOGICAL MODEL

The hydro-glaciological model developed in this study was a conceptual, semi-distributed model consisting of three parts: a rainfall–runoff model, operating in the ice-free portion of the catchment; a glacier-melt model for estimating melt from a glacier declining *in situ*; and a snowpack module, which represents the accumulation and melting of snow over the entire catchment. The model runs at a daily time-step. The nests of hypothetical catchments were divided into 100 m elevation bands. Input data were adjusted for elevation by using lapse rates. Precipitation P_{lapse} increased linearly at 500 mm km⁻¹ year⁻¹ between 2500 and 5000 m (Young and Hewitt, 1988), approximately mid-range of the 130–1060 mm km⁻¹ year⁻¹ rainfall gradient in the Beas basin

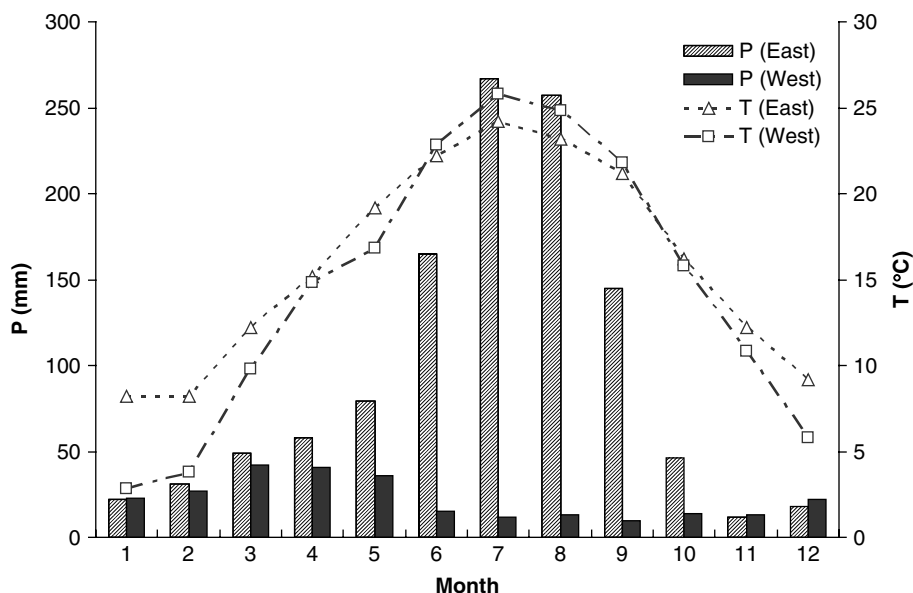


Figure 3. Monthly standard-period (1961–1990) precipitation P and air temperature T for the locations of the two nests of hypothetical catchments, as at 2000 m a.s.l.

in the central Himalaya (Singh and Kumar, 1997b). Outside the 2500–5000 m range, precipitation remained constant. An air temperature lapse rate T_{lapse} of $-6^{\circ}\text{C km}^{-1}$ was applied in each band. Precipitation in a particular band fell as snow when air temperature in that band was $\leq 2^{\circ}\text{C}$. Annual outputs generated include runoff (mm) and mean flow ($\text{m}^3 \text{s}^{-1}$) for all catchments in both nests, glacier area (km^2), glacier mass balance (mm water equivalent (w.e.)) and accumulation/area ratio.

Rainfall-runoff model

The rainfall–runoff model was based on the probability distribution model (PDM; Moore, 1985). Runoff from both rainfall and snowmelt were routed through two parallel storage reservoirs, representing rapid runoff and delayed baseflow. Daily runoff from a band was calculated as the sum of the water released from both stores each day, and basin runoff was calculated as the sum of the area-weighted runoff from all bands in the respective nested catchment.

Snowpack module

Accumulation and melting of snow in an elevation band were represented in the snowpack module by a dry store and wet store in series (Bell and Moore, 1999). New snowfall was added, as water equivalent, to the dry store. Melt from the dry store enters the wet store when daily air temperature for a band exceeds a threshold T_{melt} of 0°C , at a rate of $4 \text{ mm }^{\circ}\text{C}^{-1} \text{ day}^{-1}$, the degree-day factor for snow DDF_{snow} . Rain falling on snow contributes directly to the wet store. Daily release from the wet store is proportional to the water depth in that store.

Glacier-melt model

Uniquely, the glacier-melt component in this model allows surface area to reduce according to the glacier geometry as the receding ice thins. The *snowpack module* was also applied to ice bands whenever daily precipitation fell as snow or if snow remained in a band. Ice melt occurred in a band only when ice was exposed (i.e. when the snowpack dry and wet stores were both empty) and the air temperature at that elevation

was $T_{\text{melt}} > 0^{\circ}\text{C}$. Ice melt was calculated using a degree-day factor for ice DDF_{ice} of $10 \text{ mm }^{\circ}\text{C}^{-1} \text{ day}^{-1}$. Total discharge from the glacier was the sum of runoff generated from all ice bands.

Glacier area reduced accordingly as ice thickness in each band depleted. Once ice depth has depleted to zero the *rainfall–runoff model* was activated to calculate generated runoff in a band. At the end of each year, accumulated snow was redistributed uniformly as ice over the remaining ice bands.

MODEL APPLICATION

CRU mean monthly climatology data were disaggregated into daily values as follows: total monthly precipitation was distributed evenly between the rain-days, which were arranged randomly within each month, and mean air temperature was interpolated from linear plots of monthly values.

Key model parameter values were calibrated by iterative comparison of output from model application for an initial 5-year period using standard period climatic data, with available but sparse measurements of discharge, mass balance and accumulation/area ratio. The aim was not to achieve absolute accuracy for any particular basin, but simply to ensure that reasonably realistic estimates of flow and mass balance were generated by the model. The final parameter values used, stated above, are consistent with published data (e.g. Singh and Kumar, 1997b; Hock, 2003).

Table I. Comparison of model results with observed data

River name	Site name	Area (km ²)	Mean catchment elevation (m a.s.l.)	Long. (E)	Lat. (N)	Mean flow (m ³ s ⁻¹)	Runoff (mm year ⁻¹)	Period of record
<i>Observed (west)^a</i>								
Swat	Kalam	2 025	3 300	72°36'	35°28'	89.6	1 395	1961–1997
Astore	Doyian	3 750	3 921	74°42'	35°33'	136.8	1 150	1974–1997
Swat	Chakdara	5 400	2 499	72°01'	34°39'	178.9	1 045	1961–1997
Shigar	Shigar	6 650	4 401	75°45'	35°20'	205.4	974	1985–1997
Chitral	Chitral	12 425	3 794	71°47'	35°52'	271.9	690	1962–1996
<i>Modelled (west)</i>								
West	95% ice	53	4 722	75°00'	36°24'	4.3	2 616	—
	50% ice	100	4 481	—	—	6.0	1 814	—
	10% ice	500	3 681	—	—	13.2	736	—
	5% ice	1 000	3 280	—	—	16.0	472	—
	1% ice	5 000	2 000	—	—	20.7	130	—
<i>Observed (east)^b</i>								
Langtang	Kyangjin	333	5 430	85°30'	28°30'	14.3	1 357	1995–1996
Seti	Phoolbari	582	2 867	84°00'	28°14'	53.1	2 877	1970–1985
Balaphi	Jalbire	629	3 328	85°46'	27°49'	54.1	2 712	1970–1995
Yagdi	Mangla	1 101	3 356	83°32'	28°22'	76.7	2 197	1986–1995
Chamelia	Karkale	1 279	3 173	80°34'	29°40'	54.9	1 354	1970–1992
Tila Nala	Nagma	1 786	3 581	81°55'	29°19'	46.6	823	1976–1995
Tama K	Busti	2 983	4 228	86°05'	27°38'	145.5	1 538	1971–1987
<i>Modelled (east)</i>								
East	95% ice	53	4 722	85°30'	28°30'	4.0	2 395	—
	50% ice	100	4 481	—	—	6.7	2 100	—
	10% ice	500	3 681	—	—	21.3	1 341	—
	5% ice	1 000	3 280	—	—	31.0	977	—
	1% ice	5 000	2 000	—	—	88.4	557	—

^a Source: Water and Power Development Authority, Pakistan (Archer, 2003).

^b Source: Department of Hydrology and Meteorology, Kathmandu, Nepal.

Table I compares modelled flows with available measurements from actual catchments towards the western and eastern ends of the Himalaya. Modelled runoff for the smaller, higher elevation hypothetical sub-basins in the west was consistent with observations, but that generated for the two largest sub-basins (glacierization $\leq 5\%$) was apparently underestimated, probably because modelled precipitation at lower elevations was set too low. For the east, modelled runoff (557–2395 mm) is similar in range to that observed (823–2877 mm).

Annual mass balance estimates under baseline conditions are consistent with the limited measurement series from the region. Model estimates of -13 to -152 mm (mean -74 mm) for the hypothetical eastern glacier compare favourably with observed annual mass balances of between $+390$ to -700 mm (mean -113 mm) for Langtang Glacier between 1987 and 1997 (Dyurgerov, 2005). No direct comparison was possible for the hypothetical western glacier. However, model estimates of between -1019 and -1332 mm (mean -1215 mm) are similar in range to the -945 to -1289 mm measured at Dunagiri Glacier ($79^{\circ}54'E$, $30^{\circ}33'N$) between 1986 and 1990 (Dyurgerov, 2005). Modelled accumulation/area ratios of 0.50 and 0.68, for west and east respectively, are also consistent with observed values (Kaul, 1999).

The model was applied in both nests of hypothetical catchments under two separate scenarios, for 150 years from the arbitrary start date of 1990. First, a baseline scenario was applied, with climate data held at the standard period 1961–1990 levels throughout. Second, a transient climatic warming scenario was applied, with incremental air temperature increases of $0.06^{\circ}\text{C year}^{-1}$ but maintaining standard-period precipitation, realistic against reported values of 0.06 to $0.12^{\circ}\text{C year}^{-1}$ from 1977 in Nepal (Shrestha *et al.*, 1999) and just above the globally averaged range of IPCC predicted temperature increases (1.4 to 5.8°C by 2100) (Houghton *et al.*, 2001).

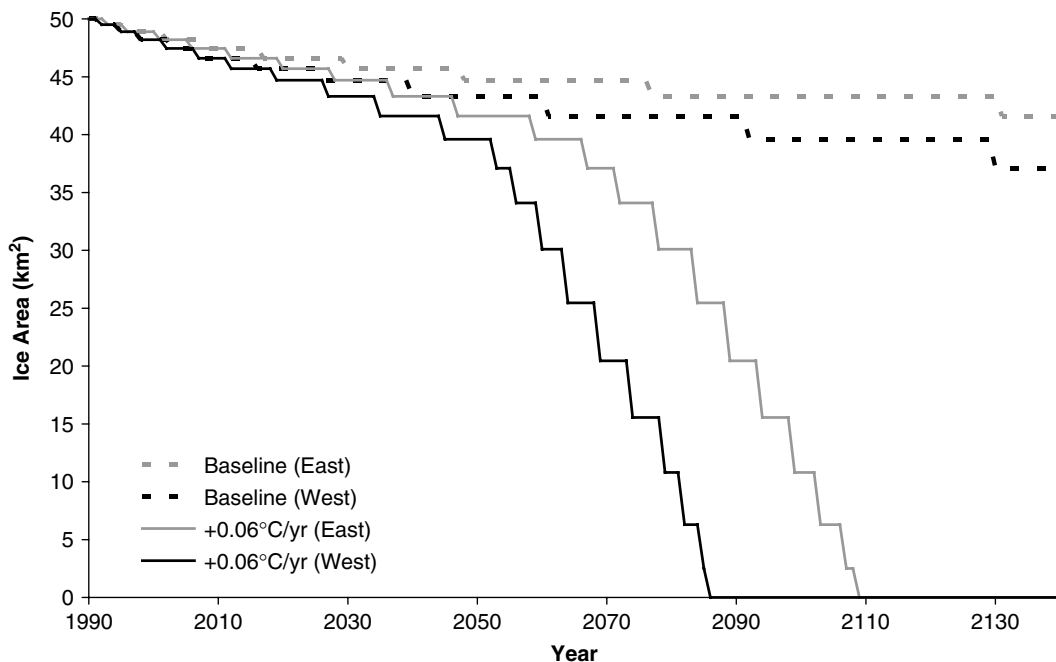


Figure 4. Comparison of decline in glacier area between west (black) and east (grey) for baseline conditions (dashed) and $0.06^{\circ}\text{C year}^{-1}$ (solid) warming scenario

ANALYSIS OF RESULTS

Glacier retreat and mass balance changes

Changes in the area of the hypothetical glaciers (Figure 4) show that glacier retreat is more rapid in the west for both baseline conditions and the warming scenario, because limited summer precipitation in the west allows ablation to continue unabated and the amount of winter snowfall is inadequate to offset loss of ice through accelerating melt. By contrast, high monsoonal precipitation in the east, which occurs as snow at higher elevations, raises albedo and protects the eastern glacier from ablation during key summer months. Recession continues, however, because the rate of loss of mass by ablation is not completely offset by total annual snow accumulation. Summer precipitation appears to be a stronger influence on glacier recession than summer energy availability. Under baseline conditions, total glacier area reduces by 26% and 17% over the 150-year period in the west and east respectively. Under climatic warming, retreat accelerates as increasing temperatures raise the limits of the transient snowline (TSL) to higher elevations to expose more ice to melting. Retreat continues apace until both glaciers disappear, in 2086 and 2109 in the west and east respectively.

Annual mass balance variation under climatic warming further emphasizes the distinction between west and east. The rate of mass loss is initially higher in the west, but steadily increases for both glaciers as temperature rises (Figure 5). Mass balance changes under climatic warming, of -41 mm year^{-1} and -27 mm year^{-1} on average ($-680 \text{ mm }^{\circ}\text{C}^{-1} \text{ year}^{-1}$ and $-442 \text{ mm }^{\circ}\text{C}^{-1} \text{ year}^{-1}$) in the west and east respectively are generally consistent with published values of mass balance sensitivity, which range globally from ± 300 to $1000 \text{ mm }^{\circ}\text{C}^{-1} \text{ year}^{-1}$ (Dyurgerov and Meier, 2000).

Future variation of river flow

Effects of glacier recession and mass balance change on annual mean flow are shown in Figures 6 and 7. Under baseline conditions, annual mean flow declines slightly in subcatchments of $\geq 50\%$ glacierization in both west and east (Figure 6). The elevation range between which the TSL fluctuates remains fixed, and the gradual loss of ice from lower ice bands gently reduces flow. Relatively small reductions in glacial melt-water

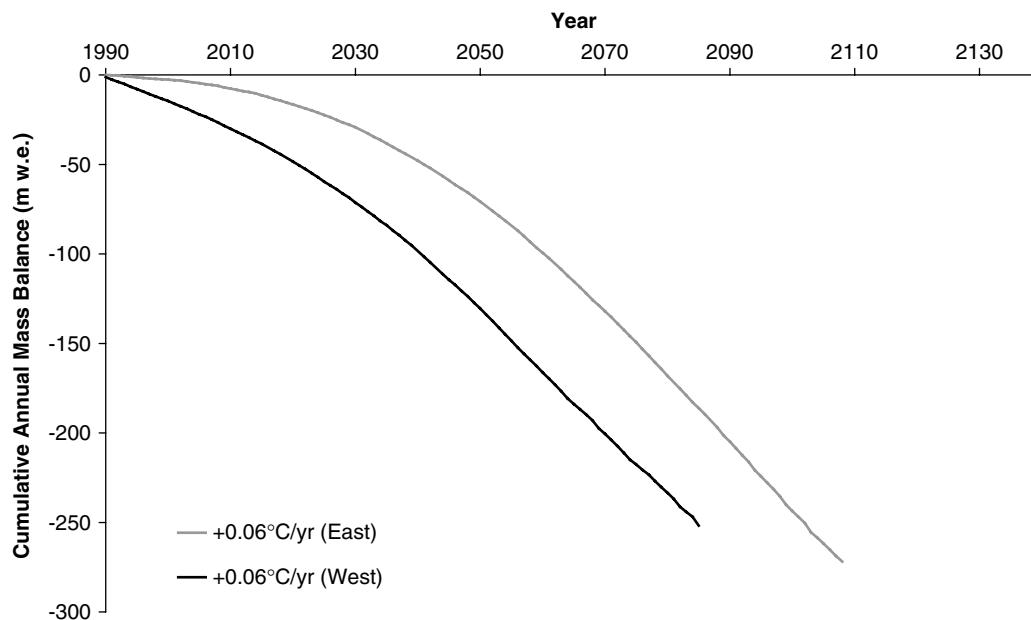


Figure 5. Cumulative annual mass balances of the hypothetical glaciers under $0.06 \text{ }^{\circ}\text{C year}^{-1}$ warming scenario

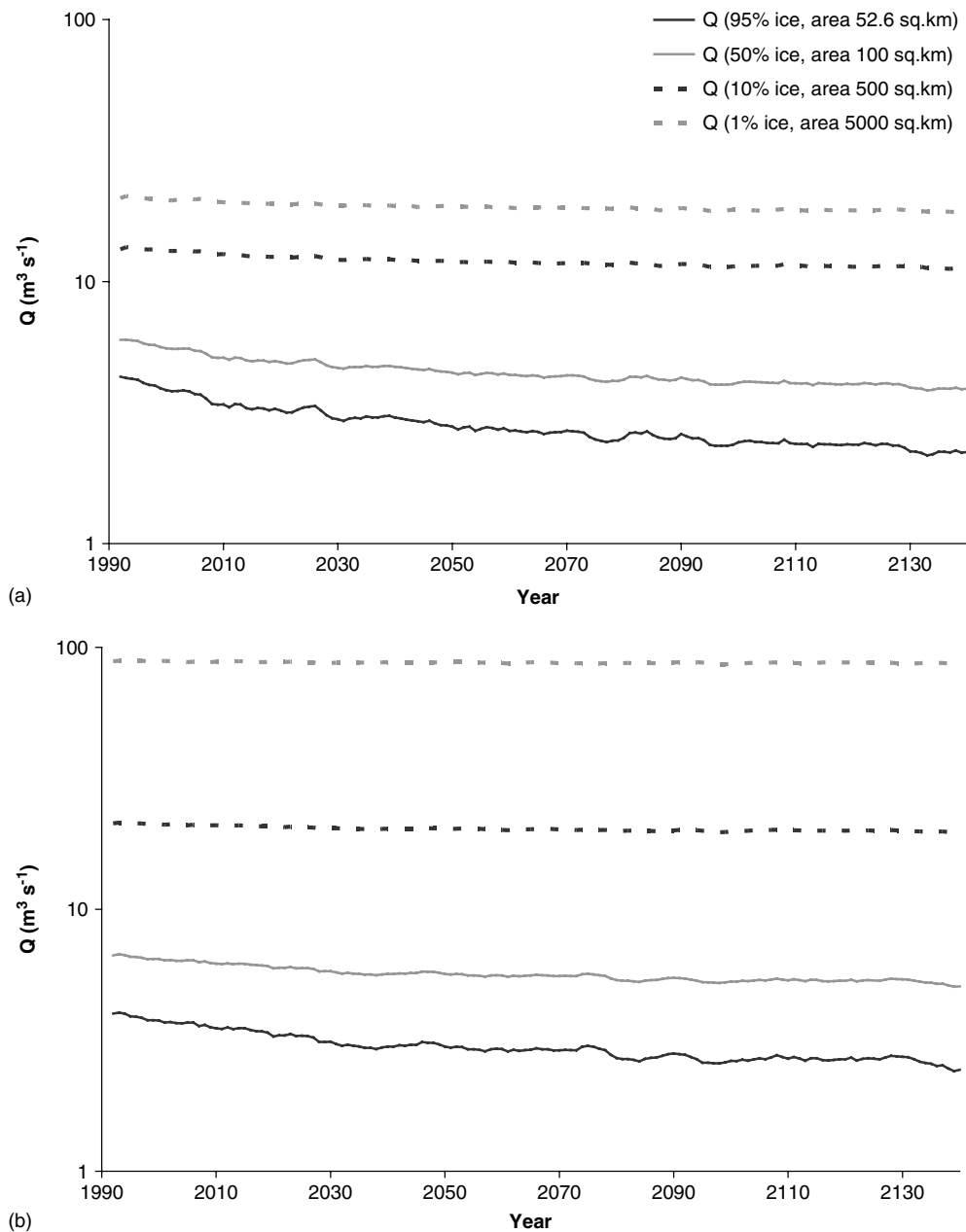


Figure 6. Variation in annual mean flow under baseline conditions for: (a) the western catchments; (b) the eastern catchments. Note the logarithmic scale on the y-axis

contributions are barely noticeable in larger downstream sub-basins, being offset by the proportion of total runoff that is generated from ice-free areas.

Figure 7 shows river flows in both nests of hypothetical catchments responding characteristically under the warming scenario. Glacier recession initially increases flows, as the area of exposed ice increases. Once the rate of addition of ice area exposed to melt by the rising TSL can no longer offset the area of ice lost around

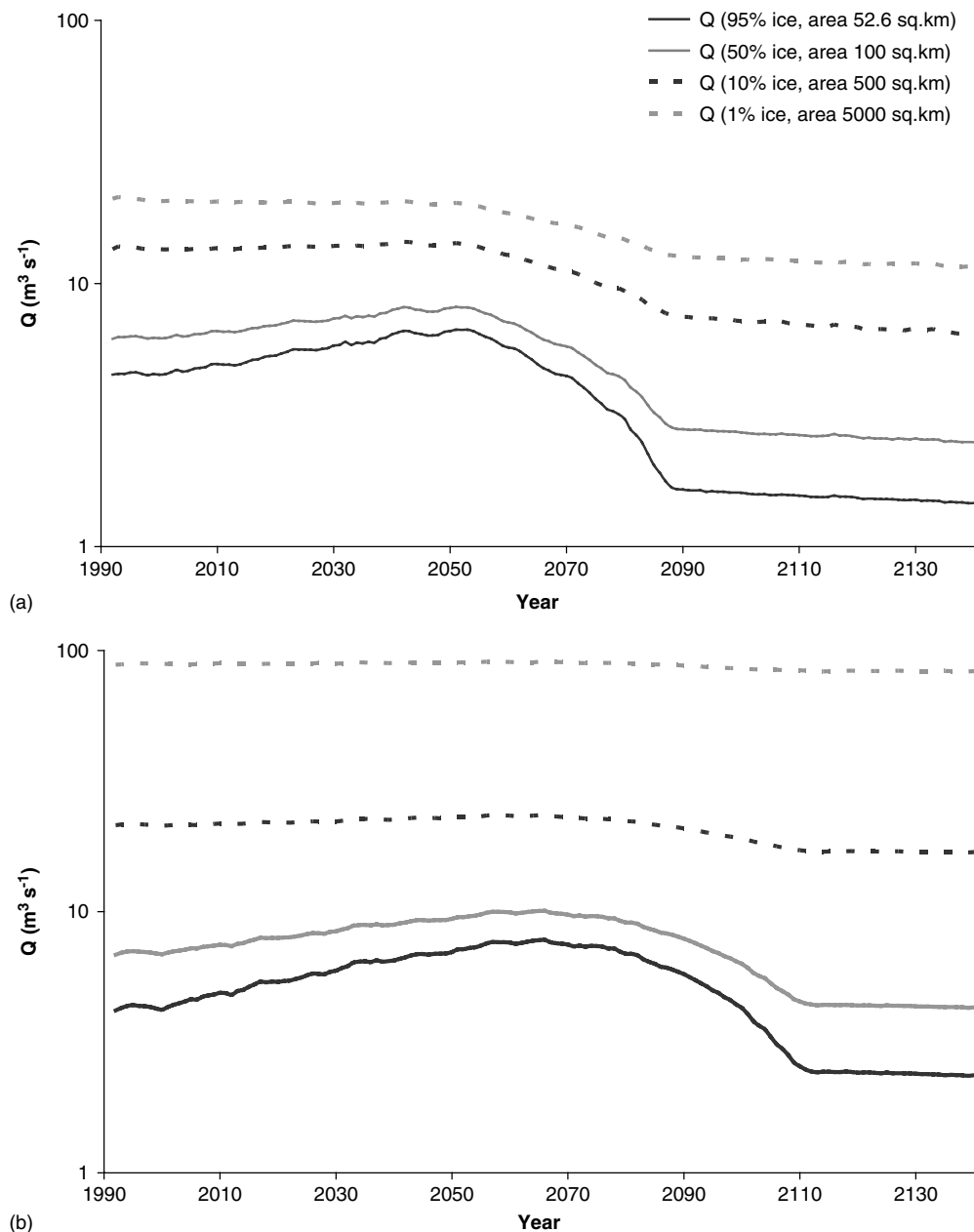


Figure 7. Variation in annual mean flow under the $0.06^\circ\text{C year}^{-1}$ warming scenario for: (a) the western catchments; (b) the eastern catchments. Note the logarithmic scale on the y-axis

the glacier terminus, flow starts to diminish. The impact of warming on runoff declines downstream in both nests of hypothetical catchments with reduction in percentage glacierization.

In the west (Figure 7a), flow from the smallest most glacierized sub-basin peaks at about 150% of initial flow around year 2060, and this impact persists downstream because declining runoff from the ice-free area downstream means that the glacier-melt component of flow remains dominant throughout. The pattern of response is similar in the east (Figure 7b), with flows in the most glacierized sub-basin rising more gently

before attaining a greater maximum, about 170% of the initial flow, some 10 to 20 years later than in the west. Changes to the melt-water contribution here have little impact downstream because runoff from rainfall over the ice-free area contributes a much larger proportion of total discharge.

Upon disappearance of the glaciers, annual mean flow is about 33% and between 4 and 18% less than in the 1990s in the west and east respectively. Removal of the glaciers leaves flow determined only by contemporary precipitation levels. The greater decline in flow in the west reflects the greater relative importance of glacial melt water at the outset.

DISCUSSION

Ideally, for modelling responses of glacierized catchments to future climatic warming, a fully distributed climate–mass-balance–hydrological model should be applied to a glacier of known geometry, known thickness and measured ice hypsometry, calibrated on a period with detailed climatic and hydrological records in order to predict the temporal pattern of glacier recession and the coupled impact on runoff accurately. However, in the Himalaya, records of mountain climatic variables and runoff are sparse and short, and glacier geometry is completely unknown. Hence, there was little choice but to develop a simple temperature-index model with parameters drawn from the literature, and apply that model to a hypothetical, but plausible, glacier geometry. Even though the modelled baseline runoff would probably deviate from reality in any actual glacierized basin, comparison between present and future modelled values can provide realistic estimates of both the pattern of change and the relative scale of change of flow into the future. Absolute timings of changes in flow and recession are strongly dependent on ice thickness and area and the range of elevation within which glaciers exist. This study describes the behaviour of relatively large glaciers descending through a considerable elevation range. The response of smaller glaciers having lesser vertical extents, located at lower elevations, would have been markedly different. Further modelling with varying glacier geometries and elevation ranges is required in order better to constrain timing for real glaciers across the Himalayan region.

Application of this model, as for all models, depends on a specific set of parameter settings. From the point of view of a west–east Himalayan comparison, the use of identical settings of parameters and the choice of the same glacier geometry mean that differences in response have arisen solely as a result of regional differences in climate, particularly in summer precipitation. Nonetheless, sensitivity analyses for the major parameters will improve confidence in absolute output forecasts, which may also have some impact on timings and scales of runoff responses. For instance, adjusting the distribution of precipitation with elevation would affect the forecasts: a reduction, say, in the precipitation lapse rate P_{lapse} would result in the annual mass balance being more negative/less positive, and time-to-peak discharge and time of glacier disappearance attained earlier as climate warms. The values taken for DDF_{snow} and DDF_{ice} also influence results. Whereas the DDF_{snow} used ($4 \text{ mm } ^\circ\text{C}^{-1} \text{ day}^{-1}$) was consistent with reported values (e.g. Hock, 2003), it is 25% lower than that for Dokriani Glacier in northwest India (Singh *et al.*, 2000) and some 60% lower than at Glacier AX010 in Nepal (Kayastha *et al.*, 2000). Using higher values would have steepened initial flow increases and given more negative/less positive annual mass balances, and led to more rapid recession. Globally, DDF_{ice} values range from 5.4 to $20 \text{ mm } ^\circ\text{C}^{-1} \text{ day}^{-1}$. The value of $10 \text{ mm } ^\circ\text{C}^{-1} \text{ day}^{-1}$ chosen for DDF_{ice} in this model matched estimates for Yala Glacier in eastern Nepal (Hock, 2003). Of course, Himalayan glaciers tend to be heavily debris covered, and this should be taken into account in future modelling.

It should be noted that the climatic warming scenario applied in this study maintained precipitation constant over the 150-year period. Air temperature increases might be expected to be accompanied by changes in precipitation. Increasing precipitation would lead to enhanced snow accumulation, more positive/less negative glacier mass balance, but more monsoonal rainfall with conflicting signals for downstream runoff. Had precipitation been allowed to increase, the results of this model would probably have shown a reduced rate of glacier retreat, less rapid changes in river flows and diminished impacts, or even reversal, downstream.

CONCLUSIONS

Application of the simple temperature-index-based hydro-glaciological model developed in this study to forecast the future response of flow in Himalayan rivers to a uniform rise in temperature highlights the issues of data requirements for modelling in areas where climatic, glaciological and hydrological data are sparse, and the characteristics of models necessary for transient treatment of climatic warming coupled with glacier decline. Not only are the data sets from which the air temperature and precipitation lapse rates could be derived deficient in the region, but sustained measurements of glacier mass balance and runoff, against which model parameters might be optimized, are also scarce, necessitating the use of hypothetical basins and generalized input data. How ice surface area and volume changes with time as glaciers recede is another essential feature of a conceptually based model for predicting future runoff. In the absence of information on appropriate three-dimensional distributions of ice volume (not only in the Himalaya), plausible glacier shapes and dimensions have to be prescribed, as hypothetical generalized glaciers.

The model described is most reliably used in comparative, or differential, mode, showing differences in future river flows between existing (baseline) climate continuing and a climatic warming scenario being applied. In differential mode also, future differences in response between two (or more) areas can be discerned when identical model glaciers in identical hypothetical catchments are exposed to the same climatic warming but differing original climatic characteristics.

Use of this model on the two identical model glaciers in the nests of hypothetical catchments located at opposite ends of the Himalayan arc demonstrates the characteristic hydrological response as ice area declines of flow initially increasing over a variable time-scale, then decreasing, over a further variable time-scale, until the glaciers eventually disappear. This response is strongly affected by differences in climate. Under the uniform warming scenario of $0.06\text{ }^{\circ}\text{C year}^{-1}$, flows for the most highly glacierized subcatchments (glacierization $\geq 50\%$) attain peaks of 150% and 170% of initial flow at around 2050 and 2070 in the west and east respectively, before declining until the respective glaciers disappear in 2086 and 2109. Such absolute estimates clearly depend on parameter values and the assumed geometries of the model glaciers. Relative differences between baseline and warming scenarios and between west and east provide a more reliable and useful indication of what might be expected as glaciers across the Himalayan region continue to recede. Glacier-fed rivers throughout the Himalaya will respond in a similar manner to climatic warming, except that summer snowfall in the east will reduce the rate of initial flow increase, delay the timing of peak discharge and postpone the eventual disappearance of the ice. Impacts of declining glacier area on river flow will be greater in smaller, more highly glacierized basins both west and east, and in the west, where precipitation is scarce, for considerable distances downstream.

ACKNOWLEDGEMENTS

The study was funded by the UK Department for International Development Knowledge and Research Programme (DFID KAR project no. R7980) and the Centre for Ecology and Hydrology (CEH). We are grateful for the constructive comments of the editor and two anonymous reviewers, and for the support of colleagues, namely: Heather Musgrave, Alan Gustard, and Andy Young, CEH; Arun Shrestha, Department of Hydrology and Meteorology, Kathmandu; Adarsha Pokhrel, Society of Hydrologists and Meteorologists of Nepal; and Rajesh Kumar and Syed Hasnain, Jawaharlal Nehru University, New Delhi. This study is a contribution to the Hindu Kush–Himalayan FRIEND project of the International Hydrological Programme of UNESCO.

REFERENCES

- Ageta Y, Naito N, Nakawo M, Fujita K, Shankar K, Pokhrel AP, Wangda D. 2001. Study project on the recent rapid shrinkage of summer-accumulation type glaciers in the Himalayas, 1997–1999. *Bulletin of Glaciological Research* **18**: 45–49.
- Archer DR. 2003. Contrasting hydrological regimes in the Indus basin. *Journal of Hydrology* **274**: 198–210.
- Bell VA, Moore RJ. 1999. An elevation-dependent snowmelt model for upland Britain. *Hydrological Processes* **13**: 1887–1903.

- Braun LN, Grabs W, Rana B. 1993. Application of a conceptual precipitation–runoff model in the Langtang Khola basin, Nepal Himalaya. In *Snow and Glacier Hydrology*, Young GJ (ed.). IAHS Publication No. 218. IAHS Press: Wallingford; 221–237.
- Collins DN, Macdonald OG, Reynolds AC, Rees HG. 2002. Climatic variation, mass balance and runoff from European glacierised mountain basins. In *Proceedings of Eighth National Hydrology Symposium, British Hydrological Society*, University of Birmingham, 8–11 September; 67–73.
- Dyurgerov MB. 2005. *Mass balance of mountain and sub-polar glaciers outside the Greenland and Antarctic ice sheets*. Supplement to Occasional Paper No. 55, Institute of Arctic and Alpine Research, University of Colorado (distributed by National Snow and Ice Data Center, Boulder, CO).
- Dyurgerov MB, Meier MF. 1997. Mass balance of mountain and subpolar glaciers: a new global assessment for 1961–1990. *Arctic and Alpine Research* **29**(4): 379–391.
- Dyurgerov MB, Meier MF. 2000. Twentieth century climate change: evidence from small glaciers. *Proceedings of the National Academy of Science of the United States of America* **97**(4): 1406–1411.
- ESRI. 1993. *Digital Chart of the World for Use with ARC/INFO: Data Dictionary*. ESRI: Redlands, CA.
- Fujita K, Kadota T, Rana B, Kayastha RB, Ageta Y. 2001. Shrinkage of Glacier AX010 in Shorong region, Nepal Himalayas in 1990s. *Bulletin of Glaciological Research* **18**: 51–54.
- Fukushima Y, Watanabe O, Higuchi K. 1991. Estimation of streamflow change by global warming in a glacier-covered high mountain area of the Nepal Himalaya. In *Snow, Hydrology and Forests in High Alpine Areas*, Bergmann H, Lang H, Frey W, Issler D, Salm B (eds). IAHS Publication No. 205. IAHS Press: Wallingford; 181–188.
- Hock R. 2003. Temperature index melt modelling in mountain area. *Journal of Hydrology* **282**(1–4): 104–115. DOI: 10.1016/S0022-1694(03)00257-9.
- Houghton JT, Ding Y, Griggs DJ, Noguer M, van der Linden PJ, Dai X, Maskell K, Johnson CA (eds). 2001. *Climate Change 2001: The Scientific Basis*. Cambridge University Press: Cambridge.
- ICIMOD. 2000. *Inventory of Glaciers, Glacial Lakes and Glacial Lake Outburst Floods—Monitoring and Early Warning Systems in the Hindu Kush–Himalayan Region–Nepal*, International Centre for Integrated Mountain Development: Kathmandu, Nepal.
- Kadota T, Seko K, Aoki T, Iwata S, Yamaguchi S. 2000. Shrinkage of the Khumbu Glacier, east Nepal 1978 to 1995. In *Debris-Covered Glaciers*, Nakawo M, Raymond CF, Fountain A (eds). IAHS Publication No. 264. IAHS Press: Wallingford; 235–243.
- Kaul MK (ed.). 1999. *Inventory of the Himalayan Glaciers. A Contribution to the International Hydrological Programme*. Geological Survey of India Special Publication No. 34. GSI: Calcutta.
- Kayastha RB, Ageta Y, Nakawo M. 2000. Positive degree-day factors for ablation on glaciers in the Nepalese Himalaya: case study on Glacier AX010 in Shorong Himal, Nepal. *Bulletin of Glaciological Research* **17**: 1–10.
- Moore RJ. 1985. The probability-distributed principle and runoff production at point and basin scales. *Hydrological Sciences Journal* **30**: 273–297.
- Müller F, Cafilish T, Müller G. 1977. *Instruction for compilation and assemblage of data for a world glacier inventory*. Temporary Technical Secretariat for World Glacier Inventory, Swiss Federal Institute of Technology, Zurich.
- Naithani AK, Nainwal HV, Sati KK, Prasad C. 2001. Geomorphological evidences of retreat of the Gangotri Glacier and its characteristics. *Current Science* **80**(1): 87–94.
- New MG, Hulme M, Jones PD. 2000. Representing twentieth-century space–time climate variability. Part II: development of 1901–1996 monthly grids of terrestrial surface climate. *Journal of Climate* **13**: 2217–2238.
- Pearce F. 1999. Flooded out: retreating glaciers spell disaster for valley communities. *New Scientist* **162**(2189): 18.
- Quick MC, Pipes A. 1977. UBC watershed model. *Hydrological Sciences Bulletin* **22**: 161–253.
- Sharma KP, Vorosmarty CJ, Moore B. 2000. Sensitivity of the Himalayan hydrology to land-use and climatic changes. *Climatic Change* **47**: 117–139.
- Shrestha AB, Wake CP, Mayewski PA, Dibb JE. 1999. Maximum temperature trends in the Himalaya and its vicinity: an analysis based on temperature records from Nepal for the period 1971–94. *Journal of Climate* **12**: 2775–2786.
- Singh P, Bengtsson L. 2003. Effect of warmer climate on the depletion of snow-covered area in the Satluj basin in the western Himalayan region. *Hydrological Sciences Journal* **48**(3): 413–425.
- Singh P, Bengtsson L. 2005. Impact of warmer climate on melt and evaporation for the rainfed, snowfed and glacierfed basins in the Himalayan region. *Journal of Hydrology* **300**: 140–154.
- Singh P, Jain SK. 2003. Modelling of streamflow and its components for a large Himalayan basin with predominant snowmelt yields. *Hydrological Sciences Journal* **48**(2): 257–276.
- Singh P, Kumar N. 1997a. Impact assessment of climate change on the hydrological response of a snow and glacier melt runoff dominated Himalayan river. *Journal of Hydrology* **193**: 316–350.
- Singh P, Kumar N. 1997b. Effect of orography on precipitation in the western Himalayan region. *Journal of Hydrology* **199**: 183–206.
- Singh P, Kumar N, Arora M. 2000. Degree-day factors for snow and ice for Dokriani Glacier, Garhwal Himalayas. *Journal of Hydrology* **235**: 1–11.
- USGS. 2001. *United States Geological Survey HYDRO1k elevation derivative database (Asia)*. Distributed by the Land Processes Distributed Active Archive Center (LPDAAC), at the USGS EROS Data Center.
- Vorosmarty CJ, Moore B, Grace AL, Gildea MP, Melillo JM, Peterson BJ, Rasetter EB, Steudler PA. 1989. Continental scale models of water balance and fluvial transport: an application to South America. *Global Biogeochemical Cycles* **3**: 241–265.
- Watson RT, Zinyowera MC, Moss RH (eds). 1996. *Climate Change 1995. Impacts, Adaptation and Mitigation of Climate Change: Scientific and Technical Analyses*. Cambridge University Press: Cambridge.
- WWF. 2005. *An overview of glaciers, glacier retreat, and subsequent impacts in Nepal, India and China*. World Wildlife Fund, Nepal Program.
- Young GJ, Hewitt K. 1988. Hydrology research in the upper Indus basin, Karakoram Himalaya, Pakistan. In *Hydrology of Mountainous Areas*, Molnár L (ed.). IAHS Publication No. 190. IAHS Press: Wallingford; 139–152.